SEVENTH FRAMEWORK PROGRAMME

Capacities Specific Programme

Research Infrastructures

Project No.: 227887

SERIES

SEISMIC ENGINEERING RESEARCH INFRASTRUCTURES FOR EUROPEAN SYNERGIES

Work package [WP9 – TA5 LNEC]

SEISMIC PERFORMANCE OF MULTI-STOREY TIMBER BUILDINGS

Rusticasa building

- Final Report -

User Group Leader: Maurizio Piazza

Revision: Final

July, 2013

ABSTRACT

This document reports the outcome of the seismic test on the Rusticasa building, the first in a total of four buildings included in the TIMBER BUILDINGS Project. This building is a log house system (LHS). The goal of the tests was to assess the seismic performance of the building, panel elements and steel connectors, defined in terms of relative displacements and hold-down forces.

Keywords: Timber buildings, Shaking Table Test, Log house system (LHS), steel connectors

ACKNOWLEDGMENTS

The research leading to these results has received funding from the European Union Seventh Framework Programme [FP7/2007-2013] under grant agreement n° 227887 [SERIES].

REPORT CONTRIBUTORS

LNEC Alfredo Campos Costa
Paulo Xavier Candeias

UNIVERSITY OF MINHO Paulo B. Lourenço
Jorge M. Branco
Chrysl Aranha

CONTENTS

List of Figures

List of Tables

1 Introduction

Timber has been used as a construction material since times immemorial. In ancient times, timber logs were either used to build entire houses or as timber frame elements in roofs. Log constructions consist of walls made by stacking horizontal logs one above the other. The logs are shaped such that they form a perfect fit with the log below. This is important as it makes the system air-tight, increases moisture resistance and improves thermal and acoustic properties. The contact area between the logs and the compression strength perpendicular to the grain determine the resistance to vertical loads and the horizontal loads are supported by cross walls, with the friction between the joints playing a pivotal role. In areas of Central and Eastern Europe with abundant forest trees, log houses date back to the Stone Age. They were constructed by stacking logs horizontally with notches provided at corner intersections. The log house construction technique followed in Western Europe was more refined as the logs were trimmed and the cross wall intersections were facilitated by dovetail notches [1]. Figure 1 depicts some of the techniques of notching for cross wall intersections.

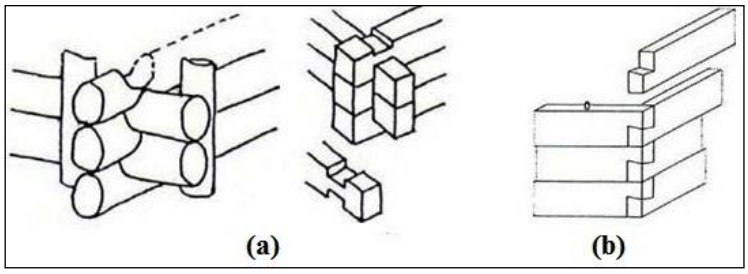

Figure 1.1: Corner log notching techniques in: (a) Central and Eastern Europe; (b) Western Europe [1]

With time, the practice of building log houses has decreased in popularity because of the development of new and improved construction materials and techniques. However, log houses are built even today in regions of Scandinavia, the United States and Canada, where there are vast forest reserves and the climate is suitable for this form of construction. Most of the traditional log houses display poor seismic performance during severe earthquakes as the

corner log connections are not sufficiently robust and come lose due to shear forces. In order to overcome that problem, modern log homes have improved carpentry joints and mechanical connections at the intersections between cross log walls. Although the practice of building log houses has existed since a very long time, the information available on the structural properties, seismic behaviour and the load resistance mechanisms of this system is limited.

In log shear walls, the resistance to lateral loads is derived from the (1) interlock between logs (2) wood or steel dowels (3) vertical through bolts and anchor bolts (4) friction between logs due to vertical loads. However, most building codes just consider the influence of dowels and vertical through bolts in lateral load resistance mechanisms [2]. According to current codes, resistance to seismic action depends only on the compression perpendicular to the grain and shear stress at interceptions between walls. Friction is not regarded as a mechanism. Since the exact contribution to resistance by friction and interlock between logs is not known and can't be quantified with current knowledge, the codes only consider the resistance provided by dowels and vertical through-bolts or anchor bolts [3].This report describes the study that was carried out based on an experimental investigation performed to improve the existing knowledge on log houses subject to seismic events. The main part of the experimental work involved a full scale shaking table test, conducted on a two-storey log house designed by the Portuguese company Rusticasa® in compliance with the design rules for timber buildings. The test was performed by the University of Minho within the framework of the SERIES (Seismic Engineering Research Infrastructures for European Synergies) Project 'Multi-storey timber buildings' and was coordinated by the University of Trento, at LNEC, Lisbon, Portugal.

This report describes the final phase of an experimental research project on a model log house, undertaken by the University of Minho in Guimarães in partnership with the Portuguese company Rusticasa. In order to obtain the European Technical Approval (ETA) for the entry of these log houses into the commercial market, a number of experimental and numerical studies have to be performed to make a detailed characterization of the construction system.

During the first phase of the project, the behaviour of connections between the sill logs and the foundation was assessed through a series of shear and tension tests under cyclic loading. Shear tests revealed that the connections have a good capacity to dissipate energy. From the tension tests, the deformation required to determine the maximum resistance of the connection was determined. In Figure 1.2, the shear and tension test set-ups are seen.

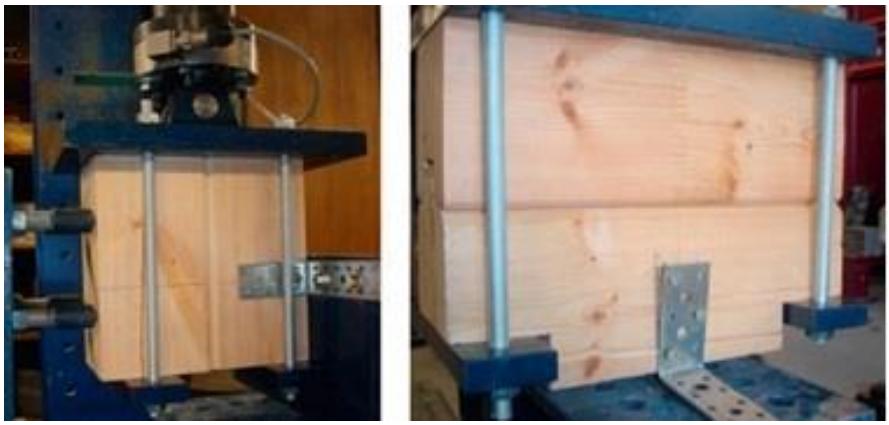

Figure 1.2: Layout of the shear test (left) and tension test (right) performed on connection of the base log and foundation [4]

The second phase focussed on the characterization of the behaviour of log walls by subjecting wall specimens to monotonic and cyclic loading. In order to assess the structural behaviour of log walls under lateral in-plane loads, a number of in-plane static tests were conducted on timber log walls and the effect of parameters like transversal stiffness, vertical compression, slenderness ratio was studied. Figure 1.3 shows the lateral view of the test set-up adopted for the timber log wall tests.

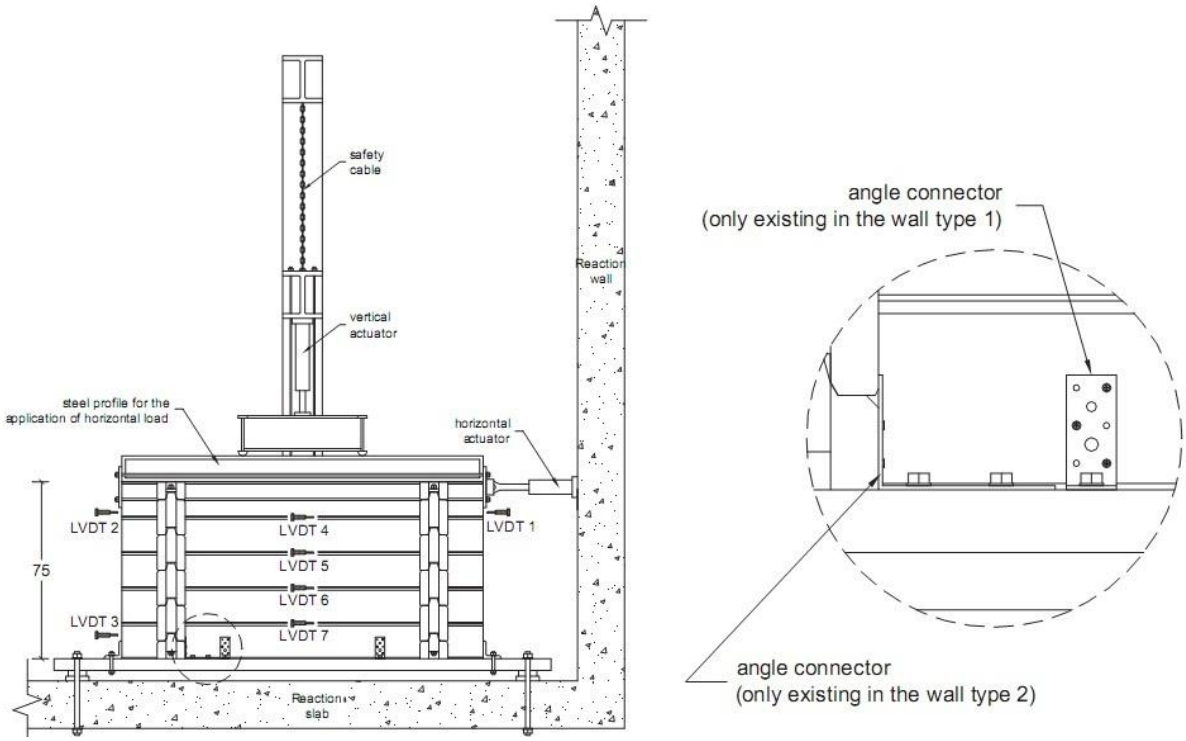

Figure 1.3: Side view of the set-up for testing the full-scale log walls [4]

From the monotonic tests, it was found that the magnitude of vertical compression was proportional to the stiffness of the wall. Due to an increase in the friction between logs, the

horizontal corresponding to the initial displacement also increased, although the ultimate load remained about the same for all walls. The cyclic tests showed that the foundation connection influenced the global behaviour of the walls whereas in the monotonic tests, the global behaviour was found to be independent of the foundation connection type. It was also observed that an increase in slenderness ratio causes a reduction in the lateral resistance of the wall [4].

Based on the results obtained from the experiments conducted in the first two phases, improvements were made in the connection between logs and the connection between the sill log and foundation. While previously, the log house relied only on the orthogonal connections between logs for resistance to loads, the introduction of metal fasteners connecting the logs was advised. Instead of an anchor plate between the wall and the foundation, the use of anchor bolts was recommended. Once the tests on individual elements were carried out, a comprehensive study of the structure itself was carried out in the third and final phase. This phase dealt with the global behaviour of the structure when subjected to seismic loads, its dynamic properties, the study of the interaction of the individual components inside the real structure during an earthquake and the assessment of the failure patterns.

2 Description of the building and construction technique

2.1 INTRODUCTION

The house, as seen in Figure 2.1, is characterized by a rectangular plan of size 5.64x7.3m and consists of two storeys. As the shaking table wasn't large enough to directly accommodate the building on the shaking table, a lattice of steel beams was used to connect the structure to the table and provide a wider base. The height of the house increases from 4.40m at the edge to 5.28m at the ridge, forming a duo-pitch (gable) roof. The ground floor has a height of 2.64m. The plan of the structure is symmetrical in the longitudinal direction and asymmetrical in the transverse direction.

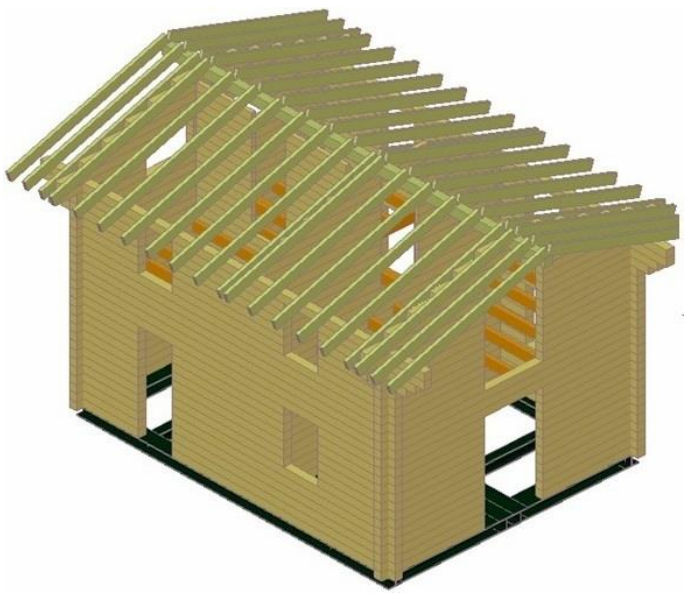

Figure 2.1: 3D model of the log house

The floor beams are of size 90x165mm. In order to guarantee rigid in-plane behaviour of the diaphragm, the beams are superimposed by Oriented Strand Board (OSB) studded panels

which are 22mm thick. In Figure 2.2, the framework of the floor beams along with their dimensions are seen.

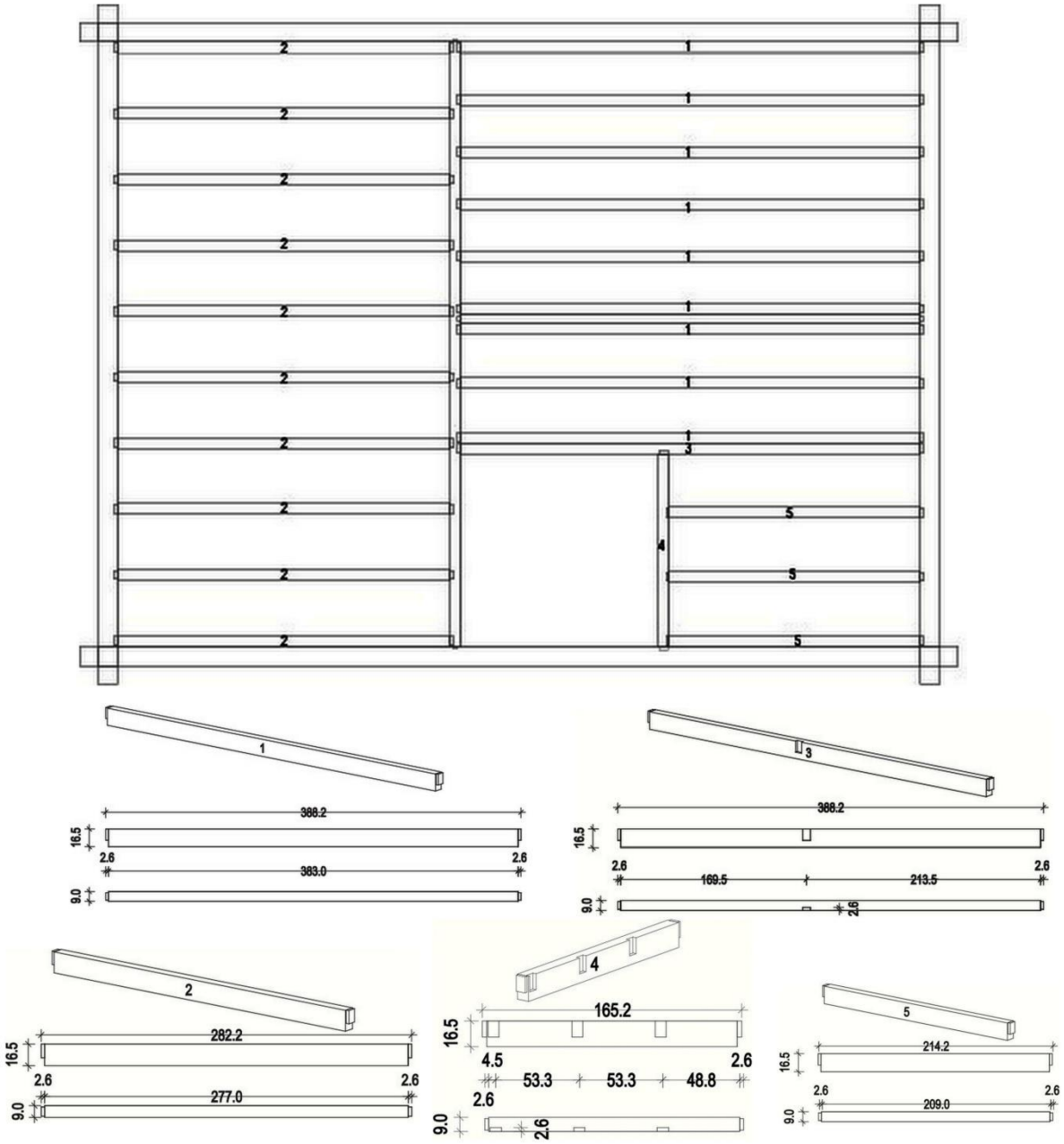

Figure 2.2: Floor beams

The roof structure is characterized by massive wooden rafters of cross-section 70x190mm. The rafters are inclined at an angle of 18°, over which OSB panels are nailed. The layout of the roof beams is seen in Figure 2.3.

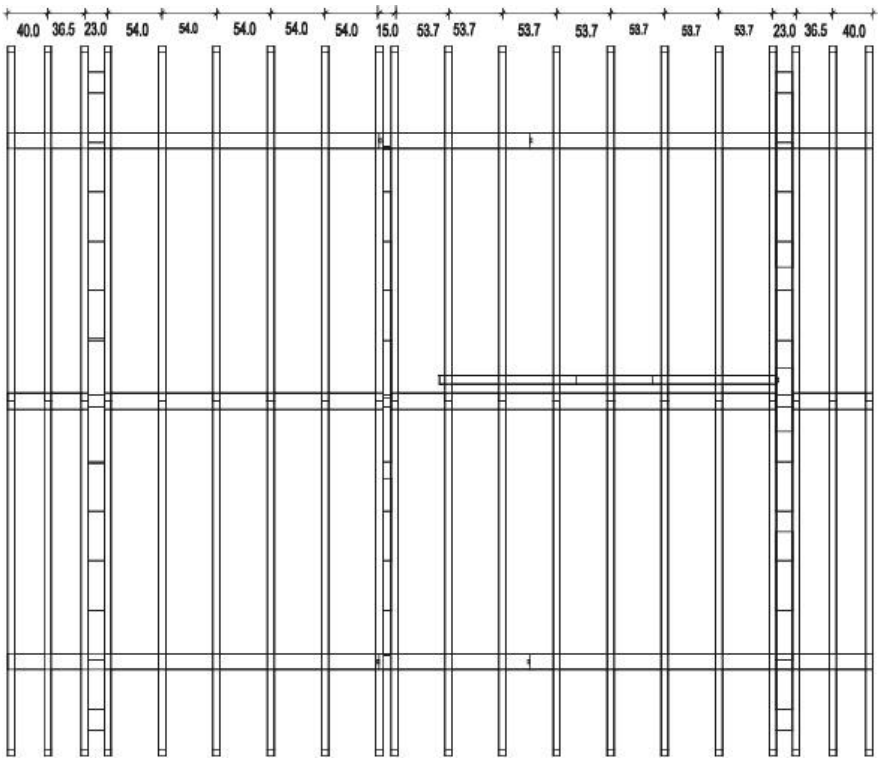

Figure 2.3: Roof framework

The ridge board has a cross-section of 120x200mm and is parallel to the longitudinal walls of the house and can be seen in Figure 2.4. Grooves are provided at the locations where the transverse walls intersect the ridge board. The top ends of the rafters lie on the ridge board and are supported near their ends by the top logs of the longitudinal walls.

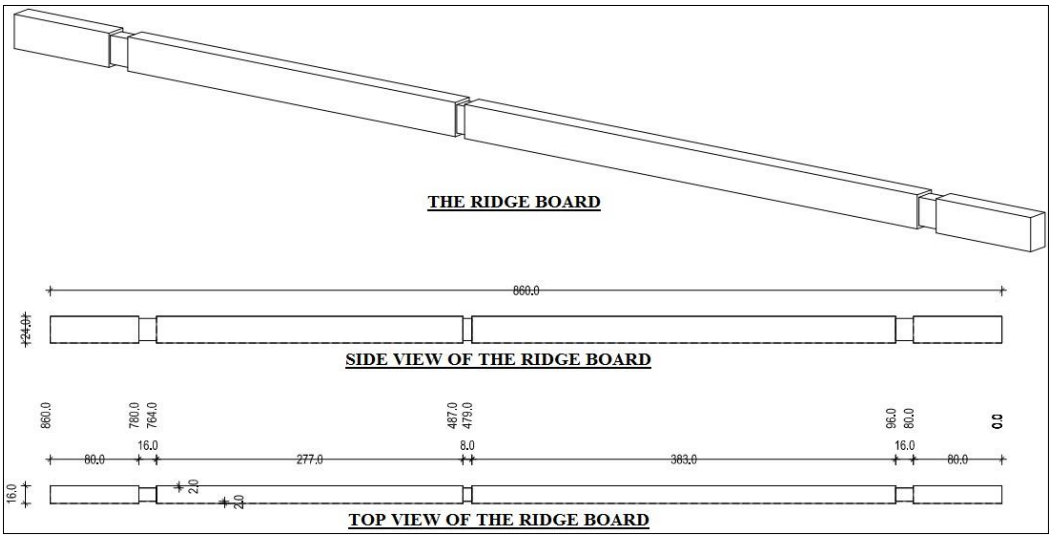

Figure 2.4: The ridge board of the log house

2.2 WALLS

The logs used in the construction of the walls form a perfect fit with each other as they are shaped both at the top and bottom. The ends of the logs are notched to facilitate the intersection of the cross walls. In Figure 2.5 it is possible to see the side profile of the logs and the corner notches.

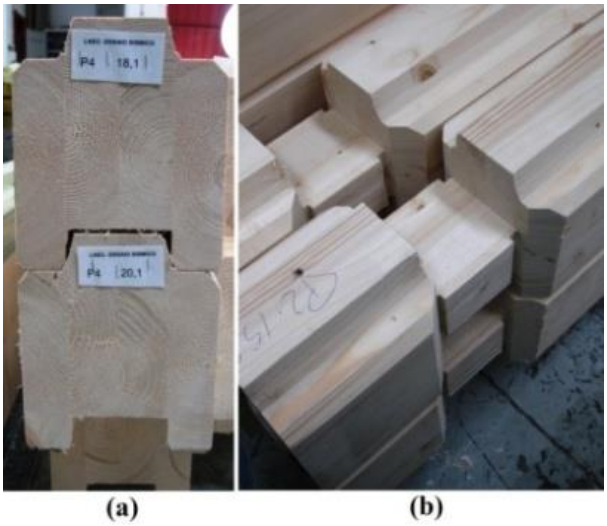

Figure 2.5: (a) Side profile of the logs; (b) Notches at corners of external wall logs

The logs are made of glued and laminated timber derived from Scots Pine trees (*Pinus sylvestris L.*) and belong to the C24 class of resistance according to [5]. The properties of the wood are listed in Table 2.1. Additional information about the geometry and the mechanical characterization of the logs can be found in [6]. The dimensions of the cross sections of the logs used in the outer walls and inner walls are 160x160mm and 80x160mm respectively and can be seen in Figure 2.6. The lamellas which constitute an individual log are each 40mm thick. The inner walls are composed of logs that have two lamellas while the outer walls are composed of four lamellas.

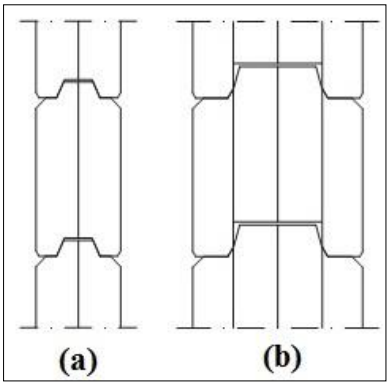

Figure 2.6: Cross-section: (a) internal walls; (b) external walls

Table 2.1 – Properties of Scots Pine wood of class C24

Mass/Volume (kg/m^3)		530
Coefficient of shrinkage	Tangential	0.33
	Radial	0.17
	Volumetric	0.53
Bending strength $f_{m,k}$ (N/mm^2)		24
Tensile strength	$f_{t,90,k}$ (N/mm^2)	14
	$f_{t,90,k}$ (N/mm^2)	0.5
Compressive strength	$f_{c,0,k}$ (N/mm^2)	21
	$f_{c,90,k}$ (N/mm^2)	2.5
Modulus of Elasticity	$E_{0,mean}$ (N/mm^2)	11000
	$E_{90,mean}$ (N/mm^2)	370
Shear Modulus G_{mean} (N/mm^2)		690
Coefficient of Thermal Expansion (C^{-1})		1.17x10^{-5}
Poisson's ratio		0.3

All the walls of the building have been provided with openings to study their influence on the seismic behaviour of the house. In the case of walls provided with openings on both the floors, they are aligned one above the other. The external walls in the longitudinal direction (P2 and P4) have identical openings, with a window and a door on the ground floor and two windows in the upper storey. One of the external walls in the transverse direction (P1) has a door provided on each floor while the other one (P3) has two windows provided on the upper floor. Both the internal walls (P5 and P6) are provided with a door on each floor. The inner wall in the longitudinal direction is connected with the exterior wall (P3) only along one edge to minimize the effect of wall linkages. The plan of the ground floor along with the dimensions is seen Figure 2.7 and Figure 2.8 show the plan of the first floor.

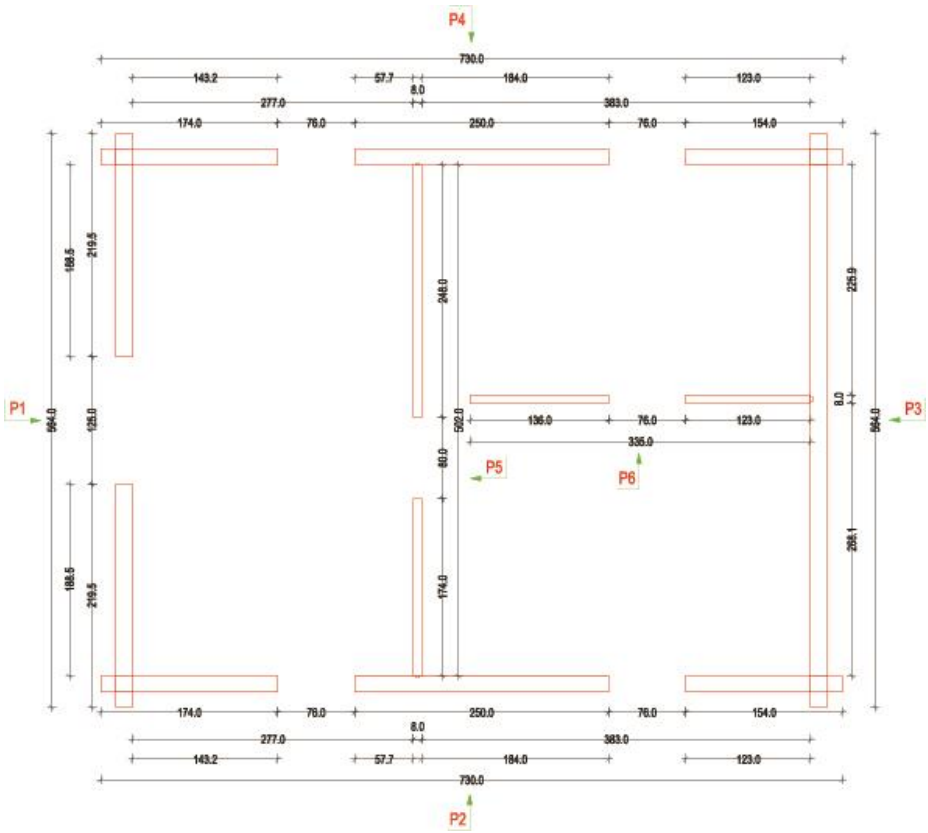

Figure 2.7: Ground floor plan

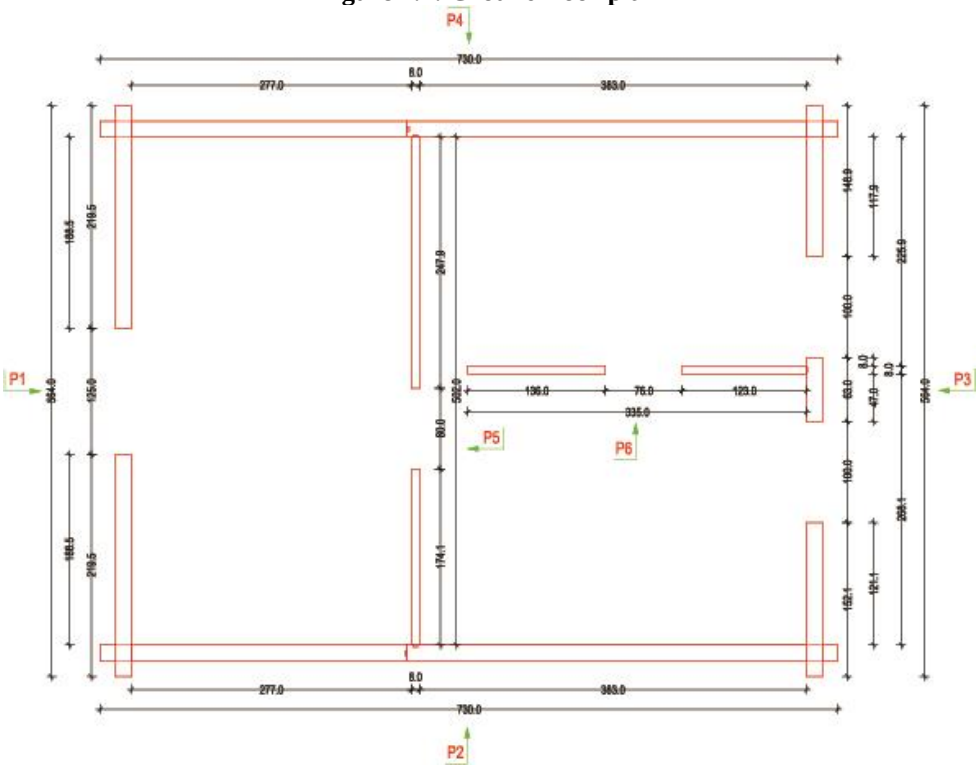

Figure 2.8: Plan of the first floor

2.3 CONNECTIONS

A number of mechanical fasteners in the form of screws have been provided at necessary locations in the house. In the log walls, screws of 10x140mm are used around the openings and screws of 8x240mm are used near the joints of the cross walls. At the intersection of the floor joists and the transverse inner wall, 6x120mm screws have been provided. The purpose of the screws placed around the openings of the house was to hold the logs in place and prevent them from sliding at the free end when the house is subjected to seismic tests. Figure 2.9 shows the location of the connections in the transverse log walls and the floor joists.

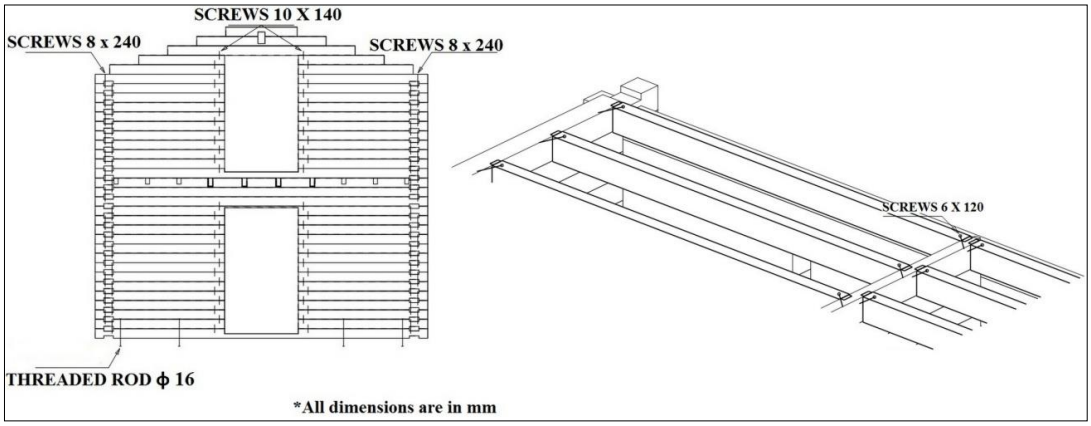

Figure 2.9: Metal fasteners in the log walls and floor beams

The fasteners used in the roof are screws of 10x140mm along with a metal sheet of size 40x140mm at the ridge and screws of size 6x120mm are drilled at the top and bottom of the rafters (Figure 2.10).

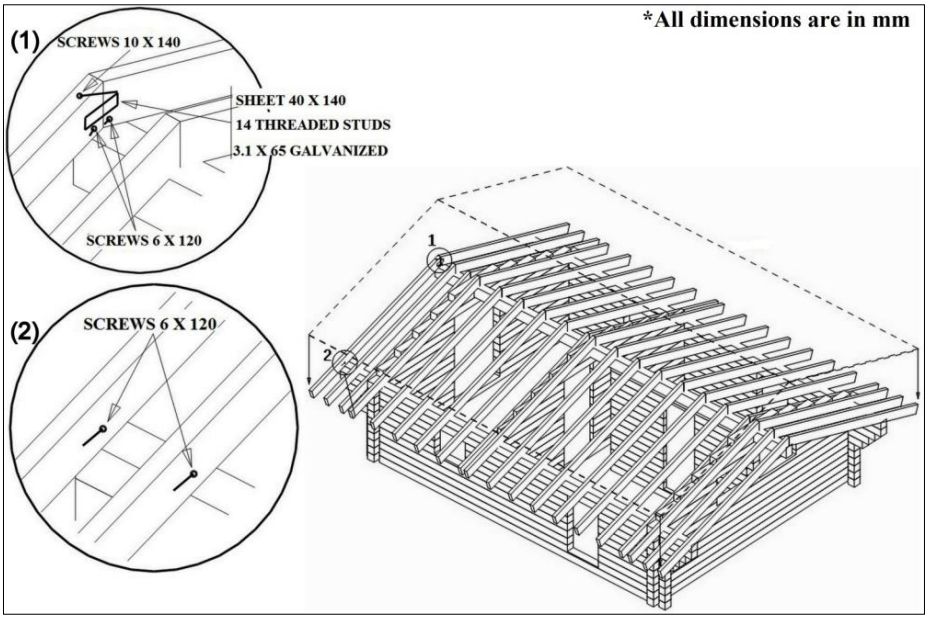

Figure 2.10: Roof connections

The sill logs are connected to the steel plate through M16 bolts of Class 8.8 that are spaced at intervals of 500mm. This ensures that the sliding between the log house and the steel lattice is minimal. The connections between wooden members are in the form of halved joints when two exterior walls meet orthogonally and dovetail joints when an exterior wall meets an interior wall. The floor end joists are also appropriately grooved to form dovetail joints with the log walls. The connections between wooden members and the base log and foundation can be seen Figure 2.11.

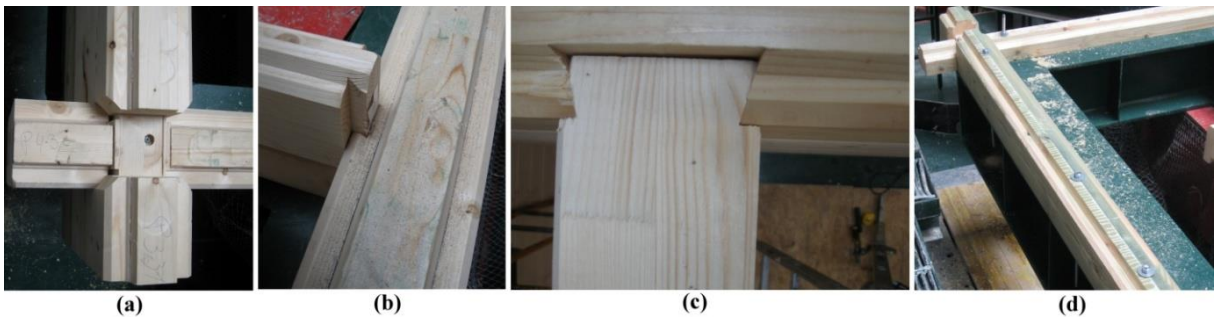

Figure 2.11: Connections between: (a) two exterior walls; (b) an exterior and an interior wall; (c) floor end joist and wall; (d) sill log and foundation

2.4 SEISMIC DESIGN CONSIDERATIONS

The behaviour factor takes into account the plastic properties of the structure and defines the relationship between the acceleration causing collapse and the acceleration causing strain to enter from an elastic zone into a plastic zone. This behaviour factor 'q' makes it possible to design the structures elastically. The seismic capacity of the structure is determined by its ability to withstand plastic strains. For structures that fail in the elastic zone itself, q=1 [7]. As a typical log-house does not dissipate a large amount of energy, the value of q should be around 1.5. However, the behaviour factor is assumed to be 2 taking into account the dissipative action contributed by friction as well.

Since the building did not incorporate any non-structural component and was constructed without any finish, additional masses were placed in order to simulate the permanent loads and accidental loads. Two steel masses weighing 600kg each were attached to the floor to represent floor loads. A representative steel platform is seen in Figure 2.12.

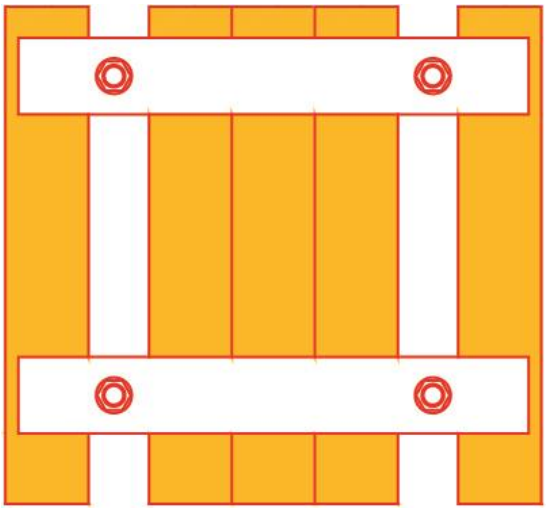

Figure 2.12: A representation of the steel mass used as additional weight

In order to simulate roof loads, 398 steel plates were nailed to the OSB boards over the rafters. The steel mass and roof plates installed in the test house can be seen in Figure 2.13.

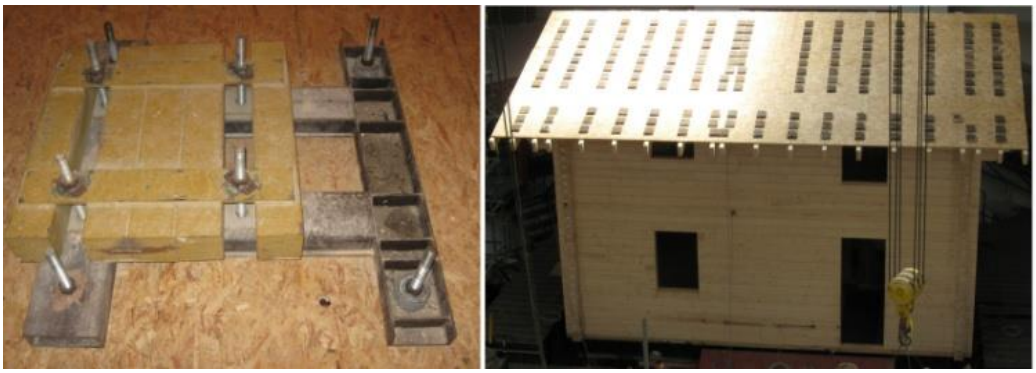

Figure 2.13: Additional weights in the form of a steel mass on the first floor (left) and steel plates on the roof (right)

2.5 ASSEMBLY OF THE HOUSE

All primary structural elements of the building were prefabricated in the factory Vila Nova de Cerveira and transported by truck for a distance of about 400km to Lisbon. The assembly of the building was done directly over the special steel foundation connected to the shaking table. The house was constructed by three workers over a period of four days.

The construction process of the house proceeded in the following manner. After connecting the steel base to the shaking table, the bottom logs were placed on the edges of the lattice and connected via anchor bolts. Successive logs were then laid in all the walls simultaneously up to the level of the floor. The floor beams were laid out as per the plans and screws were drilled at the intersections with the internal walls. Once all the floor beams had been fixed and the mechanical fasteners had been driven in, the OSB panels superposed on the floor beams and nailed in place. The additional masses in the form of steel platforms were then transferred on to the floor using the crane. The walls of the first floor were then built as before. The ridge board was placed along the longitudinal direction along the slots provided in the transverse walls. When all the walls were constructed, the roof rafters were laid out and screwed in. The rafters were superposed by OSB panels and finally the steel plates were nailed to the panels Figure 2.14 shows the sequence of construction of the log house.

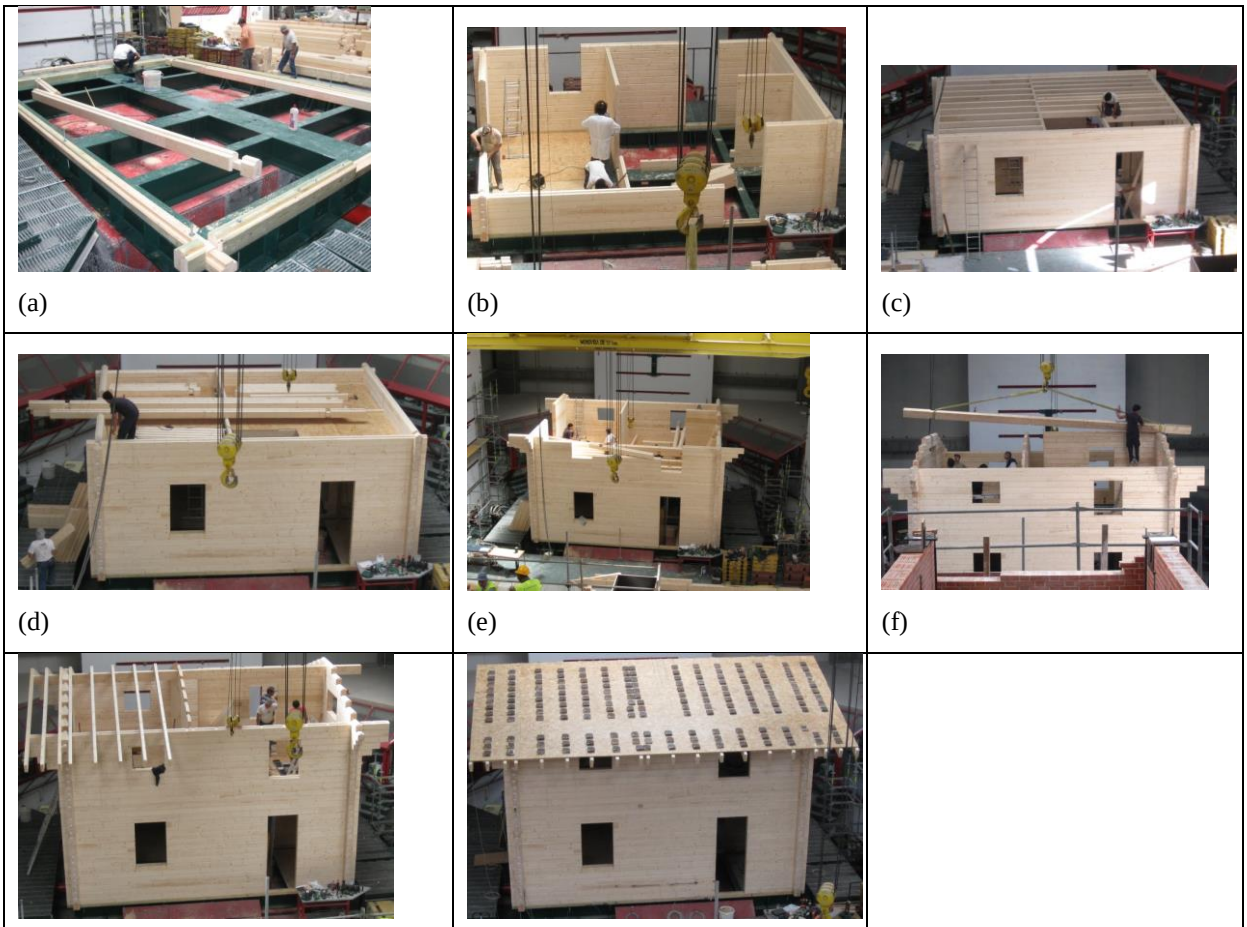

Figure 2.14: Stages of construction: (a) connecting the bottom logs with the steel lattice; (b) laying the ground floor walls; (c) placing floor beams; (d) nailing OSB planks to the floor joists; (e) laying the first floor walls; (f) positioning the ridge board; (g) connecting the roof rafters; (h) Completed house

3 Building instrumentation

To monitor the accelerations, wall sliding and uplift, shear deformations, inter-storey displacements and forces in the building components, a total of 81 sensors were placed at different points of interest in the building. In [8] was presented the list of sensors available at LNEC Earthquake Engineering facility. Table 3.5, Table 3.2, Table 3.3 and Table 3.4 summarize the list of sensors used in the seismic tests and their designations, measured quantity and type of units.

Table 3.1 – List of LVDT sensors

Channel	Name	Sensor designation	Location	Unit
1	LVDT_WU_GLW06Y_L	RDP ACT 4001	External wall P1	[mm]
2	LVDT_WU_GLW06Y_R	RDP ACT 6014		
3	LVDT_WS_GLW06Y	RDP DCTH 400AG 145870		
4	LVDT_SD_GLW06Y_L	RDP ACT 6001		
5	LVDT_SD_GLW06Y_R	RDP ACT 6013		
6	LVDT_WU_GLW07X_L	RDP ACT 4003	External wall P2	
7	LVDT_WU_GLW07X_R	RDP DCT 2000A 35025	Interior wall P2	
8	LVDT_WS_GLW07X	RDP DCTH400AG 146740		
9	LVDT_SD_GLW07X_L	RDP ACT 6007	External wall P2	
10	LVDT_SD_GLW07X_R	RDP ACT 6008		
11	LVDT_WU_GLW02Y_L	RDP ACT 2002	External wall P3	
12	LVDT_WU_GLW01Y_R	DCT 2000A 35576		
13	LVDT_WS_GLW02Y	RDP DCTH400AG 146742		
14	LVDT_SD_GLW02Y_L	RDP ACT 6009		
15	LVDT_SD_GLW01Y_R	RDP ACT 6015	External wall P3	
16	LVDT_WU_GLW04X_L	RDP ACT 2004	Internal wall P6	
17	LVDT_WU_GLW04X_R	RDP ACT 6006		
18	LVDT_WS_GLW04X	RDP DCTH 400AG 146741		
19	LVDT_SD_GLW04X_L	RDP ACT 6010		
20	LVDT_SD_GLW04X_R	RDP ACT 6004		
21	LVDT_ID_GL_X	RDP DCTH 1000A 1394		
22	LVDT_ID_GL_Y	RDP DCTH 1000A 1393	Interior wall P5	
23	LVDT_ID_L1_X	RDP DCTH 1000A 35433	External wall P6	

Table 3.2 – List of accelerometers

Channel	Name	Sensor designation	Location	Unit
24	ACC_L1_C3_X_NE_T	PCB AB31	External wall P1	[mg]
25	ACC_L1_C3_Y_NE_L	PCB AB12	External wall P2	
26	ACC_L1_A1_X_SW_T	PCB AB10	External wall P3	
27	ACC_L1_A1_Y_SW_L	PCB AB11	External wall P4	
28	ACC_RL_C3_X_NE_T	PCB AB16	External wall P1	
29	ACC_RL_C3_Y_NE_L	PCB AB07	External wall P2	
30	ACC_RL_A1_X_SW_T	PCB AB32	External wall P3	
31	ACC_RL_A1_Y_SW_L	PCB AB36	External wall P4	
32	ACC_GL_A3_X_SE_T	PCB AB25	External wall P1	
33	ACC_GL_A3_Y_SE_L	PCB AB24	External wall P4	
34	ACC_GL_C1_X_NW_T	PCB AB05	External wall P3	
35	ACC_GL_C1_Y_NW_L	PCB AB01 PCB AE05	External wall P2	
36	ACC_L1_A3_X_SE_T	PCB AB15	External wall P1	
37	ACC_L1_A3_Y_SE_L	PCB AB34	External wall P4	
38	ACC_L1_C1_X_NW_T	PCB AE05	External wall P3	
39	ACC_L1_C1_Y_NW_L	PCB AE07	External wall P2	
40	ACC_L1_C2_X_N_T	PCB AB19		
41	ACC_L1_C2_Y_N_L	PCB AB09		
42	ACC_L1_A2_X_S_T	PCB AB27	External wall P4	
43	ACC_L1_A2_Y_S_L	PCB AB21		
44	ACC_L1_B1_X_W_T	PCB AB28	External wall P3	
45	ACC_L1_B1_Y_W_L	PCB AB17		
46	ACC_L1_B2_X_I_T	PCB AB13	Interior wall P5	
47	ACC_L1_B2_Y_I_L	PCB AB29		
48	ACC_RL_C2_X_N_T	PCB AE03	External wall P2	
49	ACC_RL_C2_Y_N_L	PCB AE02		
50	ACC_RL_A2_X_S_T	PCB AE09	External wall P4	
51	ACC_RL_A2_Y_S_L	PCB AE12		
52	ACC_RL_B1_X_W_T	PCB AE01	External wall P3	
53	ACC_RL_B1_Y_W_L	PCB AE04		
54	ACC_RL_B2_X_I_T	PCB AB14	Interior wall P5	
55	ACC_RL_B2_Y_I_L	PCB AB26		
56	ACC_GLW03Y_I_T	PCB AB06		
57	ACC_GLW04Y_I_T	PCB AB08		
58	ACC_GLW04X_I_L	PCB AB35	Interior wall P6	
59	ACC_GLW05X_I_L	PCB AB30		
60	ACC_L1W03Y_I_T	PCB AB22	Interior wall P5	
61	ACC_L1W04Y_I_T	PCB AB23		
62	ACC_L1W04X_I_L	PCB AB20	Interior wall P6	
63	ACC_L1W05X_I_L	PCB AB33		

Table 3.3 – List of load cells

Channel	Name	Position		Unit
64	CF_HD_GLW06Y_L	FEUP 3	External wall P1	[kN]
65	CF_HD_GLW06X_R	LNEC 4	External wall P2	
66	CF_HD_GLW07X_L	LNEC 3		
67	CF_HD_GLW07X_R	LNEC 2		
68	CF_HD_GLW02Y_L	FEUP 4	External wall P3	
69	CF_HD_GLW01Y_R	FEUP 5		
70	CF_HD_GLW04X_L	LNEC 1	Internal wall P6	
71	CF_HD_GLW04X_R	FEUP 1		

Table 3.4 – List of Hamamatsu sensors

Channel	Name	Position		Unit
72	H_RL_C1_NW_L	HCOND04_X	External wall P3	[mm]
73	H_RL_C1_NW_T	HCOND04_Y		
74	H_L1RL_C1_NW_T	HCOND02_X	External wall P2	
75	H_L1RL_C1_NW_L	HCOND02_Y		
76	H_L1_C1_NW_L	HCOND01_X	External wall P3	
77	H_L1_C1_NW_T	HCOND01_Y		
78	H_GLL1_C1_NW_T	HCOND03_X	External wall P2	
79	H_GLL1_C1_NW_L	HCOND03_Y		
80	H_GL_C1_NW_L	HCOND05_X	External wall P3	
81	H_GL_C1_NW_T	HCOND05_Y		

Figure 3.1 to Figure 3.6 show the instrumentation that served to monitor the walls.

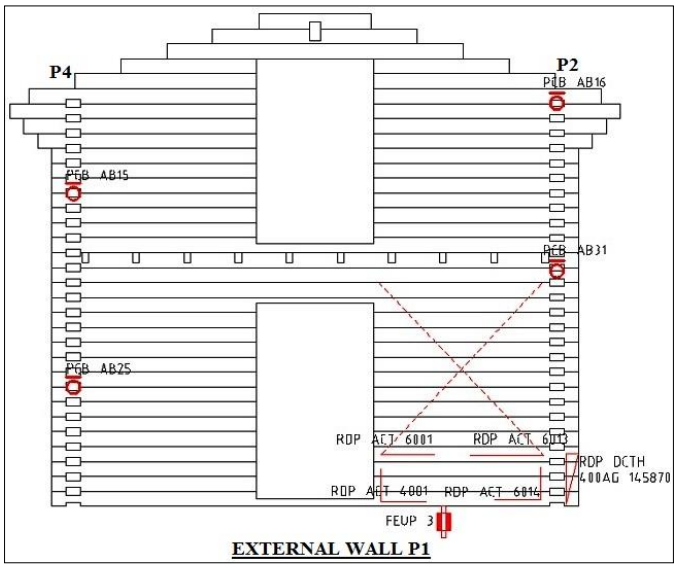

Figure 3.1: Instrumentation to monitor wall P1

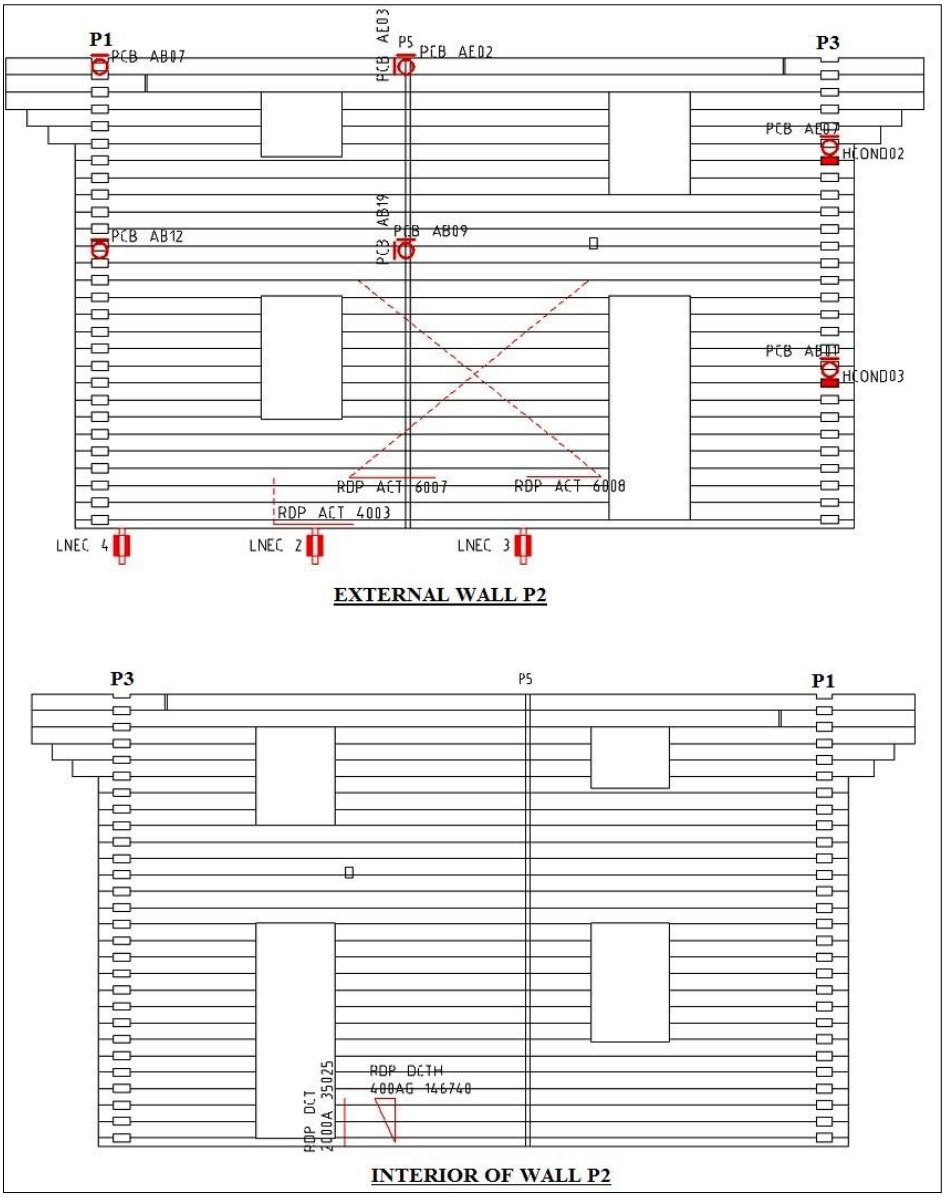

Figure 3.2: Instrumentation to monitor wall P2

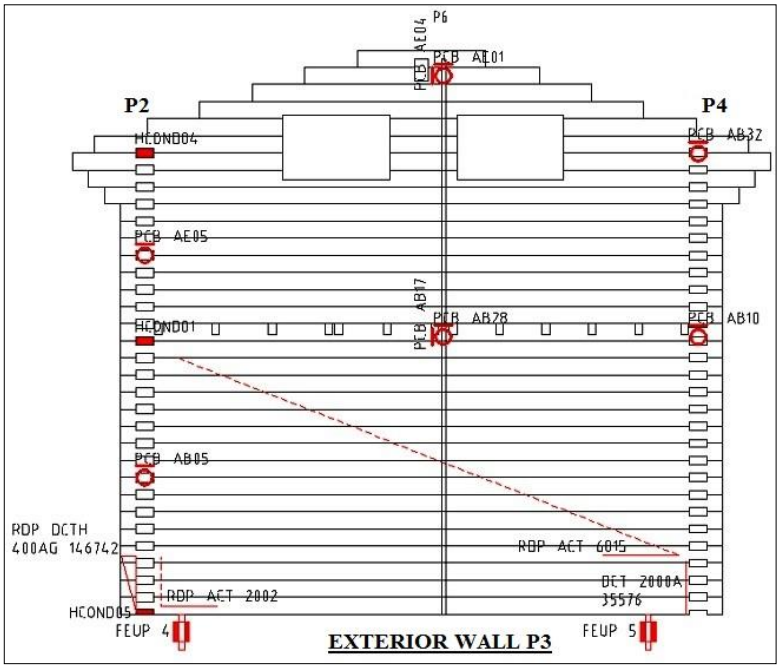

Figure 3.3: Instrumentation to monitor wall P3

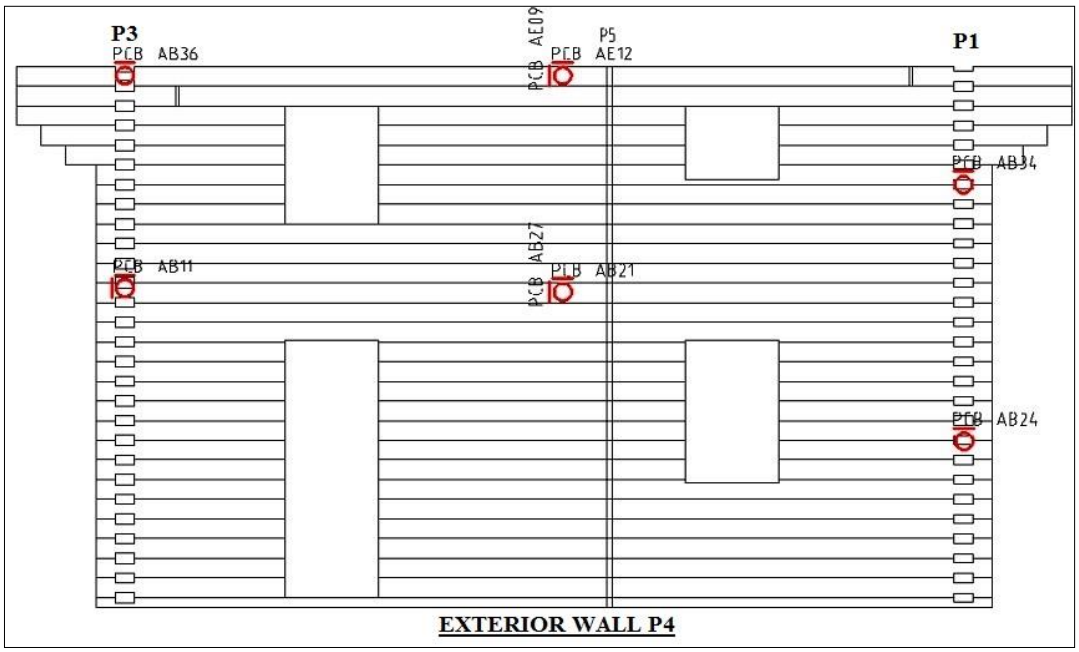

Figure 3.4: Instrumentation to monitor wall P4

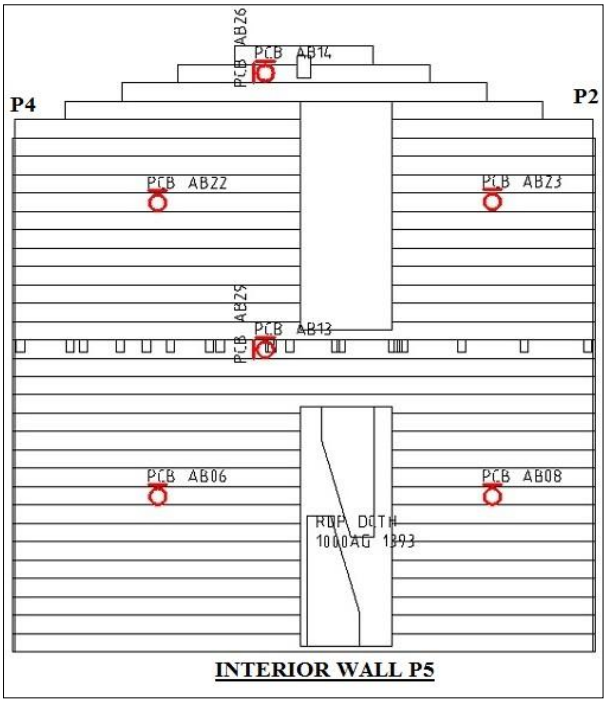

Figure 3.5: Instrumentation to monitor wall P5

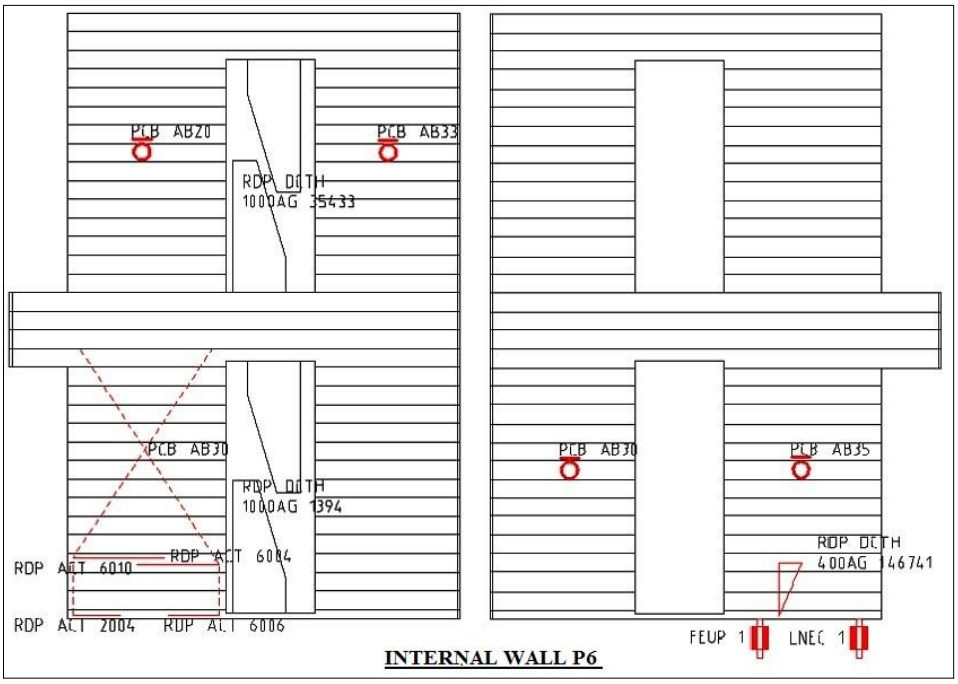

Figure 3.6: Instrumentation to monitor wall P6

The instruments were arranged to study mainly the behaviour of the building in the longitudinal and transverse directions and focused on observing the behaviour of five walls on the ground floor, two in the longitudinal direction and three in the transverse direction. Figure 3.7 shows the monitored walls on the ground floor of the log house.

Table 3.5 – Instrumentation details

Label	Measurements	Type of Sensor	No. of Sensors	No. of Channels
S 0	Wall uplift	LVDTs	8	8
S 1	Wall slippage	LVDTs	4	4
S 2	Shear deformation	LVDTs	7	7
S 3	Hold-down forces	Load Cells	8	8
S 5	Accelerations	Uniaxial Accelerometers	40	40
S 8	Inter-storey displacement	LVDTs	3	3
-	Inter-storey displacement	Optical Acquisition System	10	10
	Total		80	80

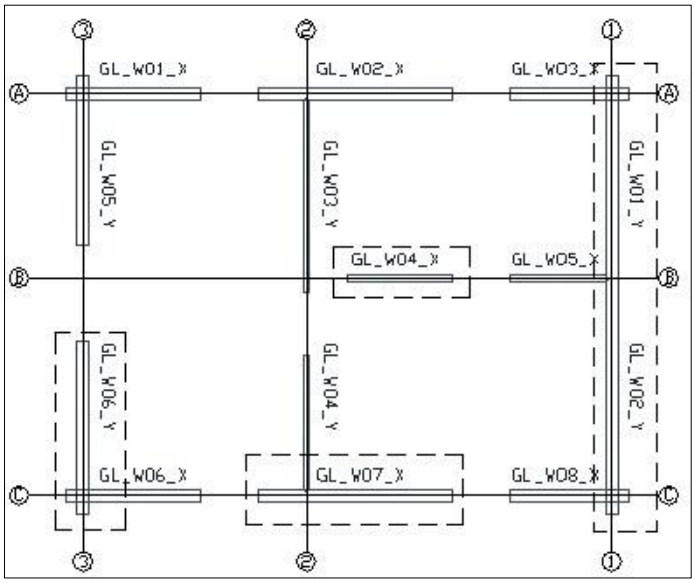

Figure 3.7: Schematic of building showing monitored walls on the ground floor

In order to measure shear deformation, were used 22 LVDT to record wall slippage, uplift, shear deformation and inter-storey displacement. In order to measure the uplift, 8 LVDT were used. The values of shear deformation and horizontal slippage were recorded in walls P1, P2, P3 and P6.

The LVDT were placed in pairs in each of the four walls. Each LVDT was connected to the point of interest using a steel cable and pulley. The steel cables connect the LVDT diagonally with the measurement point. When any movement is detected, the steel cable moves smoothly along the cable and the LVDT records the motion. It is possible to measure the angle of shear deformation by using the following formula:

$$\gamma = \frac{\overline{\Delta L}\sqrt{b^2 + d^2}}{b\ d} \tag{1}$$

When a house is subjected to seismic loads, it can induce vertical and horizontal movements in the house. Lateral forces try to lift the house and cause sliding. These LVDT were placed in contact with a triangular wooden element extending from the sill log to the third log and the wall uplift LVDT were mounted on pulleys and steel cables in a manner as seen in Figure 3.8 and Figure 3.9.

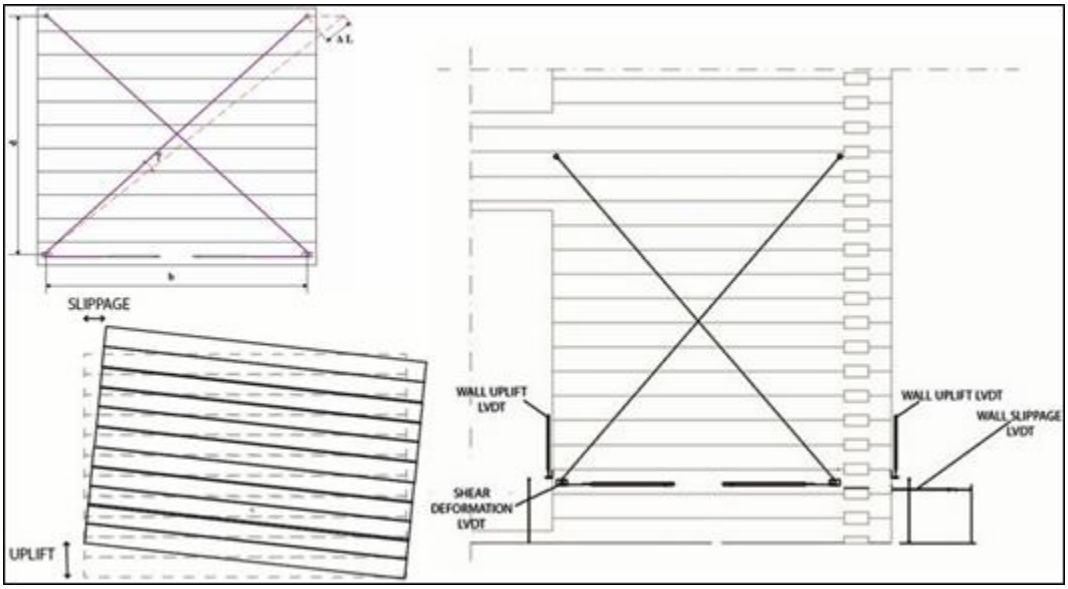

Figure 3.8: Possible wall movements measured by the LVDT

Figure 3.9: LVDT to measure (a) shear deformation (b) wall uplift (c) horizontal sliding

The LVDT used to measure the inter-storey displacement (Figure 3.10) were mounted on specially designed wooden elements so as to ensure that the measured value of relative displacement would correspond to the actual difference in movement undergone by the walls in the two storeys.

Figure 3.10: The LVDT used to measure inter-storey displacement

In order to measure the inter-storey displacements, an optical acquisition system was used in addition to the LVDTs. The system consisted of an infrared camera system HD: K600 Krypton, the camera control unit, acquisition PC/laptop, strober and linear position sensors. This system provides accurate information about the absolute displacement time history at the measuring points.

The optical acquisition system and linear position sensors was used to continuously detect and measure absolute displacement of the control points. Sensors were placed at the ground level, floor level and roof level as well as at mid-height of the corner of wall P1 on both floors.

The system makes use of a high resolution CCD camera (ten million pixels) that is mounted firmly over a steel scaffolding in order to prevent any movement and obtain still images. The camera is positioned such that it is along the axis of the desired infrared LED and at an approximate distance of 1.50 m from it. The infrared LED is attached to a steel plate placed under a rectangular wooden element that ensures certain stiffness and prevents any vertical movement of the LED. In Figure 3.11 the parts of the Hamamatsu system mounted on the log house can be seen.

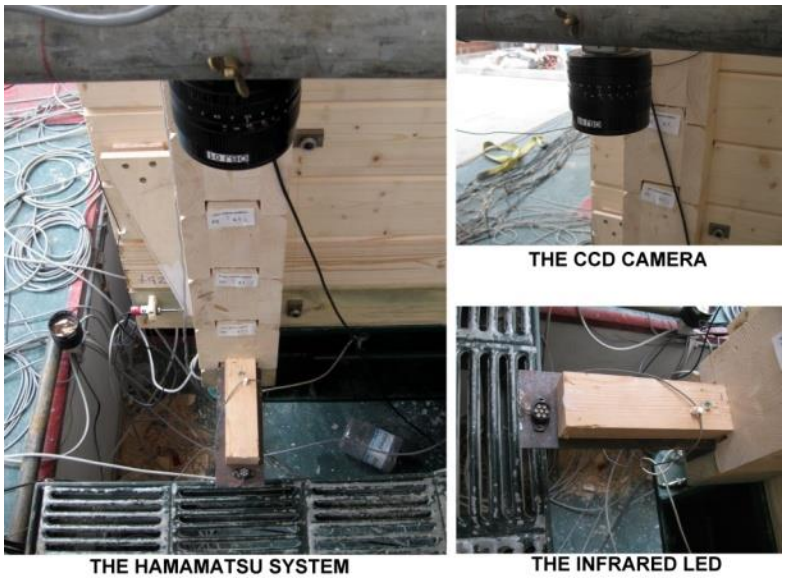

Figure 3.11: The components of the linear position sensor system

In Figure 3.12, the set-up of the optical acquistion system used to monitor the log house is shown.

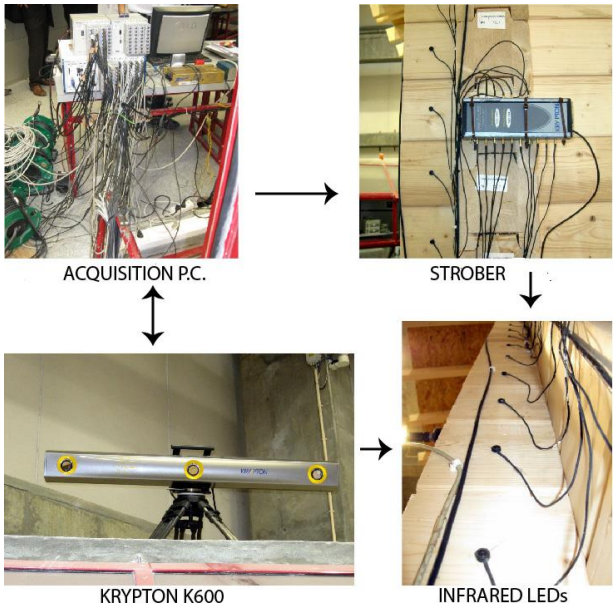

Figure 3.12: Data acquisition process of the Krypton K600 camera system

The forces acting on different structural components were measured by strategically placed load cells as seen in Figure 3.13. An individual load cell is constituted of a hollow steel cylinder where the diameter of the hole is slightly larger than that of the bolt that connects the bottom log to the steel lattice. When the log undergoes mechanical deformation, the strain gauges record the data which gives a measure of the compressive and tensile forces. A washer is placed between the cell and the nut of the bolt and another washer is placed between the cell and the steel lattice. These washers ensure that the cell is preloaded at 1kN [12]. The data

obtained from the load cells is processed and the maximum tensile forces are identified. This gives a measure of the distribution of forces in the base of the building and an indication of possible uplift. Based on this, the role of hold-downs in the building can be estimated.

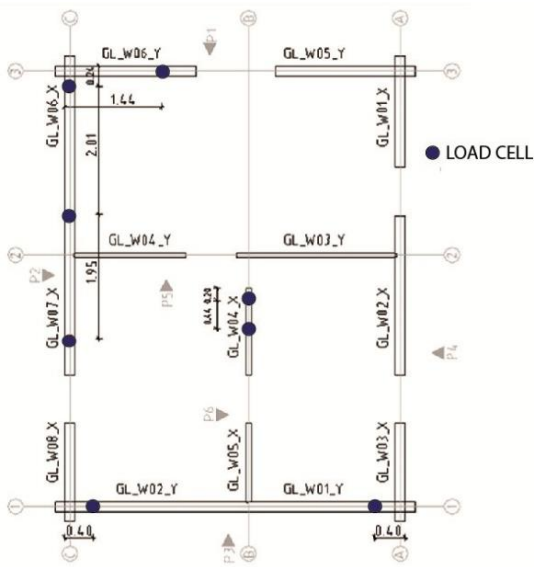

Figure 3.13: Load cell positions in the ground floor

Forty unidirectional accelerometers were used to monitor the out-of-plane behaviour of the wall. The indicator scrolls in the form of a vertical line along the height of the wall served as an indicator for slippage between the logs. The data obtained during all the stages of testing right from the tuning of the shaking table to the dynamic identification of the building and the seismic tests were sampled at a sampling frequency of 125Hz.

The accelerations at different locations in the house were recorded during the dynamic identification as well as the seismic tests using 40 unidirectional piezoelectric accelerometers. Two accelerometers were used to record the accelerations of the shaking table in the longitudinal and transverse directions. Accelerometers were placed both on the exterior and the interior walls at different locations: the roof level and floor level, at the cross wall intersections, at mid height of some of the walls. In addition to the measurement of wall accelerations, the accelerometers also give an idea of the out-of-plane displacement of the walls. No accelerometers were placed near the openings of the house as in timber structures the presence of openings doesn’t have any significant effect on the global behaviour of the structure. In Figure 3.14 the position and orientation on the accelerometers are marked on the floor plans.

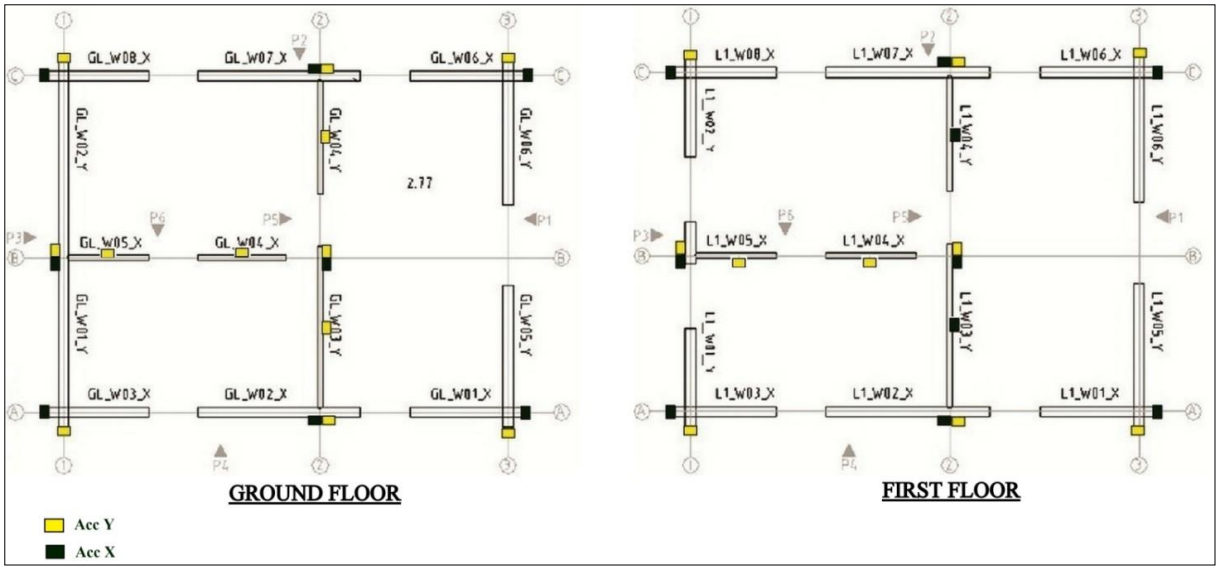

Figure 3.14: Position of accelerometers in floor plans

In Figure 3.15, the accelerometers used to monitor the house can be seen.

Figure 3.15: Accelerometers placed on interior wall (left) and close-up of an accelerometer (right)

4 Seismic testing plan

4.1 PRE-DESIGN OF THE TEST

Prior to the seismic test, it was necessary to make an analytical prediction of the expected behaviour of the building during the tests. The design of the test is the key step in the experimental campaign because the seismic input and the parameters required for phase tuning the shaking table are determined based on the model. The accelerogram used in the test should contain frequencies in the vicinity of the frequencies of interest and the control system of the shaking table must be able to reproduce the motion of the chosen reference in the range of the frequencies of interest, for the mass and stiffness of the given building.

A numerical model of the building (Figure 4.1) was developed in SAP2000 [16] to obtain information on the dynamic properties and performance capability of the structure assuming the material properties obtained from previous numerical and experimental studies performed by UMinho [6]. As seen in Figure 4.2, the first and fourth mode shapes correspond to a translational movement in the x-direction (longitudinal axis), the second and fifth mode shapes correspond to a translational movement in the y-direction while the third mode is a torsional one and is represented by a rotation around the z-axis. With regard to the damping of the structure, the value indicated by the numeric model is much higher than the value typically assumed by codes and recommendations for timber structures (ξ=5%).

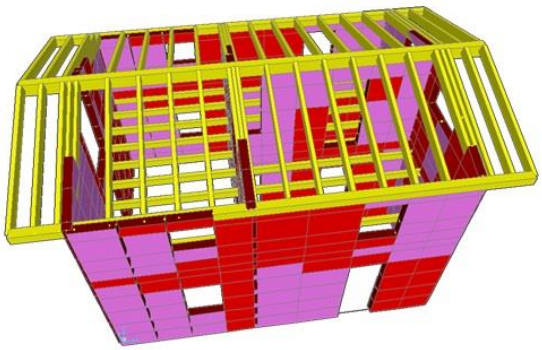

Figure 4.1: 3D FEM model of the log house developed in SAP200 during the test pre-design

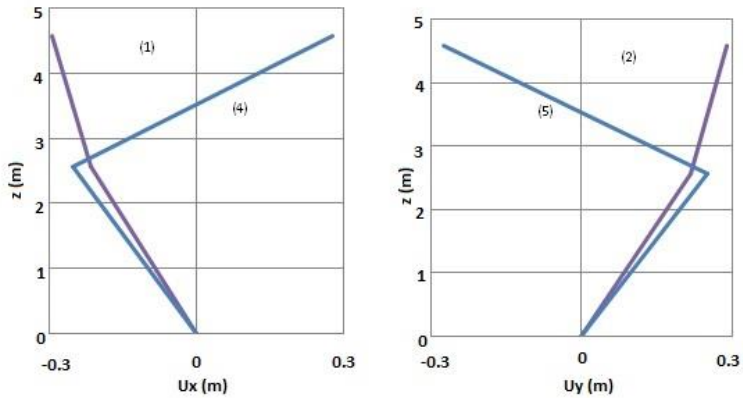

Figure 4.2: Predicted mode shapes

4.2 TESTING PROCEDURE

Once the building was constructed and the instruments were set-up, the following tasks were performed: calibration of the instruments, dynamic characterization tests and shaking table tests. The typical process is defined as follows:

- Tuning the system (at every stage);
- Dynamic characterization (before and after every seismic test);
- Preliminary test representative of low intensity earthquake (0.07g);
- Test representative of moderate intensity earthquake (0.28g);
- Test representative of high intensity earthquake (0.5g).

The dynamic characterization tests were of low intensity while the seismic tests were carried out with increasing levels of Peak Ground Acceleration (PGA). The input in the case of the characterization tests was white noise. The acceleration time history was characterized by a Gaussian distribution of RMS level of 0.05g and the frequency ranged between 0.1Hz and 30 Hz. The purpose of these tests was to calibrate the parameters necessary to control the shaking table and to conduct the dynamic identification of the structure [8]. The seismic testing procedure followed was carried out with three different PGA values - 0.07g, 0.28g and 0.5g. During this incremental test procedure, whenever damage occurred, an identification test was performed to assess any variation in the fundamental period of the house.

The testing of the log house was carried out on the 6th of April, 2012 and the following preliminary steps are shown below:

- Calibration of HAMAMATSU optical transducers – sine waves imposed in both transversal and longitudinal axes, 100mm amplitude, to determine the conversion factors from V to mm;
- Dynamic identification of ST and model (1’40’’ duration) – acquisition was shorter than the drive signal;
- Dynamic identification of ST and model (3’00’’ duration) – determination of the Frequency response Functions (FRFs);
- Calibration of HAMAMATSU optical transducers – sine wave imposed in the transversal axis, 100mm amplitude, to determine the conversion factors from V to mm;
- Calibration of HAMAMATSU optical transducers – sine wave imposed in the longitudinal axis, 100mm amplitude, to determine the conversion factors from V to mm;
- Confirmation of HAMAMATSU optical transducers calibration - sine wave imposed in the transversal axis, 100mm amplitude, to confirm the conversion factors from V to mm;
- Confirmation of HAMAMATSU optical transducers calibration - sine wave imposed in the longitudinal axis, 100mm amplitude, to confirm the conversion factors from V to mm.

Table 4.1 shows the conversion factors for Hamamatsu system used in the seismic testing. The entire testing plan for the log house specimen is presented in Table 4.2.

Table 4.1 – Conversion factors for Hamamatsu system

HAMAMATSU	X channel		Y channel	
	Direction	mm/V	Direction	mm/V
RL	L direction	-35.336	T direction	-35.336
L1-RL	T direction	-37.037	L direction	+37.037
L1	L direction	-28.944	T direction	-28.944
GL-L1	T direction	-32.895	L direction	+32.895
GL	L direction	+20.182	T direction	-20.182

The seismic tests on this building were carried out in 2012-06-04 and only the 1979 Montenegro earthquake was used [8]. The test procedure is presented in Table 4.2, showing all the stages carried out. The signals were imposed with increasing amplitudes until the corresponding targets were achieved.

Table 4.2 – Rusticasa building test procedure (target: 1979 Montenegro earthquake)

Test	Drive	Target [g]	Video
	Dynamic Identification (CAT 1)		
	Dynamic Identification (CAT 2)		
01	5	0.07	Test_01
02	6	0.07	Test_02
03	7	0.07	Test_03
04	8	0.07	Test_04
	Dynamic Identification (CAT 3)		
05	11	0.28	Test_05
06	12	0.28	Test_06
07	13	0.28	Test_07
	Dynamic Identification (CAT 4)		
	Dynamic Identification (CAT 5)		
08	13 (repeat)	0.28	Test_08
09	14	0.28	Test_09
10	15	0.28	Test_10
	Dynamic Identification (CAT 6)		
11	16	0.5	Test_11
12	17	0.5	Test_12
	Dynamic Identification (CAT 7)		

A grand total of 12 seismic tests, plus 7 intermediate dynamic identification tests, were carried out with the Rusticasa building.

5 Analysis of results

The most relevant results are presented in the following sections. Annex I present the time histories acquired during the seismic tests TEST_04, TEST_09 and TEST_11. Annex II presents the digital signal processing results. To compute the simultaneous maximum values were specifically developed MathCAD [19] sheets and the LNEC-SPA software [20] developed at the LNEC Earthquake Engineering and Structural Dynamics Division (NESDE) was used to process the FRF estimates.

5.1 SHAKING TABLE FIDELITY (COMPARISON OF REFERENCE AND ACHIEVED INPUT MOTIONS)

The following figures show the response spectra for the seismic tests TEST_04, TEST_09 and TEST_11 for the two horizontal directions that represent the final tests in each stage. In each direction is given: i) the input reference signal; and ii) the achieved motion which is the signal recorded on the shaking table.

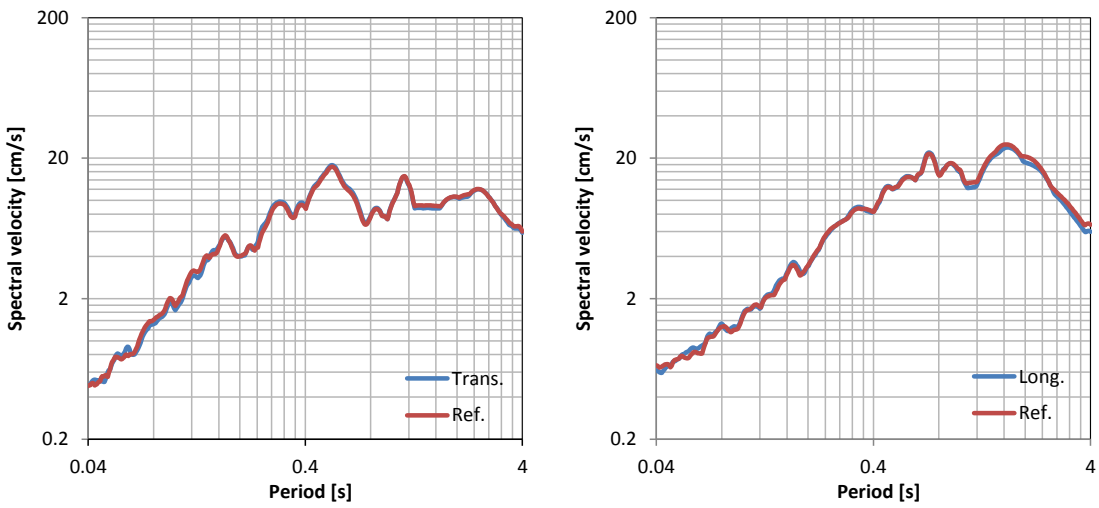

Figure 5.1: Response spectra for the reference and achieved signals, TEST_04

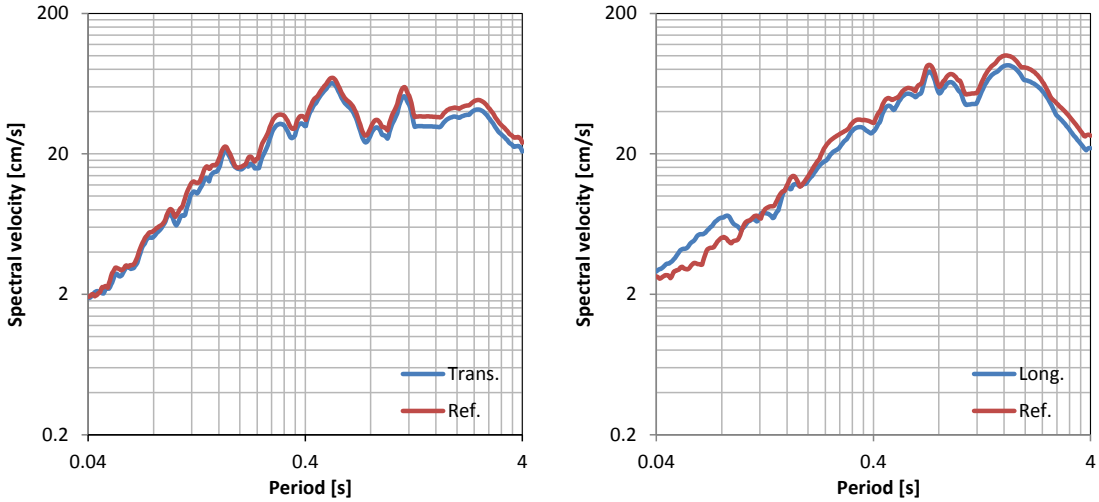

Figure 5.2: Response spectra for the reference and achieved signals, TEST_09

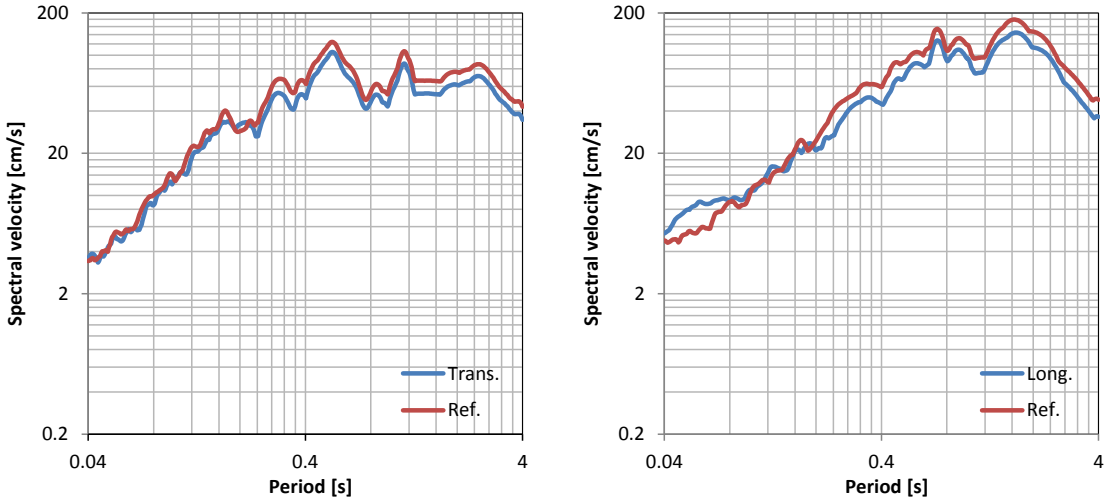

Figure 5.3: Response spectra for the reference and achieved signals, TEST_11

5.2 BUILDING MOTIONS MAXIMUM AND SPECTRAL CONTENT GENERAL RESULTS

5.2.1 Processing of Results

The maximum acceleration values, the maximum simultaneous values on all uplifts, slippages, inter-storey displacement and hold down forces were measured by processing the data from the accelerometers, the LVDTs, the optical acquisition system and the load cells using MathCad [19] sheets developed for this purpose. The data from tests TEST_03 and TEST_12 were not used as there were some errors in some of the instruments.

The tables with simultaneous values are read in the following way: each line contains the simultaneous values corresponding to the maximum of the channel in the main diagonal (background in grey). The maximum value in each channel is read directly from the table main diagonal. Only the data from tests TEST_04, TEST_09 and TEST_11 are presented in this section.

5.2.2 Acceleration

Table 5.1 shows the maximum acceleration values for the seismic tests TEST_04, TEST_09 and TEST_12. The peak value is not available (N/A) when the sensors exceed their measurement range. A small sample of the accelerations recorded in seismic tests is presented from Figure 5.4 to Figure 5.6.

Table 5.1 – Maximum acceleration for the seismic tests TEST_04, TEST_09 and TEST_12

Designation	TEST_04	TEST_09	TEST_11
	Max [mg]	Max [mg]	Max [mg]
ACC_L1_C3_X_NE_T	93.63	240.88	330.33
ACC_L1_C3_Y_NE_L	90.02	233.34	449.79
ACC_L1_A1_X_SW_T	88.08	305.84	N/A
ACC_L1_A1_Y_SW_L	86.98	224.73	422.97
ACC_RL_C3_X_NE_T	112.45	238.94	332.38
ACC_RL_C3_Y_NE_L	127.20	300.38	393.16
ACC_RL_A1_X_SW_T	136.73	238.94	371.31
ACC_RL_A1_Y_SW_L	114.08	235.22	385.19
ACC_GL_A3_X_SE_T	78.58	270.62	409.59
ACC_GL_A3_Y_SE_L	78.85	293.33	588.31
ACC_GL_C1_X_NW_T	68.54	276.98	435.50
ACC_GL_C1_Y_NW_L	N/A	403.20	561.66
ACC_L1_A3_X_SE_T	106.61	217.48	302.93
ACC_L1_A3_Y_SE_L	95.44	274.72	400.33
ACC_L1_C1_X_NW_T	105.52	259.64	341.95
ACC_L1_C1_Y_NW_L	N/A	283.11	414.20
ACC_L1_C2_X_N_T	92.25	229.68	339.30
ACC_L1_C2_Y_N_L	89.77	221.76	410.73
ACC_L1_A2_X_S_T	88.07	212.28	366.51
ACC_L1_A2_Y_S_L	88.15	217.59	416.62
ACC_L1_B1_X_W_T	78.86	190.39	312.08
ACC_L1_B1_Y_W_L	84.45	231.30	416.55
ACC_L1_B2_X_I_T	80.58	193.48	320.23
ACC_L1_B2_Y_I_L	89.60	221.56	403.88
ACC_RL_C2_X_N_T	110.59	246.49	321.58
ACC_RL_C2_Y_N_L	135.90	282.80	409.54
ACC_RL_A2_X_S_T	135.62	236.45	366.68
ACC_RL_A2_Y_S_L	140.22	281.41	453.38
ACC_RL_B1_X_W_T	135.10	225.54	300.05
ACC_RL_B1_Y_W_L	127.05	224.96	381.07
ACC_RL_B2_X_I_T	137.44	224.40	310.92
ACC_RL_B2_Y_I_L	142.40	262.83	392.34
ACC_GLW03Y_I_T	156.42	373.62	N/A
ACC_GLW04Y_I_T	85.65	342.18	528.19
ACC_GLW04X_I_L	125.68	398.03	634.63
ACC_GLW05X_I_L	99.89	542.86	828.50
ACC_L1W03Y_I_T	157.21	295.37	430.37
ACC_L1W04Y_I_T	115.26	305.48	433.21
ACC_L1W04X_I_L	306.13	610.80	693.55
ACC_L1W05X_I_L	122.81	330.32	515.84
ACC MESA TRANS	62.27	228.30	432.59
ACC MESA LONG	71.98	327.22	633.46

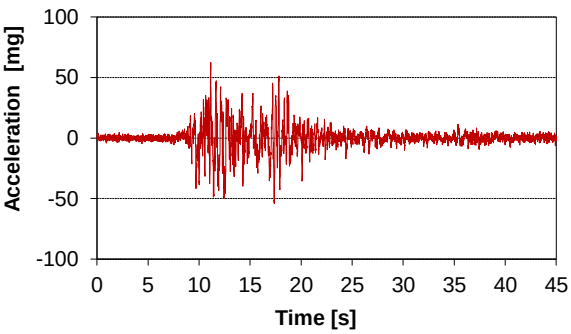

a) Shake table transverse acceleration

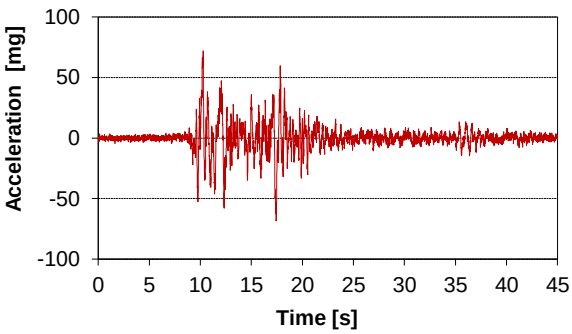

b) Shake table longitudinal acceleration

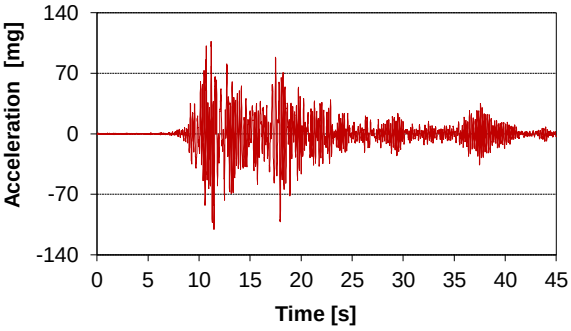

c) Roof level transverse acceleration (channel ACC_RL_C2_X_N_T)

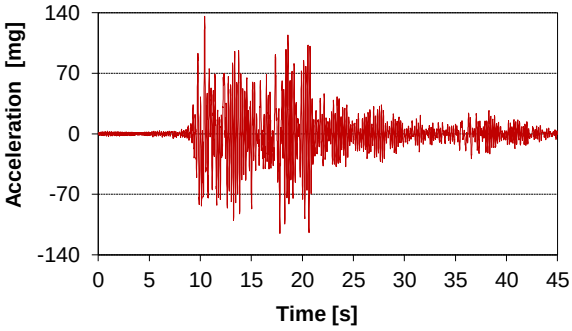

d) Roof level longitudinal acceleration (channel ACC_RL_C2_Y_N_L)

Figure 5.4: Sample of the records obtained in seismic test TEST_04 of the Rusticasa building

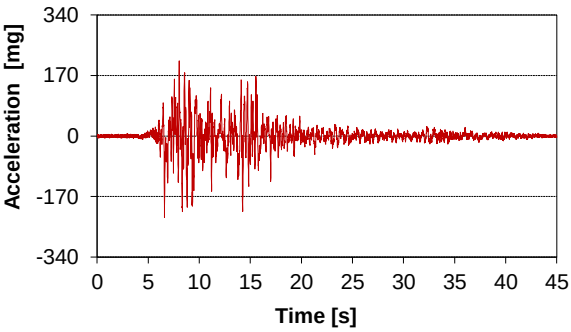

a) Shake table transverse acceleration

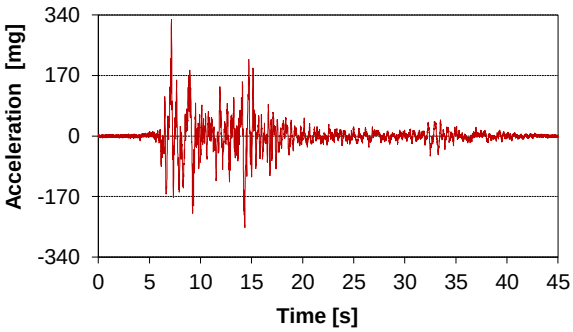

b) Shake table longitudinal acceleration

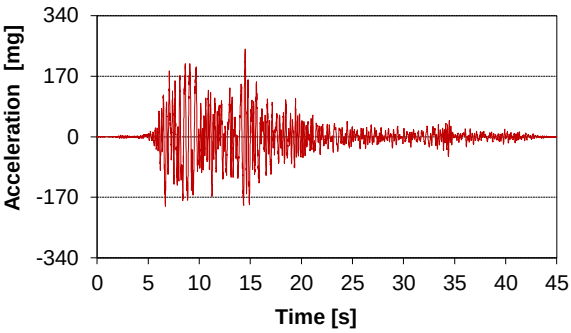

c) Roof level transverse acceleration (channel ACC_RL_C2_X_N_T)

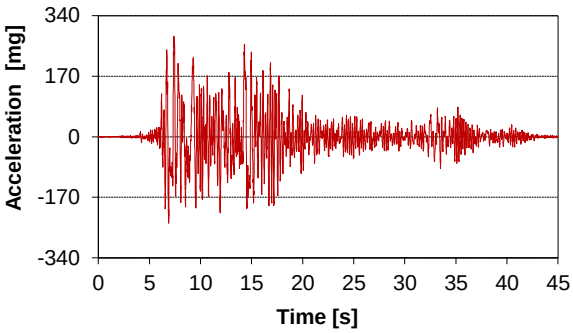

d) Roof level longitudinal acceleration (channel ACC_RL_C2_Y_N_L)

Figure 5.5: Sample of the accelerations records obtained in seismic test TEST_09 of the Rusticasa building

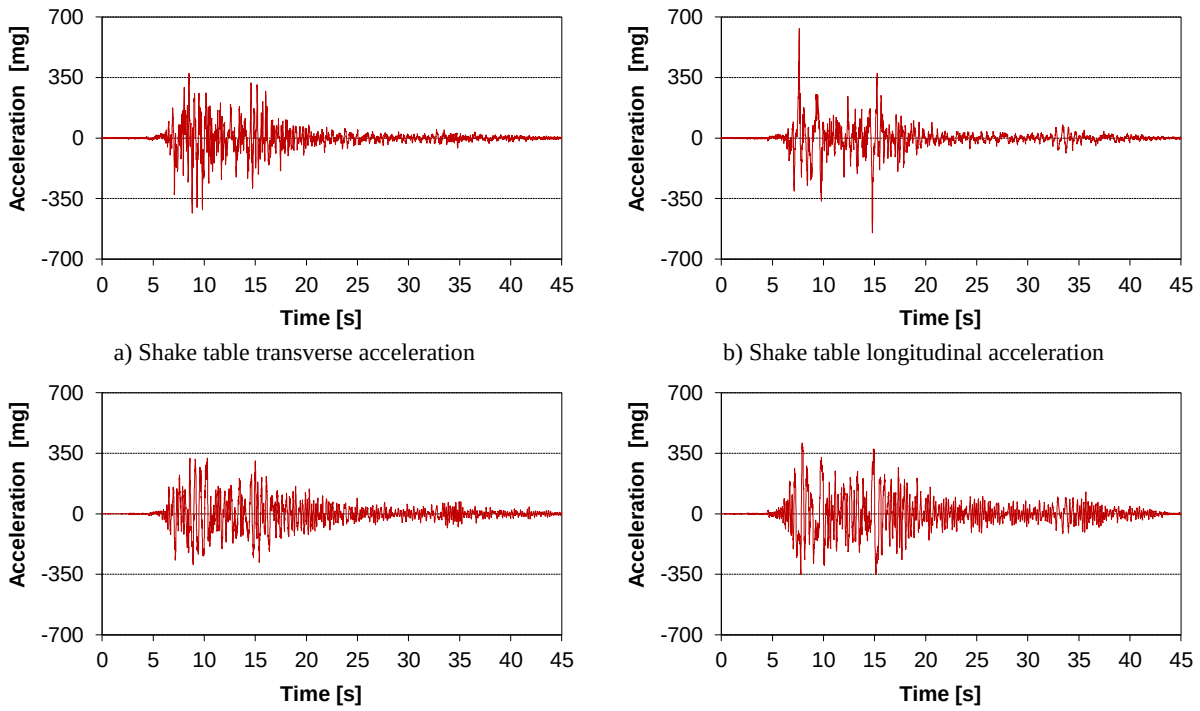

a) Shake table transverse acceleration

b) Shake table longitudinal acceleration

c) Roof level transverse acceleration (channel ACC_RL_C2_X_N_T)

d) Roof level longitudinal acceleration (channel ACC_RL_C2_Y_N_L)

Figure 5.6: Sample of the accelerations records obtained in seismic test TEST_11 of the Rusticasa building

5.2.3 Wall uplift

The values of the maximum wall uplift were calculated and presented in Table 5.2**.** There was almost no uplift measured in the walls for the tests of 0.07g. The highest value of wall uplift measured in the tests of 0.28g PGA was just 4mm and it was recorded at the wall 07X_R on the ground floor. During the tests of 0.5g, the highest recorded uplift was in wall 04X_L and was approximately 8.9mm. The wall 07X_R recorded an uplift of about 8.4 mm.

Table 5.2 – Maximum wall uplift values recorded by LVDT

Wall	01Y_R	02Y_L	04X_L	04X_R	06Y_L	06Y_R	07X_L	07X_R
TEST_01	0.32	0.18	0.10	0.18	0.09	0.18	0.10	0.96
TEST_02	0.29	0.21	0.07	0.12	0.08	0.14	0.09	0.90
TEST_04	0.26	0.16	0.09	0.12	0.09	0.19	0.10	0.85
TEST_05	1.49	0.19	1.63	0.56	0.17	0.47	0.34	2.36
TEST_06	2.05	0.18	2.78	0.72	0.20	0.63	0.48	3.24
TEST_07	2.66	0.25	3.41	0.95	0.21	0.78	0.62	4.17
TEST_08	0.97	0.20	1.20	0.60	0.21	0.38	0.29	1.81
TEST_09	1.78	0.21	2.66	0.79	0.20	0.55	0.45	3.11
TEST_10	3.22	0.86	3.15	1.16	0.21	1.11	0.85	4.08
TEST_11	6.97	1.21	8.88	1.98	0.46	2.11	1.88	8.42

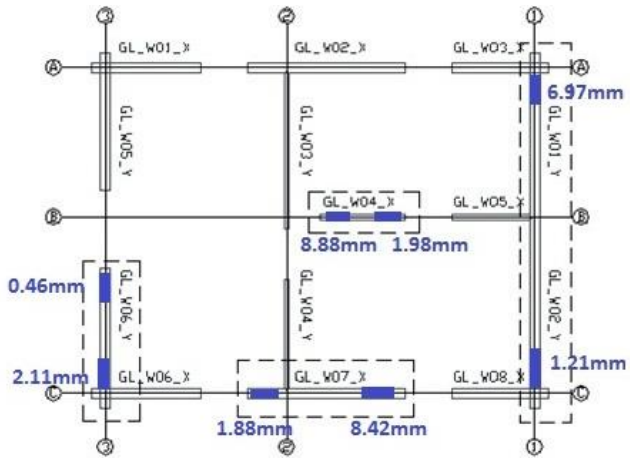

Figure 5.7: Values of maximum uplift recorded during the 0.5g test

Figure 5.8 to Figure 5.10 show a small sample (four channels) of the ground level wall uplift displacements recorded in seismic tests TEST_04, TEST_09 and TEST_11.

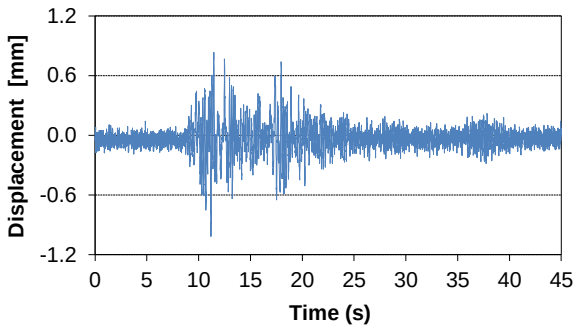

a) Ground level wall uplift displacement (channel LVDT_WU_GLW07X_R)

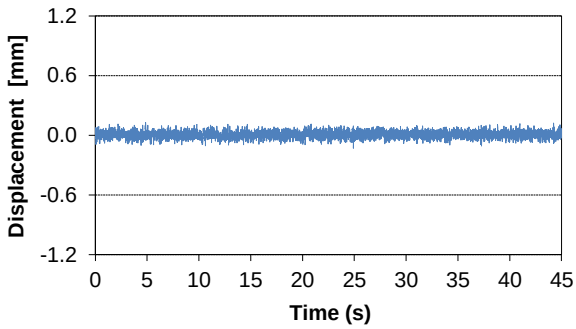

b) Ground level wall uplift displacement (channel LVDT_WU_GLW07X_L)

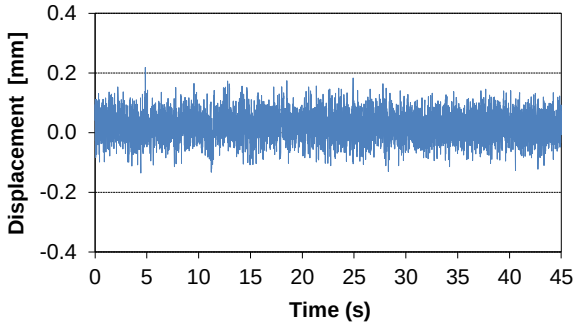

c) Ground level wall uplift displacement (channel LVDT_WU_GLW04X_R)

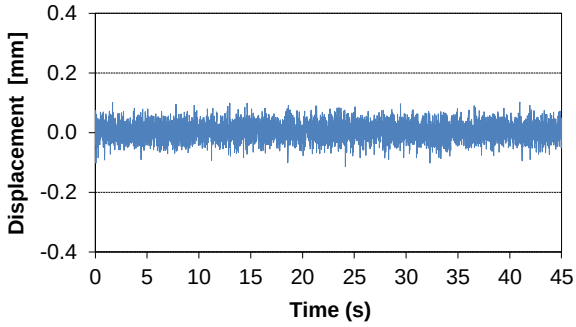

d) Ground level wall uplift displacement (channel LVDT_WU_GLW04X_L)

Figure 5.8: Sample of the wall uplift records obtained in seismic test TEST_04 of the Rusticasa building

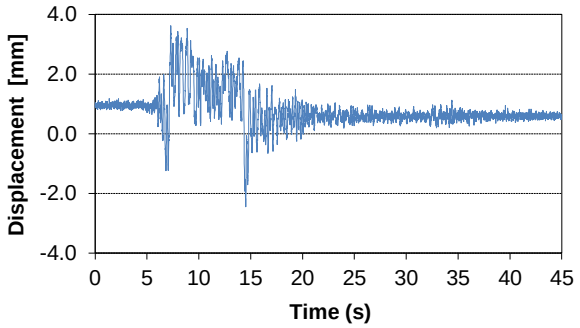

a) Ground level wall uplift displacement (channel LVDT_WU_GLW07X_R)

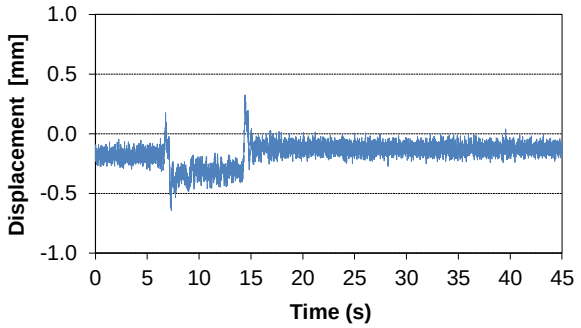

b) Ground level wall uplift displacement (channel LVDT_WU_GLW07X_L)

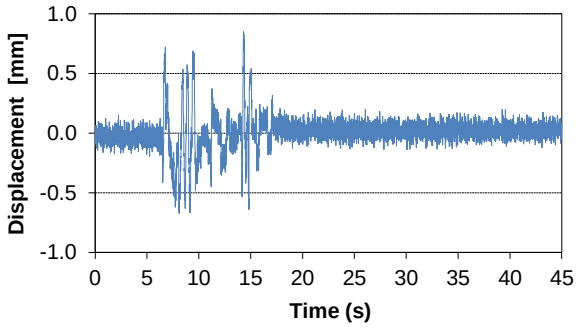

c) Ground level wall uplift displacement (channel LVDT_WU_GLW04X_R)

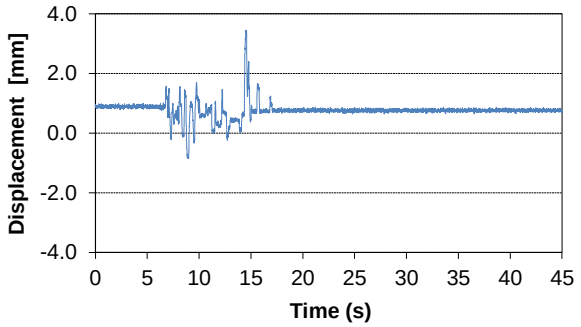

d) Ground level wall uplift displacement (channel LVDT_WU_GLW04X_L)

Figure 5.9: Sample of the wall uplift records obtained in seismic test TEST_09 of the Ruscticasa building

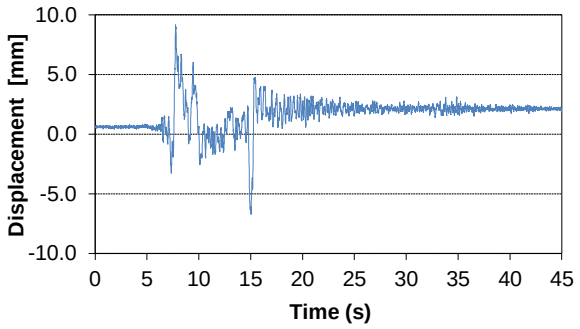

a) Ground level wall uplift displacement (channel LVDT_WU_GLW07X_R)

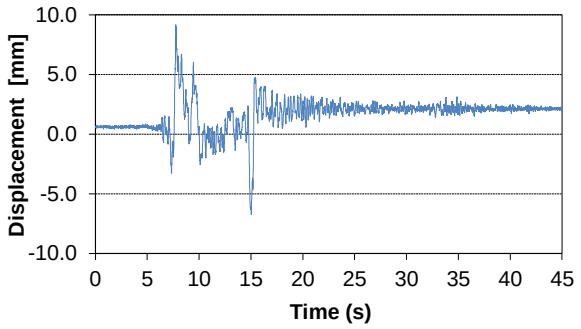

b) Ground level wall uplift displacement (channel LVDT_WU_GLW07X_L)

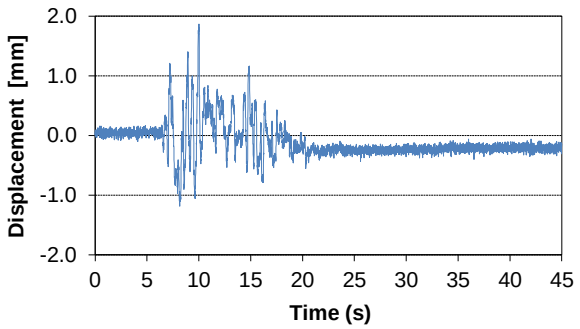

c) Ground level wall uplift displacement (channel LVDT_WU_GLW04X_R)

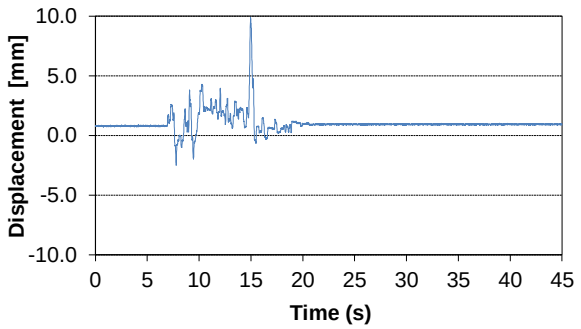

d) Ground level wall uplift displacement (channel LVDT_WU_GLW04X_L)

Figure 5.10: Sample of the wall uplift records obtained in seismic test TEST_11 of the Rusticasa building

The values of the maximum simultaneous on all wall uplifts were and presented in Table 5.3 to Table 5.5 for the seismic tests TEST_04, TEST_09 and TEST_11 that represents the tests 0.07g, 0.28g and 0.5g. In Annex III were presented all the results.

The highest value of wall uplifts measured was 12.64mm and it was recorded at the wall 07X_R on the ground floor in the seismic test TEST_11. It is on this wall that the higher values were recorded for the entire testing plan.

Table 5.3 – Maximum simultaneous values on all wall uplifts for seismic test TEST_04

TEST_04	WU_GLW01Y_R	WU_GLW02Y_L	WU_GLW04X_L	WU_GLW04X_R	WU_GLW06Y_L	WU_GLW06Y_R	WU_GLW07X_L	WU_GLW07X_R
WU_GLW01Y_R	0.31	0.03	0.03	0.09	0.04	0.07	0.03	1.02
WU_GLW02Y_L	0.02	0.27	0.05	0.08	0.08	0.18	0.10	0.13
WU_GLW04X_L	0.06	0.01	0.11	0.07	0.09	0.16	0.07	0.02
WU_GLW04X_R	0.12	0.04	0.06	0.22	0.12	0.23	0.13	0.14
WU_GLW06Y_L	0.12	0.08	0.10	0.13	0.12	0.23	0.12	0.06
WU_GLW06Y_R	0.12	0.04	0.06	0.22	0.12	0.23	0.13	0.14
WU_GLW07X_L	0.04	0.12	0.06	0.10	0.11	0.20	0.13	0.06
WU_GLW07X_R	0.31	0.03	0.03	0.09	0.04	0.07	0.03	1.02

Table 5.4 – Maximum simultaneous values on all wall uplifts for seismic test TEST_09

TEST_09	WU_GLW01Y_R	WU_GLW02Y_L	WU_GLW04X_L	WU_GLW04X_R	WU_GLW06Y_L	WU_GLW06Y_R	WU_GLW07X_L	WU_GLW07X_R
WU_GLW01Y_R	2.65	0.14	1.55	0.55	0.12	0.10	0.33	1.36
WU_GLW02Y_L	1.44	0.32	0.71	0.06	0.04	0.50	0.20	0.38
WU_GLW04X_L	2.27	0.12	3.45	0.26	0.10	0.22	0.19	2.22
WU_GLW04X_R	0.03	0.01	0.66	0.85	0.01	0.49	0.18	2.03
WU_GLW06Y_L	2.08	0.00	0.71	0.45	0.28	0.04	0.28	1.31
WU_GLW06Y_R	0.07	0.09	0.82	0.39	0.01	0.88	0.48	2.26
WU_GLW07X_L	0.51	0.05	0.22	0.31	0.01	0.86	0.64	3.19
WU_GLW07X_R	0.23	0.05	0.10	0.07	0.18	0.51	0.46	3.62

Table 5.5 – Maximum simultaneous values on all wall uplifts for seismic test TEST_11

TEST_11	WU_GLW01Y_R	WU_GLW02Y_L	WU_GLW04X_L	WU_GLW04X_R	WU_GLW06Y_L	WU_GLW06Y_R	WU_GLW07X_L	WU_GLW07X_R
WU_GLW01Y_R	5.11	0.99	1.82	1.81	0.13	1.24	0.05	0.11
WU_GLW02Y_L	4.92	1.21	1.88	1.87	0.18	1.15	0.14	0.57
WU_GLW04X_L	1.06	0.46	9.90	0.31	0.03	1.63	1.53	6.16
WU_GLW04X_R	4.92	1.21	1.88	1.87	0.18	1.15	0.14	0.57
WU_GLW06Y_L	1.78	0.01	1.89	0.71	0.49	0.88	1.22	9.12
WU_GLW06Y_R	3.55	0.18	1.97	0.77	0.03	1.82	0.87	5.74
WU_GLW07X_L	1.25	0.47	9.86	0.29	0.03	1.65	1.54	6.16
WU_GLW07X_R	1.93	0.01	2.15	0.76	0.44	0.99	1.26	9.15

5.2.4 Wall sliding

The values of wall sliding were negligible for the tests of 0.07g. The highest value of wall sliding during the tests of 0.28g (2.09mm) and 0.50g (5.6mm) was recorded by the LVDT that was placed at the base of the western wall (GLW02_Y), closer to the north-west corner, where sliding between the logs in the upper portion, near the window, was seen. The values of maximum wall sliding are presented in Table 5.6.

Table 5.6 - Maximum wall sliding values recorded by LVDTs (mm)

Wall	GLW02Y	GLW04X	GLW06Y	GLW 07X
TEST_01	0.04	0.02	0.01	0.04
TEST_02	0.02	0.01	0.01	0.03
TEST_04	0.02	0.01	0.02	0.03
TEST_05	1.21	1.49	0.22	0.54
TEST_06	2.16	1.06	0.52	0.70
TEST_07	2.09	0.48	0.68	0.89
TEST_08	1.08	0.11	0.15	0.52
TEST_09	1.76	0.24	0.40	0.76
TEST_10	1.86	0.27	0.63	0.85
TEST_11	5.59	1.22	2.73	3.11

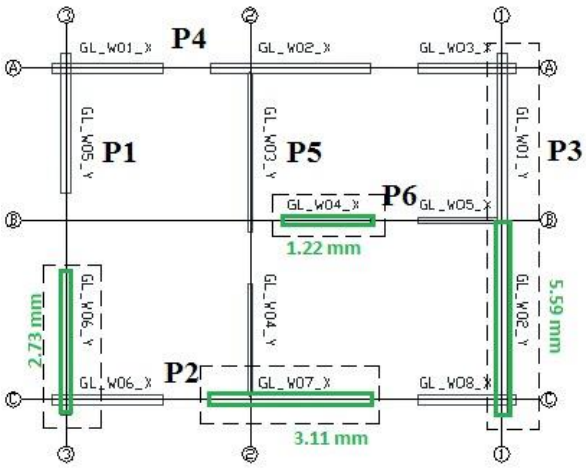

Figure 5.11: Maximum sliding values obtained during the 0.50g test

Figure 5.12 to Figure 5.14 show a small sample (four channels) of the ground and first levels wall sliding displacements recorded in seismic tests TEST_04, TEST_09 and TEST_11.

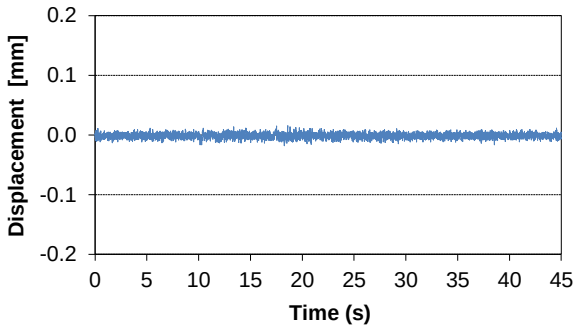

a) Ground level wall sliding displacement (channel LVDT_WS_GLW06Y)

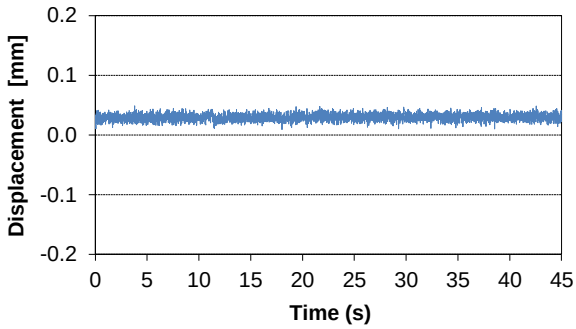

b) Ground level wall sliding displacement (channel LVDT_WS_GLW02Y)

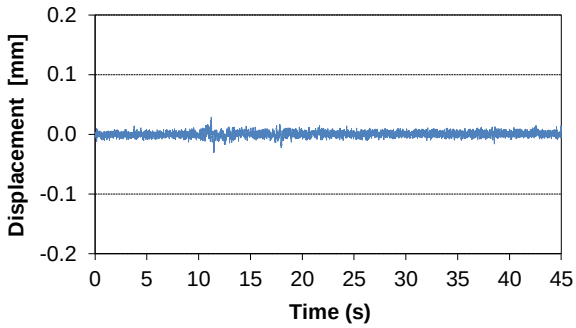

c) First level wall sliding displacement (channel LVDT_WS_GLW07X)

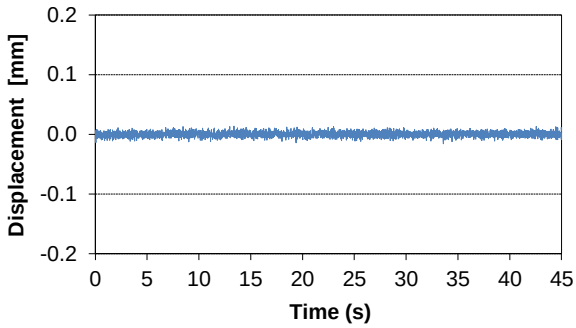

d) First level wall sliding displacement (channel LVDT_WS_GLW04X)

Figure 5.12: Sample of the wall sliding records obtained in seismic test TEST_04 of the Rusticasa building

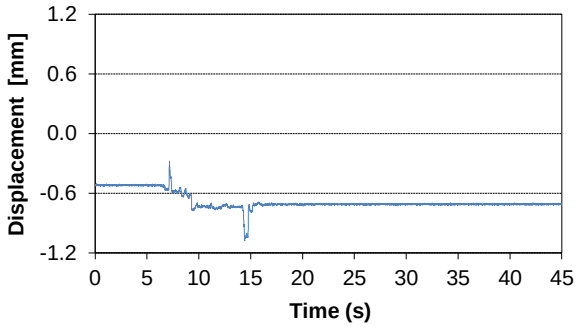

a) Ground level wall sliding displacement (channel LVDT_WS_GLW06Y)

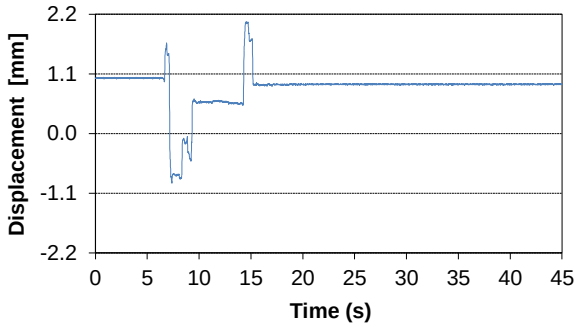

b) Ground level wall sliding displacement (channel LVDT_WS_GLW02Y)

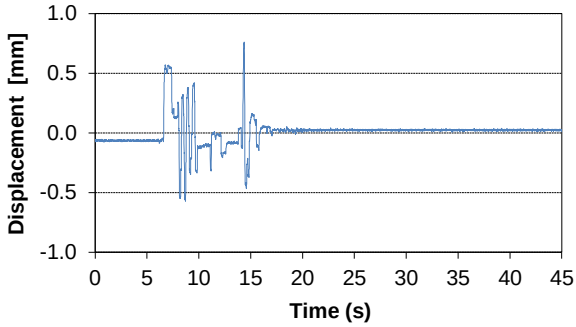

c) First level wall sliding displacement (channel LVDT_WS_GLW07X)

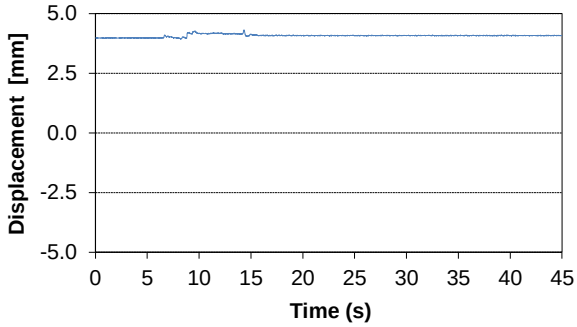

d) First level wall sliding displacement (channel LVDT_WS_GLW04X)

Figure 5.13: Sample of the wall sliding records obtained in seismic test TEST_09 of the Rusticasa building

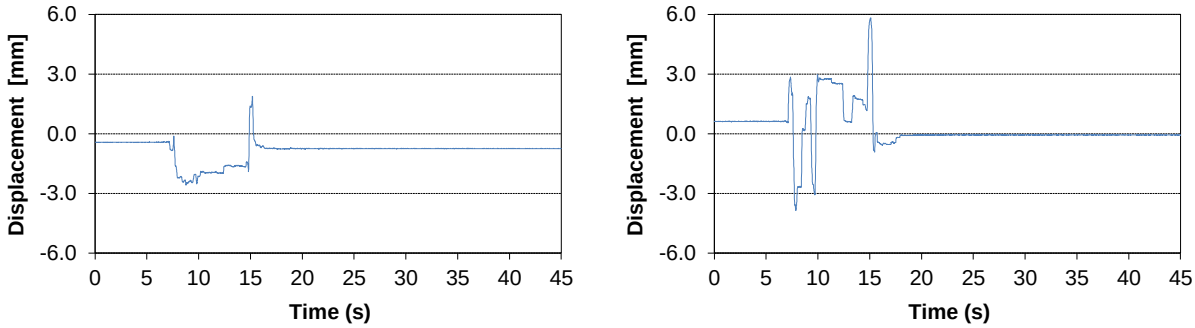

a Ground level wall sliding displacement (channel LVDT_WS_GLW06Y)

b) Ground level wall sliding displacement (channel LVDT_WS_GLW02Y)

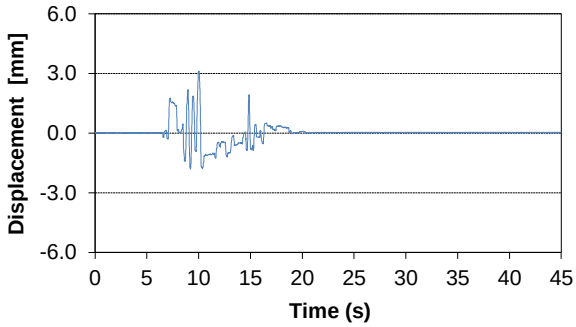

c)) First level wall sliding displacement (channel LVDT_WS_GLW07X)

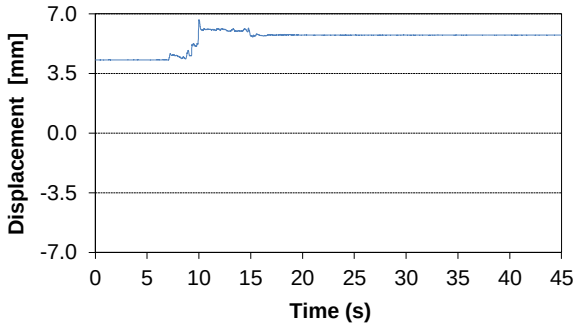

d) First level wall sliding displacement (channel LVDT_WS_GLW04X)

Figure 5.14: Sample of the wall sliding records obtained in seismic test TEST_11 of the Rusticasa building

The values of the maximum simultaneous on all wall sliding were and presented in Table 5.7 to Table 5.9 for the seismic tests TEST_04, TEST_09 and TEST_11 that represents the tests 0.07g, 0.28g and 0.5g. In Annex III were presented all the results.

The highest value of wall sliding measured was 7.21mm and it was recorded at the base of the western wall (W02Y), on the ground floor in the seismic test TEST_11. It is on this wall that the higher values were recorded for the entire testing plan.

Table 5.7 – Maximum simultaneous values on all walls sliding for seismic test TEST_04

TEST_04	WS_GLW02Y	WS_GLW04X	WS_GLW06Y	WS_GLW07X
WS_GLW02Y	0.05	0.01	0.01	0.00
WS_GLW04X	0.02	0.02	0.01	0.00
WS_GLW06Y	0.02	0.00	0.02	0.00
WS_GLW07X	0.02	0.00	0.00	0.03

Table 5.8 – Maximum simultaneous values on all walls sliding for seismic test TEST_09

TEST_09	WS_GLW02Y	WS_GLW04X	WS_GLW06Y	WS_GLW07X
WS_GLW02Y	2.06	4.07	1.03	0.42
WS_GLW04X	1.66	4.31	0.92	0.76
WS_GLW06Y	1.92	4.14	1.08	0.03
WS_GLW07X	1.70	4.29	0.91	0.76

Table 5.9 – Maximum simultaneous values on all wall sliding for seismic test TEST_11

TEST_11	WS_GLW02Y	WS_GLW04X	WS_GLW06Y	WS_GLW07X
WS_GLW02Y	5.83	5.72	1.39	0.84
WS_GLW04X	2.87	6.64	2.15	3.08
WS_GLW06Y	0.19	4.38	2.58	0.90
WS_GLW07X	2.63	6.62	2.16	3.12

5.2.5 Shear deformation

In the first stage of the test (0.07g), the shear deformation was negligible. During the tests with 0.28g PGA, the maximum shear deformation measured was 70mm in the wall GLW01_Y. The shear deformation was largest in the tests of 0.50g PGA with the highest value being 140mm measured in the same wall as the previous stage. The readings taken by LVDT_SD_GLW02Y_L and LVDT_SD_GLW04X_L were not included in Table 5.10 as they were faulty.

Table 5.10 - Maximum shear deformation of monitored walls (mm)

Wall	GLW01Y_R	GLW04X_R	GLW06Y_L	GLW06Y_R	GLW07X_L	GLW07X_R
TEST_01	0.22	0.15	0.21	0.21	0.18	0.65
TEST_02	0.14	0.13	0.17	0.18	0.12	0.43
TEST_04	0.13	0.13	0.19	0.25	0.16	0.45
TEST_05	37.45	0.93	3.46	4.03	1.59	4.21
TEST_06	66.22	1.42	5.16	5.93	2.22	6.25
TEST_07	79.02	2.24	5.82	6.44	3.20	5.37
TEST_08	25.04	0.70	2.26	2.84	1.51	3.95
TEST_09	76.91	2.44	7.35	6.61	2.43	5.77
TEST_10	70.45	1.89	6.42	6.47	2.63	6.91
TEST_11	139.50	6.37	15.28	17.31	7.87	19.75

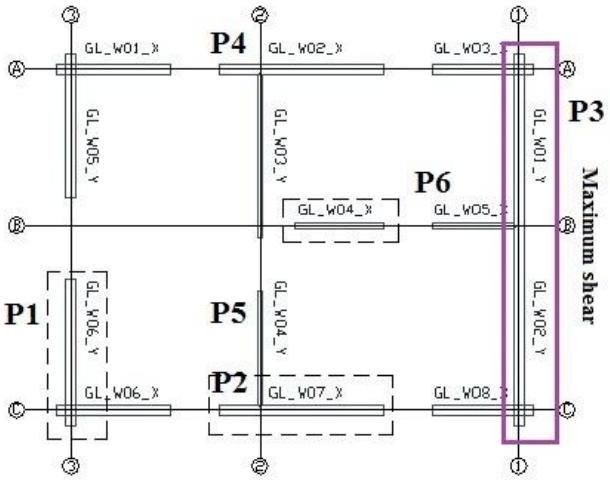

Figure 5.15: Plan of the house showing position of maximum shear deformation

Figure 5.16 to Figure 5.18 show a small sample (four channels) of the ground and first levels shear deformation recorded in seismic tests TEST_04, TEST_09 and TEST_11.

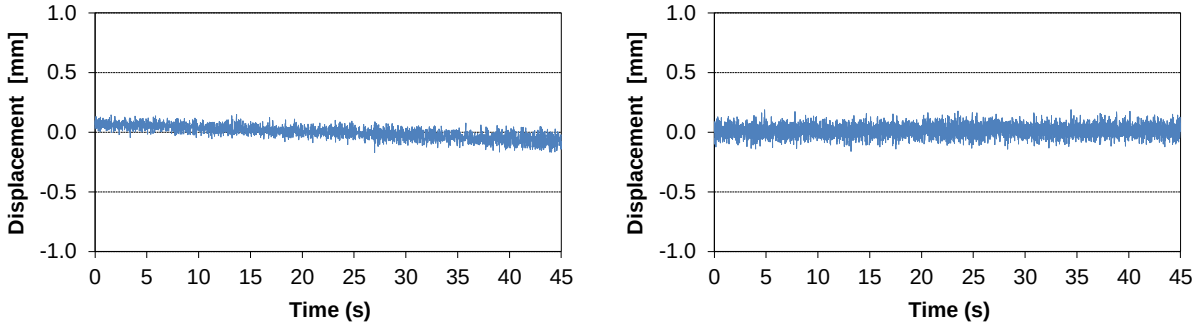

a) Ground level shear deformation (channel LVDT_SD_GLW04X_L)

b) Ground level shear deformation (channel LVDT_SD_GLW04X_R)

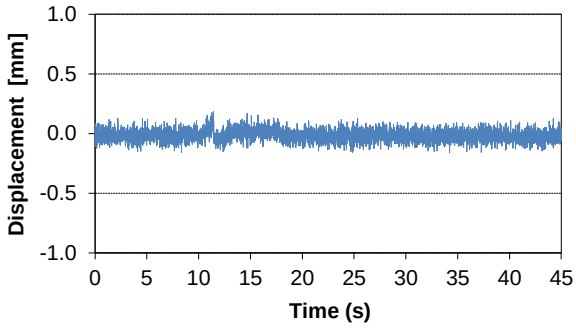

c) Ground level shear deformation (channel LVDT_SD_GLW07X_L)

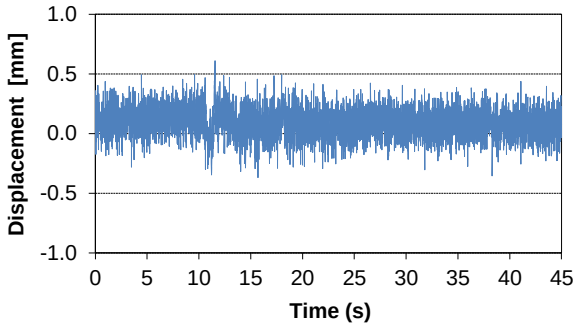

d) Ground level shear deformation (channel LVDT_SD_GLW07X_R)

Figure 5.16: Sample of the shear deformation records obtained in seismic test TEST_04 of the Rusticasa building

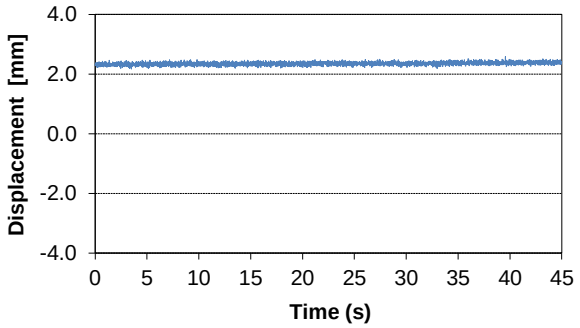

a) Ground level shear deformation (channel LVDT_SD_GLW04X_L)

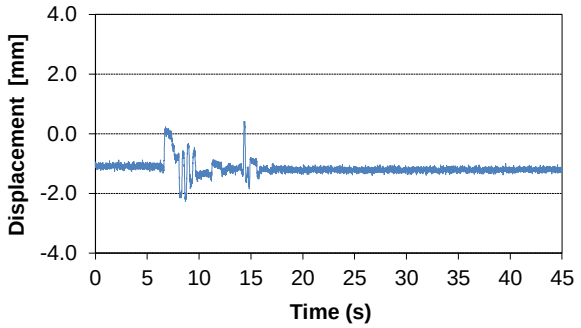

b) Ground level shear deformation (channel LVDT_SD_GLW04X_R)

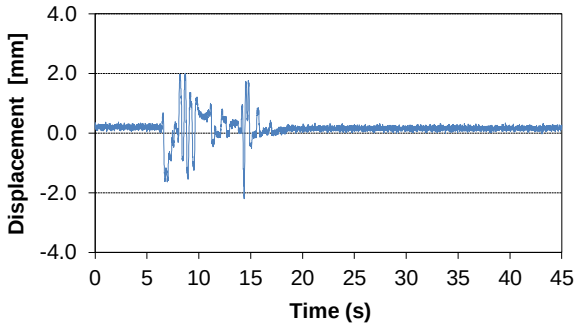

c) Ground level shear deformation (channel LVDT_SD_GLW07X_L)

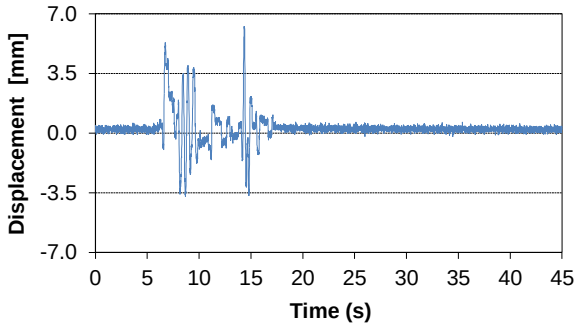

d) Ground level shear deformation (channel LVDT_SD_GLW07X_R)

Figure 5.17: Sample of the shear deformation records obtained in seismic test TEST_09 of the Rusticasa building

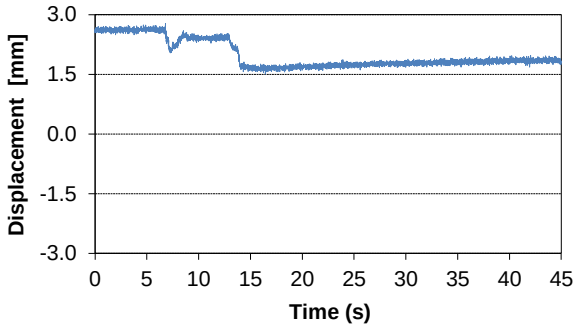

a) Ground level shear deformation (channel LVDT_SD_GLW04X_L)

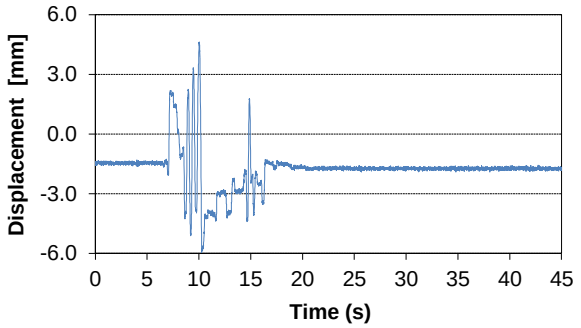

b) Ground level shear deformation (channel LVDT_SD_GLW04X_R)

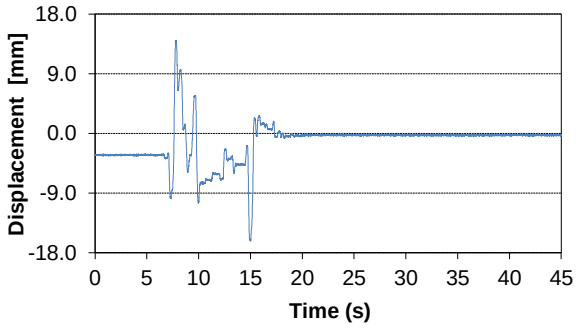

c) Ground level shear deformation (channel LVDT_SD_GLW07X_L)

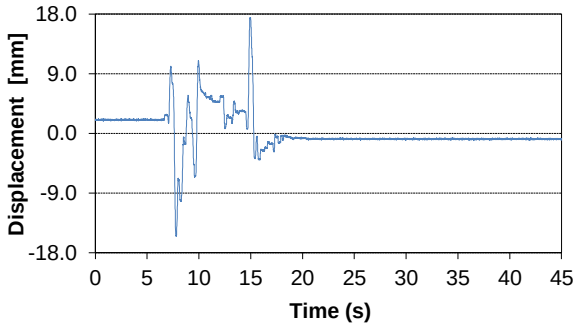

d) Ground level shear deformation (channel LVDT_SD_GLW07X_R)

Figure 5.18: Sample of the shear deformation records obtained in seismic test TEST_11 of the Rusticasa building

The values of the maximum simultaneous on all shear deformation were and presented in Table 5.11 to Table 5.13 for the seismic tests TEST_04, TEST_09 and TEST_11 that represents the tests 0.07g, 0.28g and 0.5g. In Annex III were presented all the results.

The highest value of the shear deformation measured was 143.09mm and it was recorded at the base of the western wall (W01Y_R), on the ground floor in the seismic test TEST_11. It is on this wall that the higher values were recorded for the entire testing plan.

Table 5.11 – Maximum simultaneous values on all shear deformation for seismic test TEST_04

TEST_04	SD_GLW01Y_R	SD_GLW02Y_L	SD_GLW04X_L	SD_GLW04X_R	SD_GLW06Y_L	SD_GLW06Y_R	SD_GLW07X_L	SD_GLW07X_R
SD_GLW01Y_R	0.24	0.41	0.45	0.15	0.21	0.21	0.11	0.33
SD_GLW02Y_L	0.08	0.42	0.48	0.13	0.18	0.18	0.16	0.00
SD_GLW04X_L	0.07	0.34	0.72	0.14	0.14	0.13	0.05	0.40
SD_GLW04X_R	0.18	0.16	0.67	0.19	0.24	0.19	0.10	0.20
SD_GLW06Y_L	0.09	0.25	0.46	0.10	0.25	0.24	0.15	0.16
SD_GLW06Y_R	0.13	0.26	0.47	0.03	0.16	0.27	0.11	0.06
SD_GLW07X_L	0.12	0.18	0.58	0.08	0.08	0.10	0.18	0.17
SD_GLW07X_R	0.05	0.18	0.54	0.00	0.01	0.00	0.07	0.61

Table 5.12 – Maximum simultaneous values on all shear deformation for seismic test TEST_09

TEST_09	SD_GLW01Y_R	SD_GLW02Y_L	SD_GLW04X_L	SD_GLW04X_R	SD_GLW06Y_L	SD_GLW06Y_R	SD_GLW07X_L	SD_GLW07X_R
SD_GLW01Y_R	72.82	3.91	2.38	0.65	6.96	6.52	0.68	0.49
SD_GLW02Y_L	72.79	3.92	2.31	1.47	7.03	6.28	1.53	2.78
SD_GLW04X_L	19.74	1.59	2.58	1.00	2.58	2.01	0.33	0.35
SD_GLW04X_R	8.99	0.89	2.23	2.26	0.29	0.83	1.77	3.73
SD_GLW06Y_L	69.63	3.82	2.29	0.36	7.08	6.40	0.05	1.07
SD_GLW06Y_R	67.51	3.67	2.40	0.23	6.56	6.65	0.55	3.14
SD_GLW07X_L	41.22	2.70	2.31	0.29	5.49	4.77	2.20	6.09
SD_GLW07X_R	37.09	2.51	2.37	0.40	4.77	4.63	2.09	6.26

Table 5.13 – Maximum simultaneous values on all shear deformation for seismic test TEST_11

TEST_11	SD_GLW01Y_R	SD_GLW02Y_L	SD_GLW04X_L	SD_GLW04X_R	SD_GLW06Y_L	SD_GLW06Y_R	SD_GLW07X_L	SD_GLW07X_R
SD_GLW01Y_R	142.71	4.48	2.24	1.42	11.86	12.17	2.33	5.54
SD_GLW02Y_L	133.22	7.94	1.60	1.02	15.94	17.36	1.19	5.14
SD_GLW04X_L	18.49	1.82	2.78	1.40	3.68	2.82	0.05	1.24
SD_GLW04X_R	70.32	3.92	2.41	5.96	7.49	6.37	5.93	11.51
SD_GLW06Y_L	133.22	7.89	1.63	2.32	16.23	16.13	3.37	5.82
SD_GLW06Y_R	133.22	7.75	1.72	1.59	15.88	17.45	2.61	8.73
SD_GLW07X_L	91.79	4.61	2.38	4.44	9.54	8.72	7.43	18.26
SD_GLW07X_R	94.12	4.67	2.44	4.61	10.30	10.11	7.40	19.60

5.2.6 Inter-storey drift

The relative displacement between the floors was measured by LVDTs whereas the optical acquisition system measured the absolute displacement. After processing the data obtained from the tests and comparing the displacements obtained from both the measurement systems, it was found that the values differed vastly. Since it is known that the optical acquisition system gives accurate measurements and the LVDTs are extremely sensitive, only the

displacements measured by the LEDs of the optical acquisition system have been used to compute the maximum inter-storey drift and are expressed in Table 5.14.

Table 5.14 - Inter-storey displacements obtained from Hamamatsu system (mm)

Wall	GL-L1 (long)	L1-RL (long)	GL-L1 (trans)	L1-RL (trans)
TEST_01	2.36	0.95	1.80	2.28
TEST_02	2.16	1.08	1.78	1.33
TEST_04	2.41	1.03	1.50	1.16
TEST_05	9.61	4.71	7.02	2.82
TEST_06	14.79	5.97	9.06	3.14
TEST_07	17.32	6.53	10.98	3.84
TEST_08	8.25	3.46	6.32	2.49
TEST_09	13.76	5.40	8.95	3.21
TEST_10	17.59	5.88	9.70	3.64
TEST_11	177.41	17.26	36.26	7.03

Table 5.15 - Maximum inter-storey drift obtained from Hamamatsu system (%)

Wall	GL-L1	L1-RL
TEST_01	0.001	0.001
TEST_02	0.001	0.001
TEST_04	0.001	0.001
TEST_05	0.004	0.003
TEST_06	0.006	0.003
TEST_07	0.007	0.004
TEST_08	0.003	0.002
TEST_09	0.005	0.003
TEST_10	0.007	0.003
TEST_11	0.067	0.01

Figure 5.19 to Figure 5.21 show a small sample (four channels) of the ground and first levels inter-storey drift displacements recorded in seismic tests TEST_04, TEST_09 and TEST_11.

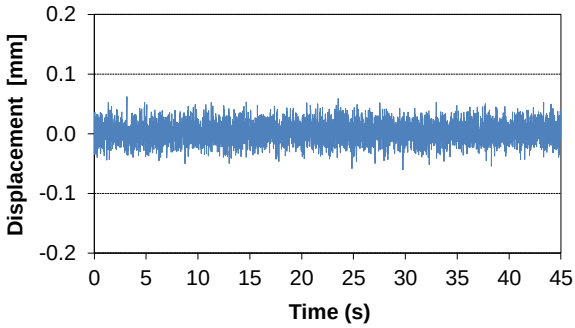

a) Ground level interstorey displacement (channel LVDT_ID_GL_X)

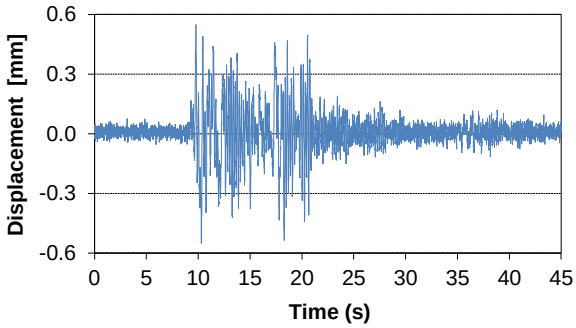

b) Ground level interstorey displacement (channel LVDT_ID_GL_Y)

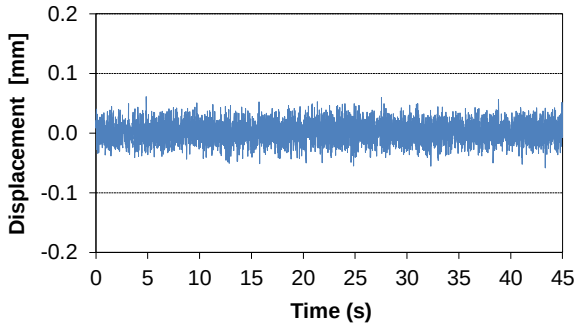

c) First level interstorey displacement (channel LVDT_ID_L1_X)

Figure 5.19: Sample of the inter-storey drift records obtained in seismic test TEST_04 of the Rusticasa building

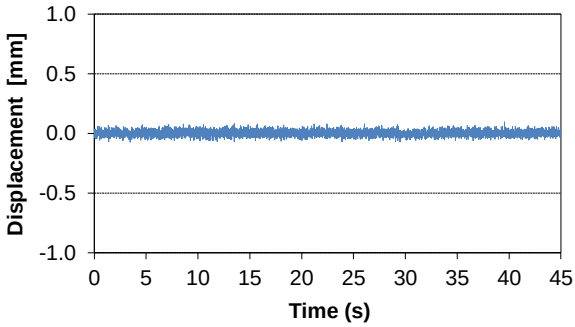

a) Ground level interstorey displacement (channel LVDT_ID_GL_X)

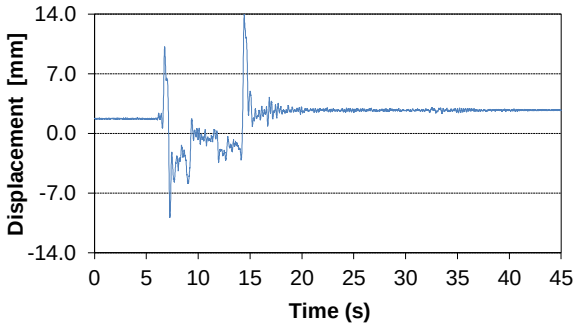

b) Ground level interstorey displacement (channel LVDT_ID_GL_Y)

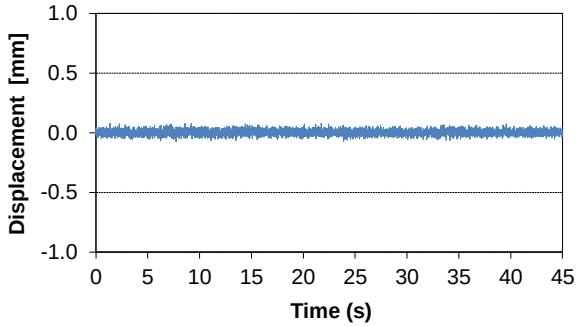

c) First level inter-storey displacement (channel LVDT_ID_L1_X)

Figure 5.20: Sample of the inter-storey drift records obtained in seismic test TEST_09 of the Rusticasa building

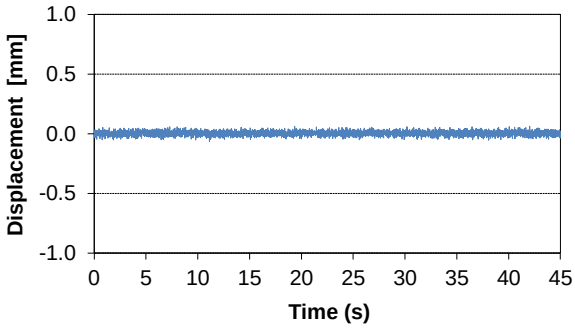

a) Ground level interstorey displacement (channel LVDT_ID_GL_X)

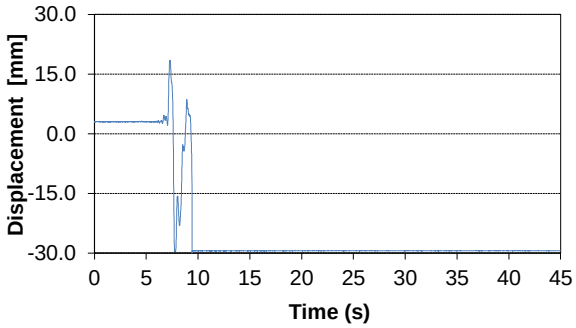

b) Ground level interstorey displacement (channel LVDT_ID_GL_Y)

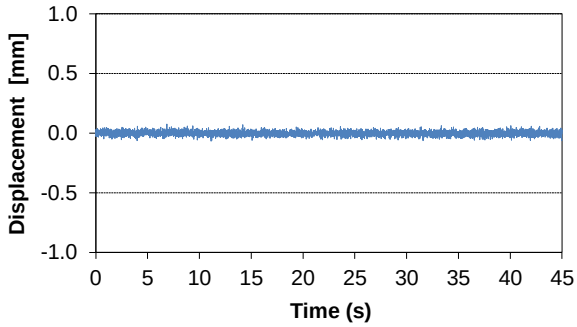

c) First level interstorey displacement (channel LVDT_ID_L1_X)

Figure 5.21: Sample of the inter-storey drift records obtained in seismic test TEST_11 of the Rusticasa building

The values of the maximum simultaneous on all inter-storey drift were and presented in Table 5.16 to

Table 5.17 for the seismic tests TEST_04, TEST_09 and TEST_11 that represents the tests 0.07g, 0.28g and 0.5g. In Annex III were presented all the results.

The highest value of the inter-storey drift measured was 30.49mm and it was recorded at the GL_Y, on the ground floor in the seismic test TEST_11. It is on this wall that the higher values were recorded for the entire testing plan.

Table 5.16 – Maximum simultaneous values on all inter-storey drift for seismic test TEST_04

TEST_04	ID_GL_X	ID_GL_Y	L1_X
ID_GL_X	0.06	0.08	0.05
ID_GL_Y	0.03	0.55	0.03
L1_X	0.06	0.07	0.06

Table 5.17 – Maximum simultaneous values on all inter-storey drift for seismic test TEST_09

TEST_09	ID_GL_X	ID_GL_Y	L1_X
ID_GL_X	0.09	2.86	0.07
ID_GL_Y	0.04	13.94	0.04
L1_X	0.06	2.93	0.08

Table 5.18 – Maximum simultaneous values on all inter-storey drift for seismic test TEST_11

TEST_11	ID_GL_X	ID_GL_Y	L1_X
ID_GL_X	0.07	29.37	0.04
ID_GL_Y	0.01	29.97	0.00
L1_X	0.03	29.48	0.08

5.2.7 Hold-down forces

The peak tensile hold down forces measured during the tests with PGAs of 0.07g and 0.28g are negligible. In the 0.50g test, the magnitude of the forces is also low with the peak tensile force measured being 0.82kN. The low magnitude of the hold-down forces can be attributed in part to the fact that the load cells were attached to the vertical through bolts provided between the sill logs and the foundation that were very rigid and did not give scope for any sort of rocking motion. The values of the peak hold down forces recorded during each test are shown in Table 5.19. It is interesting to note that the walls with lower values of hold down forces recorded higher values of uplift. At the internal wall, the uplift was found to be the highest and was found to be 9mm. The wall with the lowest recorded hold down force (0.15kN) underwent an uplift of 8.5mm. However the wall GLW06_Y with a hold-down force of 0.19kN showed low values of uplift, 0.5mm and 2.1mm on either side of the load cell. The maximum tensile forces recorded by the load cells during the 0.50g test are seen in Figure 5.22.

Table 5.19 - Peak hold down forces (kN)

Wall	01Y_R	02Y_L	04X_L	04X_R	06Y_L	06Y_R	07X_L	07X_R
TEST_01	0.11	0.12	0.12	0.13	0.14	0.15	0.16	0.12
TEST_02	0.09	0.14	0.11	0.11	0.15	0.10	0.14	0.10
TEST_04	0.11	0.12	0.10	0.10	0.15	0.10	0.12	0.13
TEST_05	0.15	0.19	0.15	0.18	0.45	0.12	0.40	0.10
TEST_06	0.16	0.16	0.16	0.15	0.61	0.11	0.41	0.11
TEST_07	0.15	-	0.18	0.17	0.58	0.18	0.45	0.15
TEST_08	0.15	-	0.15	0.16	0.35	0.16	0.25	0.11
TEST_09	0.15	-	0.15	0.15	0.53	0.12	0.36	0.09
TEST_10	0.16	-	0.15	0.15	0.52	0.11	0.38	0.12
TEST_11	0.30	0.77	0.24	0.26	0.82	0.19	0.60	0.15

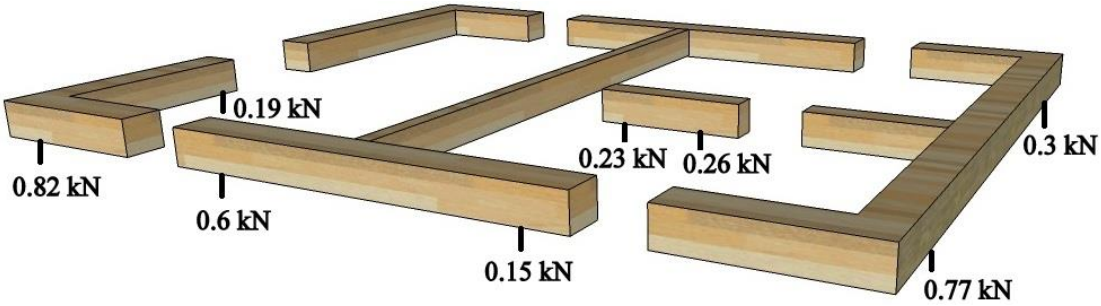

Figure 5.22: Peak hold down forces measured during the 0.50g PGA test

Figure 5.23 to Figure 5.25 show a small sample (four channels) of hold-down forces recorded in seismic tests TEST_04, TEST_09 and TEST_11.

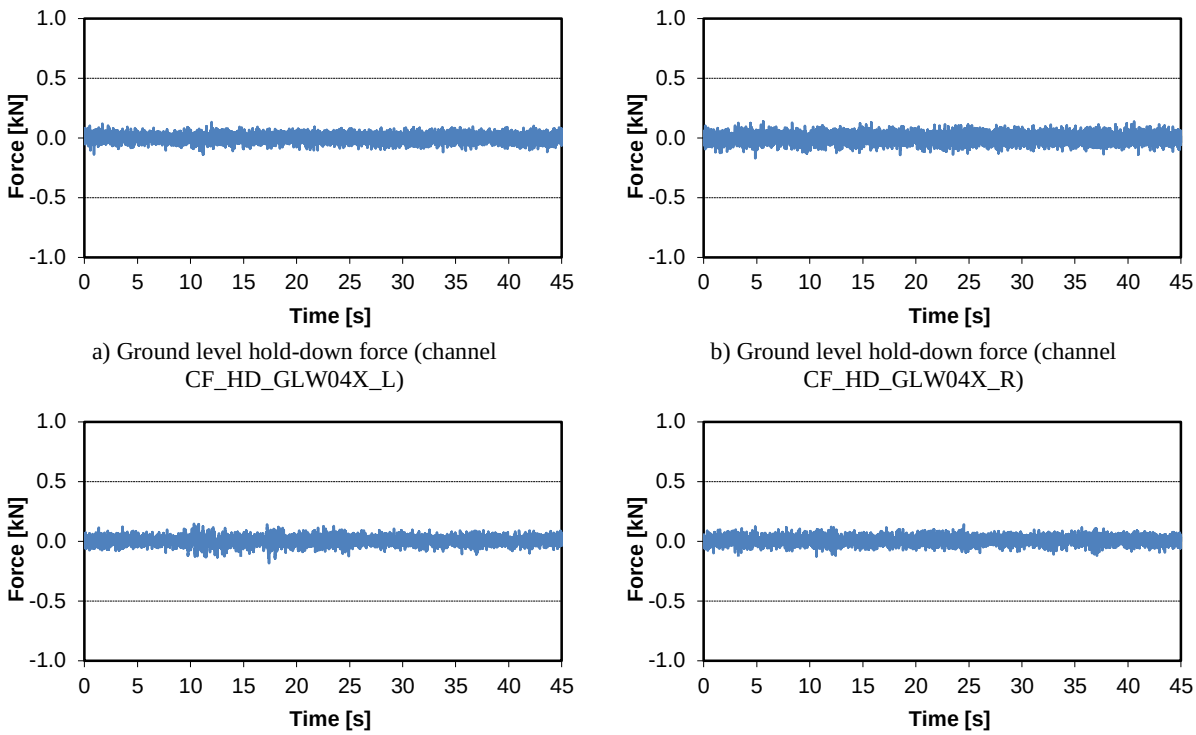

a) Ground level hold-down force (channel CF_HD_GLW04X_L)

b) Ground level hold-down force (channel CF_HD_GLW04X_R)

c) Ground level hold-down force (channel CF_HD_GLW07X_L)

d) Ground level hold-down force (channel CF_HD_GLW07X_R)

Figure 5.23: Sample of the hold-down forces records obtained in seismic test TEST_04 of the Rusticasa building

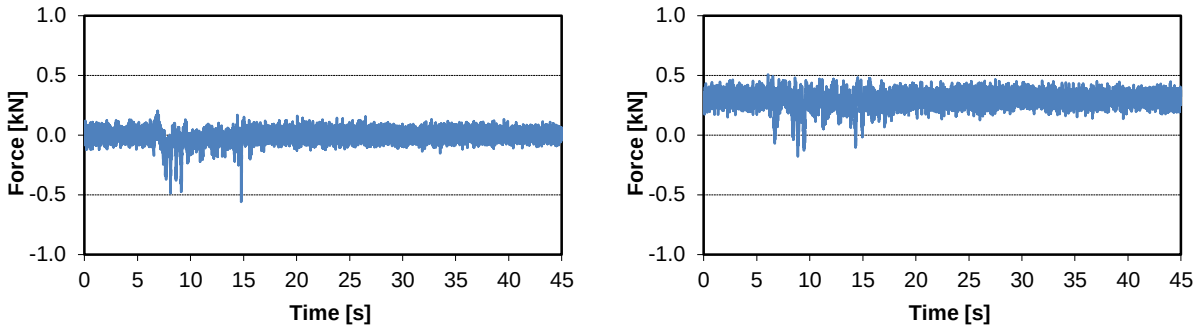

a) Ground level hold-down force (channel CF_HD_GLW04X_L)

b) Ground level hold-down force (channel CF_HD_GLW04X_R)

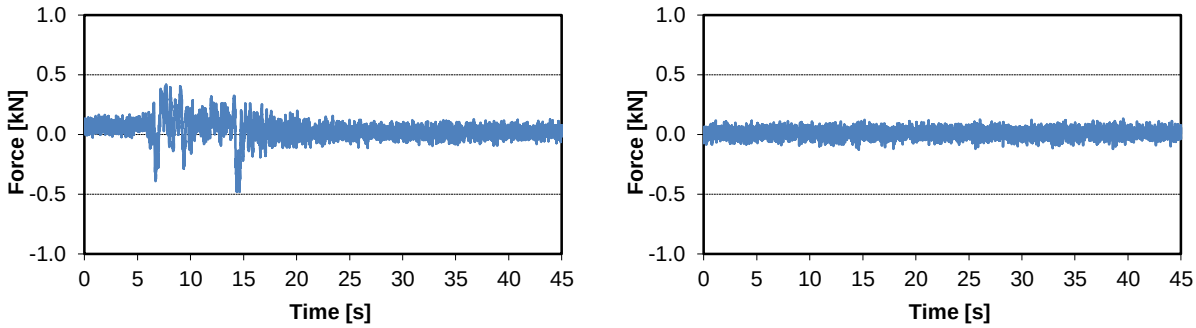

c) Ground level hold-down force (channel CF_HD_GLW07X_L)

d) Ground level hold-down force (channel CF_HD_GLW07X_R)

Figure 5.24: Sample of the hold-down forces records obtained in seismic test TEST_09 of the Rusticasa building

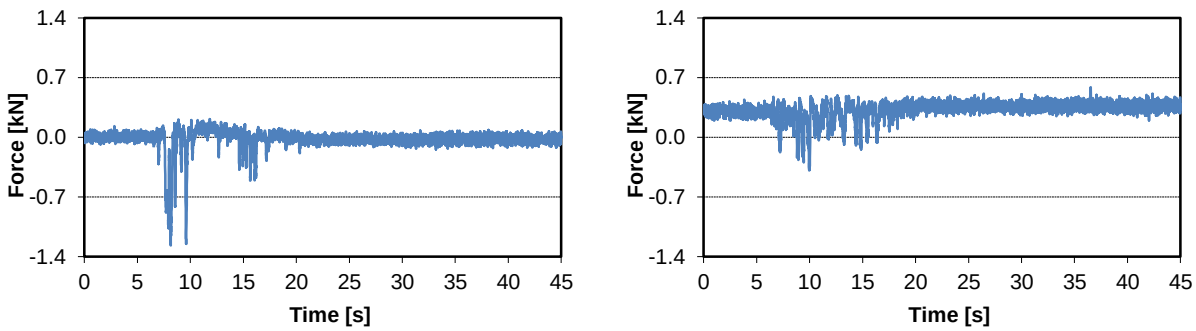

a) Ground level hold-down force (channel CF_HD_GLW04X_L)

b) Ground level hold-down force (channel CF_HD_GLW04X_R)

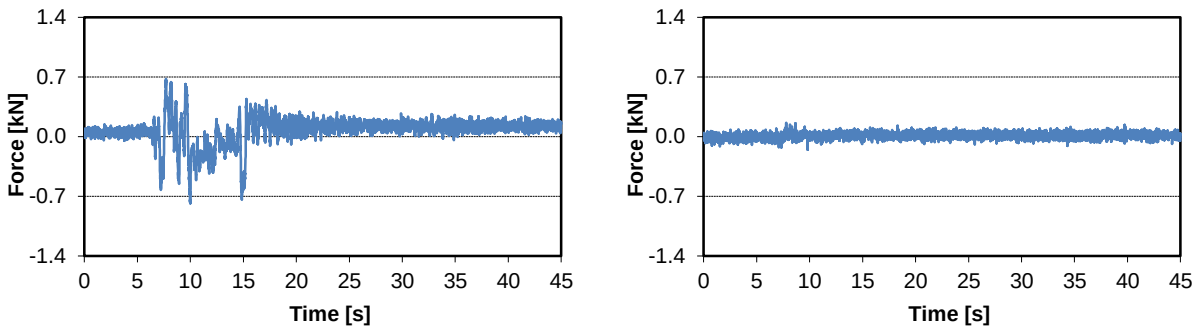

c) Ground level hold-down force (channel CF_HD_GLW07X_L)

d) Ground level hold-down force (channel CF_HD_GLW07X_R)

Figure 5.25: Sample of the hold-down forces records obtained in seismic test TEST_11 of the Rusticasa building

Table 5.20 Table 5.22 illustrated maximum simultaneous values on all load cells for the seismic tests 0.07g, 0.15g, 0.28g and 0.50g. The load cells measured are increased from the seismic test of 0.07g to 0.50g. The highest value of the force measured in the test of 0.50g was 31.64kN and it was recorded at the wall 07X_R on the ground floor.

Table 5.20 – Maximum simultaneous values on all load cells for seismic test TEST_04

TEST_04	CF_GLW01Y_R	CF_GLW02Y_L	CF_GLW04X_L	CF_GLW04X_R	CF_GLW06X_R	CF_GLW06Y_L	CF_GLW07X_L	CF_GLW07X_R
CF_GLW01Y_R	0.15	0.03	0.10	0.09	0.08	0.07	0.07	0.07
CF_GLW02Y_L	0.06	0.13	0.04	0.02	0.03	0.02	0.02	0.01
CF_GLW04X_L	0.11	0.08	0.14	0.05	0.15	0.01	0.09	0.05
CF_GLW04X_R	0.06	0.03	0.03	0.17	0.09	0.16	0.08	0.12
CF_GLW06X_R	0.07	0.03	0.01	0.07	0.23	0.03	0.03	0.05
CF_GLW06Y_L	0.06	0.03	0.03	0.17	0.09	0.16	0.08	0.12
CF_GLW07X_L	0.06	0.07	0.04	0.00	0.09	0.03	0.18	0.05
CF_GLW07X_R	0.00	0.05	0.02	0.02	0.10	0.05	0.10	0.14

Table 5.21 – Maximum simultaneous values on all load cells for seismic test TEST_09

TEST_09	CF_GLW01Y_R	CF_GLW02Y_L	CF_GLW04X_L	CF_GLW04X_R	CF_GLW06X_R	CF_GLW06Y_L	CF_GLW07X_L	CF_GLW07X_R
CF_GLW01Y_R	0.23	0.10	0.06	0.44	0.78	0.06	0.36	0.02
CF_GLW02Y_L	0.09	47.06	0.04	0.29	0.53	0.04	0.34	0.05
CF_GLW04X_L	0.01	0.19	0.56	0.37	0.10	0.02	0.17	0.00
CF_GLW04X_R	0.09	0.15	0.08	0.51	0.08	0.12	0.06	0.06
CF_GLW06X_R	0.07	0.11	0.07	0.29	0.81	0.14	0.32	0.03
CF_GLW06Y_L	0.04	0.09	0.10	0.12	0.27	0.20	0.12	0.12
CF_GLW07X_L	0.00	0.03	0.09	0.02	0.15	0.00	0.48	0.02
CF_GLW07X_R	0.06	0.09	0.13	0.14	0.31	0.17	0.12	0.13

Table 5.22 – Maximum simultaneous values on all load cells for seismic test TEST_11

TEST_11	CF_GLW01Y_R	CF_GLW02Y_L	CF_GLW04X_L	CF_GLW04X_R	CF_GLW06X_R	CF_GLW06Y_L	CF_GLW07X_L	CF_GLW07X_R
CF_GLW01Y_R	0.38	0.01	0.66	0.09	1.09	0.18	0.44	0.16
CF_GLW02Y_L	0.04	0.92	0.10	0.36	0.40	0.06	0.33	0.00
CF_GLW04X_L	0.08	0.30	1.27	0.26	0.43	0.05	0.58	0.00
CF_GLW04X_R	0.18	0.18	0.11	0.59	0.24	0.11	0.09	0.07
CF_GLW06X_R	0.33	0.13	0.34	0.38	2.89	0.06	0.63	0.09
CF_GLW06Y_L	0.04	0.11	0.12	0.34	0.34	0.25	0.62	0.01
CF_GLW07X_L	0.00	0.04	0.02	0.33	0.14	0.12	0.78	0.04
CF_GLW07X_R	0.38	0.01	0.66	0.09	1.09	0.18	0.44	0.16

5.2.8 Wall in-plane and out-of-plane displacements

Using the acceleration time histories recorded by the accelerometers, the maximum displacement of the walls can be obtained. The accelerometers PCB AB01 and PCB AE05 did not function correctly until the calibration process for the 0.28g Montenegro earthquake was restarted after the 7th Test. The values of the accelerations were integrated twice in respect to time to obtain the values of the approximate maximum displacements of the walls of the house. The values of the maximum out-of-plane displacement at wall P6 obtained from the accelerometer readings for different values of PGA are presented in Table 5.23 and Figure 5.26 shows the graphical representation of the same.

Table 5.23 - Out-of-plane displacement of internal wall P6

Test No.	P.G.A.(g)	Displacement at 1.28m (mm)	Displacement at 4m (mm)
TEST_04	0.07	2.1	4.1
TEST_10	0.28	8.6	14.1
TEST_11	0.50	13.8	22.7

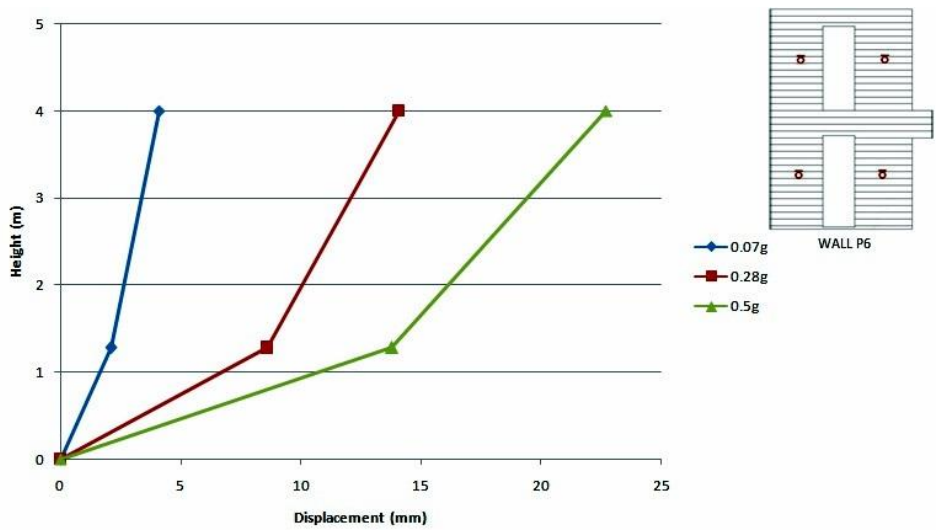

Figure 5.26: Maximum values of out-of-plane displacement of wall P6

The maximum values of the out-of-plane and in-plane displacements of wall P5 at the level of the accelerometers are presented in Table 5.24 and Table 5.25 respectively while the graphical representations can be seen in Figure 5.27 and Figure 5.28 respectively.

Table 5.24 - Out-of-plane displacement of internal wall P5

Test No.	P.G.A.(g)	Displacement at 2.64m (mm)	Displacement at 5.04m (mm)
TEST_04	0.07	2.1	2.4
TEST_10	0.28	6.3	6.3
TEST_11	0.50	12.2	12.8

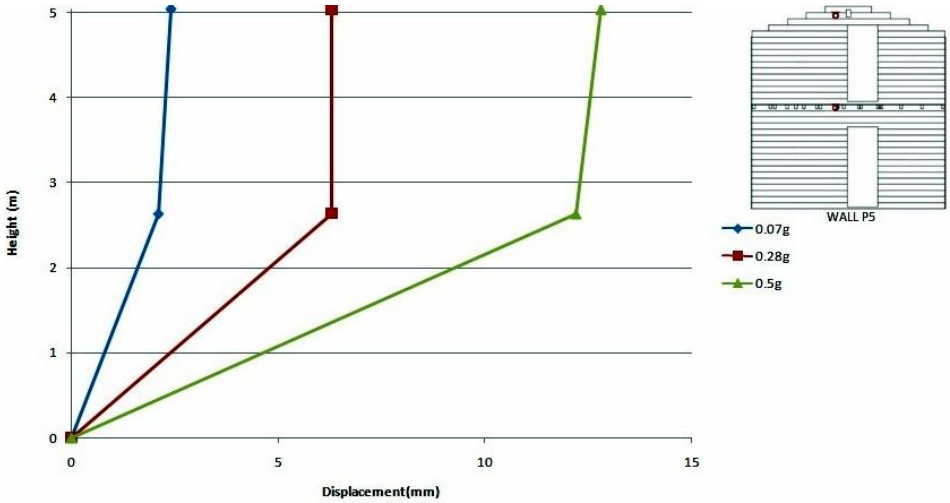

Figure 5.27: Maximum values of out-of-plane displacement of wall P5

Table 5.25 - In-plane displacement of internal wall P5

Test No.	P.G.A.(g)	Displacement at 2.64m (mm)	Displacement at 5.04m (mm)
TEST_04	0.07	3.5	2.6
TEST_10	0.28	14.1	8.8
TEST_11	0.50	21.7	10.9

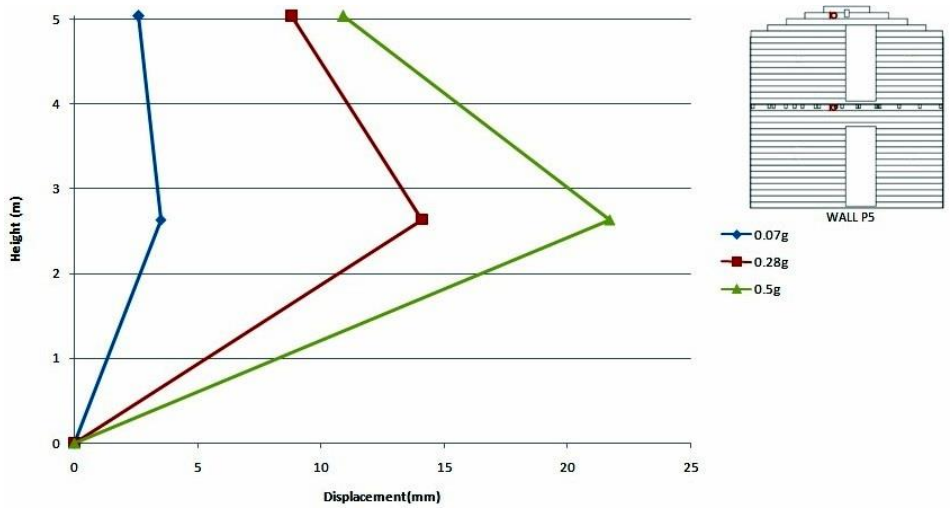

Figure 5.28: Maximum values of in-plane displacement of wall P5

The values of the maximum displacements at the corners of the exterior orthogonal walls are presented below. The displacement at corner A3 in the transverse direction represents the out-of-plane displacement of wall P4 and the in-plane displacement of wall P1 at the point of their intersection. These values are presented in Figure 5.29 and Table 5.26.

Table 5.26 - Displacement at A3 in the transverse direction

Test No.	P.G.A.(g)	Displacement at 1.36m (mm)	Displacement at 3.36m (mm)
TEST_04	0.07	2.7	2.8
TEST_10	0.28	7.5	7.6
TEST_11	0.50	11	9.7

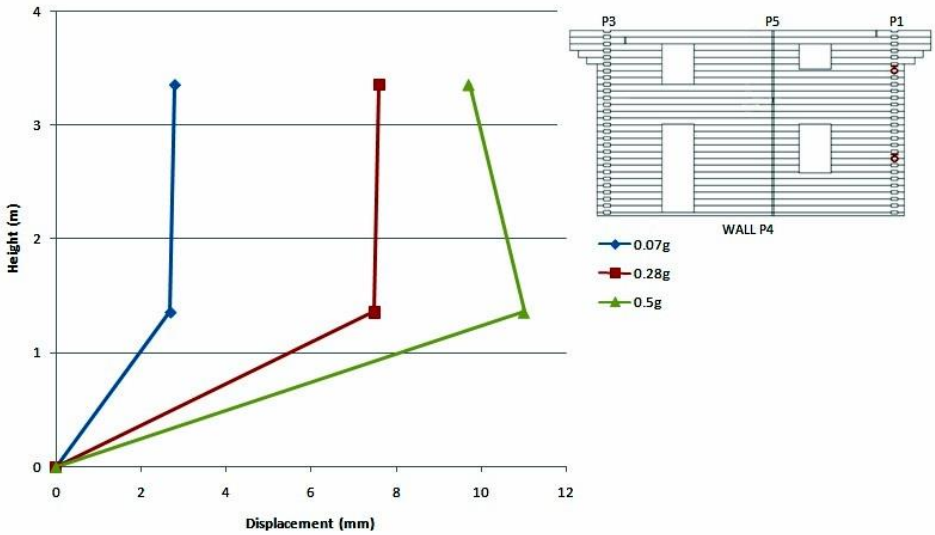

Figure 5.29: Maximum displacement at corner A3 in the transverse direction

The displacement at corner C1 in the transverse direction presented in Table 5.27 represents the out-of-plane displacement of wall P2 and the in-plane displacement of wall P3 at the point of their intersection. In Figure 5.30, values of the maximum displacements at the positions of the accelerometers are determined only for the tests of 0.28g and 0.50g as the accelerometers started functioning correctly only after the re-calibration of instruments following the 7th test.

Table 5.27 - Displacement at C1 in the transverse direction

Test No.	P.G.A.(g)	Displacement at 1.36m (mm)	Displacement at 3.52m (mm)
TEST_04	0.07	-	-
TEST_10	0.28	13.9	13.4
TEST_11	0.50	17.3	20.7

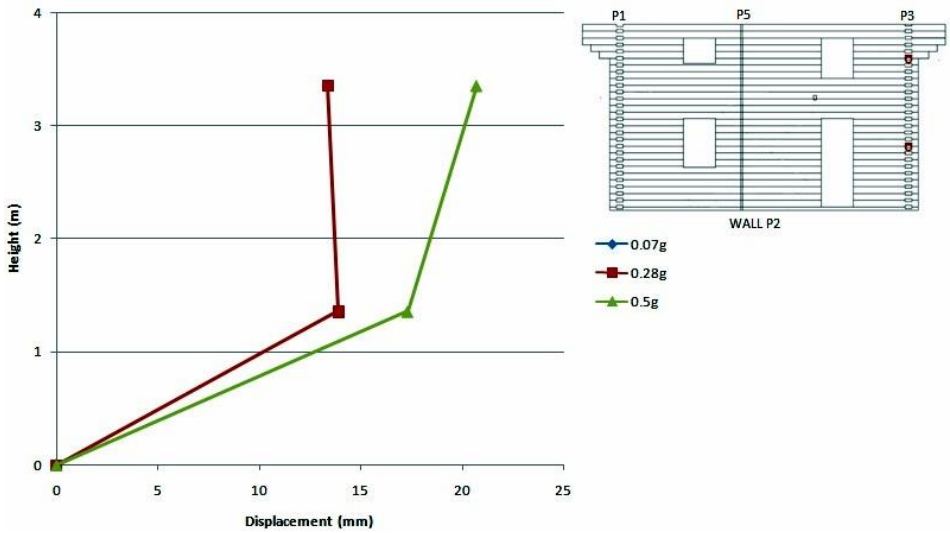

Figure 5.30: Maximum displacement at corner C1 in the transverse direction

The displacement at corner C1 in the longitudinal direction presented in represents the out-of-plane displacement of wall P3 and the in-plane displacement of wall P2 at the point of their intersection. In Table 5.28, values of the maximum displacements at the positions of the accelerometers are listed followed by a graphic representation in Figure 5.31.

Table 5.28 - Displacement at C1 in the longitudinal direction

Test No.	P.G.A.(g)	Displacement at 1.28m (mm)	Displacement at 3.52m (mm)
TEST_04	0.07	2.5	2.4
TEST_10	0.28	8.4	10.8
TEST_11	0.50	14.3	36.9

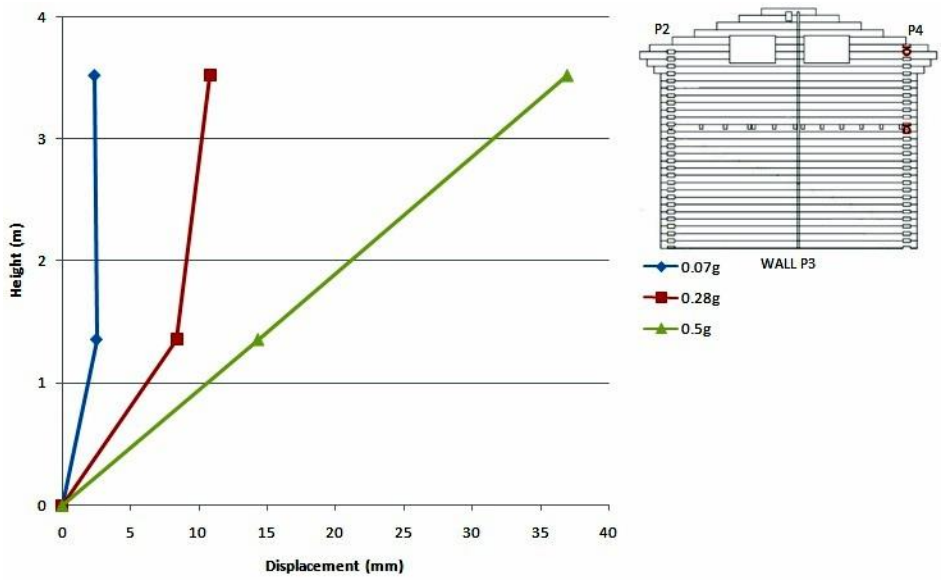

Figure 5.31: Maximum displacement at corner C1 in the longitudinal direction

Table 5.29 gives the values of the maximum displacement at corner A3 in the transverse direction which represents the out-of-plane displacement of wall P1 and the in-plane displacement of wall P4 at the point of their intersection. In Figure 5.32, the maximum displacements at the positions of the accelerometers are represented by a suitable graph.

Table 5.29 - Displacement at A3 in the longitudinal direction

Test No.	P.G.A.(g)	Displacement at 1.36m (mm)	Displacement at 3.36m (mm)
TEST_04	0.07	2.5	2.2
TEST_10	0.28	11.3	8.2
TEST_11	0.50	12.9	12.6

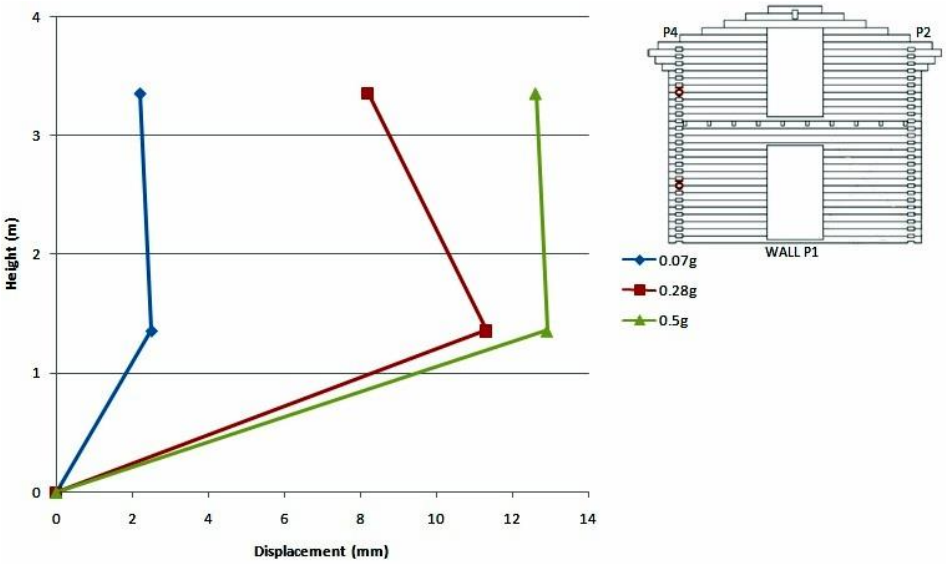

Figure 5.32: Maximum displacement at corner A3 in the longitudinal direction

The out-of-plane displacement of wall P2 and the in-plane displacement of wall P1 are given by the displacement at corner C3 in the transverse direction at the point of their intersection. These values are presented in Table 5.30 and graphically represented in Figure 5.33.

Table 5.30 - Displacement at C3 in the transverse direction

Test No.	P.G.A.(g)	Displacement at 2.64m (mm)	Displacement at 4.4m (mm)
TEST_04	0.07	3.9	4.2
TEST_10	0.28	29.1	35.1
TEST_11	0.50	36.6	30.8

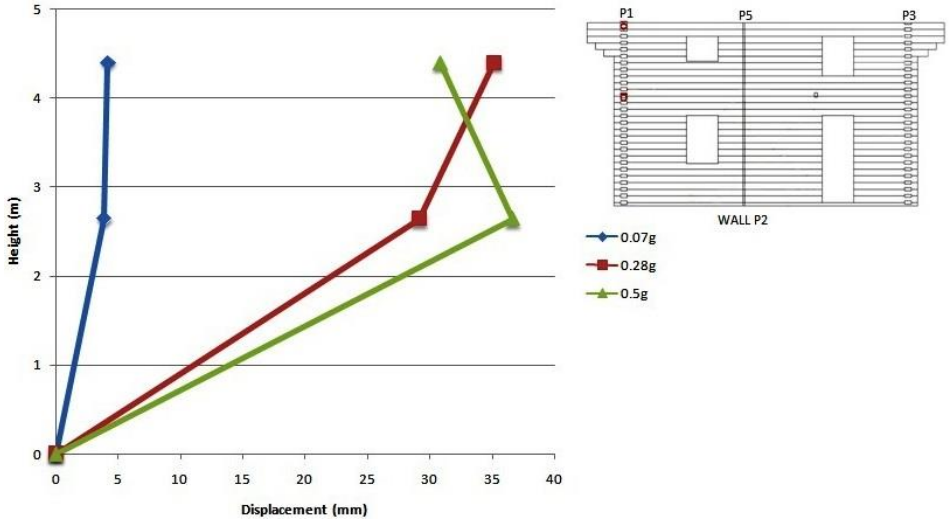

Figure 5.33 - Maximum displacement at corner C3 in the transverse direction

Table 5.31 gives the values of the maximum displacement at corner C3 in the longitudinal direction which represents the out-of-plane displacement of wall P1 and the in-plane displacement of wall P2 at the point of their intersection. The maximum displacements at the positions of the accelerometers are represented by a suitable graph as seen in Figure 5.34.

Table 5.31 - Displacement at C3 in the longitudinal direction

Test No.	P.G.A.(g)	Displacement at 2.64m (mm)	Displacement at 4.4m (mm)
TEST_04	0.07	2.4	2.6
TEST_10	0.28	19.1	22.2
TEST_11	0.50	-	-

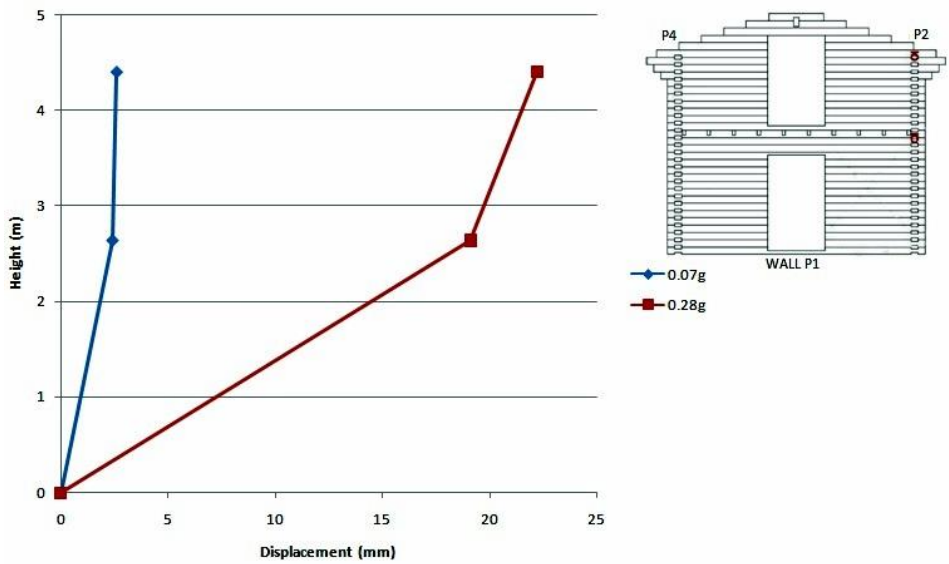

Figure 5.34: Maximum displacement at corner C3 in the longitudinal direction

The displacement at corner A1 in the transverse direction represents the out-of-plane displacement of wall P4 and the in-plane displacement of wall P3 at the point of their intersection. These values are presented in Table 5.32 and Figure 5.35.

Table 5.32 - Displacement at A1 in the transverse direction

Test No.	P.G.A.(g)	Displacement at 2.64m (mm)	Displacement at 4.4m (mm)
TEST_04	0.07	1.9	2.2
TEST_10	0.28	-	-
TEST_11	0.50	29.3	22.9

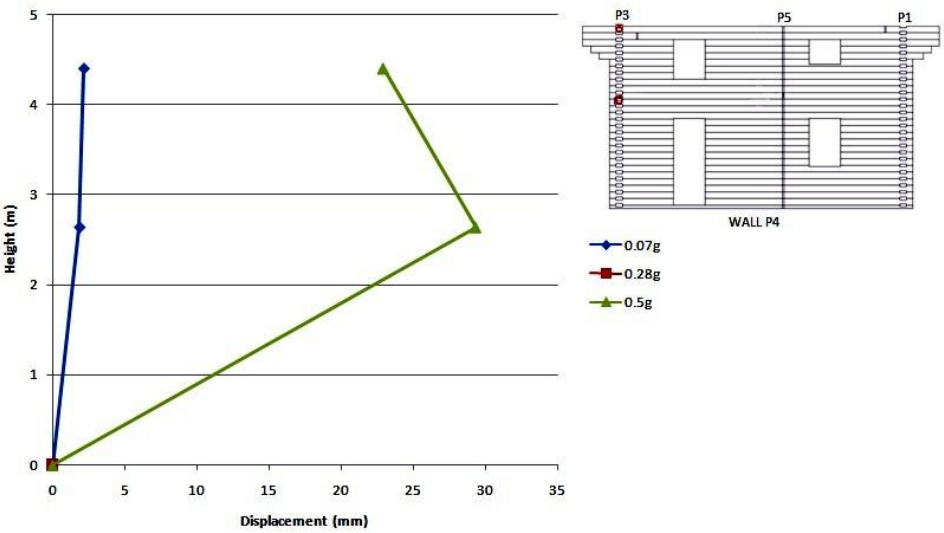

Figure 5.35: Maximum displacement at corner A1 in the transverse direction

For the longitudinal displacement at corner A1, only the accelerometer readings of the tests with PGA 0.07g could be processed as the accelerometer readings were erroneous in the subsequent tests. The displacement at the level of the inter-storey floor was 2.5mm and the maximum displacement at a height of 4.4m was 2.8mm.

The values of the displacements obtained from the accelerometers were compared with the values of the displacements obtained from sensors of the Hamamatsu system, which were located in the same position, at the intersection of the walls P2 and P3. They are presented in the table below. Most of the values are similar, but there are discrepancies in some tests. The values of the displacements at corner C1 in the transverse direction could not be calculated for the tests with 0.07g as the accelerometers in this position did not function correctly.

Table 5.33 - Comparison of displacements obtained from the accelerometers and the Hamamatsu system

		Displacement between GL and L1(mm)		Displacement between L1 and RL(mm)	
		Accelerometer	Hamamatsu	Accelerometer	Hamamatsu
TEST_04	C1-L	2.5	2.08	2.4	1.57
TEST_10	C1-L	8.37	7.37	10.84	12.97
	C1-T	13.87	6.35	13.44	16.13
TEST_04	C1-L	14.3	20.76	36.84	28.37
	C1-T	17.27	17.75	20.7	54.73

5.2.9 Spectral content

To identify the dynamic characteristics of the Rusticasa building, the frequency response functions (FRF's) were computed with LNEC SPA [20] taking into account single input, multi output relations (SIMO) obtained from the characterization signals CAT 1 and CAT 7. Figure 5.36 and Figure 5.37 show an example of the frequency response function, phase and coherence in the transverse and longitudinal directions calculated for the channel ACC_RL_B2_X_I_T and for the dynamic identification CAT 1. In Figure 5.38 and Figure 5.39 are shown the same but for the dynamic identification CAT 7.

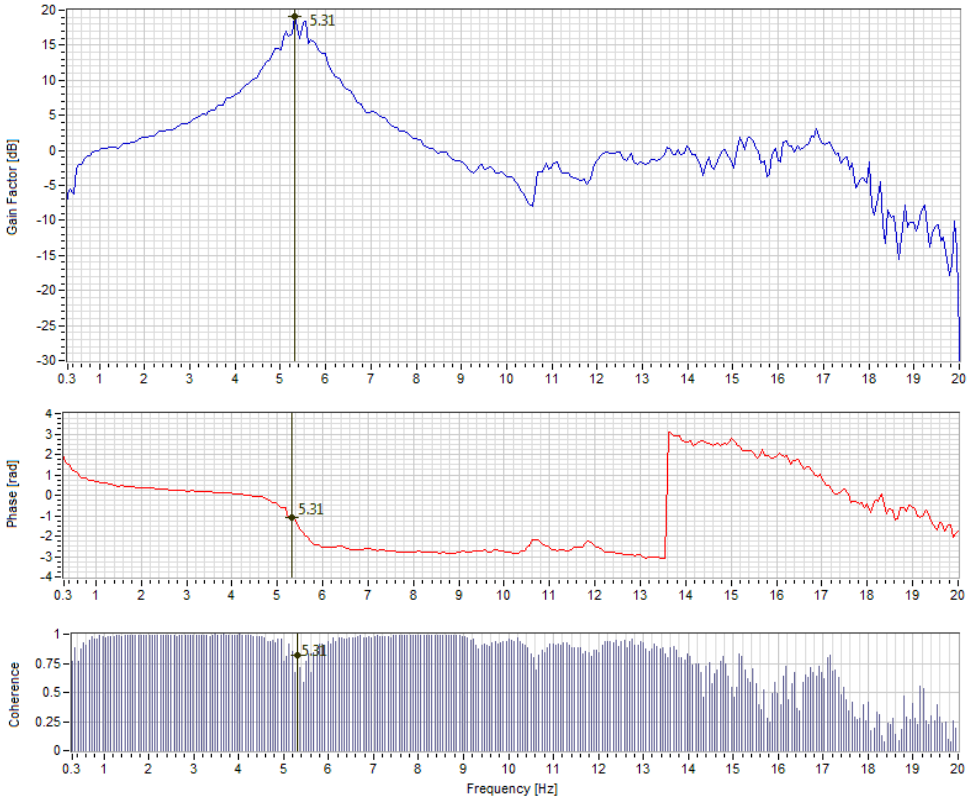

Figure 5.36: Frequency response function, phase and coherence (Cat 1): ACC MESA TRANS; ACC_RL_B2_X_I_T

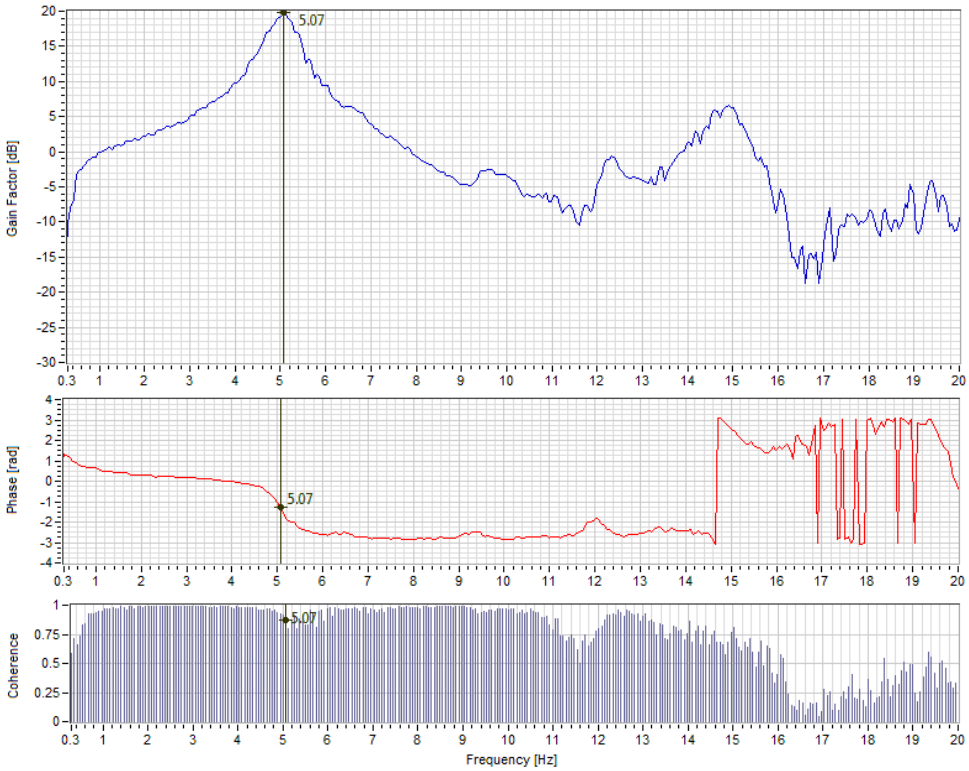

Figure 5.37: Frequency response function, phase and coherence (Cat 1): ACC MESA LONG; ACC_L1_C2_X_N_L

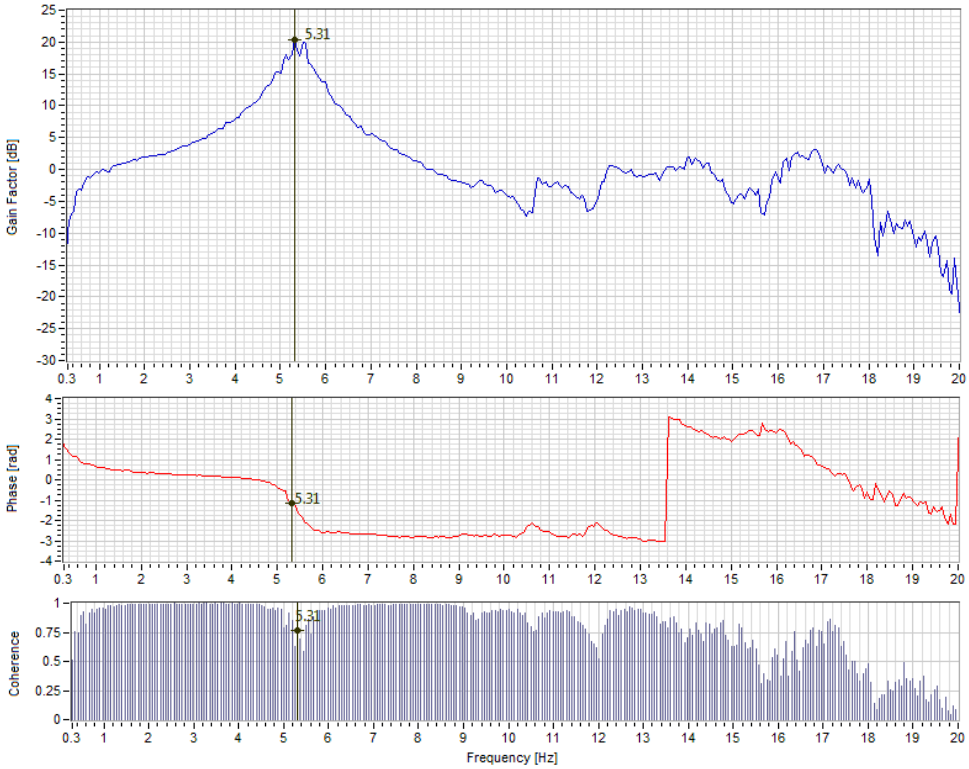

Figure 5.38: Frequency response function, phase and coherence (Cat 7): ACC MESA TRANS; ACC_L1_C2_Y_N_T

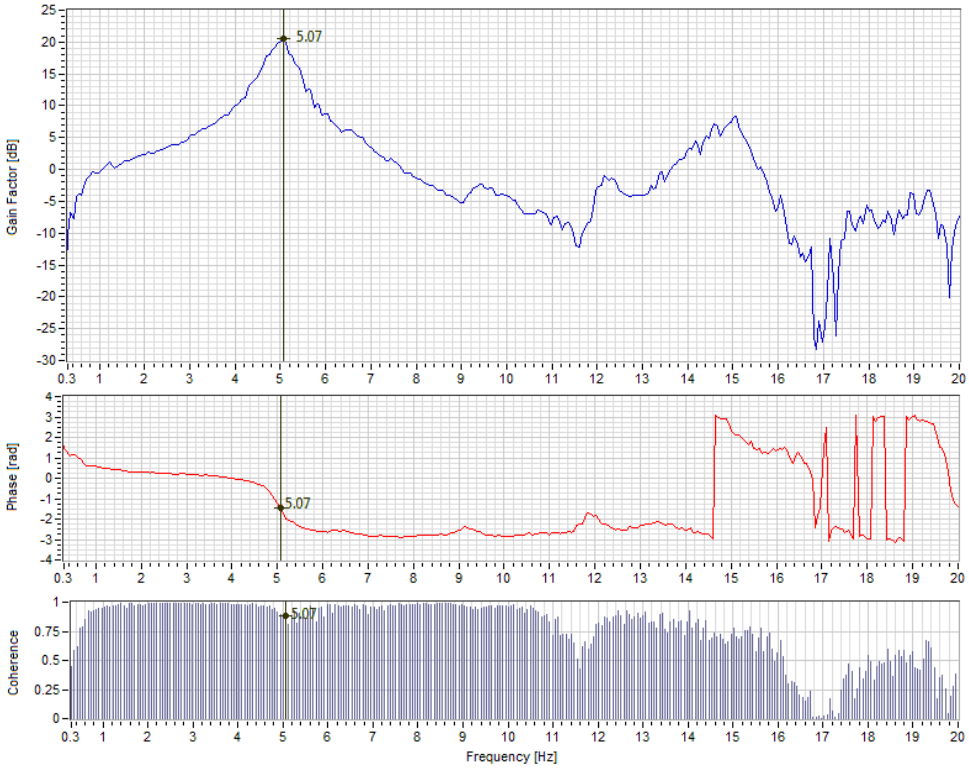

Figure 5.39: Frequency response function, phase and coherence (Cat 7): ACC MESA LONG; ACC_L1_C2_X_N_L

5.3 MODE SHAPES AND NATURAL FREQUENCIES CHARACTERIZATION

Since the dynamic properties of the system play an important role in determining the seismic response of the structure, it is essential to estimate the natural frequencies, damping and mode shapes. In low-rise buildings, the seismic response mainly depends on the fundamental mode. For the log house, the first four modes of the structure were identified. There were seven dynamic characterization tests conducted in total, but the mode shapes from only four of the tests were evaluated:

- CAT 1- corresponding to the characterization test at the start of the experiment;
- CAT 2- corresponding to the characterization test after the four seismic tests with 0.07g PGA;
- CAT 6- corresponding to the characterization test after the six seismic tests with 0.28g PGA;
- CAT 7- corresponding to the characterization test after the two seismic tests with 0.50g PGA.

The data recorded by the accelerometers during the dynamic characterization tests correspond to the data obtained from input-output modal identification techniques. In order to obtain the mode shapes of the structure using ARTeMIS, the information needs to be converted into equivalent data obtained from the output-only modal identification technique. ARTeMIS is a state-of-the-art software platform which is one of the most powerful and versatile tools for Operational Modal Analysis available. Figure 5.40 shows the log house modelled in ARTeMIS and Figure 5.41 shows the accelerometer positions and directions mapped out on the house.

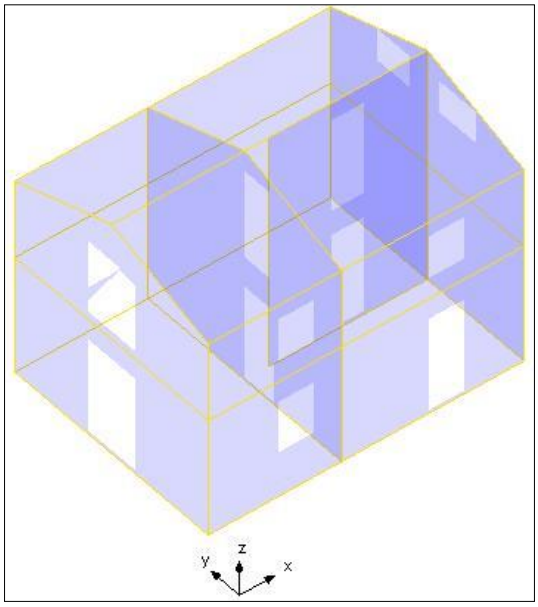

Figure 5.40: Log house modelled in ARTeMIS

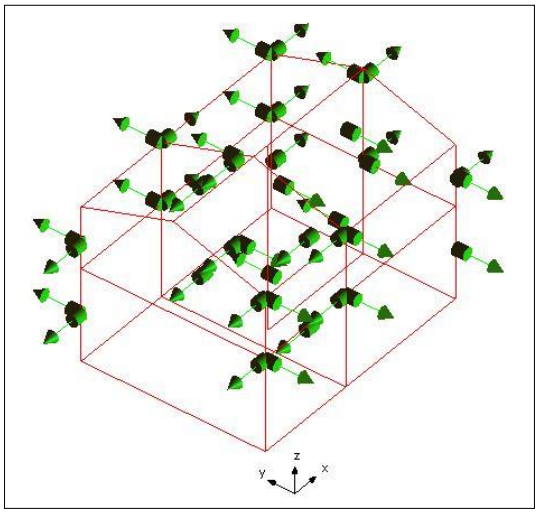

Figure 5.41: Positions of the accelerometers in the house modelled in ARTeMIS

On completion of the analysis, it was found that since the log house corners are formed by intersections of cross logs, it is difficult to obtain purely longitudinal or translational modes. The movement of the logs of one of the walls influences the movement of the orthogonal walls. However, based on the magnitude of movement, it was possible to characterize the mode shape. If the displacement of the walls in the X-direction was far greater than the displacement in the Y-direction, the mode was classified as longitudinal and similarly if the displacement of the walls in the Y-direction was much higher than in the X-direction, the mode was classified as a transverse.

The fundamental frequency obtained was 5.39Hz [T=0.185s] during the initial characterization test (before 0.07g) which reduced to 5.109Hz [T=0.196s] during the final

characterization test (after 0.50g). As there was an equal movement in the longitudinal as well as translational direction, the first mode was classified as a mixed mode and can be seen in Figure 5.42. The second natural frequency of the structure was 11.85Hz at the beginning and reduced to 11.53Hz at the end. From Figure 5.44 one can observe that the mode was longitudinal. The third frequency of the house was 14.93 Hz at the beginning and reduced to 14.54Hz at the end. This mode was torsional as seen in Figure 5.46. The fourth mode (Figure 5.48) was transverse and was characterized by a frequency of 20.53Hz in the beginning and 20.19Hz at the end. The frequencies of the structure evaluated during Test 2 (after the 0.07g PGA tests) were slightly different from the results obtained in all the other tests. There was no observed mode around the region of 20Hz. The reduction in the frequencies of the tests for each mode suggests the lowering in the stiffness of the structure corresponding to an increase in the Peak Ground Acceleration. However, the decrease in the frequency is small, indicating that the structure suffered only minor damage. Even if there were hidden damages internally, they were small.

Table 5.34 - Natural frequencies of the log house

	Before 0.07g tests		After 0.07g tests		After 0.28g tests		After 0.50g tests	
	f (Hz)	T (s)	f (Hz)	T (s)	f (Hz)	T (s)	f (Hz)	T (s)
Mode 1 Mixed mode	5.389	0.185	5.315	0.188	5.171	0.193	5.109	0.196
Mode 2 Longitudinal	11.85	0.084	11.83	0.085	11.77	0.085	11.53	0.087
Mode 3 Torsional	14.93	0.067	14.91	0.067	14.87	0.067	14.54	0.069
Mode 4 Transverse	20.53	0.049	-	-	20.38	0.049	20.19	0.05

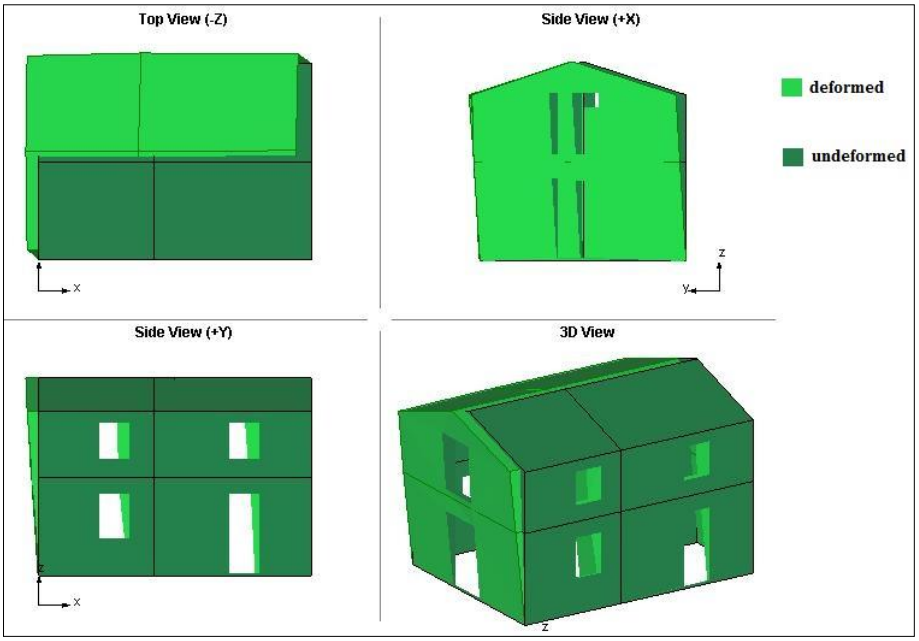

Figure 5.42: Views of the house for the first mode

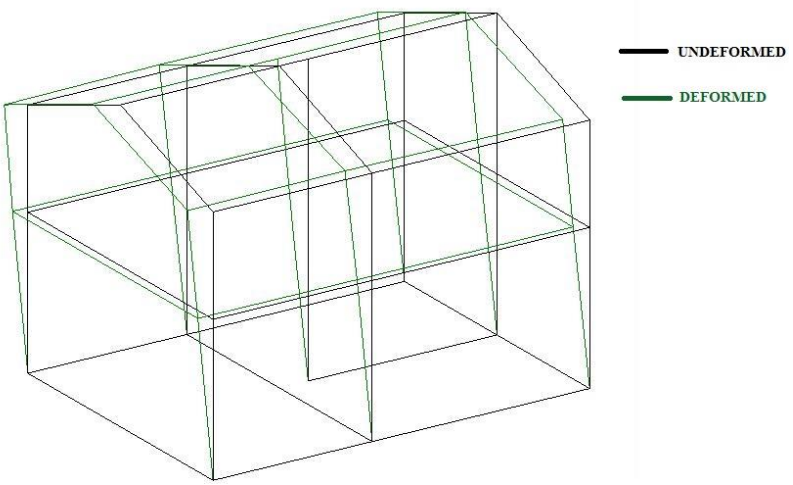

Figure 5.43: The outlines of the deformed and undeformed structure of the log-house during the first mode

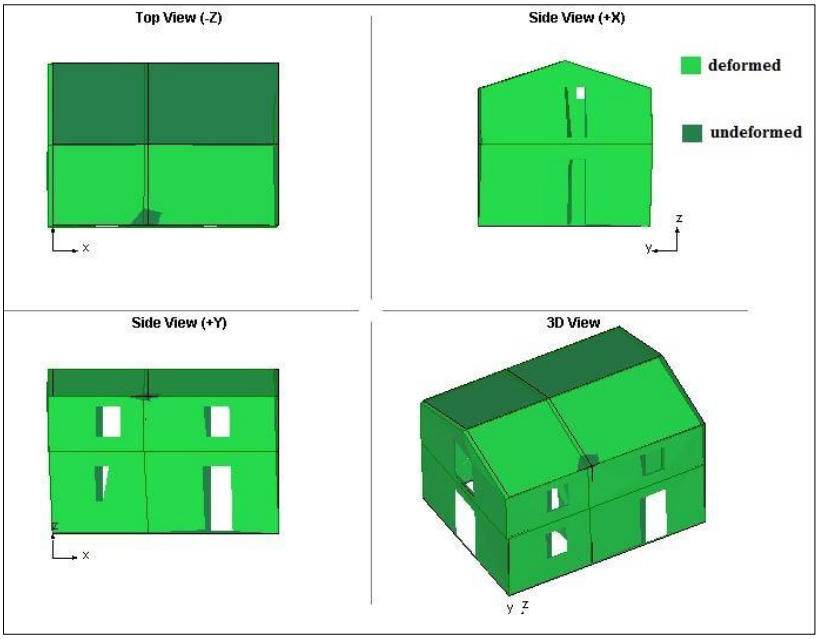

Figure 5.44: Views of the house for the second mode

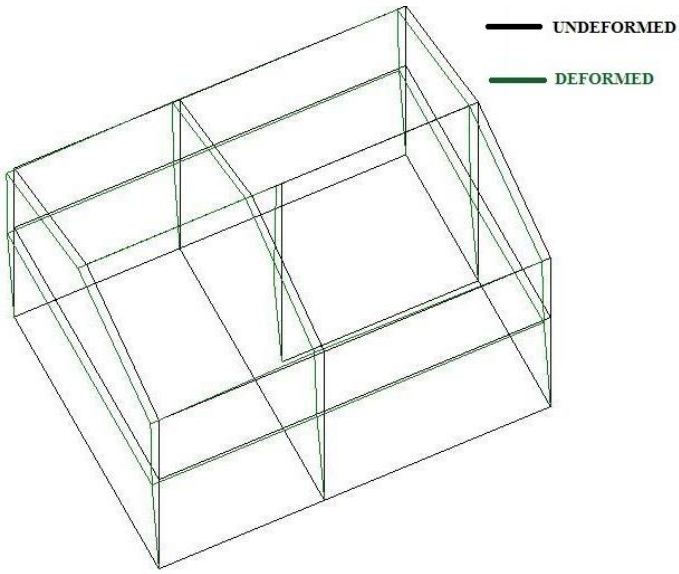

Figure 5.45: The outlines of the deformed and undeformed structure of the log-house during the second mode

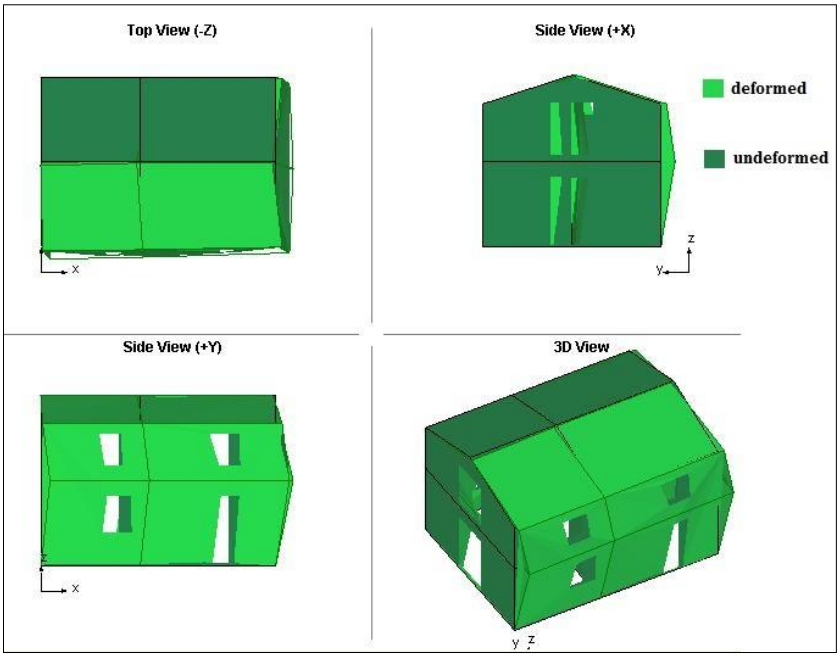

Figure 5.46: Views of the house for the third mode

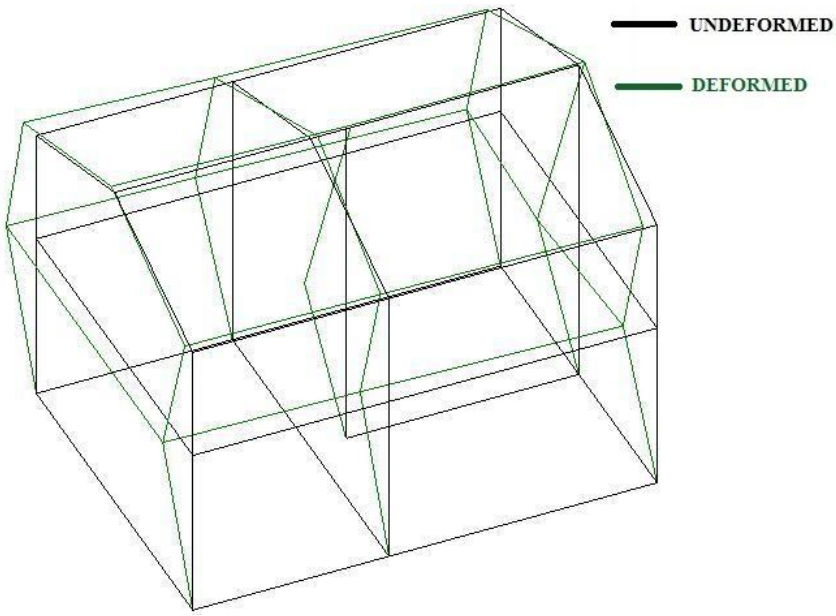

Figure 5.47: The outlines of the deformed and undeformed structure of the log-house during the third mode

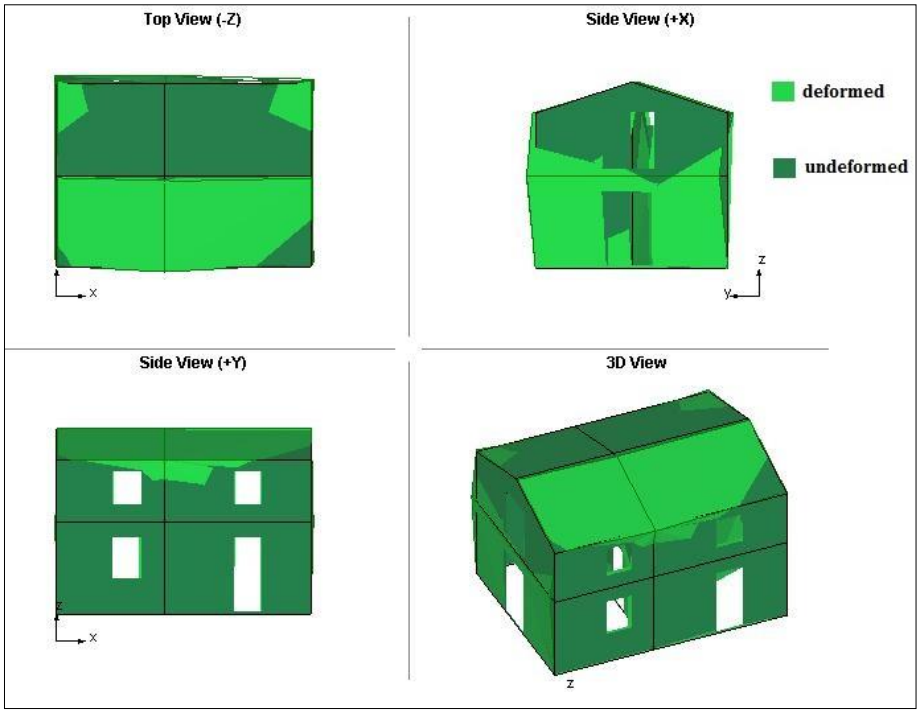

Figure 5.48: Views of the house for the fourth mode

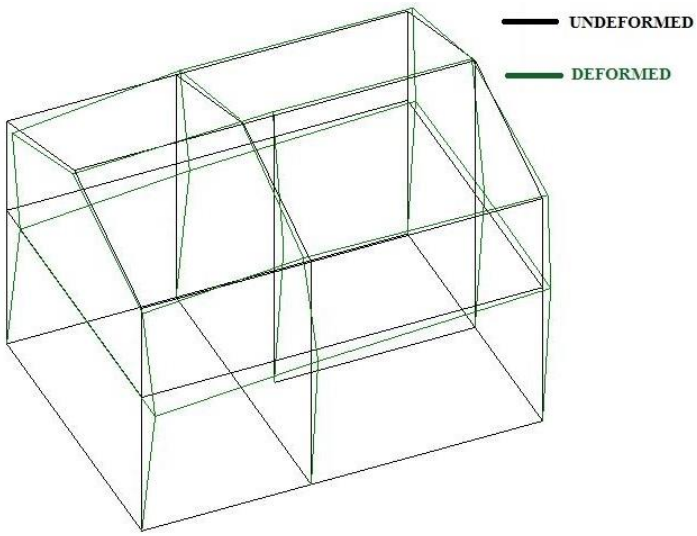

Figure 5.49: The outlines of the deformed and undeformed structure of the log-house during the fourth mode

The results of the CAT 1 test correspond to the value of the undamaged structure while the results from CAT 2, CAT 3, CAT 6 and CAT 7 correspond to the damaged structure. The numerical correlation of the mode shape vectors of the undamaged and damaged structure can be obtained by computing the Modal Assurance Criteria (MAC) value as shown in the equation below.

$$\mathrm{MAC}_{u,d} = \frac{\left|\sum_{i=1}^{n} \varphi_i^u \varphi_i^d\right|^2}{\sum_{i=1}^{n} (\varphi_i^u)^2 \sum_{i=1}^{n} \left(\varphi_i^d\right)^2} \tag{2}$$

where φ^u is the mode shape vector corresponding to the undamaged condition of the structure, φ^d is the mode shape vector corresponding to the damaged condition of the structure and, n is the number of estimated degrees of freedom.

The result of the expression is a scalar value in the range of 0 and 1 and indicates the extent of correlation between the two cases. However, the MAC values are global quantities that are not sensitive to low damage in the structure. In order to overcome this drawback, the Normalised Modal Difference (NMD) value is calculated, which is more sensitive to the differences between the shape vectors [18].

$$\mathrm{NMD}_{u,d} = \sqrt{\frac{1 - \mathrm{MAC}_{u,d}}{\mathrm{MAC}_{u,d}}} \tag{3}$$

In practice, one might consider that a NMD value less that 33% (MAC value > 0.90) between two modes is an indicator of a good correlation between the modes [9].

Table 5.35 - MAC values of the mode shapes of the characterization tests

	Mode 1	Mode 2	Mode 3	Mode 4
CAT1-CAT2	0.9525	0.8616	0.8788	-
CAT1-CAT6	0.9817	0.9327	0.9847	0.9408
CAT1-CAT7	0.9449	0.9204	0.9396	0.9191

Table 5.36 - NMD values of the mode shapes of the characterization tests

	Mode 1	Mode 2	Mode 3	Mode 4
CAT1-CAT2	0.22	0.40	0.37	-
CAT1-CAT6	0.14	0.27	0.12	0.25
CAT1-CAT7	0.24	0.29	0.25	0.30

5.4 DAMAGE PERFORMANCE ASSESSMENT OF THE BUILDING

5.4.1 Observed Damages

There were no signs of visible damage in the structure after the tests of 0.07g PGA were carried out. The only damage that was noticed after Test 7 (0.28g) was the sliding of the logs in the North Western Corner of the house, located near the window in wall P3. Once all the seismic tests were carried out, the following damages were observed:

- Fracture along the length of the log due to out-of-plane flexure

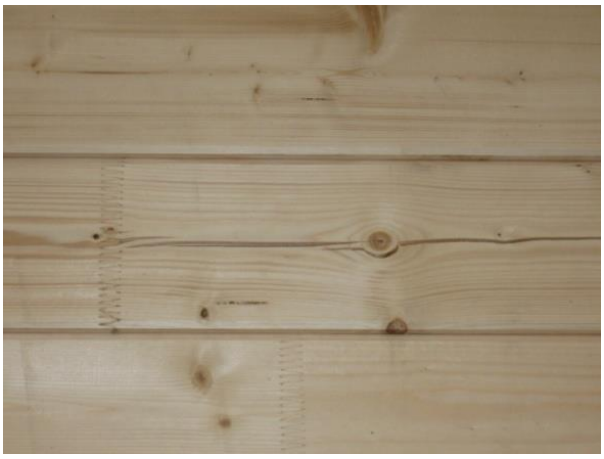

Figure 5.50: Crack seen along the grain of the log

- Fracture along the grain at connections between orthogonal walls due to shear

Figure 5.51: Cracks seen in logs at cross wall intersections

- Sliding of logs due to shear

Figure 5.52: Sliding of logs near the window openings in the NW part of the house

- Damage in the vicinity of the screws

Figure 5.53: Chipping of wood around screws

- Internal cracks in the log section

Figure 5.54: Cracks visible in the cross section of the log

- Fracture at the top and bottom notches of the logs

Figure 5.55: Damage to the top and bottom profiles of the log

- Fracture at the intersection between floor beams and the wall

Figure 5.56: Cracks seen near the intersection of the floor beams with the log wall

6 Main conclusions

The work presented in this report describes the study of the seismic behaviour of a log-house system (LHS) building as part of the SERIES Project on multi-storey timber buildings. This project is coordinated by the University of Trento and involves the University of Minho and the Graz University of Technology, at LNEC, in Lisbon.

Regarding the time taken for construction, it can be concluded that using this technology, a single house of this kind can be constructed within a period of four days once all the prefabricated elements are on the site. After the seismic tests were carried out, no major damages were seen on visual inspection. Dynamic characterization tests revealed that the fundamental frequency of the structure was initially 5.389 Hz (0.186s) and then decreased to 5.109Hz (0.196s). The low magnitude of the decrease in frequency corroborates the fact that there were hardly any damages seen. The numerical model developed during the pre-design of the test indicated a fundamental frequency of 4.97Hz (0.201s) for the undamaged structure, which is close to the observed frequency. However, the mode shapes that were predicted by the numerical model differed from the experimental mode shapes. This suggests that a more sophisticated numerical model of the structure needs to be developed. The magnitude of the hold down forces that were measured during the test was low and the displacements of the walls were also within limits. This suggests that the house possesses good seismic resistance.

The carpentry joints remained intact and the log profiles enabled a perfect fit between successive logs, which is a significant improvement from traditional log houses. The fast pace and ease of construction and the absence of major damage in the building indicate that this form of log construction would be a viable option in areas that have high seismic risk, provided the climatic conditions are suitable.

References

[1] KUKLIK P. - **History of Timber Structures**. In Educational Materials for Designing and Testing of Timber Structures-TEMTIS "Handbook I- Timber Structures, 1-14. Leonardo da Vinci Pilot Projects, September 2008.

[2] National institute for land and infrastructure management et al. - **Technical standard and design examples for log constructions**. Kogaku Tosho, 2003.

[3] HIRAI T., TAKEO K., KUNIYOSHI Y., YOSHIHISA S., AKIO K. - **Lateral resistance of log constructions**. Proceedings of the 8th World Conference on Timber Engineering, WCTE. Lahti, Finland 163, 2004, 251-254.

[4] BRANCO J.M., ARAUJO J.P. - **Structural behaviour of log timber walls under lateral in-plane loads**. Engineering Structures. 40, 2012, 371-382. URL: http://hdl.handle.net/1822/19907.

[5] European committee for standardization - **Structural timber – Strength classes EN 338:2003**. CEN, Brussels, Belgium, 2003.

[6] BRANCO J.M., CRUZ, P.J.S. - **Caracterização mecânica de toros de madeira lamelada colada**. 7º Congresso Nacional de Mecânica Experimental, UTAD, 23-25, Jan 2008.

[7] TORATTI T. - **Seismic Design of Timber Structures**. Wood focus Publications, 2001. (http://customers.evianet.fi/woodfocus/download.php/download/document_data/3944/Seismic_design_of_timber_structures.pdf)

[8] CAMPOS COSTA, A., CANDEIAS, P., PIAZZA, M., TOMASI, R., LOURENÇO, P.B., BRANCO, J., SCHICKHOFER, G., FLATSCHER, G. - **The LNEC Earthquake Engineering Testing Facility. Background information: LNEC testing facility, testing setup and protocol and data processing**, SERIES Report, July 2013.

[9] COELHO E., CARVALHAL F. - **Breve descrição da plataforma triaxial.** 2010 (http://www.lnec.pt/organizacao/de/nesde/ptriaxialdescricao).

[10] Seismic Engineering Research Infrastructures for European Synergies, European Commission, LNEC Shaking table. (http://www.series.upatras.gr/LNEC).

[11] RAMOS J.L. - **Damage Identification on Masonry Structures Based on Vibration Signatures**. PhD Thesis, University of Minho, Portugal, 2007, http://hdl.handle.net/1822/7380.

[12] TESTONI M. - **Avaliação sísmica de casas log-house através de ensaios em mesa sísmica**. Tese de Mestrado. Universidade de Trento. (Em Italiano).

[13] Krypton Electronic Engineering n.v., Krypton Help Pages on K400/K600 - Hardware & Software Guide, Leuven, April 2003.

[14] http://blog.nikonmetrology.com

[15] http://www.datasheetcatalog.org/datasheet/hamamatsu/C5949.pdf

[16] SAP - **CSI Analysis Reference Manual for SAP2000. Version v14**. Computers & Structures Inc., Berkeley, USA, 2000.

[17] GENTILE, C., MARTINEZ, F., and CABRERA - D**ynamic assessment of a curved cable-stayed bridge at the Malpensa 2000 Airport, Milan, Italy**. Structural Engineering International, (1). 2001, 52–58.

[18] LNEC (2010). http://www.lnec.pt/organizacao/de/nesde

[19] Mathcad software (version 14), PTC.

[20] MENDES, L., CAMPOS COSTA, A. - **LNEC-SPA – Signal Processing and Analysis Tool for Civil Engineers. Version 1.0 – Build 12**. Report LNEC 29/2007-NESDE, 2007.

ANNEX I
Shaking Figure tests: Time histories

Seismic test – TEST_04

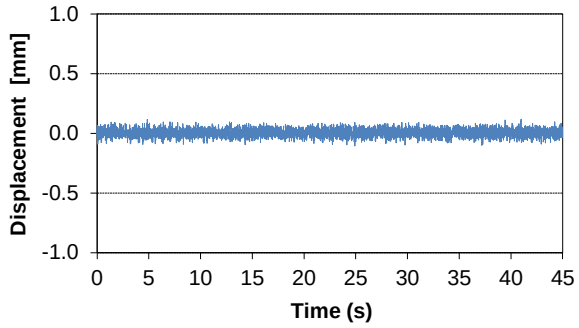

Figure AI. 1 – Channel LVDT_WU_GLW06Y_L

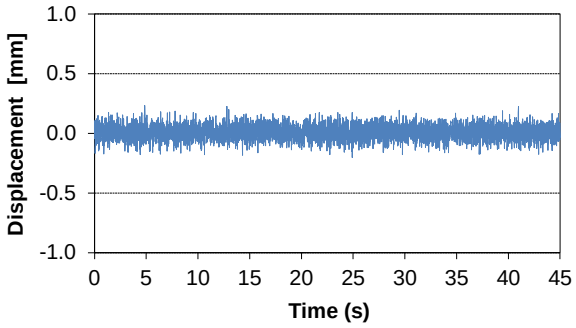

Figure AI. 2 - Channel LVDT_WU_GLW06Y_R

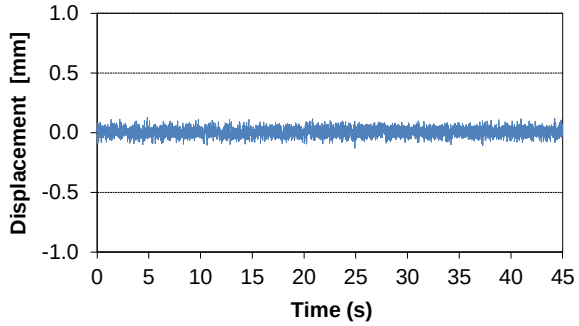

Figure AI. 3 - Channel LVDT_WU_GLW07X_L

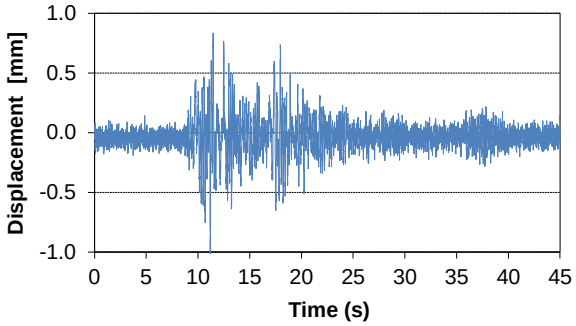

Figure AI. 4 - Channel LVDT_WU_GLW07X_R

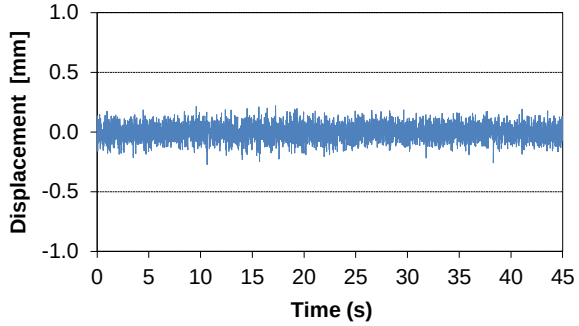

Figure AI. 5 - Channel LVDT_WU_GLW02Y_L

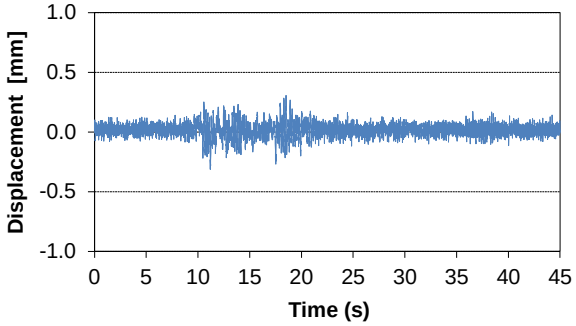

Figure AI. 6 - Channel LVDT_WU_GLW01Y_R

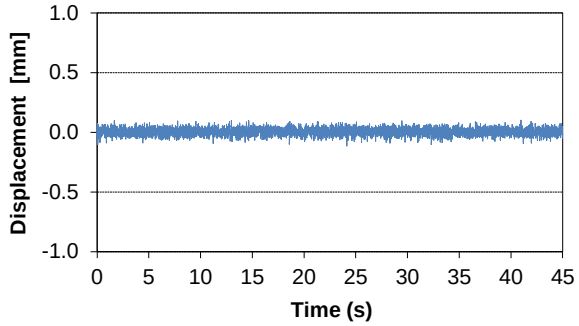

Figure AI. 7 - Channel LVDT_WU_GLW04X_L

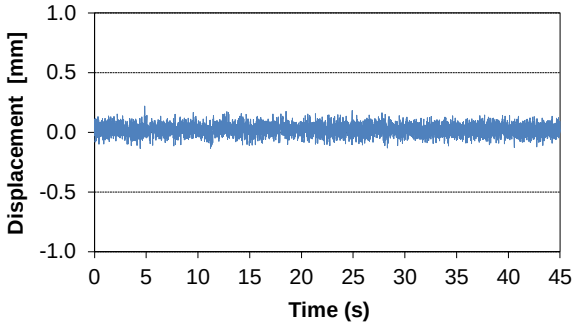

Figure AI. 8 - Channel LVDT_WU_GLW04X_R

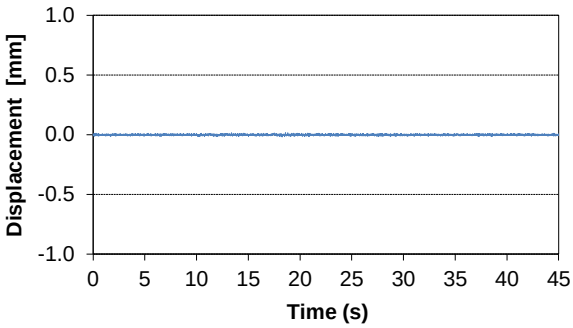

Figure AI. 9 - Channel LVDT_WS_GLW06Y

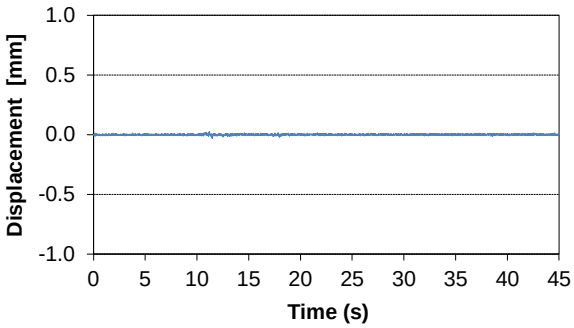

Figure AI. 10 – Channel LVDT_WS_GLW07X

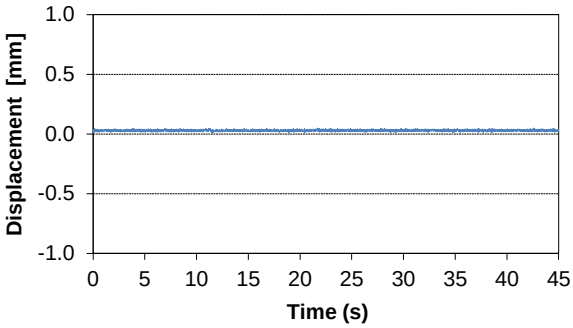

Figure AI. 11 - Channel LVDT_WS_GLW02Y

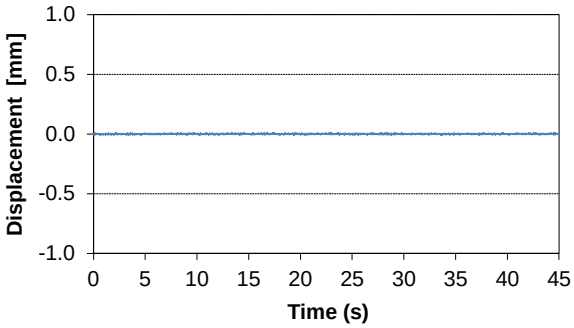

Figure AI. 12 - Channel LVDT_WS_GLW04X

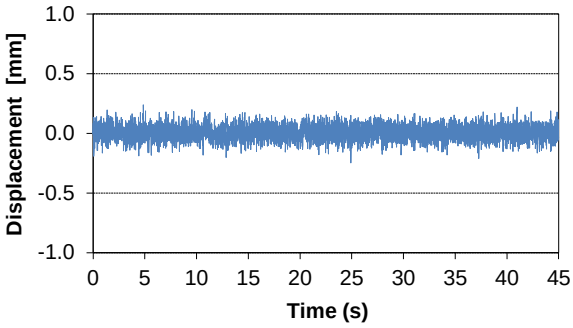

Figure AI. 13 - Channel LVDT_SD_GLW06Y_L

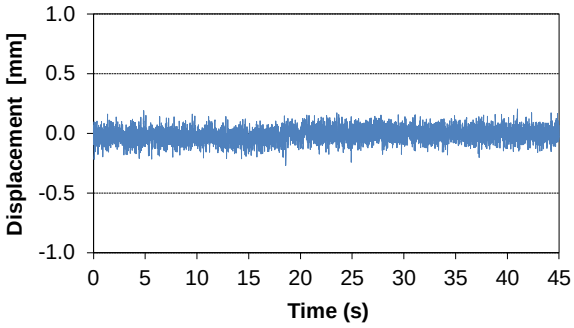

Figure AI. 14 - Channel LVDT_SD_GLW06Y_R

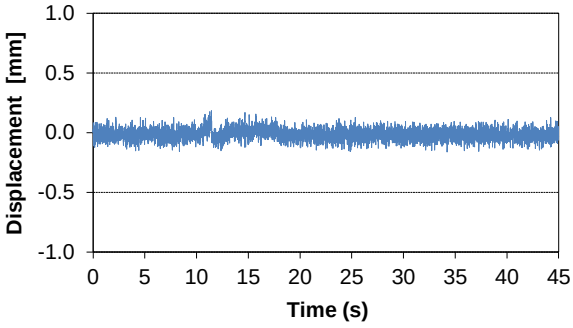

Figure AI. 15 - Channel LVDT_SD_GLW07X_L

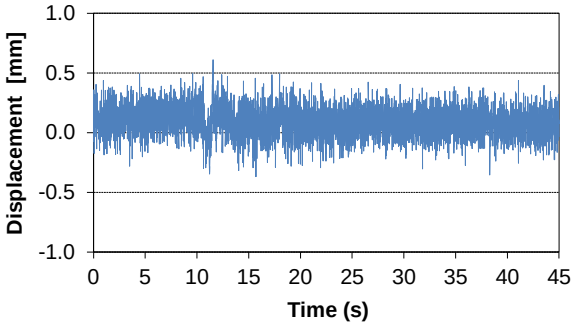

Figure AI. 16 - Channel LVDT_SD_GLW07X_R

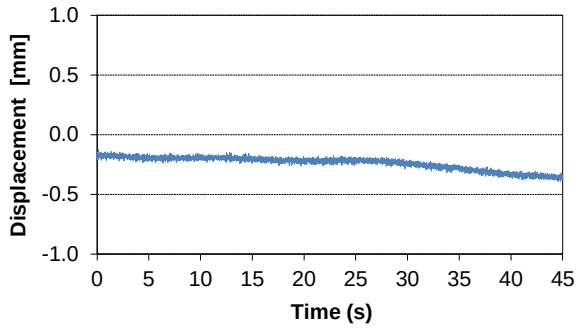

Figure AI. 17 - Channel LVDT_SD_GLW02Y_L

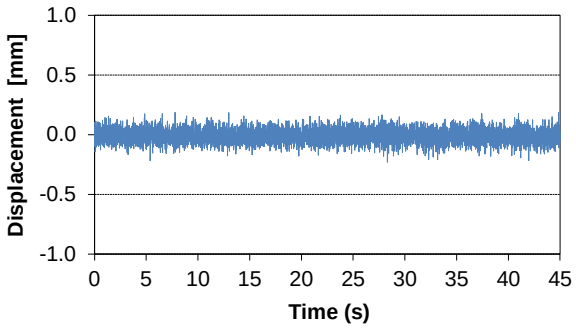

Figure AI. 18 - Channel LVDT_SD_GLW01Y_R

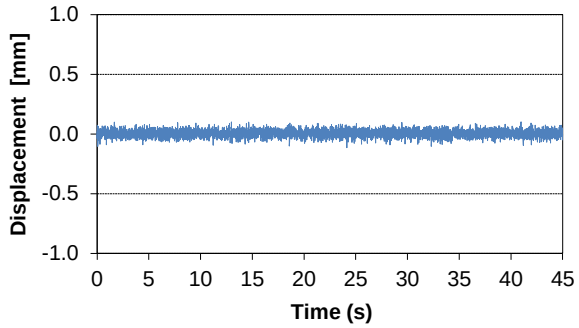

Figure AI. 19 - Channel LVDT_SD_GLW04X_L

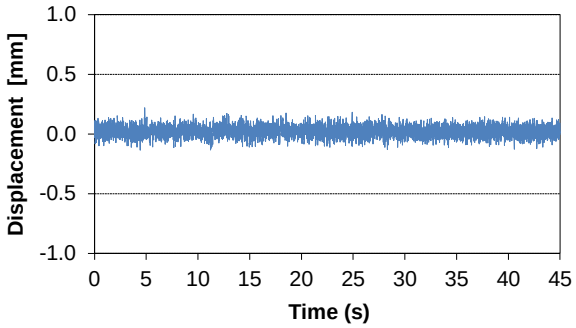

Figure AI. 20 - Channel LVDT_SD_GLW04X_R

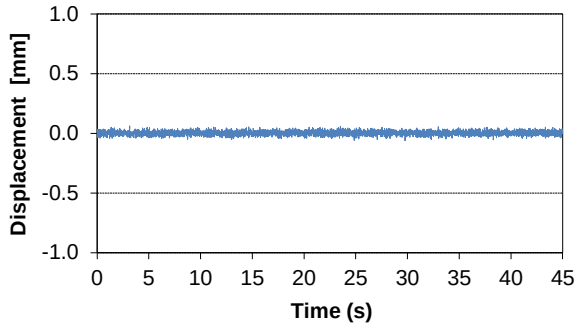

Figure AI. 21 - Channel LVDT_ID_GL_X

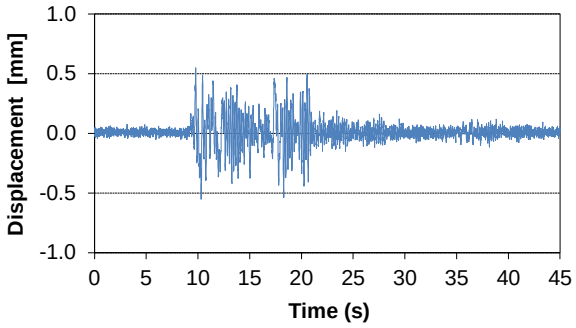

Figure AI. 22 - Channel LVDT_ID_GL_Y

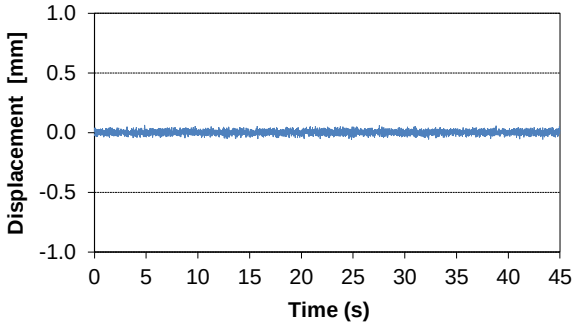

Figure AI. 23 - Channel LVDT_ID_L1_X

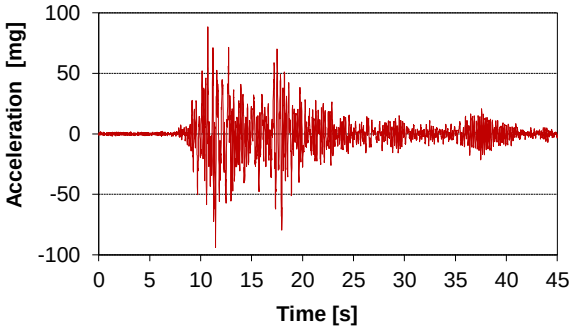

Figure AI. 24 - Channel ACC_L1_C3_X_NE_T

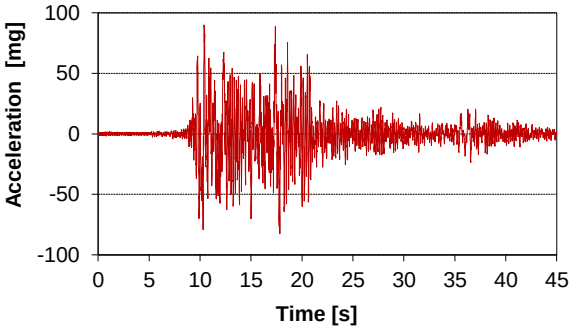

Figure AI. 25 - Channel ACC_L1_C3_Y_NE_L

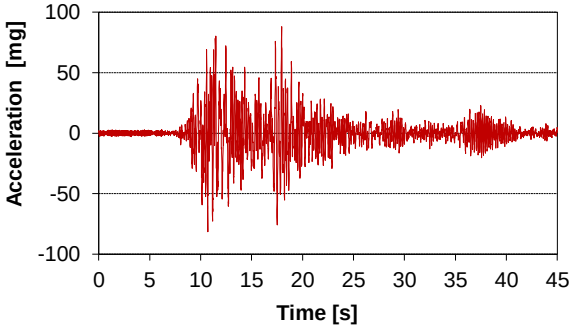

Figure AI. 26 - Channel ACC_L1_A1_X_SW_T

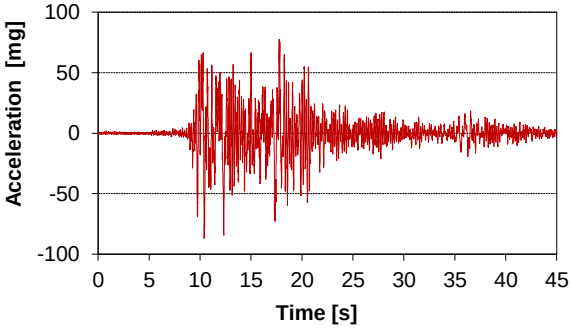

Figure AI. 27 - Channel ACC_L1_A1_Y_SW_L

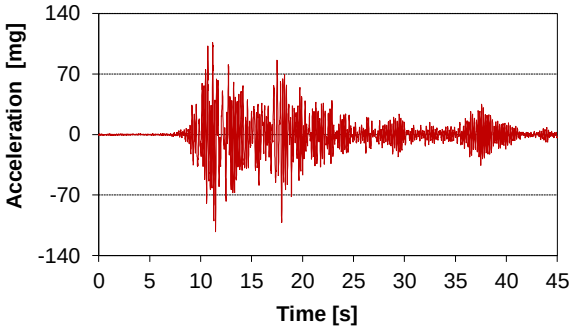

Figure AI. 28 - Channel ACC_RL_C3_X_NE_T

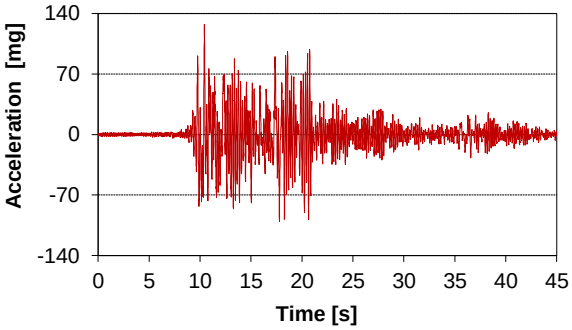

Figure AI. 29 - Channel ACC_RL_C3_Y_NE_L

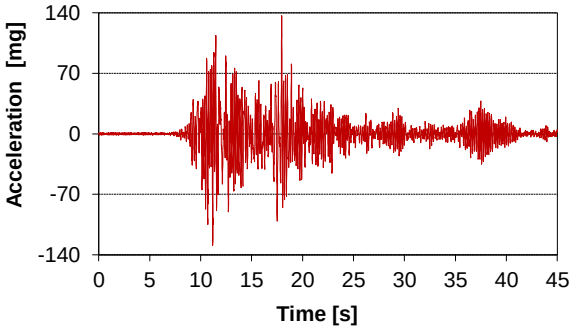

Figure AI. 30 - Channel ACC_RL_A1_X_SW_T

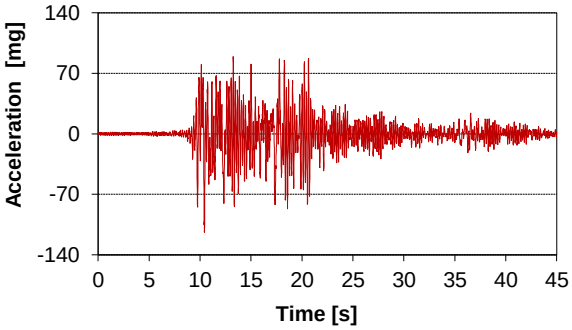

Figure AI. 31 - Channel ACC_RL_A1_Y_SW_L

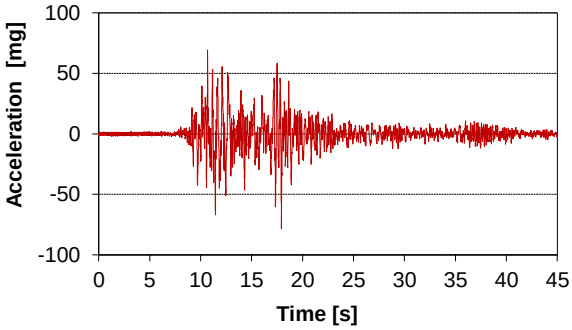

Figure AI. 32 - Channel ACC_GL_A3_X_SE_T

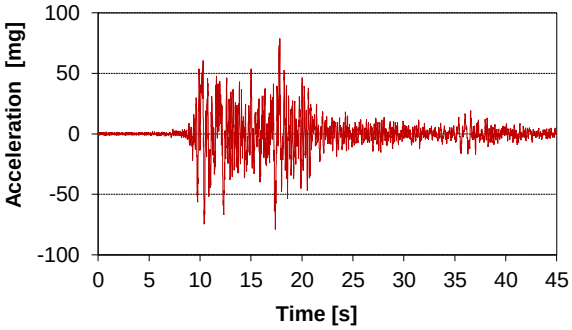

Figure AI. 33 - Channel ACC_GL_A3_Y_SE_L

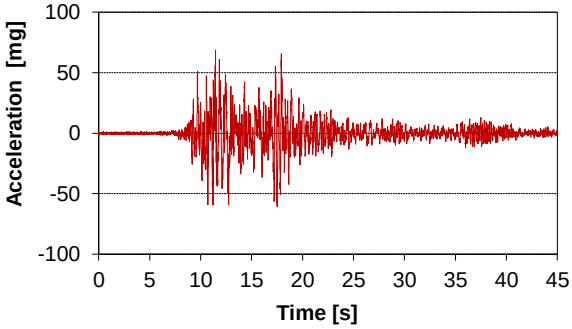

Figure AI. 34 - Channel ACC_GL_C1_X_NW_T

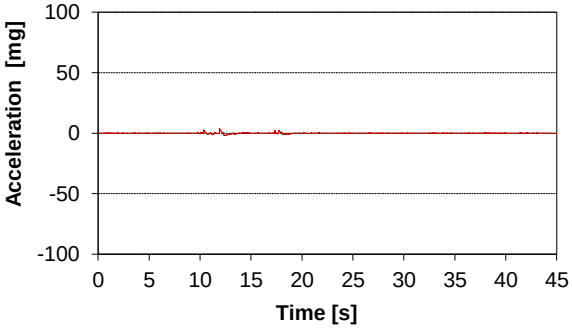

Figure AI. 35 - Channel ACC_GL_C1_Y_NW_L

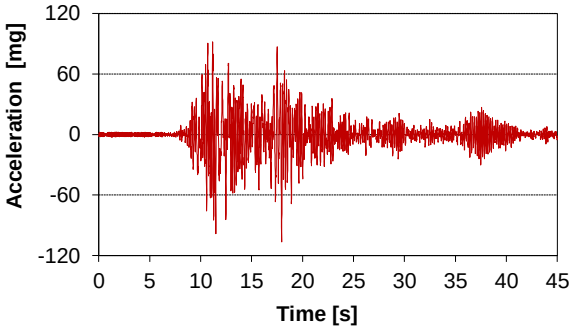

Figure AI. 36 - Channel ACC_L1_A3_X_SE_T

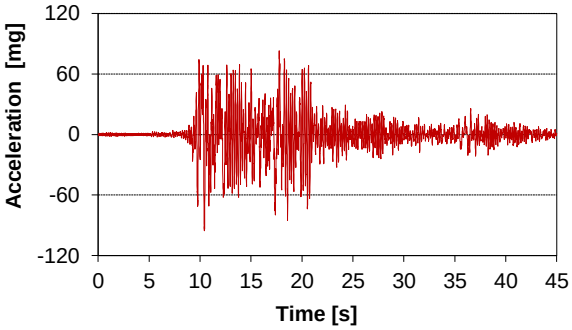

Figure AI. 37 - Channel ACC_L1_A3_Y_SE_L

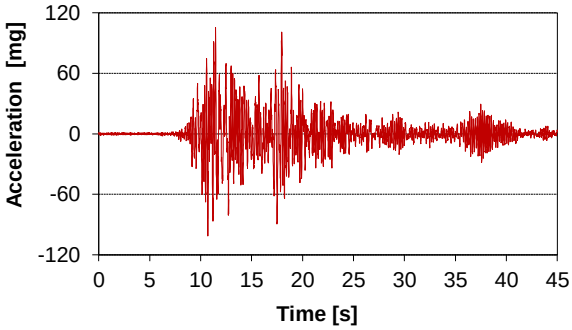

Figure AI. 38 - Channel ACC_L1_C1_X_NW_T

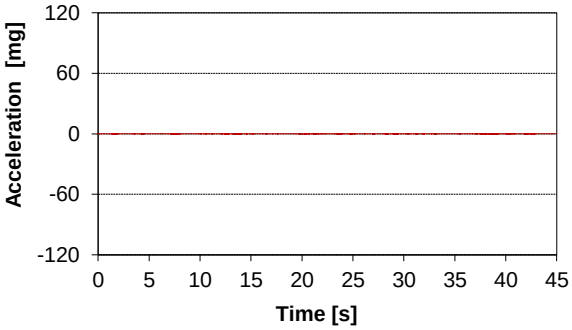

Figure AI. 39 - Channel ACC_L1_C1_Y_NW_L

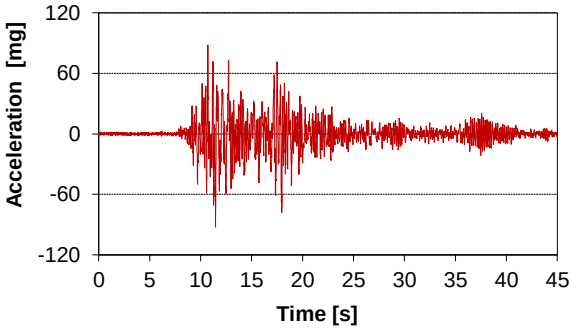

Figure AI. 40 - Channel ACC_L1_C2_X_N_T

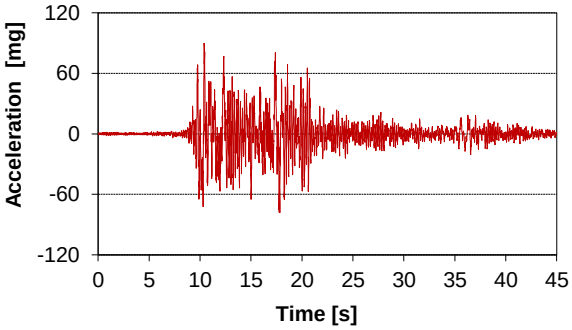

Figure AI. 41 - Channel ACC_L1_C2_Y_N_L

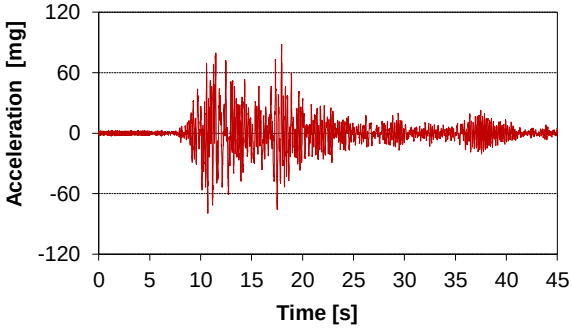

Figure AI. 42 - Channel ACC_L1_A2_X_S_T

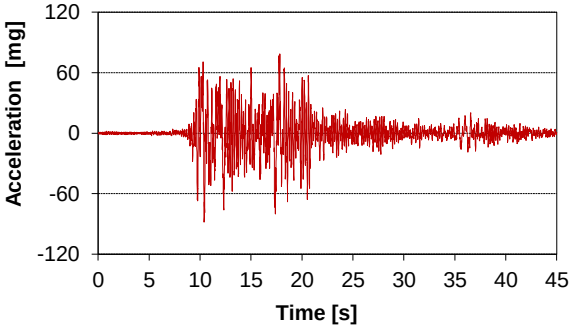

Figure AI. 43 - Channel ACC_L1_A2_Y_S_L

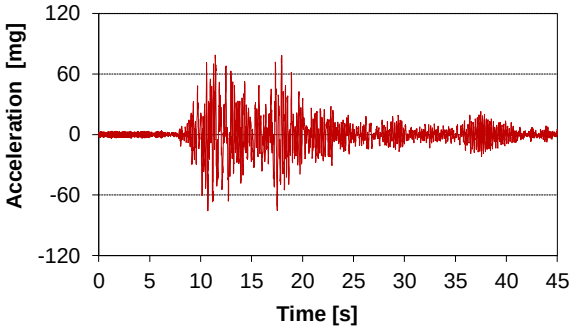

Figure AI. 44 - Channel ACC_L1_B1_X_W_T

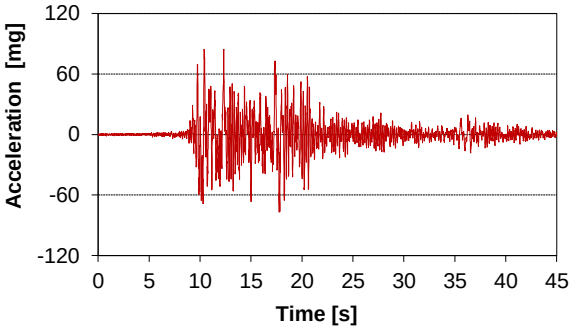

Figure AI. 45 - Channel ACC_L1_B1_Y_W_L

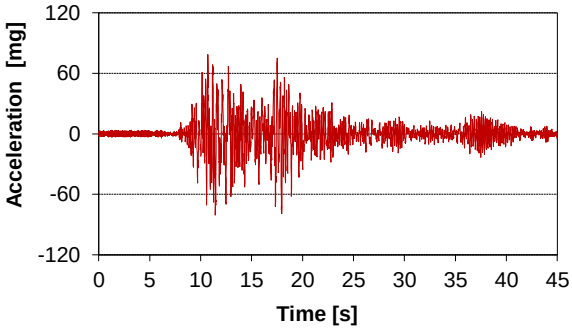

Figure AI. 46 - Channel ACC_L1_B2_X_I_T

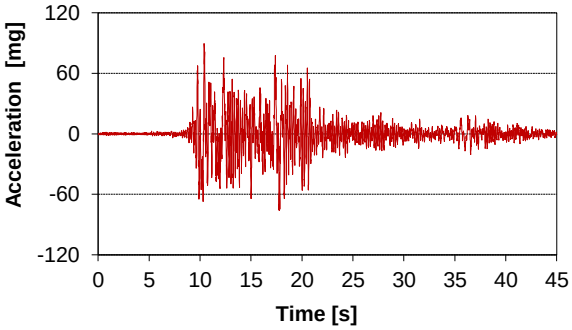

Figure AI. 47 - Channel ACC_L1_B2_Y_I_L

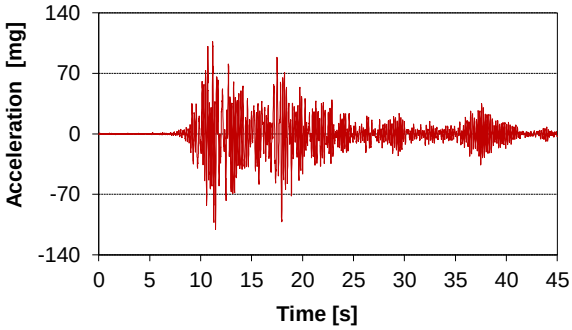

Figure AI. 48 - Channel ACC_RL_C2_X_N_T

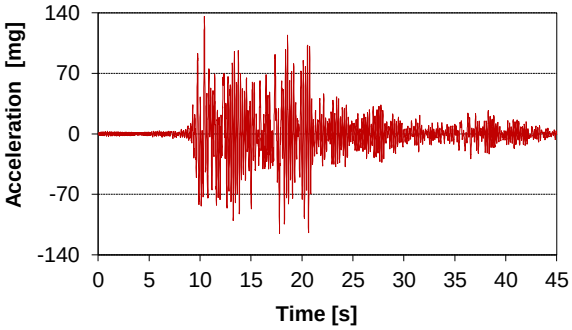

Figure AI. 49 - Channel ACC_RL_C2_Y_N_L

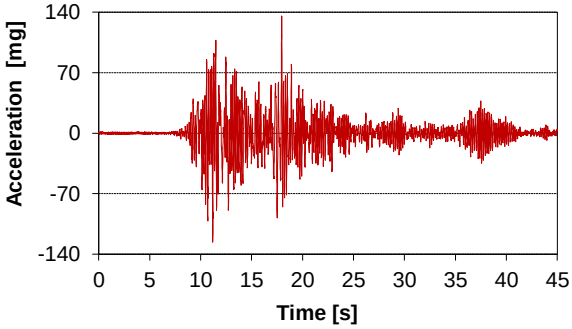

Figure AI. 50 - Channel ACC_RL_A2_X_S_T

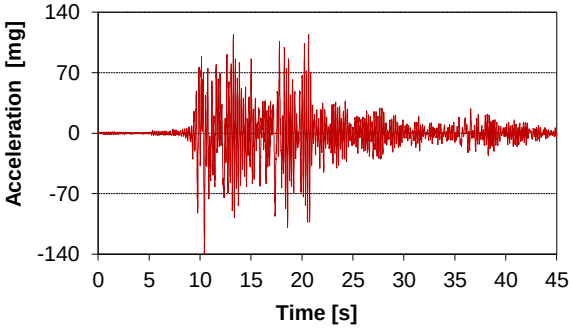

Figure AI. 51 - Channel ACC_RL_A2_Y_S_L

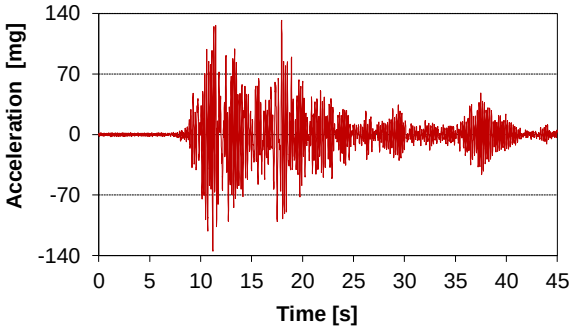

Figure AI. 52 - Channel ACC_RL_B1_X_W_T

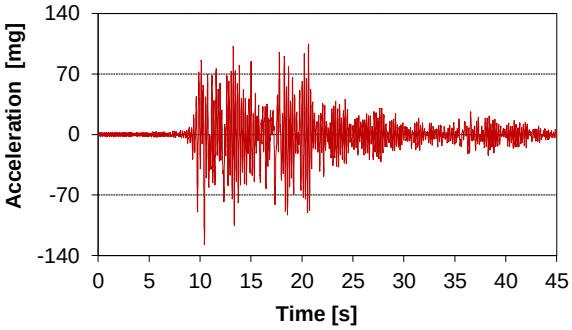

Figure AI. 53 - Channel ACC_RL_B1_Y_W_L

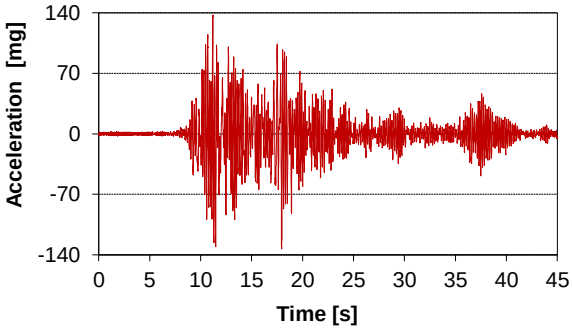

Figure AI. 54 - Channel ACC_RL_B2_X_I_T

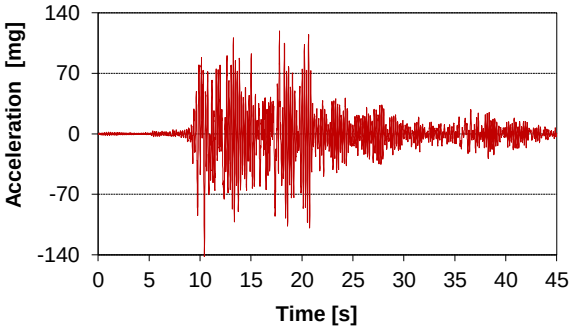

Figure AI. 55 - Channel ACC_RL_B2_Y_I_L

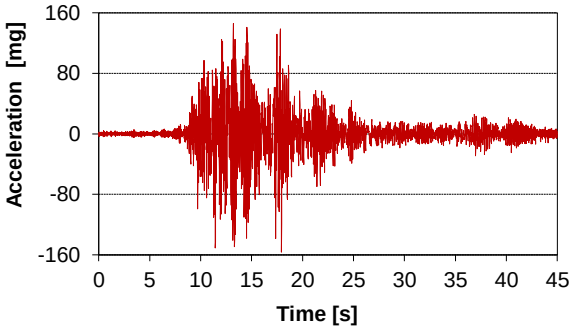

Figure AI. 56 - Channel ACC_GLW03Y_I_T

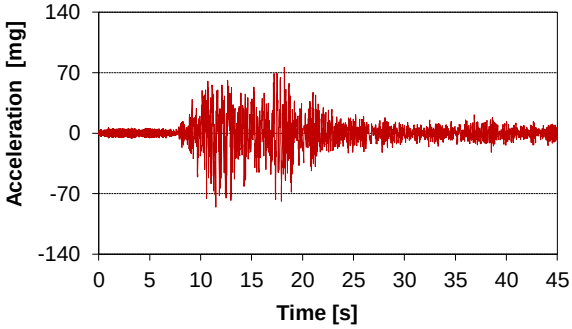

Figure AI. 57 - Channel ACC_GLW04Y_I_T

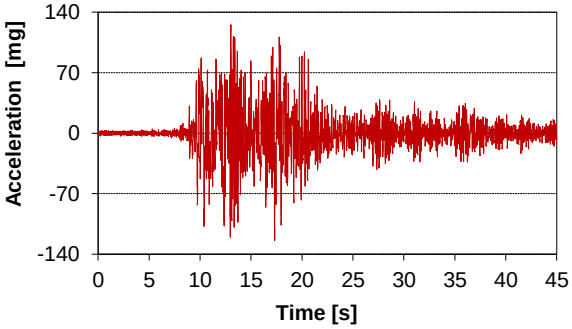

Figure AI. 58 - Channel ACC_GLW04X_I_L

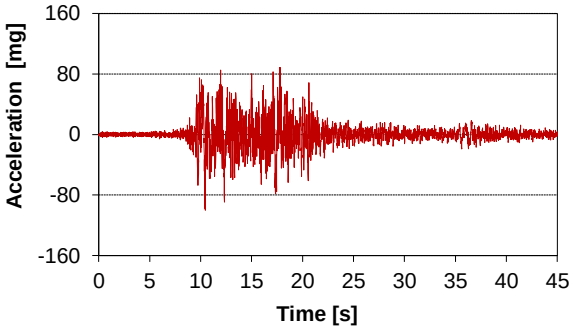

Figure AI. 59 - Channel ACC_GLW05X_I_L

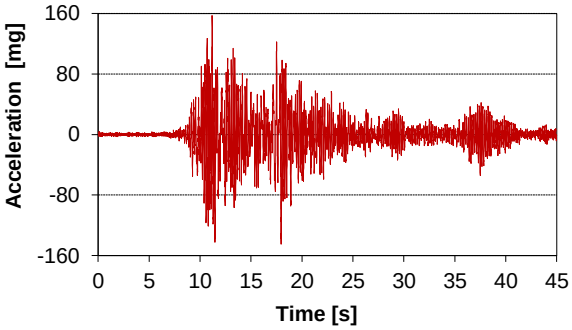

Figure AI. 60 - Channel ACC_L1W03Y_I_T

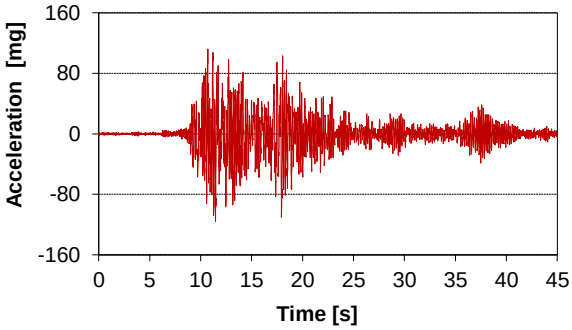

Figure AI. 61 - Channel ACC_L1W04Y_I_T

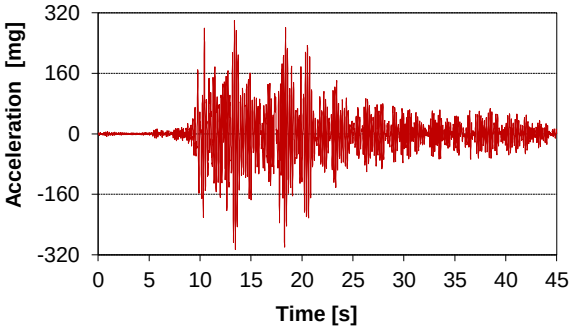

Figure AI. 62 - Channel ACC_L1W04X_I_L

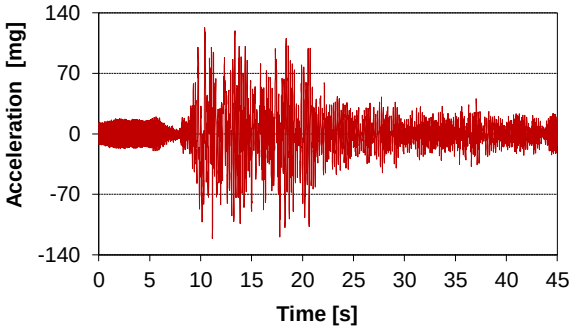

Figure AI. 63 - Channel ACC_L1W05X_I_L

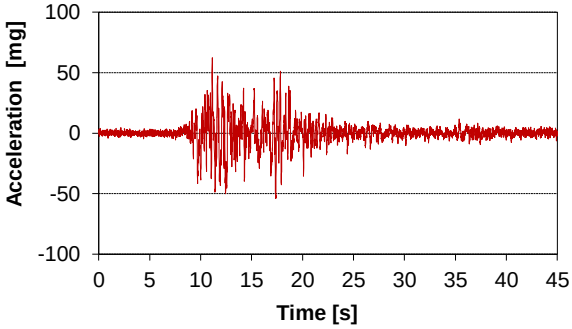

Figure AI. 64 - Channel ACC MESA TRANS

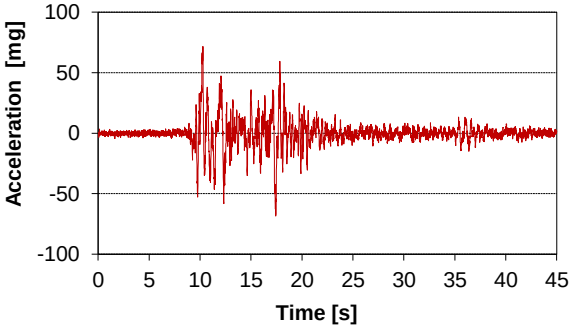

Figure AI. 65 - Channel ACC MESA LONG

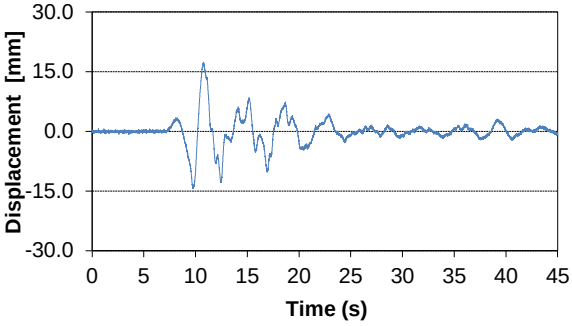

Figure AI. 66 - Channel DISP MESA TRANS

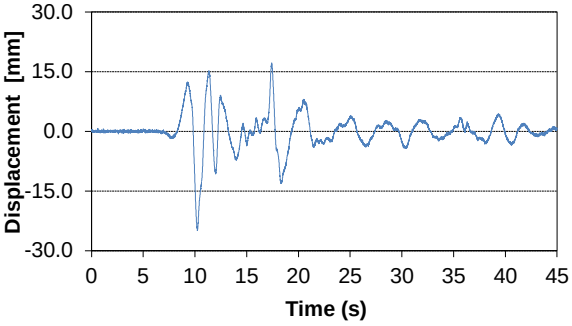

Figure AI. 67 - Channel DISP MESA LONG

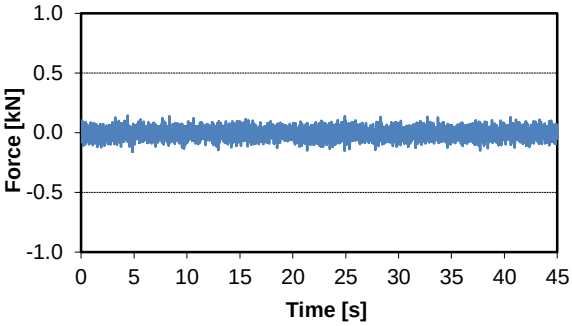

Figure AI. 68 - Channel CF_HD_GLW06Y_L

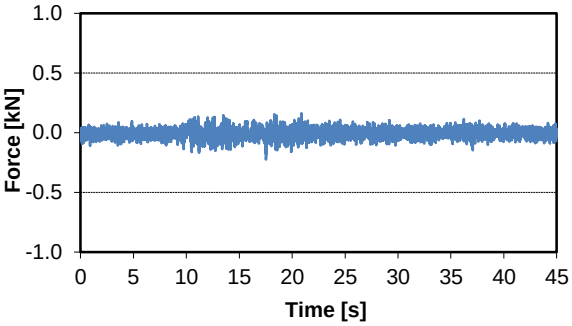

Figure AI. 69 - Channel CF_HD_GLW06X_R

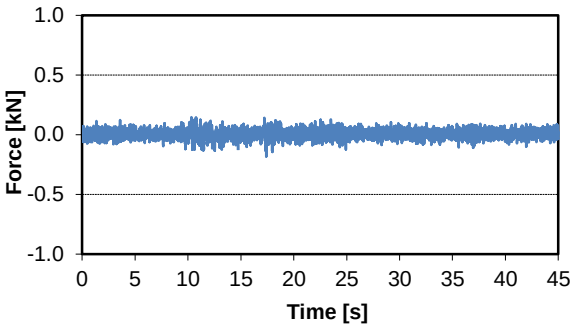

Figure AI. 70 - Channel CF_HD_GLW07X_L

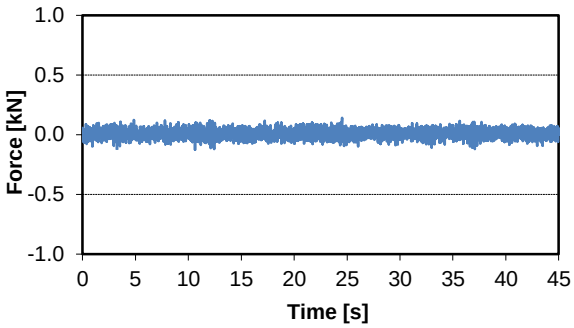

Figure AI. 71 - Channel CF_HD_GLW07X_R

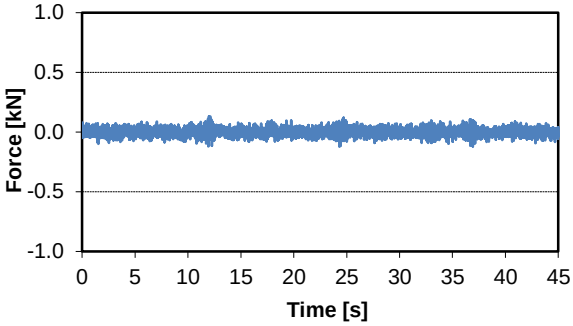

Figure AI. 72 - Channel CF_HD_GLW02Y_L

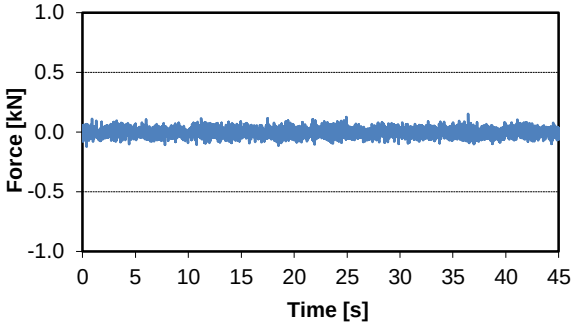

Figure AI. 73 - Channel CF_HD_GLW01Y_R

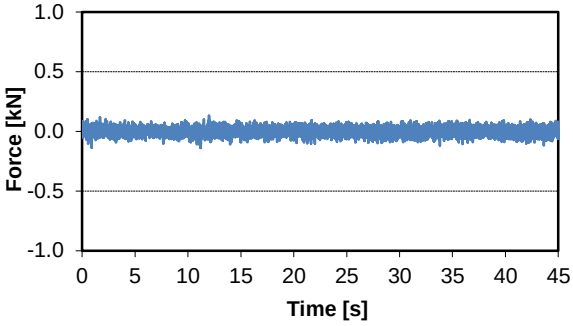

Figure AI. 74 - Channel CF_HD_GLW04X_L

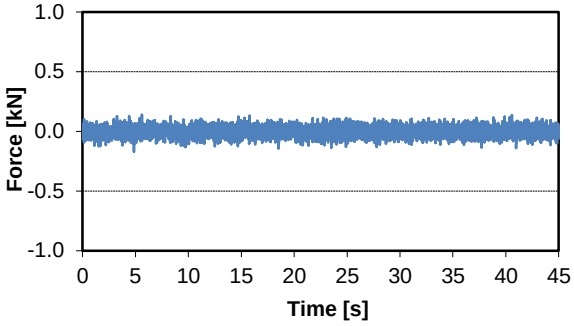

Figure AI. 75 - Channel CF_HD_GLW04X_R

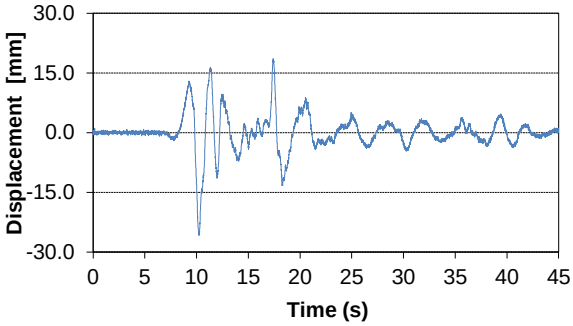

Figure AI. 76 - Channel H_RL_C1_NW_L

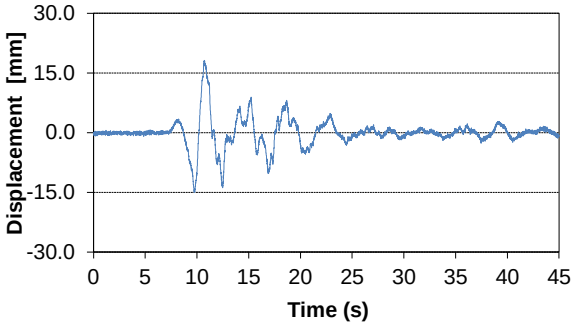

Figure AI. 77 - Channel H_RL_C1_NW_T

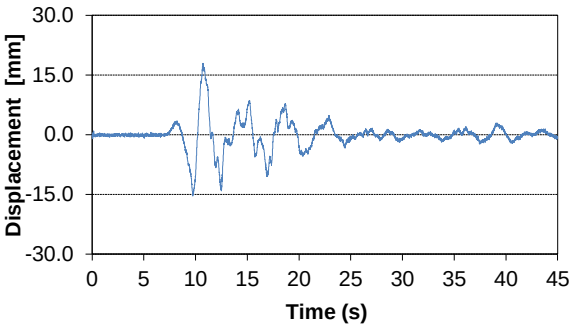

Figure AI. 78 - Channel H_L1RL_C1_NW_T

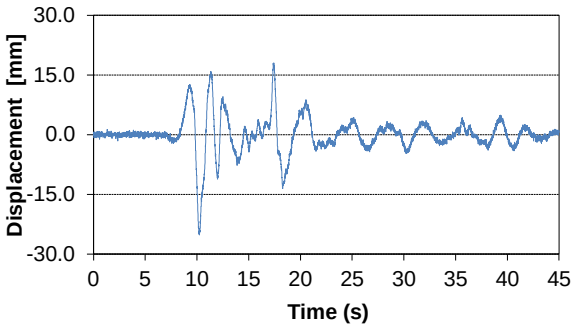

Figure AI. 79 - Channel H_L1RL_C1_NW_L

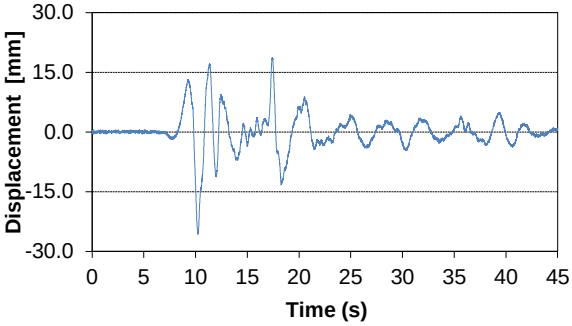

Figure AI. 80 - Channel H_L1_C1_NW_L

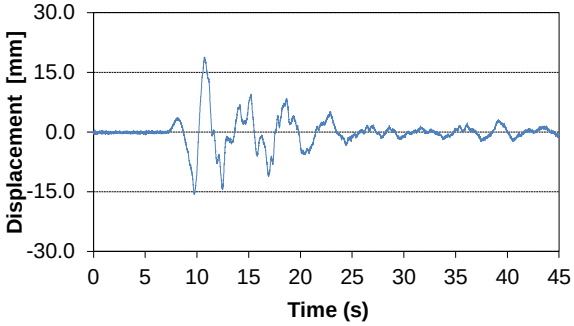

Figure AI. 81 - Channel H_L1_C1_NW_T

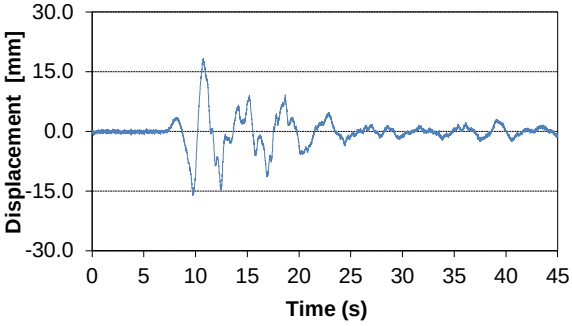

Figure AI. 82 - Channel H_GLL1_C1_NW_T

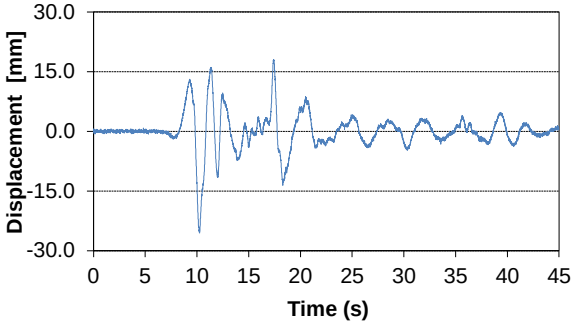

Figure AI. 83 - Channel H_GLL1_C1_NW_L

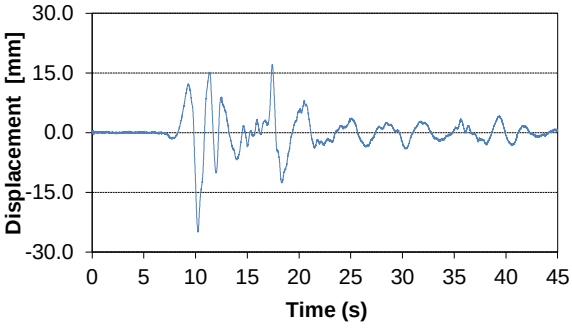

Figure AI. 84 - Channel H_GL_C1_NW_L

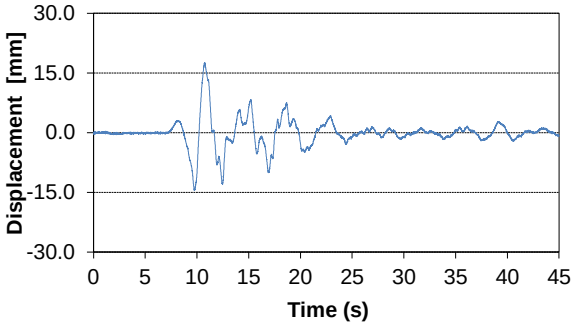

Figure AI. 85 - Channel H_GL_C1_NW_T

Seismic test – TEST_09

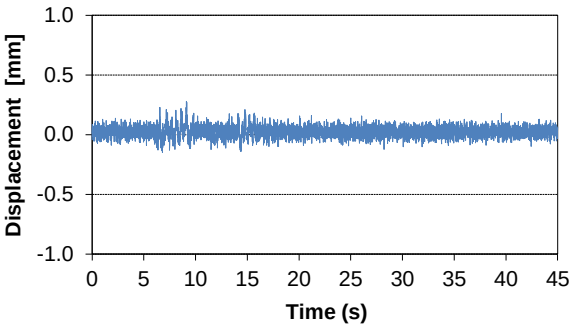

Figure AI. 86 – Channel LVDT_WU_GLW06Y_L

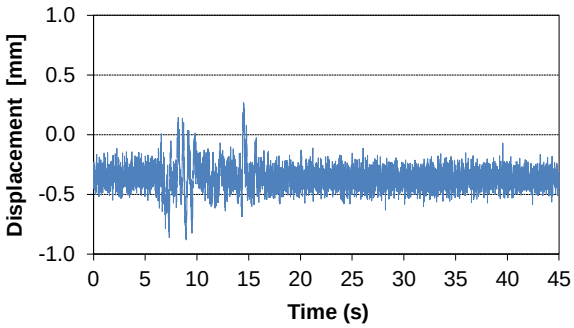

Figure AI. 87 - Channel LVDT_WU_GLW06Y_R

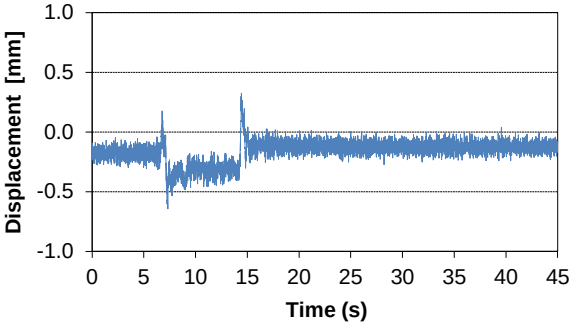

Figure AI. 88 - Channel LVDT_WU_GLW07X_L

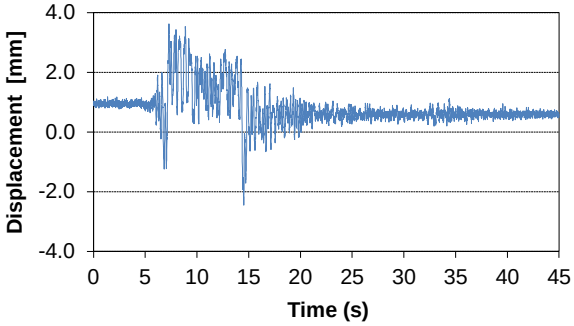

Figure AI. 89 - Channel LVDT_WU_GLW07X_R

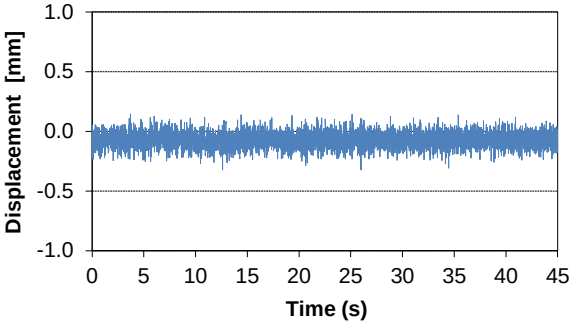

Figure AI. 90 - Channel LVDT_WU_GLW02Y_L

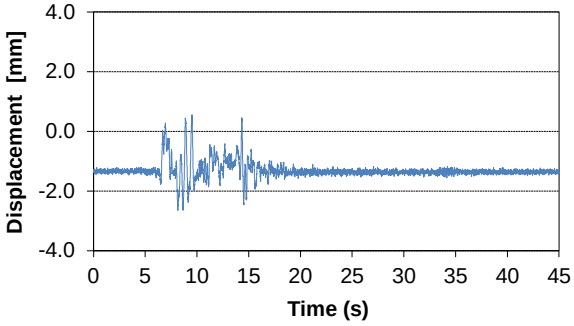

Figure AI. 91 - Channel LVDT_WU_GLW01Y_R

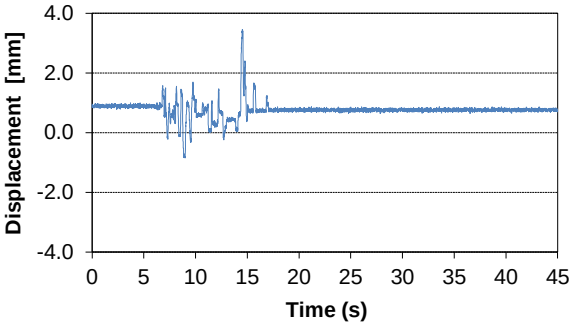

Figure AI. 92 - Channel LVDT_WU_GLW04X_L

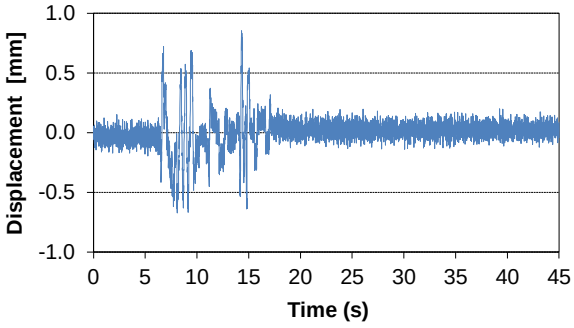

Figure AI. 93 - Channel LVDT_WU_GLW04X_R

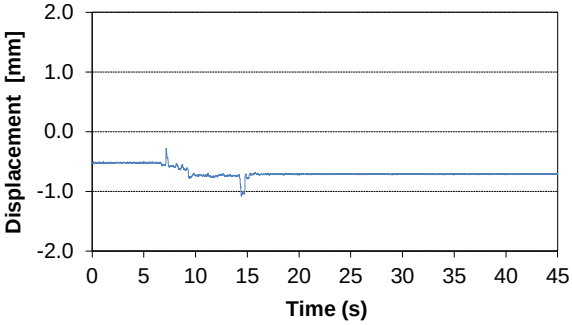

Figure AI. 94 - Channel LVDT_WS_GLW06Y

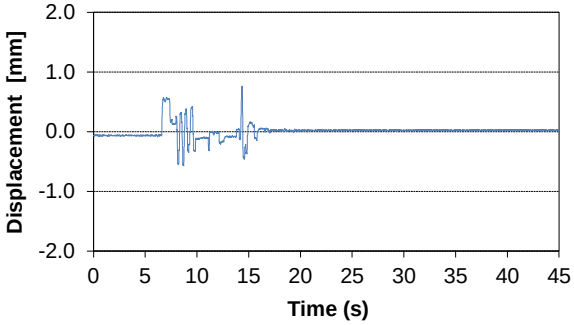

Figure AI. 95 - LVDT_WS_GLW07X

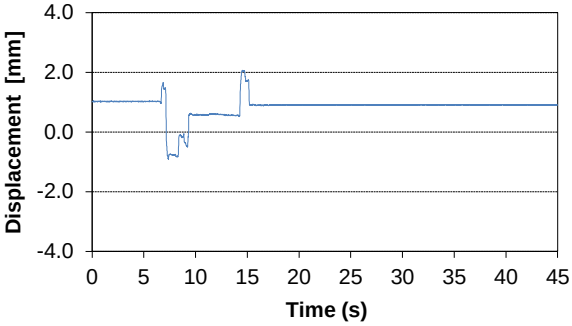

Figure AI. 96 - Channel LVDT_WS_GLW02Y

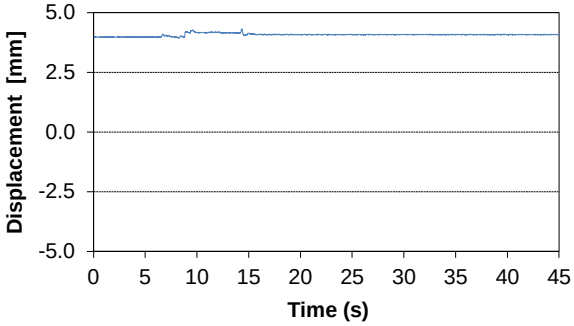

Figure AI. 97 - Channel LVDT_WS_GLW04X

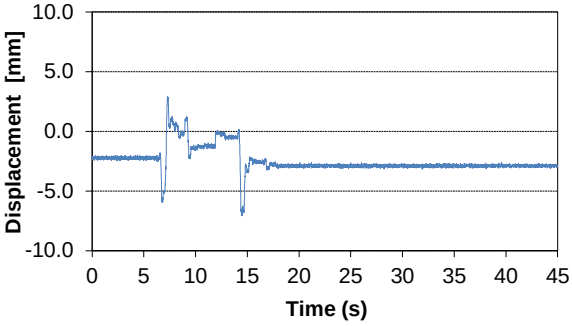

Figure AI. 98 - Channel LVDT_SD_GLW06Y_L

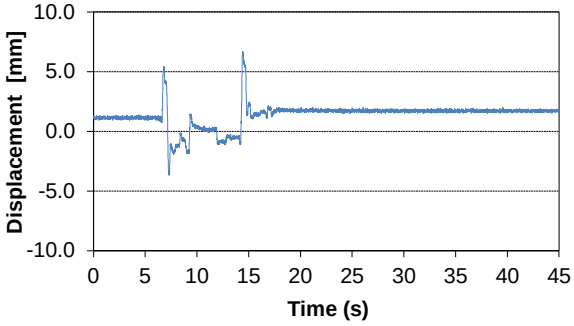

Figure AI. 99 - Channel LVDT_SD_GLW06Y_R

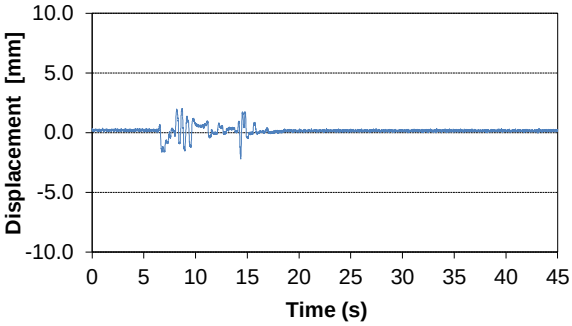

Figure AI. 100 - Channel LVDT_SD_GLW07X_L

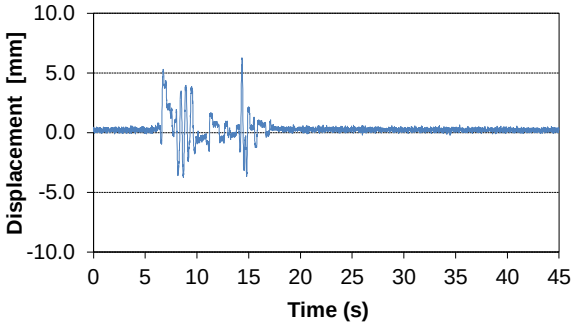

Figure AI. 101 - Channel LVDT_SD_GLW07X_R

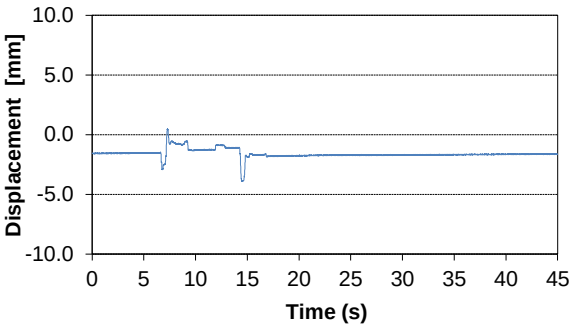

Figure AI. 102 - Channel LVDT_SD_GLW02Y_L

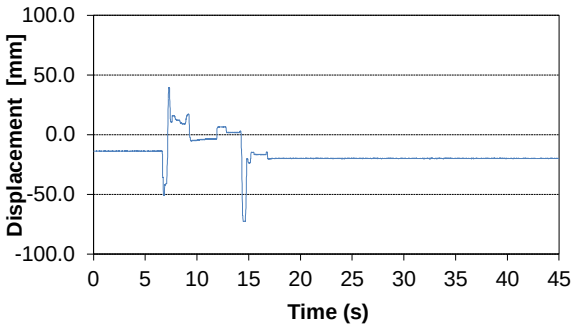

Figure AI. 103 - Channel LVDT_SD_GLW01Y_R

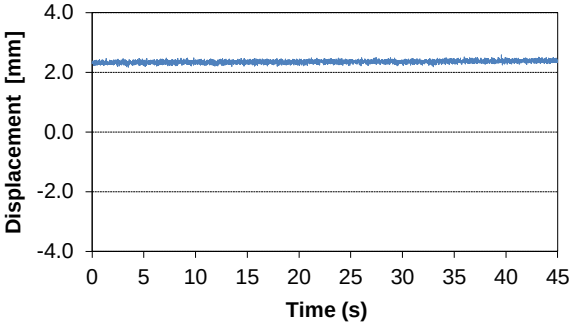

Figure AI. 104 - Channel LVDT_SD_GLW04X_L

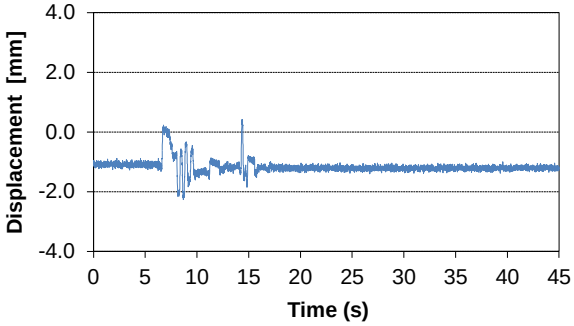

Figure AI. 105 - Channel LVDT_SD_GLW04X_R

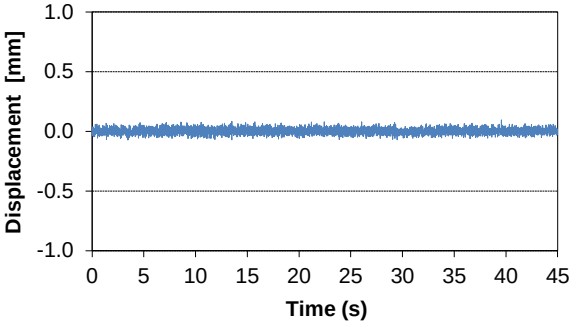

Figure AI. 106 - Channel LVDT_ID_GL_X

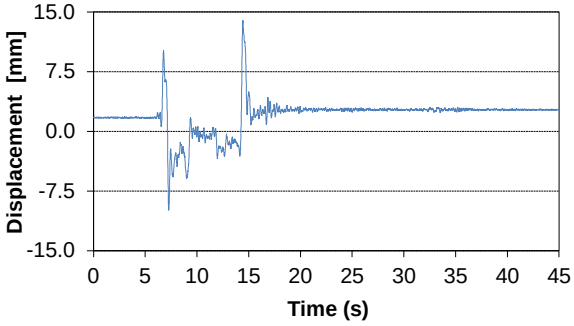

Figure AI. 107 - Channel LVDT_ID_GL_Y

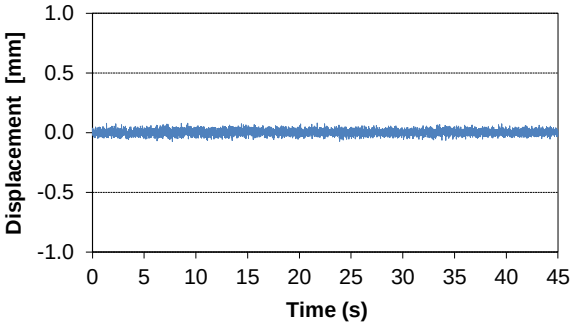

Figure AI. 108 - Channel LVDT_ID_L1_X

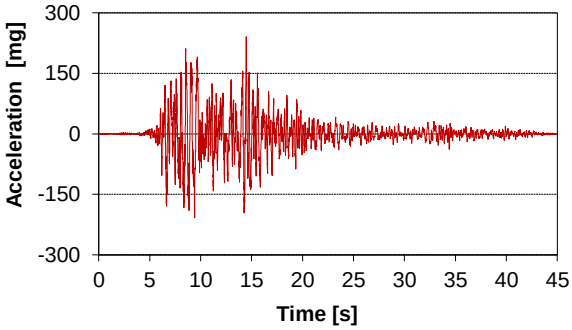

Figure AI. 109 - Channel ACC_L1_C3_X_NE_T

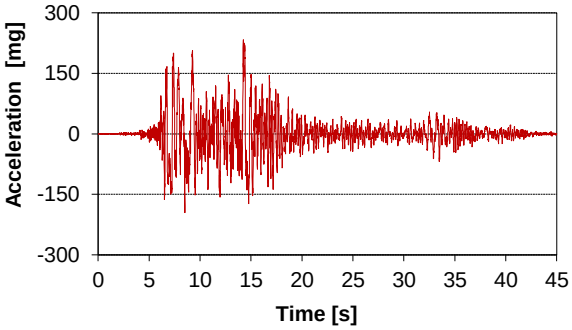

Figure AI. 110 - Channel ACC_L1_C3_Y_NE_L

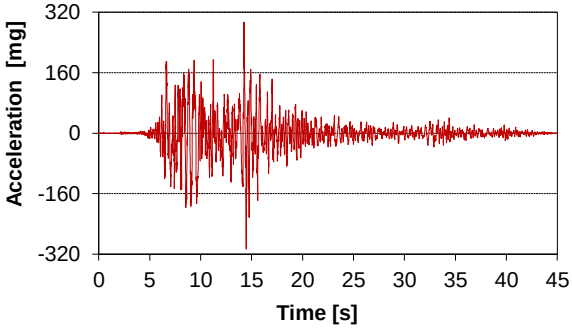

Figure AI. 111 - Channel ACC_L1_A1_X_SW_T

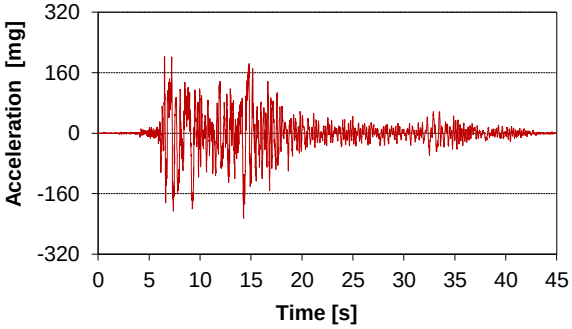

Figure AI. 112 - Channel ACC_L1_A1_Y_SW_L

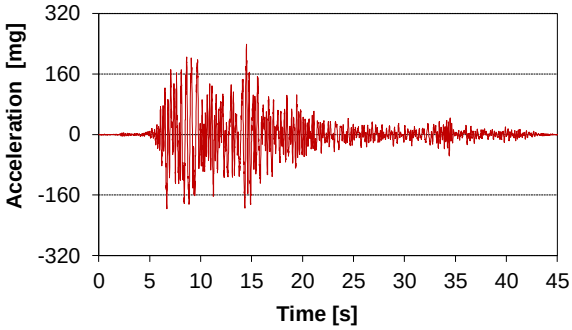

Figure AI. 113 - Channel ACC_RL_C3_X_NE_T

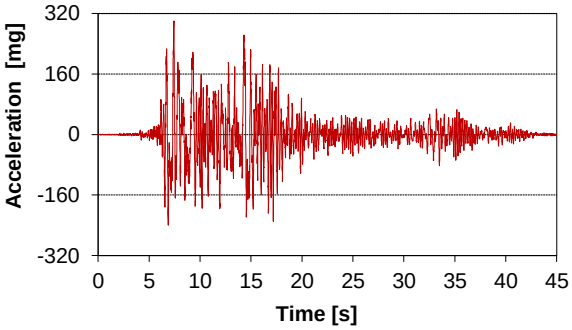

Figure AI. 114 - Channel ACC_RL_C3_Y_NE_L

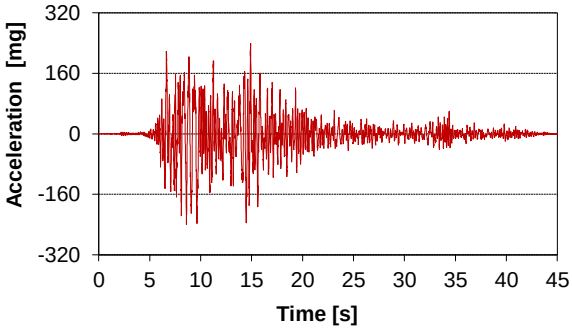

Figure AI. 115 - Channel ACC_RL_A1_X_SW_T

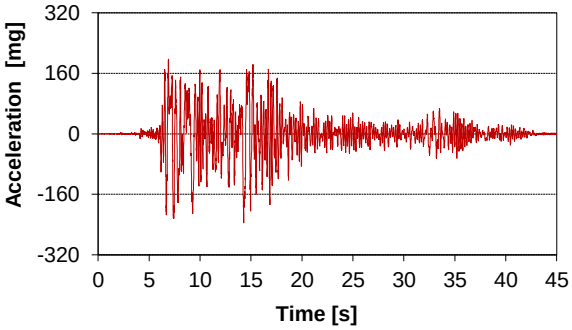

Figure AI. 116 - Channel ACC_RL_A1_Y_SW_L

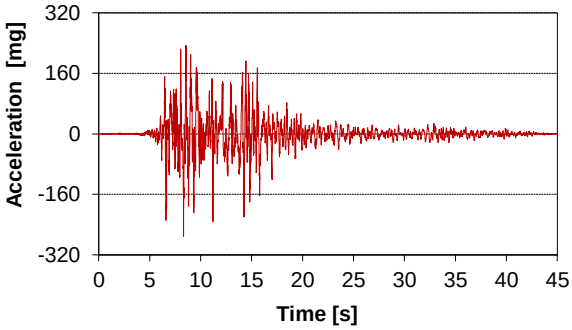

Figure AI. 117 - Channel ACC_GL_A3_X_SE_T

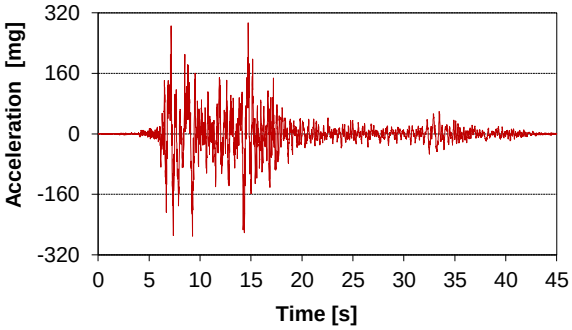

Figure AI. 118 - Channel ACC_GL_A3_Y_SE_L

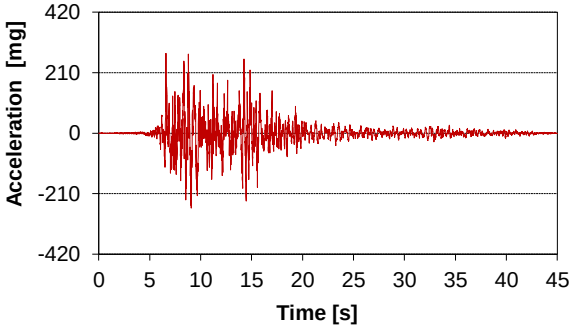

Figure AI. 119 - Channel ACC_GL_C1_X_NW_T

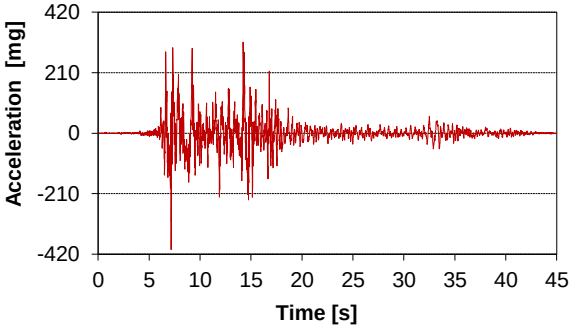

Figure AI. 120 - Channel ACC_GL_C1_Y_NW_L

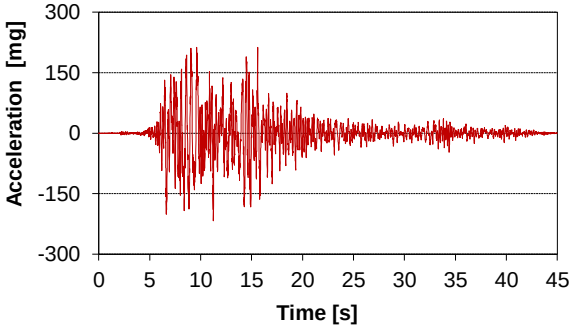

Figure AI. 121 - Channel ACC_L1_A3_X_SE_T

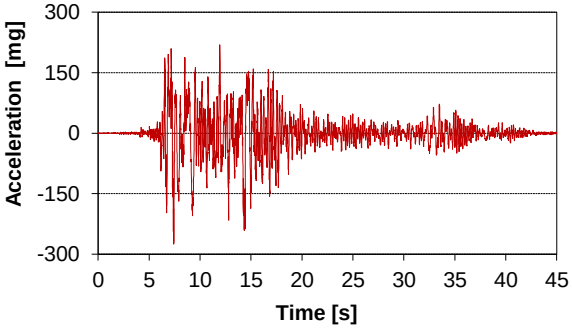

Figure AI. 122 - Channel ACC_L1_A3_Y_SE_L

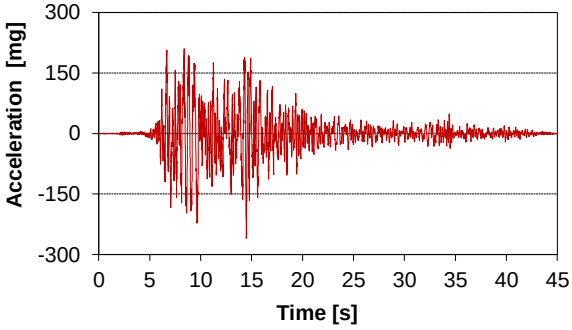

Figure AI. 123 - Channel ACC_L1_C1_X_NW_T

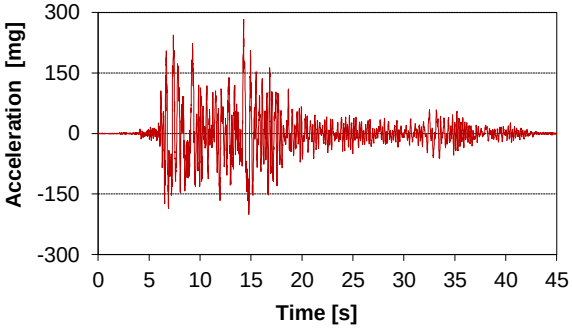

Figure AI. 124 - Channel ACC_L1_C1_Y_NW_L

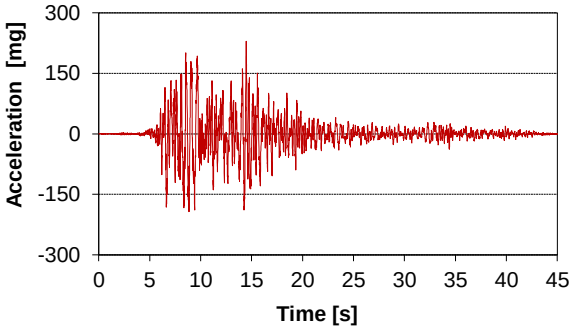

Figure AI. 125 - Channel ACC_L1_C2_X_N_T

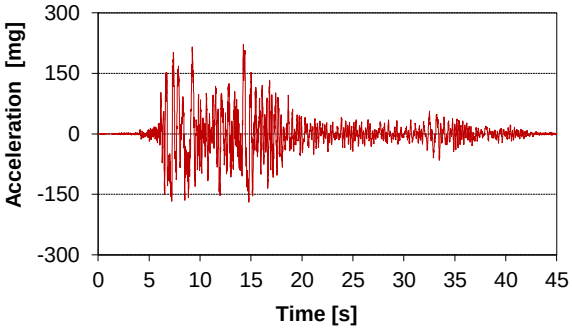

Figure AI. 126 - Channel ACC_L1_C2_Y_N_L

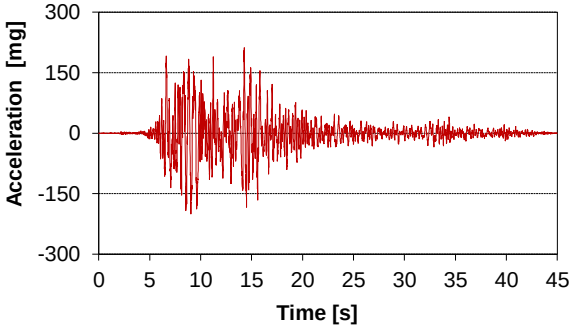

Figure AI. 127 - Channel ACC_L1_A2_X_S_T

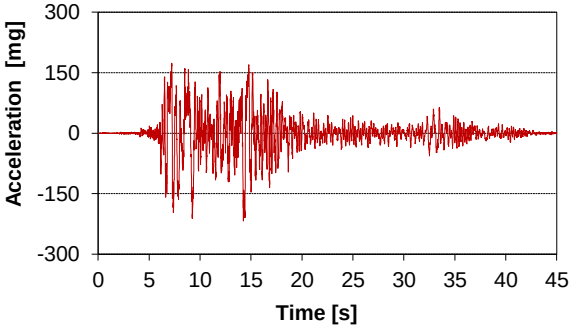

Figure AI. 128 - Channel ACC_L1_A2_Y_S_L

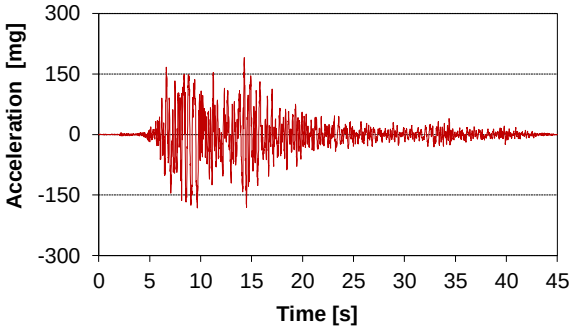

Figure AI. 129 - Channel ACC_L1_B1_X_W_T

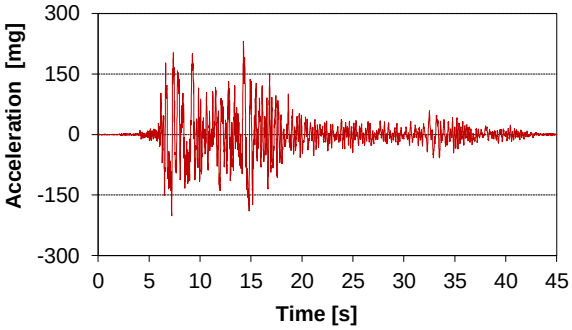

Figure AI. 130 - Channel ACC_L1_B1_Y_W_L

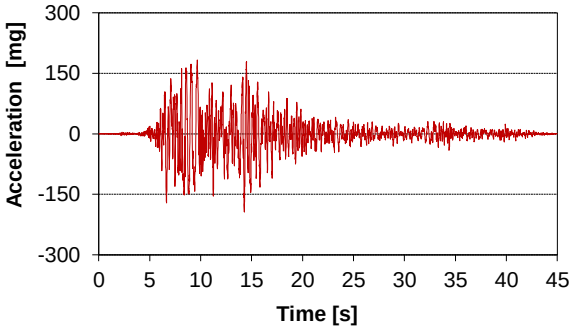

Figure AI. 131 - Channel ACC_L1_B2_X_I_T

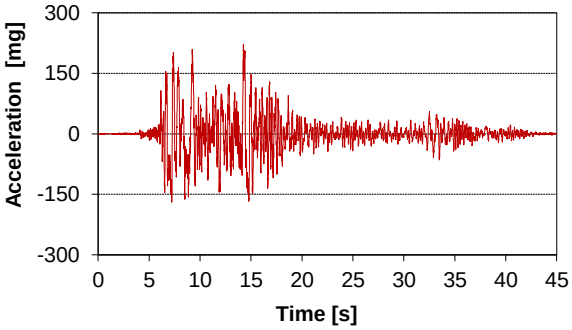

Figure AI. 132 - Channel ACC_L1_B2_Y_I_L

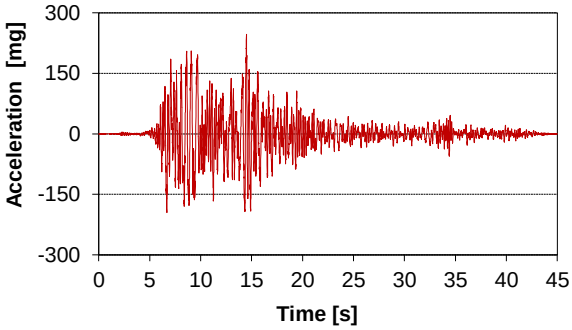

Figure AI. 133 - Channel ACC_RL_C2_X_N_T

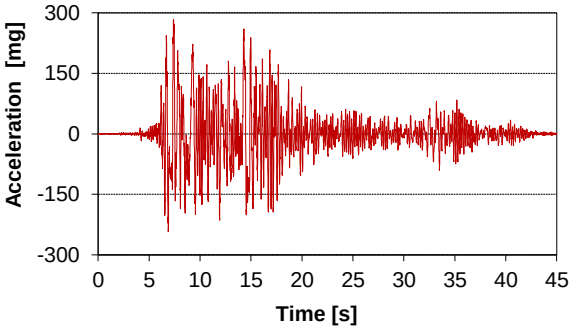

Figure AI. 134 - Channel ACC_RL_C2_Y_N_L

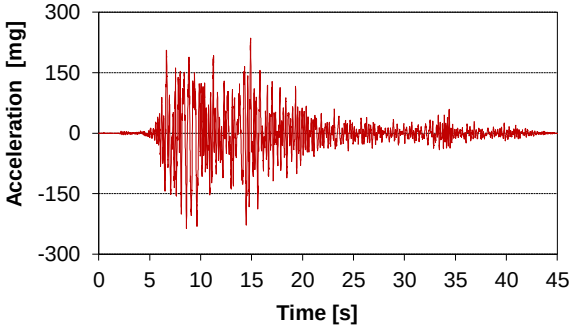

Figure AI. 135 - Channel ACC_RL_A2_X_S_T

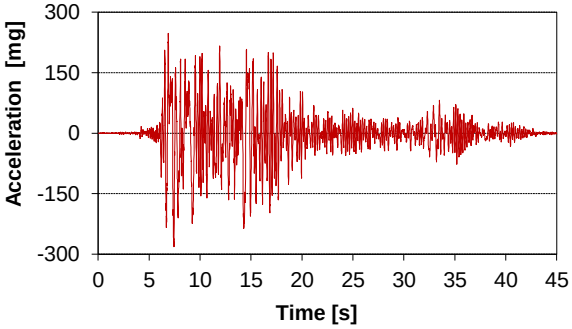

Figure AI. 136 - Channel ACC_RL_A2_Y_S_L

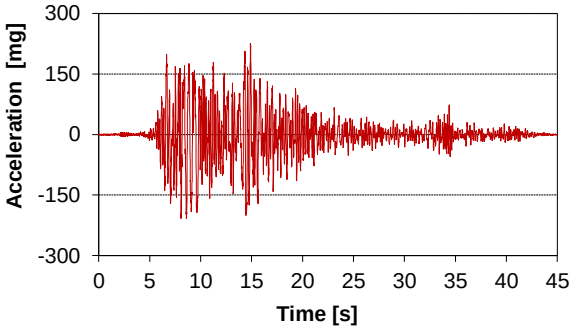

Figure AI. 137 - Channel ACC_RL_B1_X_W_T

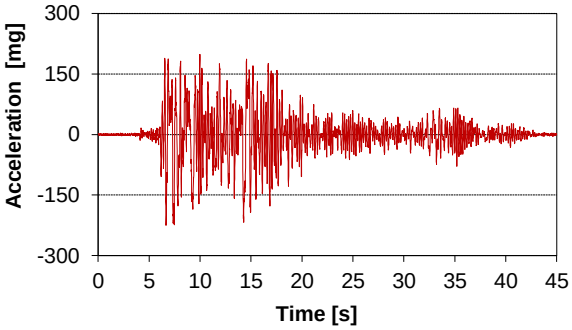

Figure AI. 138 - Channel ACC_RL_B1_Y_W_L

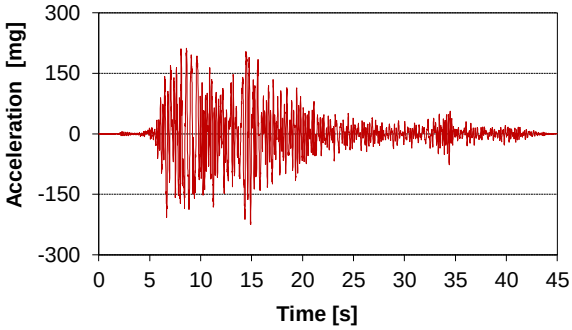

Figure AI. 139 - Channel ACC_RL_B2_X_I_T

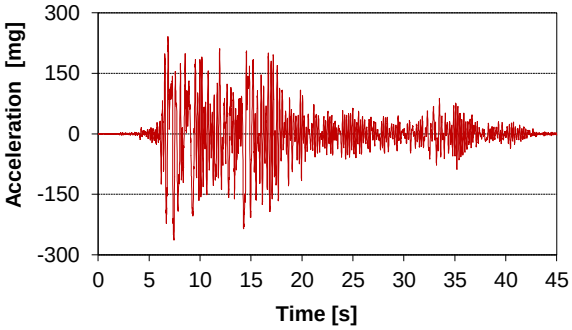

Figure AI. 140 - Channel ACC_RL_B2_Y_I_L

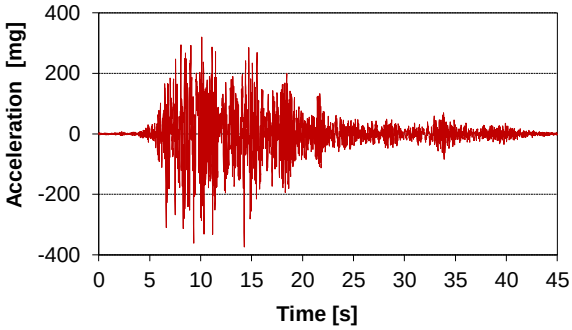

Figure AI. 141 - Channel ACC_GLW03Y_I_T

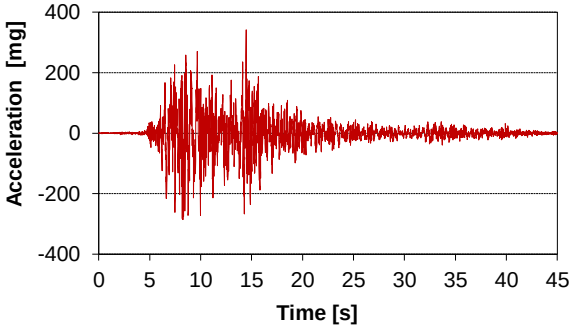

Figure AI. 142 - Channel ACC_GLW04Y_I_T

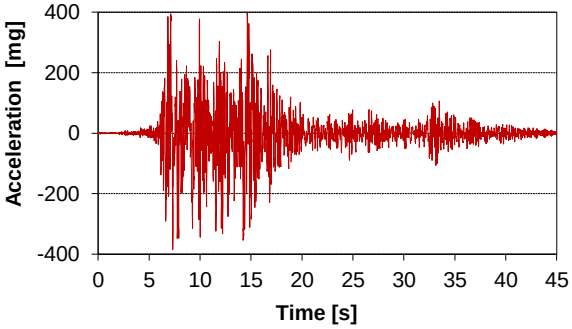

Figure AI. 143 - Channel ACC_GLW04X_I_L

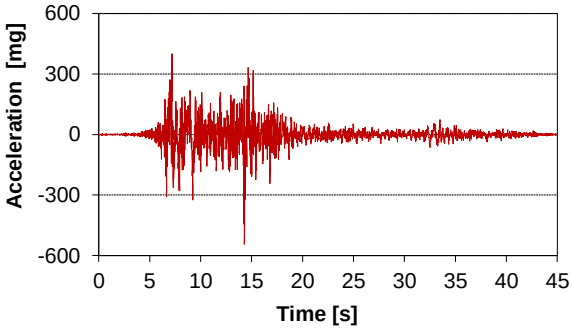

Figure AI. 144 - Channel ACC_GLW05X_I_L

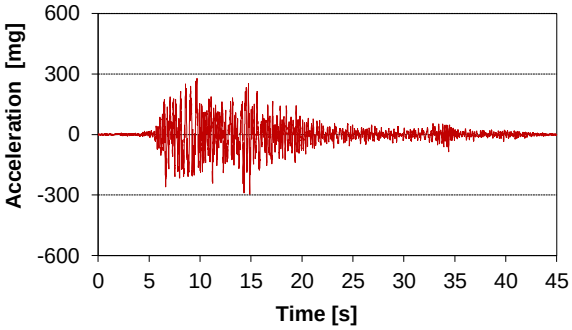

Figure AI. 145 - Channel ACC_L1W03Y_I_T

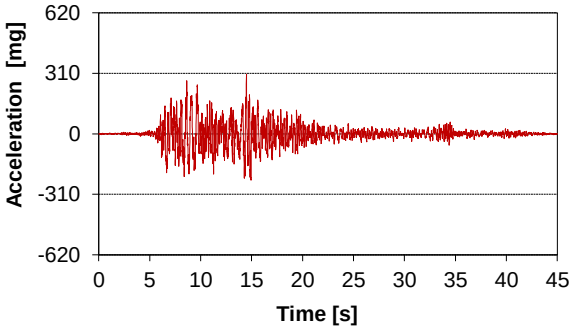

Figure AI. 146 - Channel ACC_L1W04Y_I_T

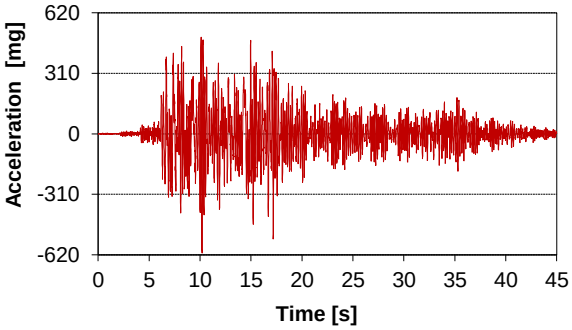

Figure AI. 147 - Channel ACC_L1W04X_I_L

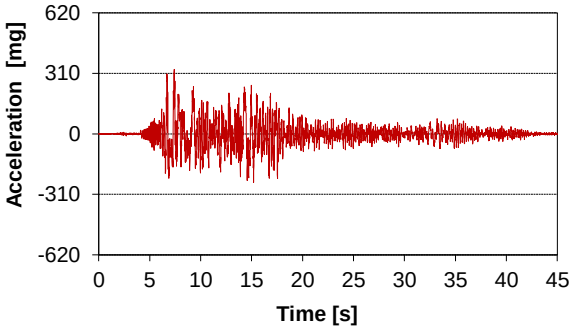

Figure AI. 148 - Channel ACC_L1W05X_I_L

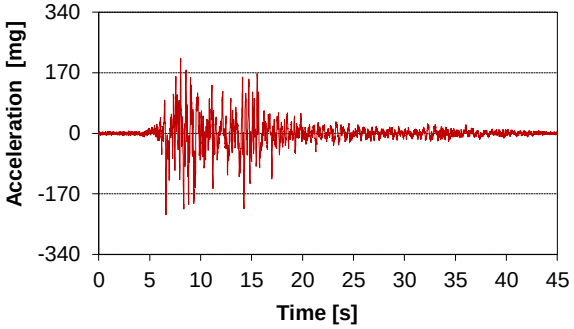

Figure AI. 149 - Channel ACC MESA TRANS

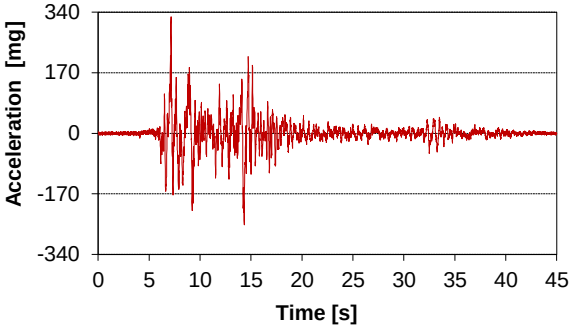

Figure AI. 150 - Channel ACC MESA LONG

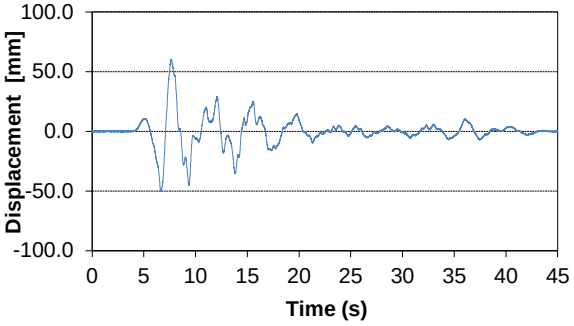

Figure AI. 151 - Channel DISP MESA TRANS

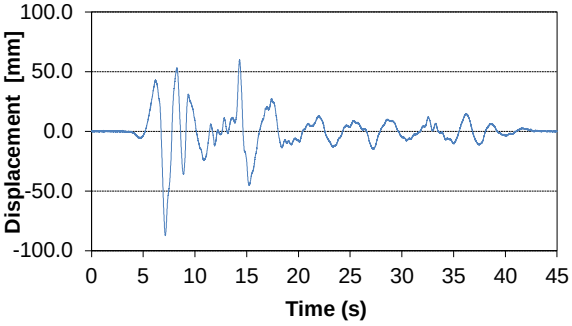

Figure AI. 152 - Channel DISP MESA LONG

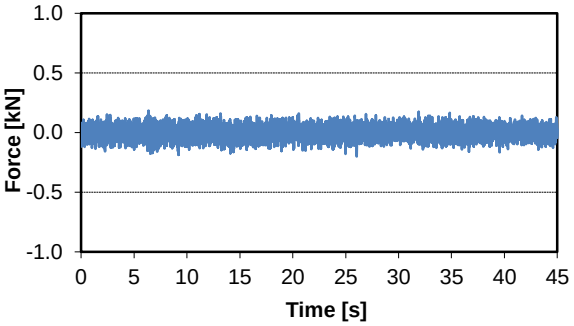

Figure AI. 153 - Channel CF_HD_GLW06Y_L

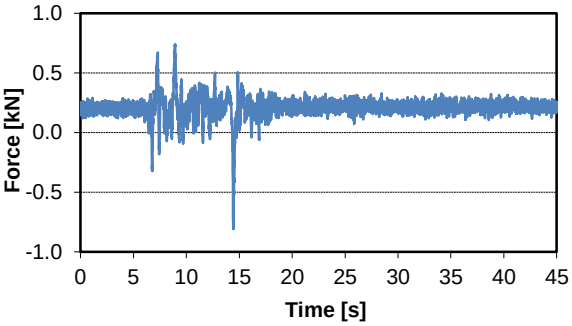

Figure AI. 154 - Channel CF_HD_GLW06X_R

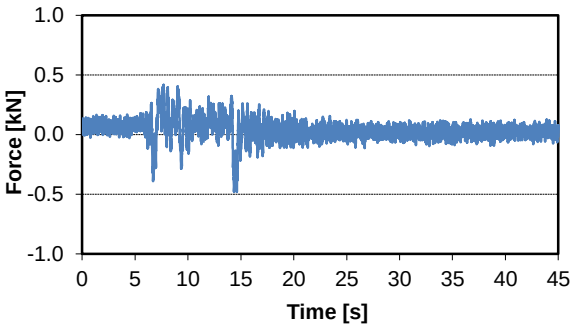

Figure AI. 155 - Channel CF_HD_GLW07X_L

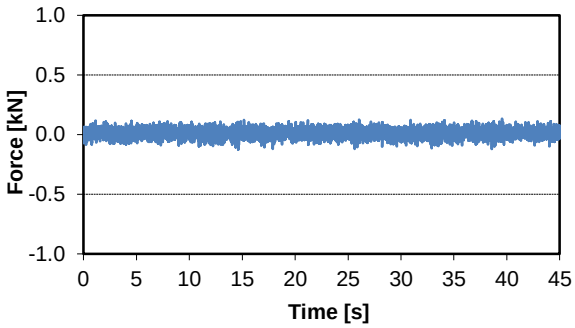

Figure AI. 156 - Channel CF_HD_GLW07X_R

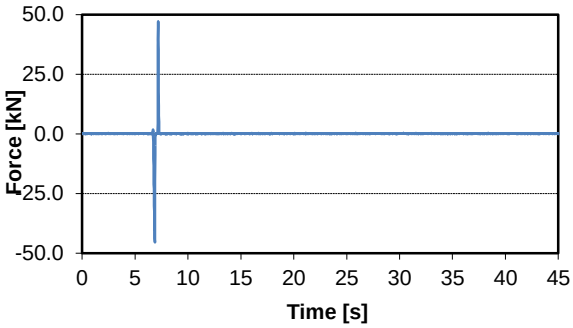

Figure AI. 157 - Channel CF_HD_GLW02Y_L

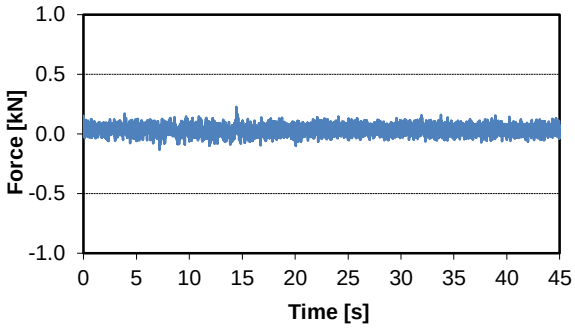

Figure AI. 158 - Channel CF_HD_GLW01Y_R

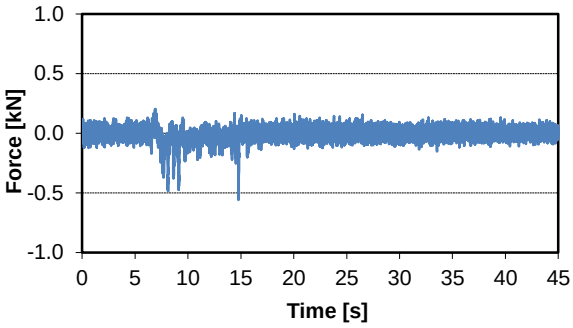

Figure AI. 159 - Channel CF_HD_GLW04X_L

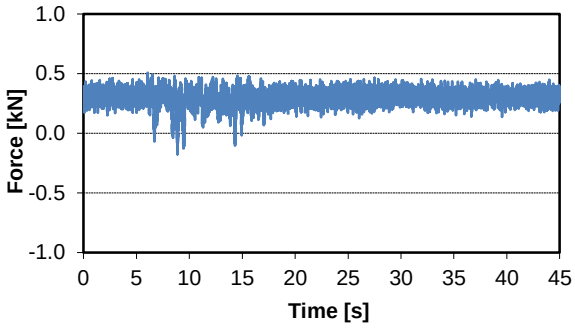

Figure AI. 160 - Channel CF_HD_GLW04X_R

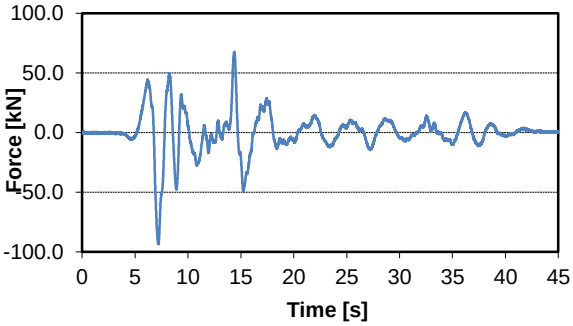

Figure AI. 161 - Channel H_RL_C1_NW_L

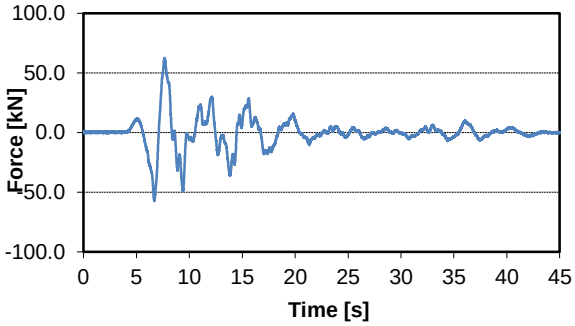

Figure AI. 162 - Channel H_RL_C1_NW_T

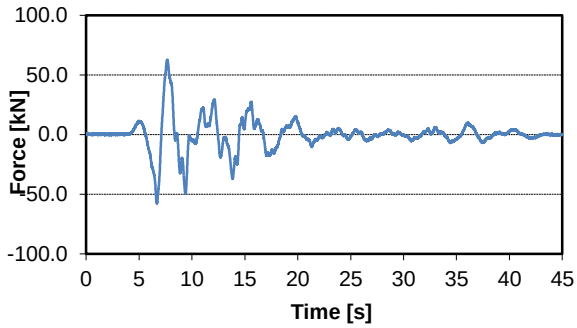

Figure AI. 163 - Channel H_L1RL_C1_NW_T

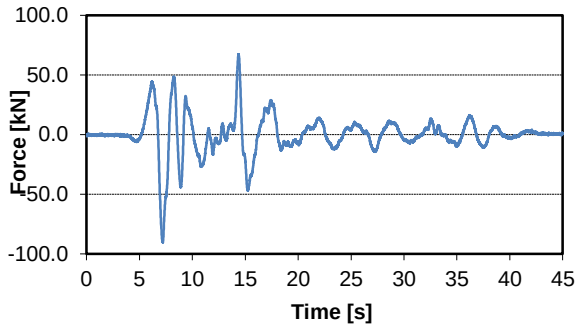

Figure AI. 164 - Channel H_L1RL_C1_NW_L

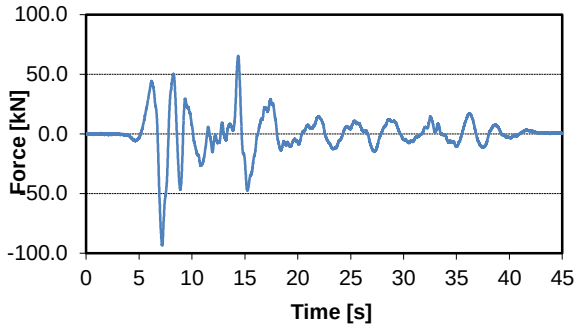

Figure AI. 165 - Channel H_L1_C1_NW_L

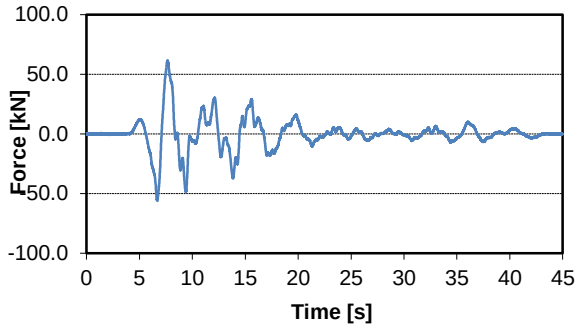

Figure AI. 166 - Channel H_L1_C1_NW_T

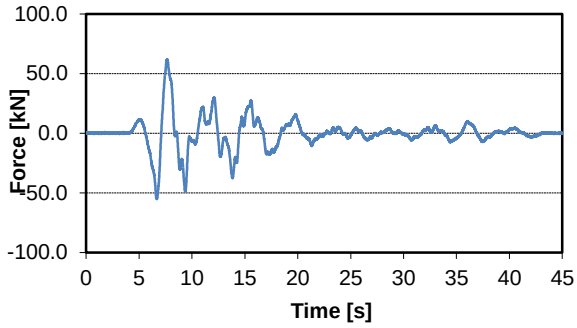

Figure AI. 167 - Channel H_GLL1_C1_NW_T

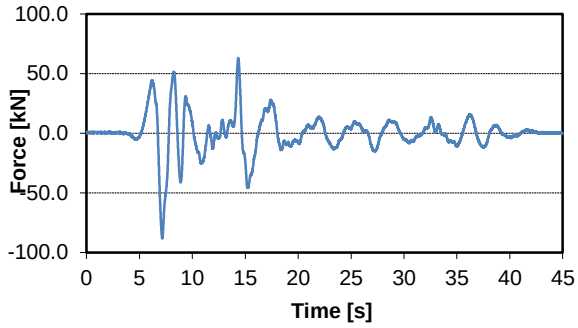

Figure AI. 168 - Channel H_GLL1_C1_NW_L

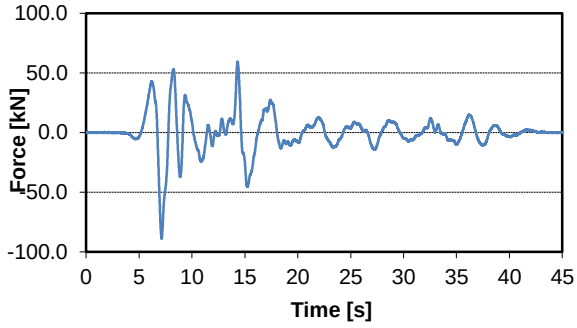

Figure AI. 169 - Channel H_GL_C1_NW_L

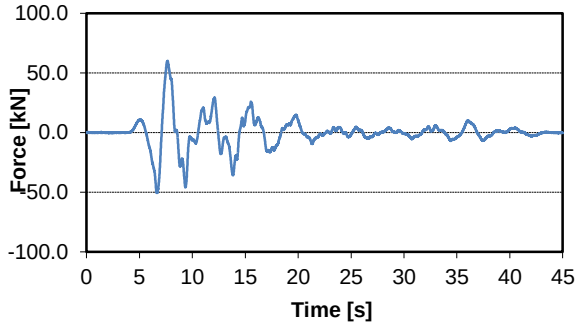

Figure AI. 170 - Channel H_GL_C1_NW_T

Seismic test – TEST_11

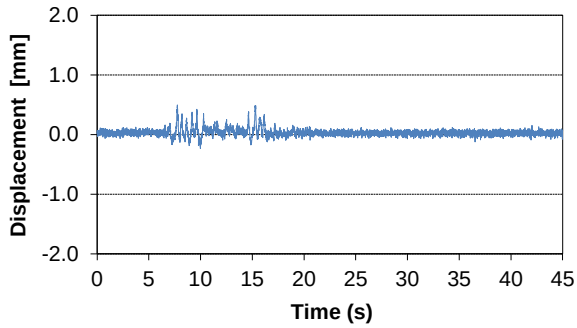

Figure AI. 171 – Channel LVDT_WU_GLW06Y_L

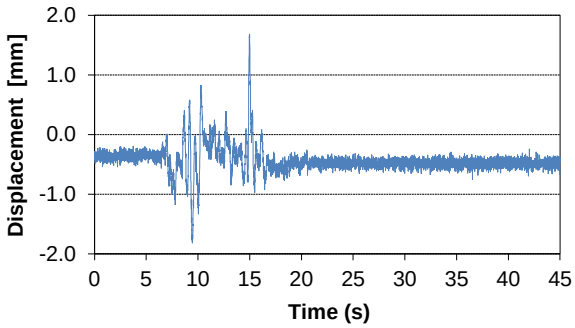

Figure AI. 172 - Channel LVDT_WU_GLW06Y_R

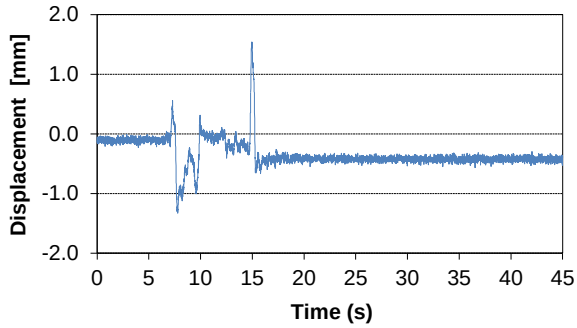

Figure AI. 173 - Channel LVDT_WU_GLW07X_L

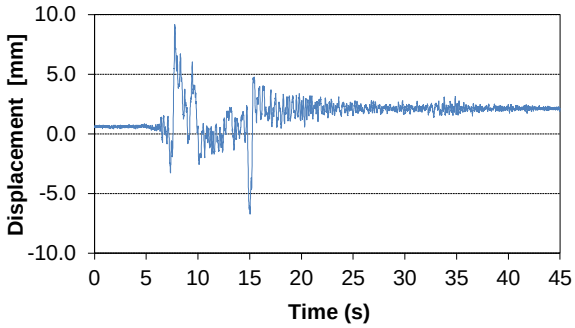

Figure AI. 174 - Channel LVDT_WU_GLW07X_R

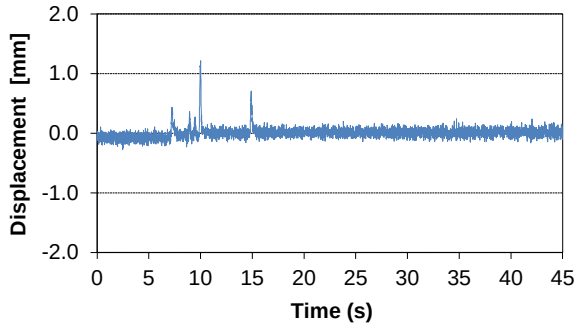

Figure AI. 175 - Channel LVDT_WU_GLW02Y_L

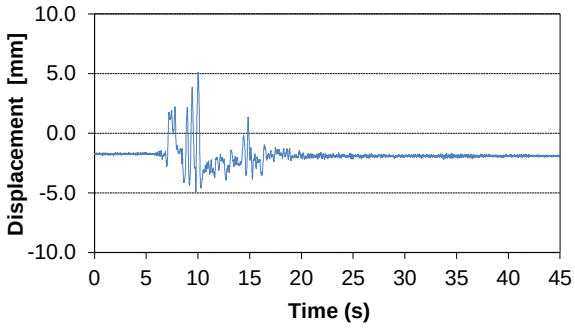

Figure AI. 176 - Channel LVDT_WU_GLW01Y_R

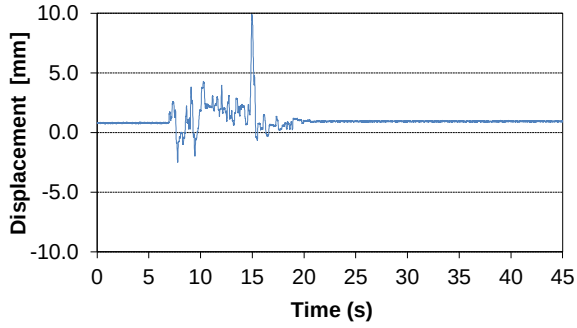

Figure AI. 177 - Channel LVDT_WU_GLW04X_L

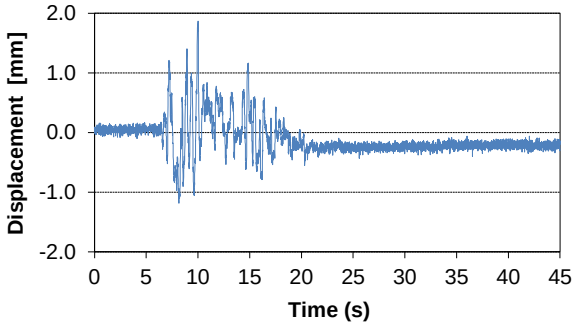

Figure AI. 178 - Channel LVDT_WU_GLW04X_R

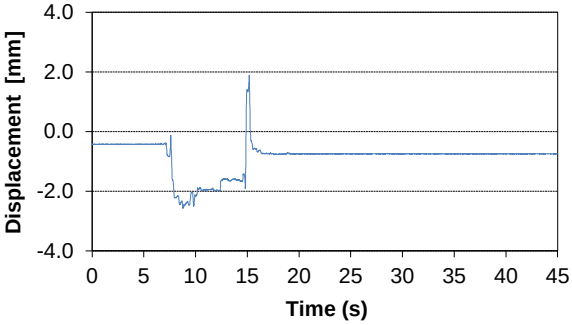

Figure AI. 179 - Channel LVDT_WS_GLW06Y

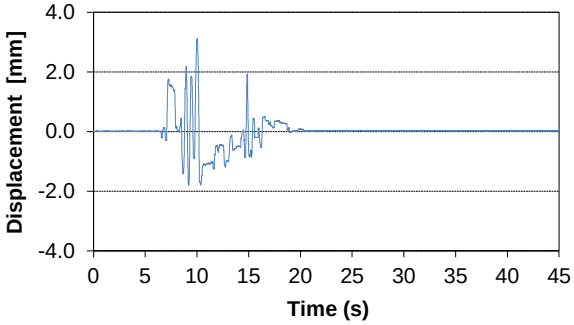

Figure AI. 180 - LVDT_WS_GLW07X

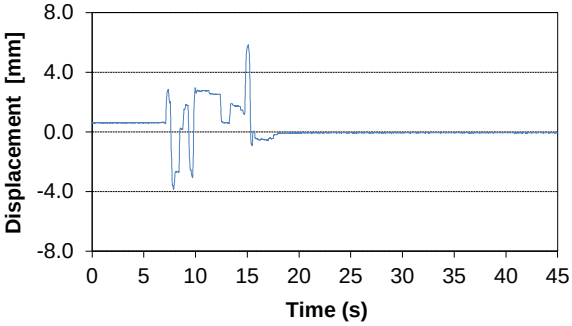

Figure AI. 181 - Channel LVDT_WS_GLW02Y

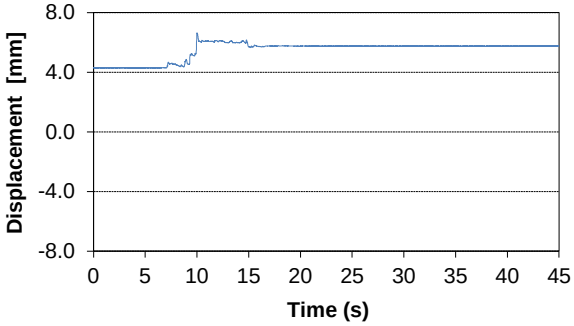

Figure AI. 182 - Channel LVDT_WS_GLW04X

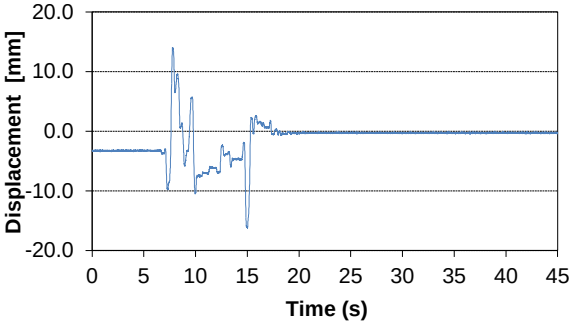

Figure AI. 183 - Channel LVDT_SD_GLW06Y_L

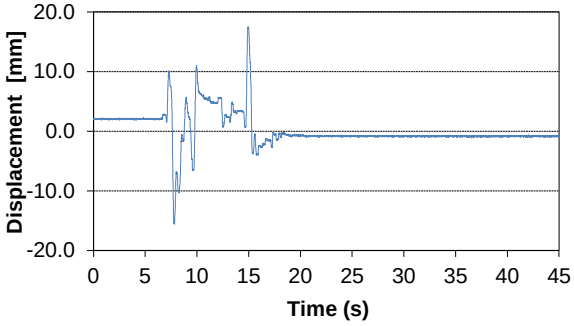

Figure AI. 184 - Channel LVDT_SD_GLW06Y_R

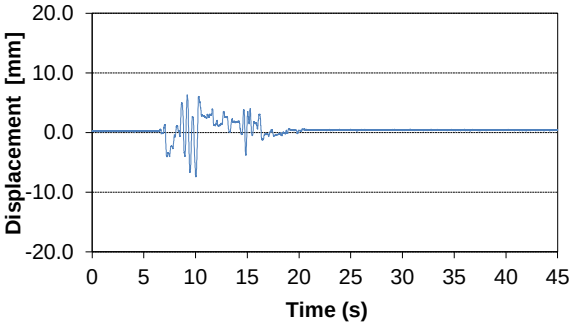

Figure AI. 185 - Channel LVDT_SD_GLW07X_L

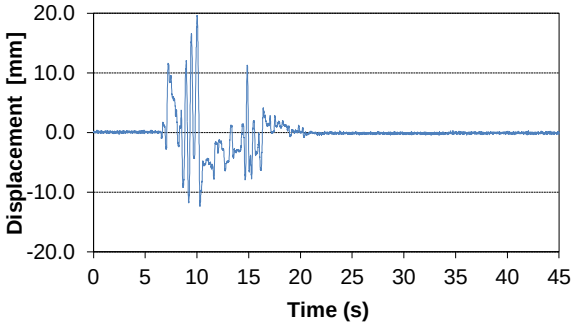

Figure AI. 186 - Channel LVDT_SD_GLW07X_R

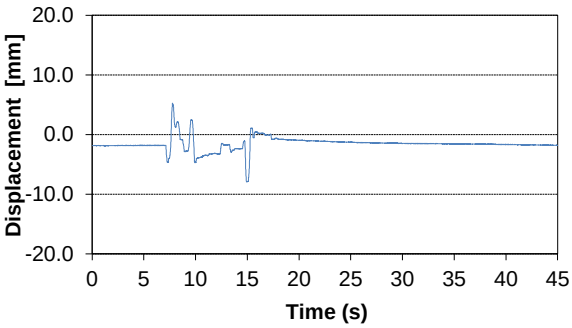

Figure AI. 187 - Channel LVDT_SD_GLW02Y_L

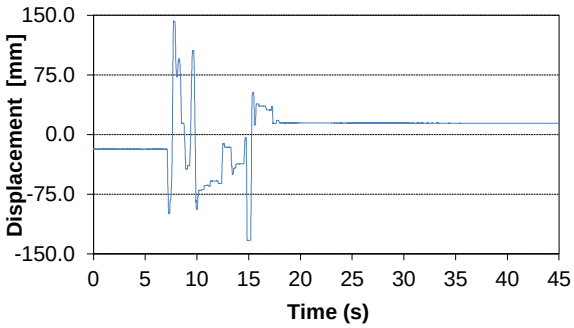

Figure AI. 188 - Channel LVDT_SD_GLW01Y_R

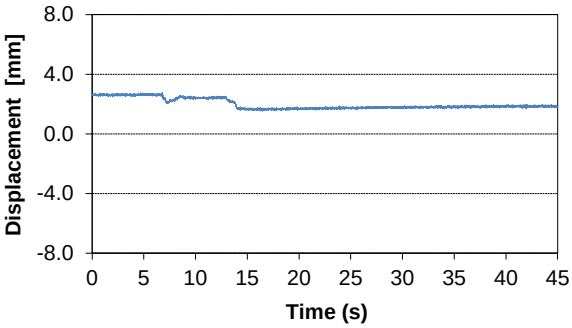

Figure AI. 189 - Channel LVDT_SD_GLW04X_L

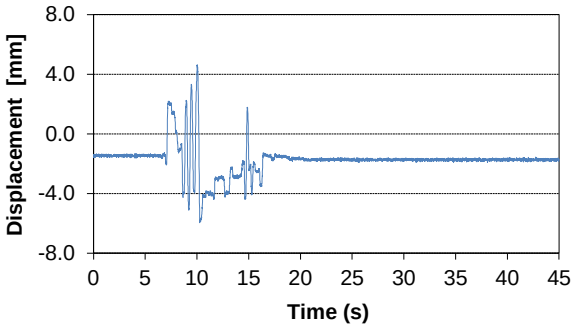

Figure AI. 190 - Channel LVDT_SD_GLW04X_R

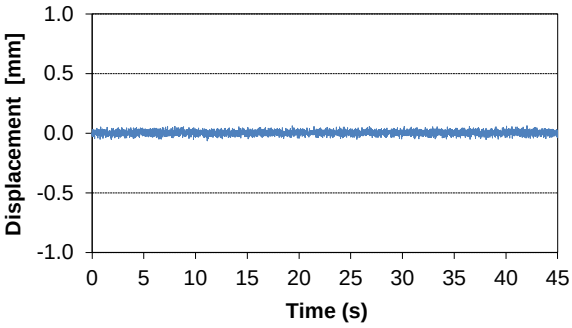

Figure AI. 191 - Channel LVDT_ID_GL_X

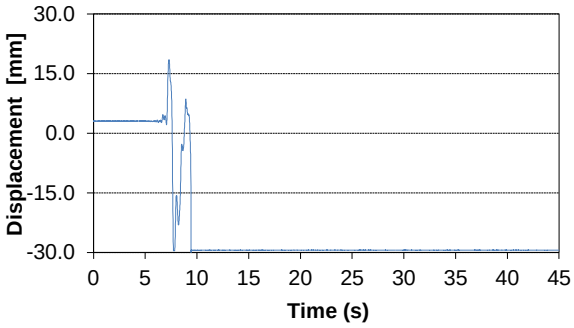

Figure AI. 192 - Channel LVDT_ID_GL_Y

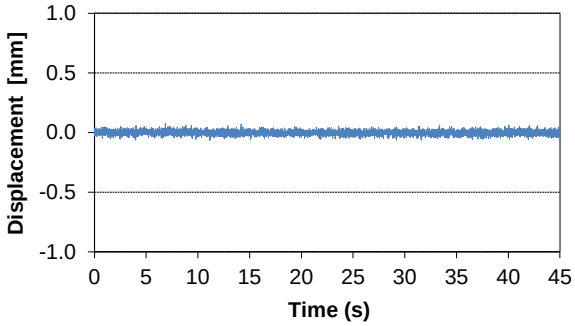

Figure AI. 193 - Channel LVDT_ID_L1_X

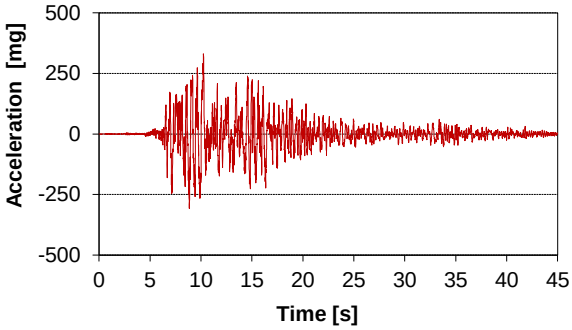

Figure AI. 194 - Channel ACC_L1_C3_X_NE_T

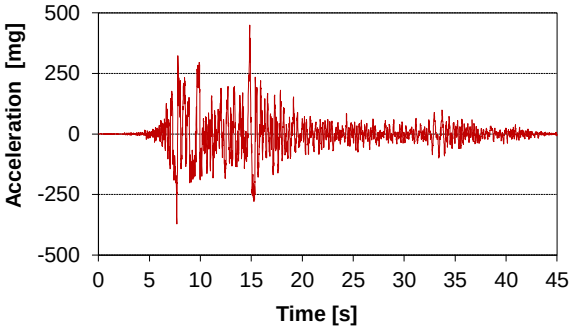

Figure AI. 195 - Channel ACC_L1_C3_Y_NE_L

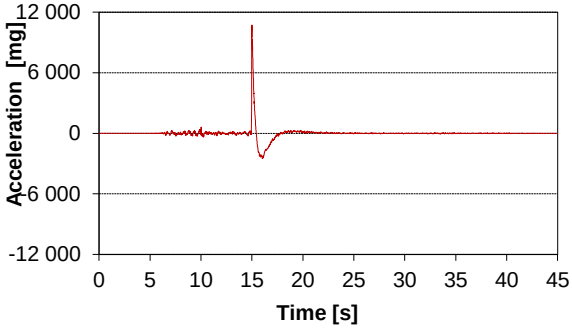

Figure AI. 196 - Channel ACC_L1_A1_X_SW_T

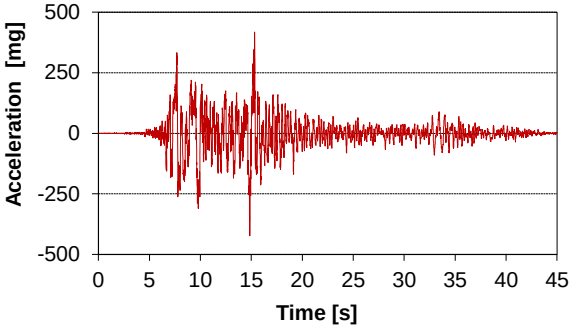

Figure AI. 197 - Channel ACC_L1_A1_Y_SW_L

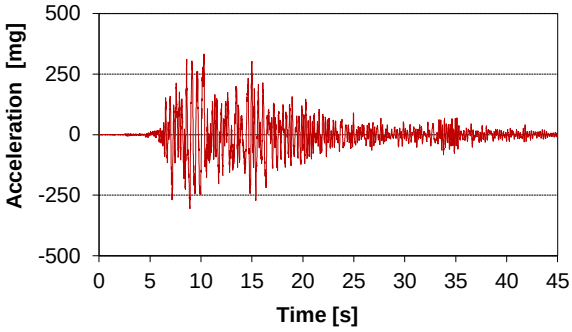

Figure AI. 198 - Channel ACC_RL_C3_X_NE_T

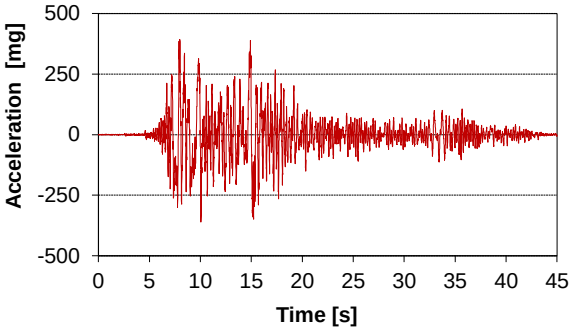

Figure AI. 199 - Channel ACC_RL_C3_Y_NE_L

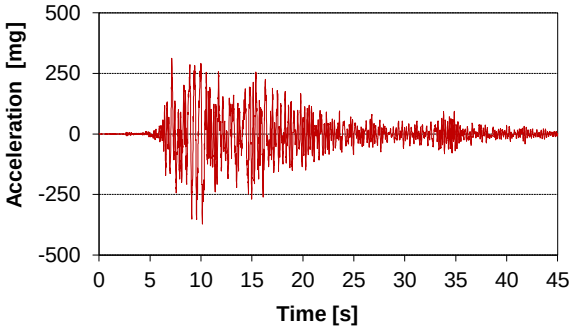

Figure AI. 200 - Channel ACC_RL_A1_X_SW_T

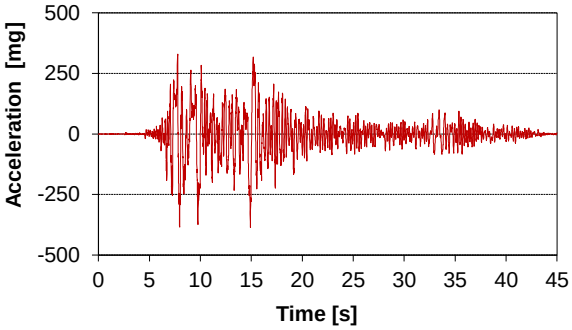

Figure AI. 201 - Channel ACC_RL_A1_Y_SW_L

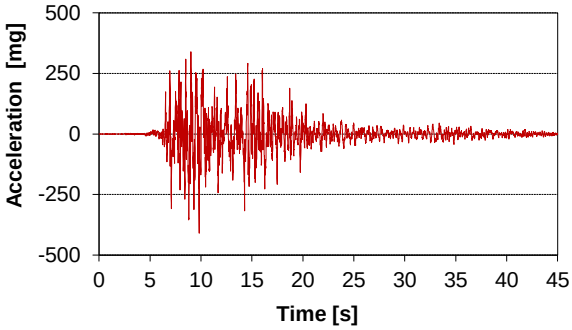

Figure AI. 202 - Channel ACC_GL_A3_X_SE_T

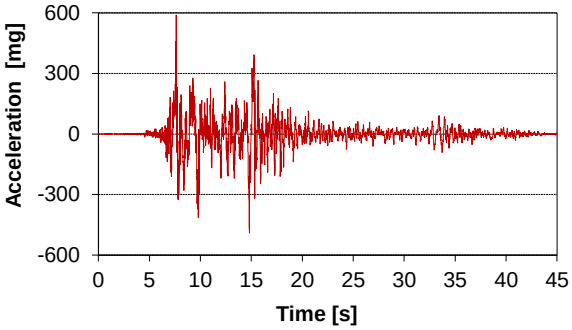

Figure AI. 203 - Channel ACC_GL_A3_Y_SE_L

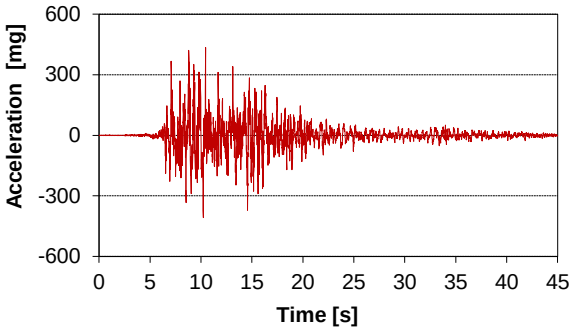

Figure AI. 204 - Channel ACC_GL_C1_X_NW_T

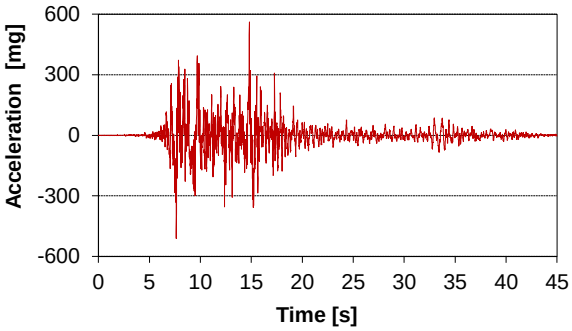

Figure AI. 205 - Channel ACC_GL_C1_Y_NW_L

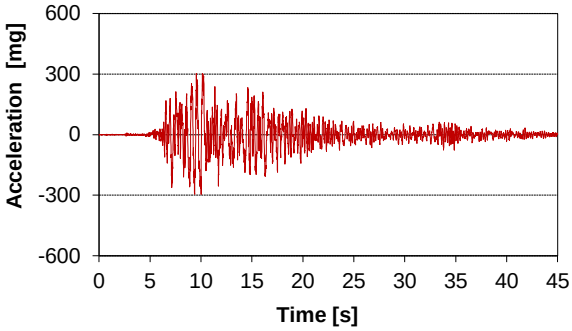

Figure AI. 206 - Channel ACC_L1_A3_X_SE_T

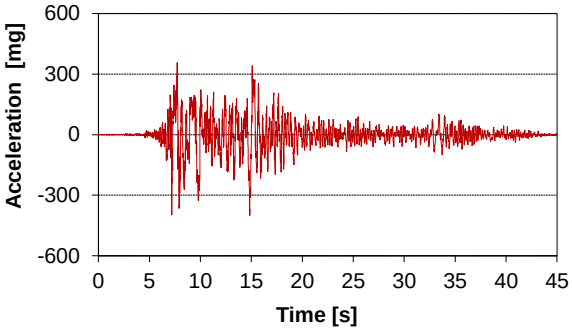

Figure AI. 207 - Channel ACC_L1_A3_Y_SE_L

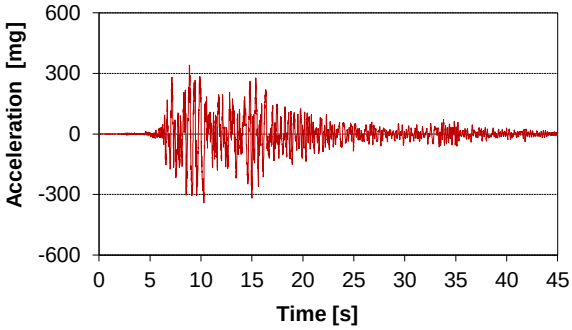

Figure AI. 208 - Channel ACC_L1_C1_X_NW_T

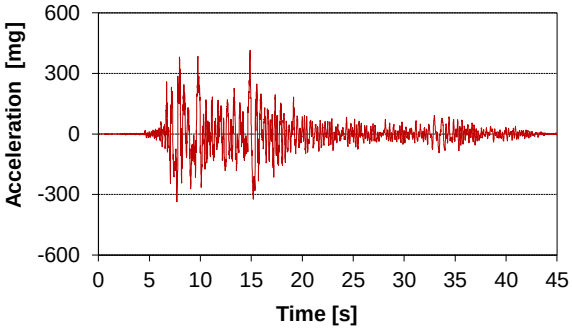

Figure AI. 209 - Channel ACC_L1_C1_Y_NW_L

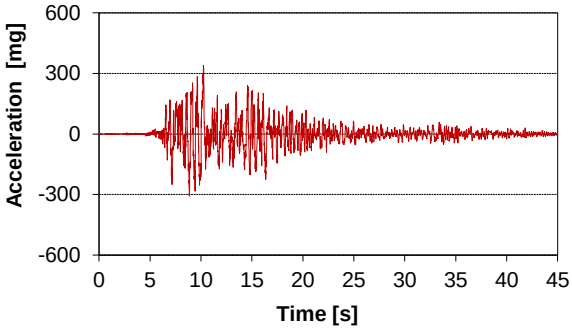

Figure AI. 210 - Channel ACC_L1_C2_X_N_T

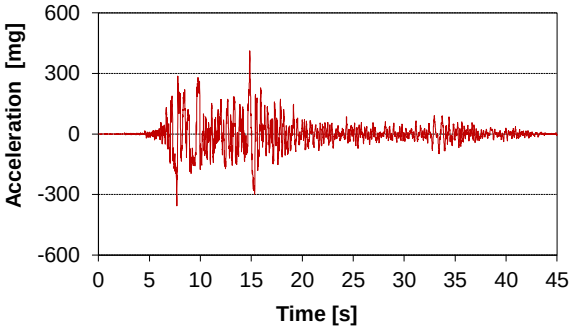

Figure AI. 211 - Channel ACC_L1_C2_Y_N_L

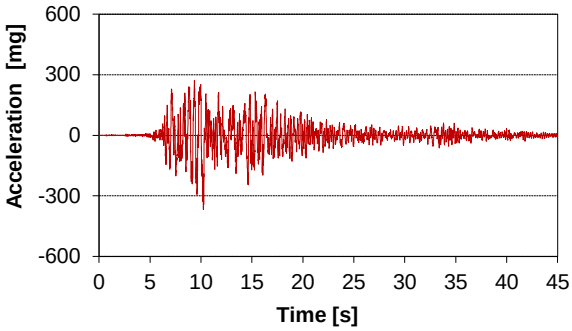

Figure AI. 212 - Channel ACC_L1_A2_X_S_T

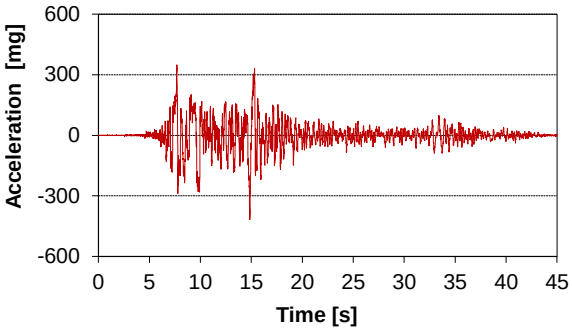

Figure AI. 213 - Channel ACC_L1_A2_Y_S_L

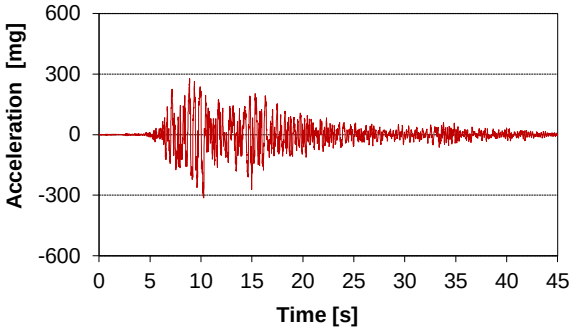

Figure AI. 214 - Channel ACC_L1_B1_X_W_T

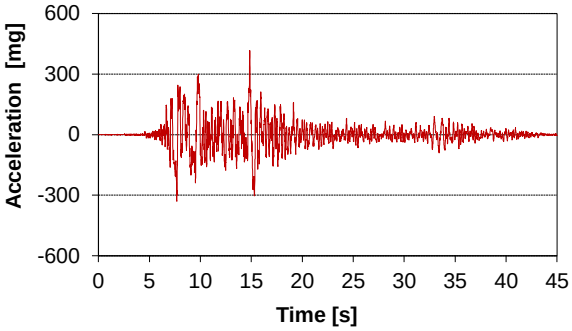

Figure AI. 215 - Channel ACC_L1_B1_Y_W_L

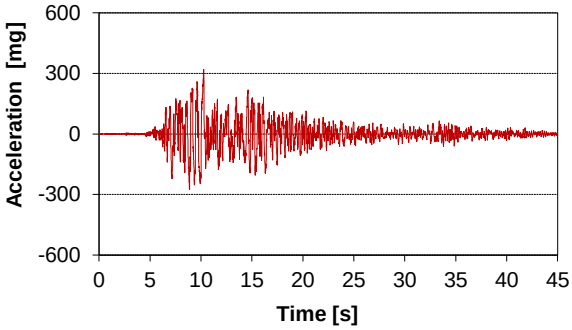

Figure AI. 216 - Channel ACC_L1_B2_X_I_T

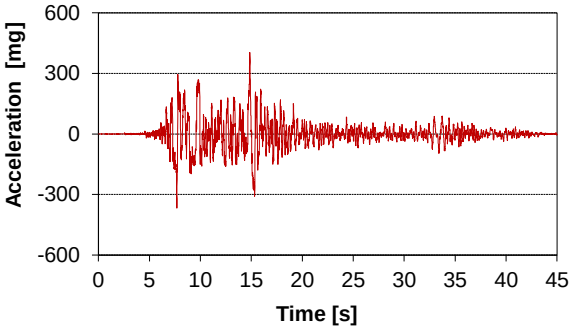

Figure AI. 217 - Channel ACC_L1_B2_Y_I_L

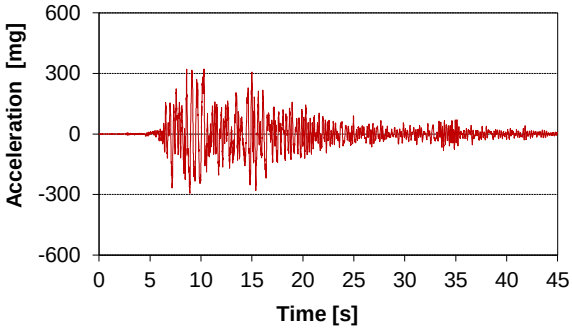

Figure AI. 218 - Channel ACC_RL_C2_X_N_T

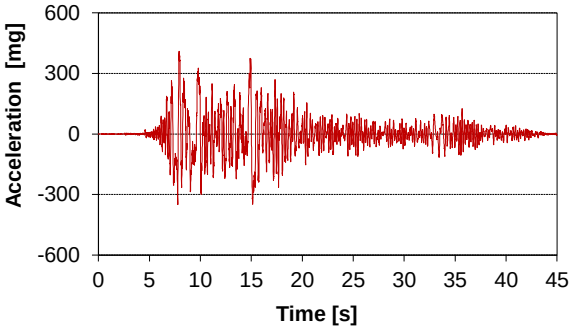

Figure AI. 219 - Channel ACC_RL_C2_Y_N_L

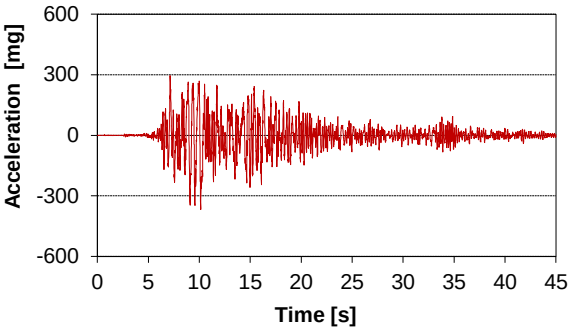

Figure AI. 220 - Channel ACC_RL_A2_X_S_T

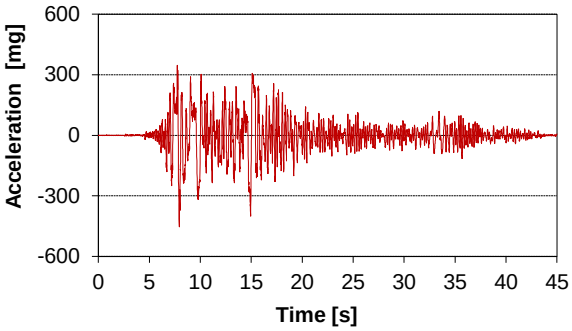

Figure AI. 221 - Channel ACC_RL_A2_Y_S_L

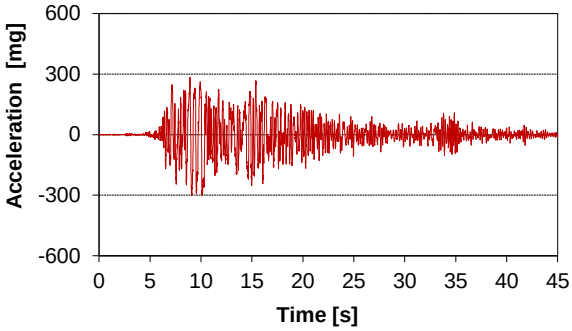

Figure AI. 222 - Channel ACC_RL_B1_X_W_T

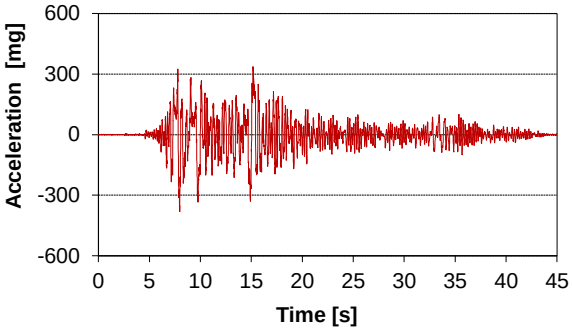

Figure AI. 223 - Channel ACC_RL_B1_Y_W_L

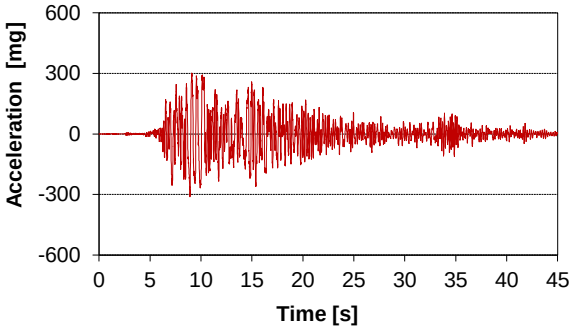

Figure AI. 224 - Channel ACC_RL_B2_X_I_T

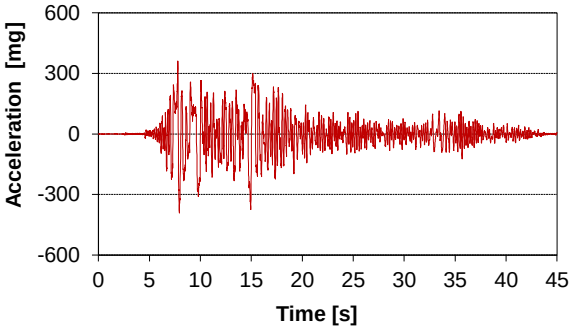

Figure AI. 225 - Channel ACC_RL_B2_Y_I_L

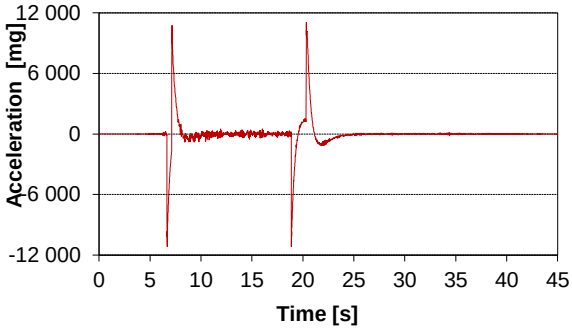

Figure AI. 226 - Channel ACC_GLW03Y_I_T

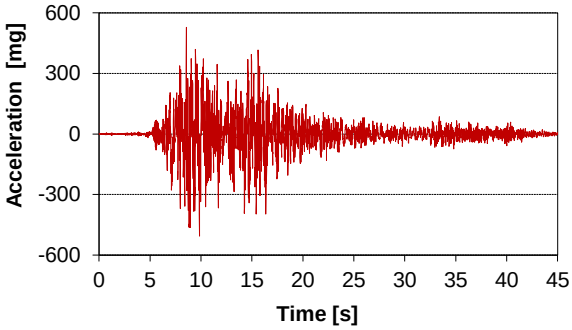

Figure AI. 227 - Channel ACC_GLW04Y_I_T

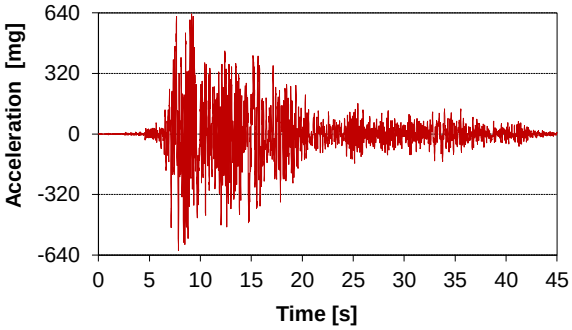

Figure AI. 228 - Channel ACC_GLW04X_I_L

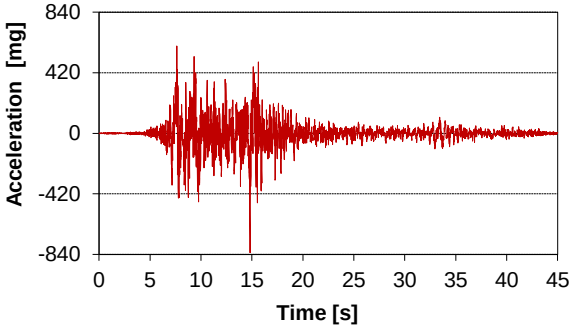

Figure AI. 229 - Channel ACC_GLW05X_I_L

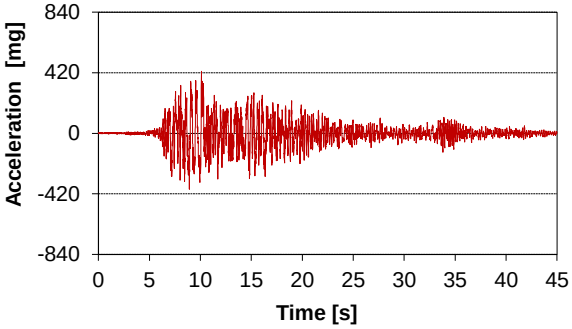

Figure AI. 230 - Channel ACC_L1W03Y_I_T

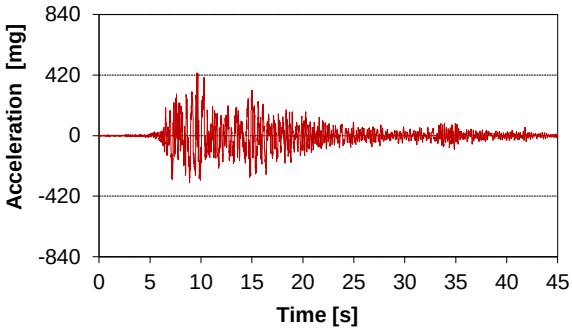

Figure AI. 231 - Channel ACC_L1W04Y_I_T

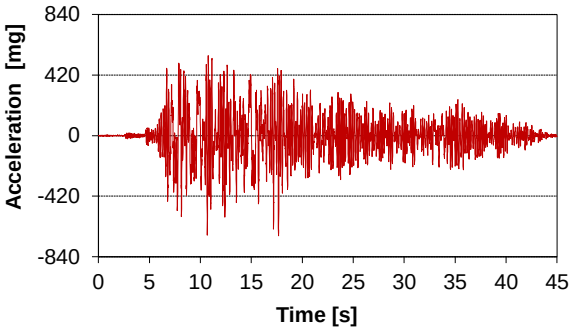

Figure AI. 232 - Channel ACC_L1W04X_I_L

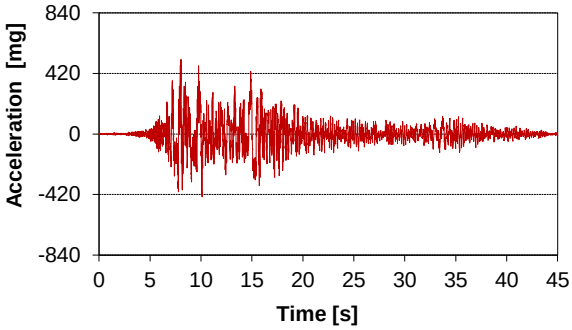

Figure AI. 233 - Channel ACC_L1W05X_I_L

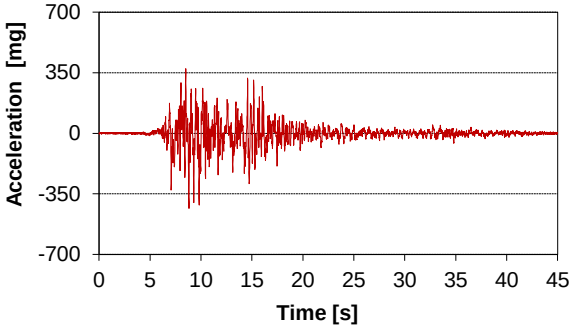

Figure AI. 234 - Channel ACC MESA TRANS

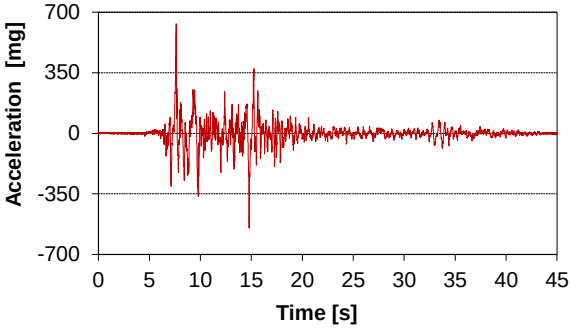

Figure AI. 235 - Channel ACC MESA LONG

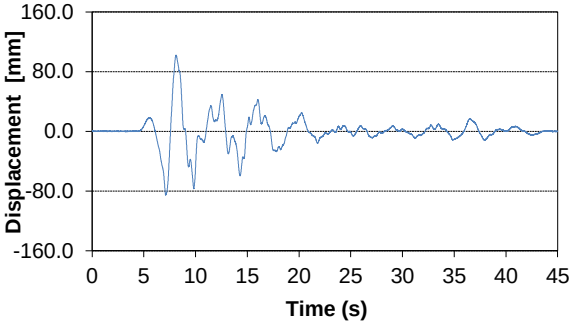

Figure AI. 236 - Channel DISP MESA TRANS

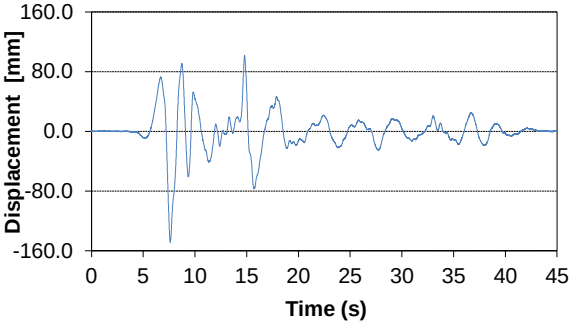

Figure AI. 237 - Channel DISP MESA LONG

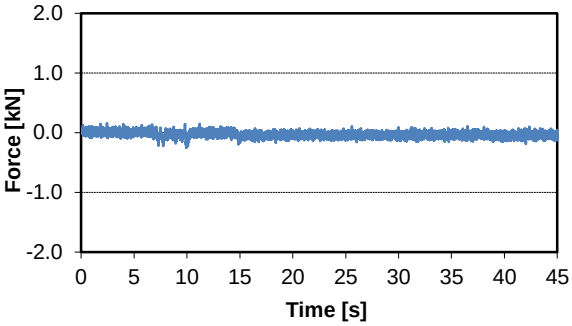

Figure AI. 238 - Channel CF_HD_GLW06Y_L

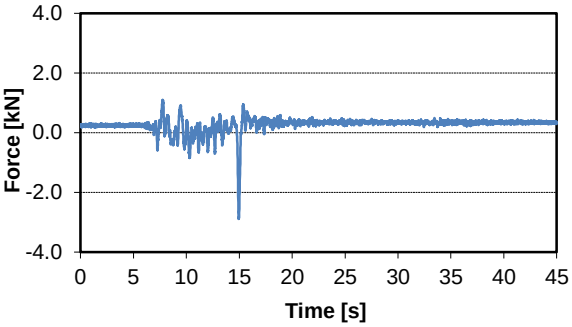

Figure AI. 239 - Channel CF_HD_GLW06X_R

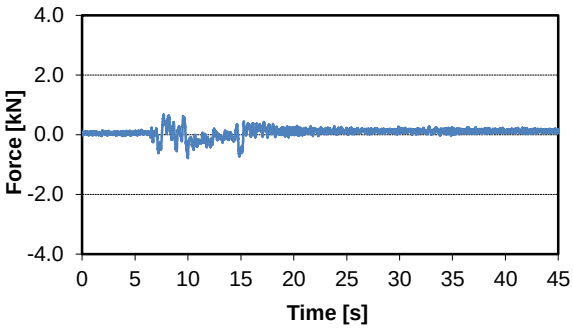

Figure AI. 240 - Channel CF_HD_GLW07X_L

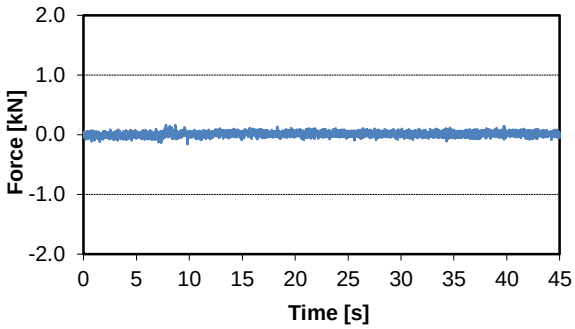

Figure AI. 241 - Channel CF_HD_GLW07X_R

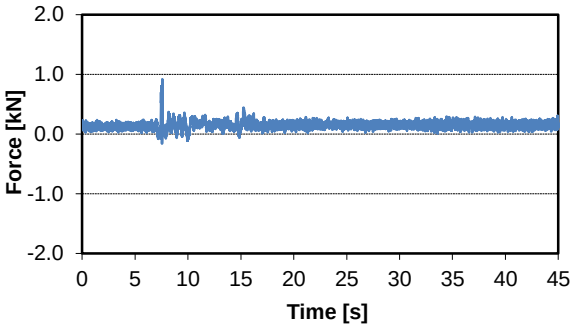

Figure AI. 242 - Channel CF_HD_GLW02Y_L

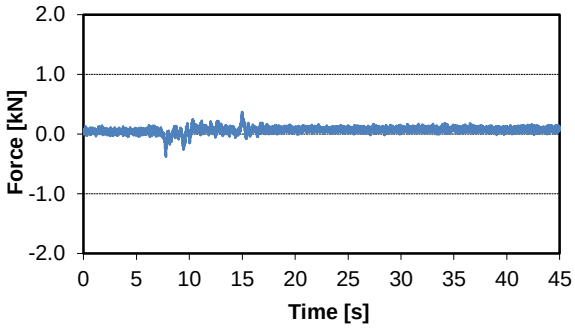

Figure AI. 243 - Channel CF_HD_GLW01Y_R

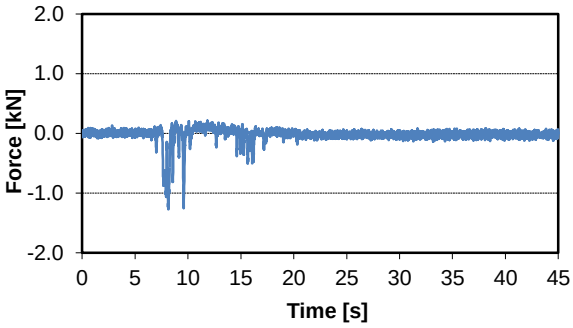

Figure AI. 244 - Channel CF_HD_GLW04X_L

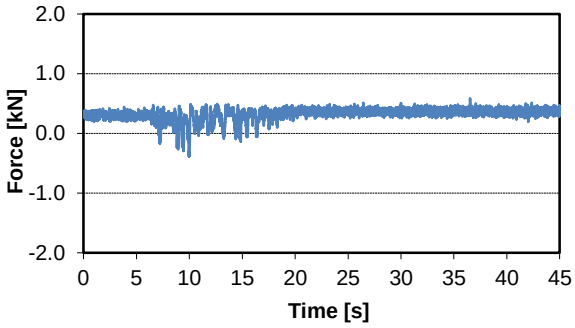

Figure AI. 245 - Channel CF_HD_GLW04X_R

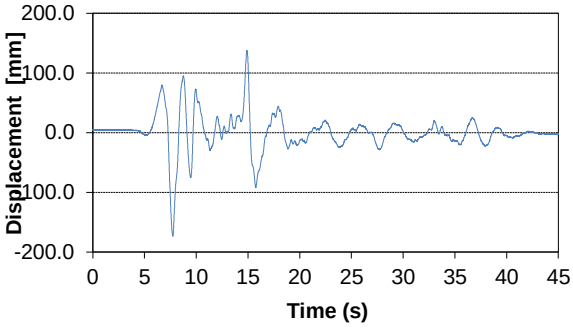

Figure AI. 246 - Channel H_RL_C1_NW_L

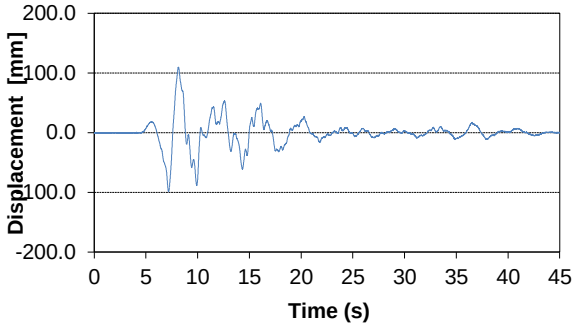

Figure AI. 247 - Channel H_RL_C1_NW_T

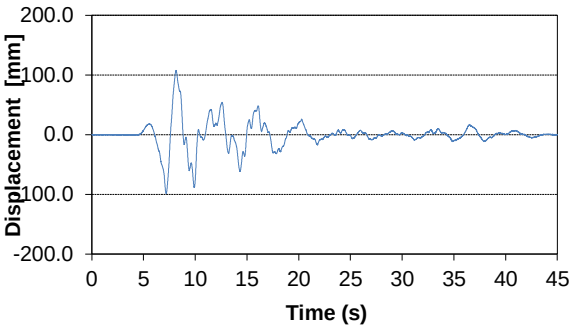

Figure AI. 248 - Channel H_L1RL_C1_NW_T

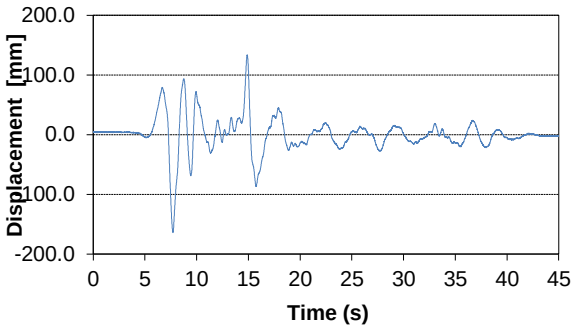

Figure AI. 249 - Channel H_L1RL_C1_NW_L

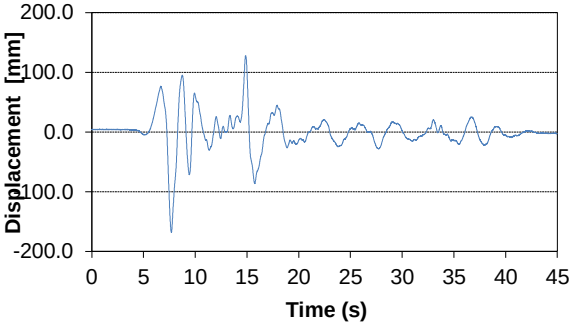

Figure AI. 250 - Channel H_L1_C1_NW_L

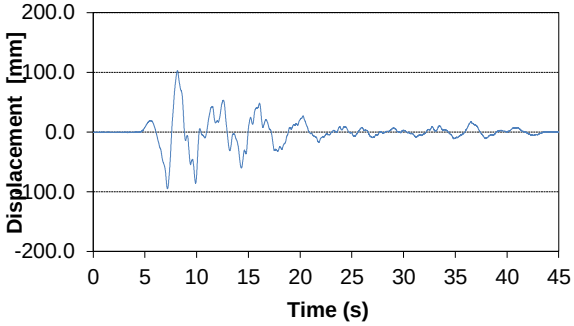

Figure AI. 251 - Channel H_L1_C1_NW_T

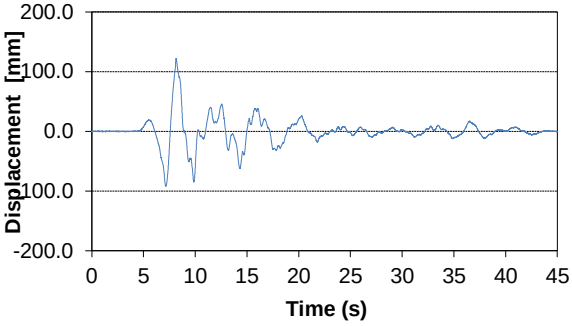

Figure AI. 252 - Channel H_GLL1_C1_NW_T

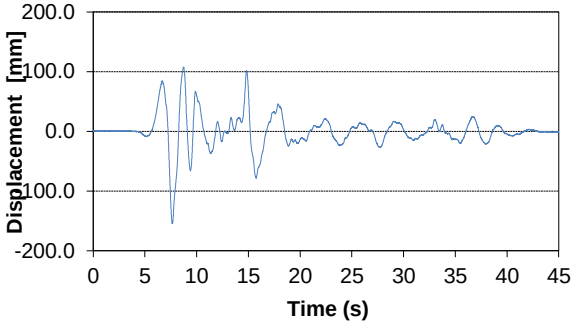

Figure AI. 253 - Channel H_GLL1_C1_NW_L

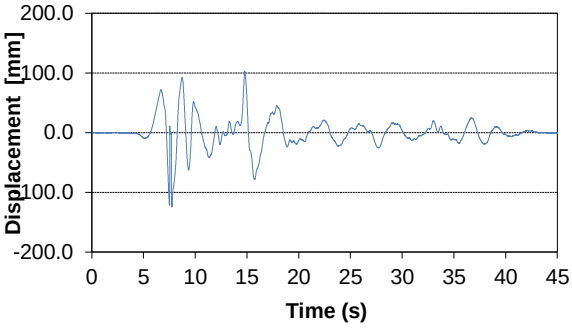

Figure AI. 254 - Channel H_GL_C1_NW_L

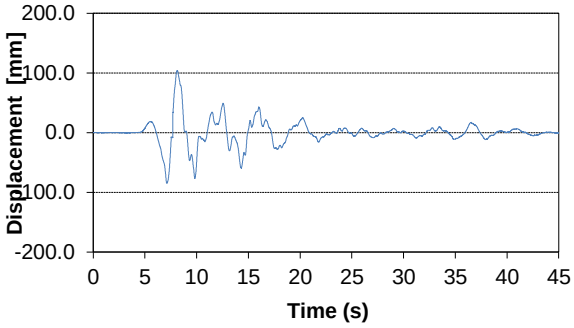

Figure AI. 255 - Channel H_GL_C1_NW_T

ANNEX II
Digital signal processing results

Maximum simultaneous values

Table AII.1 – Maximum simultaneous values on all wall uplifts for seismic test TEST_01

TEST007_01	GLW01Y_R	GLW02Y_L	GLW04X_L	GLW04X_R	GLW06Y_L	GLW06Y_R	GLW07X_L	GLW07X_R
GLW01Y_R	0.33	0.01	0.04	0.02	0.04	0.02	0.01	0.91
GLW02Y_L	0.16	0.28	0.09	0.11	0.09	0.20	0.12	0.16
GLW04X_L	0.18	0.03	0.13	0.19	0.12	0.24	0.10	0.25
GLW04X_R	0.19	0.11	0.05	0.22	0.05	0.10	0.07	0.12
GLW06Y_L	0.12	0.10	0.07	0.16	0.15	0.28	0.16	0.22
GLW06Y_R	0.12	0.10	0.07	0.16	0.15	0.28	0.16	0.22
GLW07X_L	0.12	0.10	0.07	0.16	0.15	0.28	0.16	0.22
GLW07X_R	0.31	0.09	0.02	0.10	0.03	0.02	0.04	1.04

Table AII.2 – Maximum simultaneous values on all wall uplifts for seismic test TEST_02

TEST007_02	GLW01Y_R	GLW02Y_L	GLW04X_L	GLW04X_R	GLW06Y_L	GLW06Y_R	GLW07X_L	GLW07X_R
GLW01Y_R	0.31	0.04	0.06	0.09	0.05	0.08	0.03	0.74
GLW02Y_L	0.07	0.32	0.06	0.13	0.11	0.22	0.12	0.19
GLW04X_L	0.09	0.09	0.11	0.12	0.14	0.25	0.15	0.15
GLW04X_R	0.14	0.06	0.06	0.21	0.08	0.19	0.12	0.31
GLW06Y_L	0.09	0.09	0.11	0.12	0.14	0.25	0.15	0.15
GLW06Y_R	0.09	0.09	0.11	0.12	0.14	0.25	0.15	0.15
GLW07X_L	0.09	0.09	0.11	0.12	0.14	0.25	0.15	0.15
GLW07X_R	0.22	0.02	0.02	0.04	0.00	0.01	0.01	0.99

Table AII.3 – Maximum simultaneous values on all wall uplifts for seismic test TEST_03

TEST007_03	GLW01Y_R	GLW02Y_L	GLW04X_L	GLW04X_R	GLW06Y_L	GLW06Y_R	GLW07X_L	GLW07X_R
GLW01Y_R	0.30	0.01	0.08	0.11	0.07	0.11	0.04	0.30
GLW02Y_L	0.02	0.26	0.02	0.05	0.06	0.13	0.09	0.20
GLW04X_L	0.10	0.06	0.10	0.14	0.08	0.15	0.11	0.07
GLW04X_R	0.10	0.11	0.05	0.18	0.09	0.16	0.11	0.08
GLW06Y_L	0.05	0.18	0.09	0.12	0.12	0.24	0.13	0.00
GLW06Y_R	0.05	0.18	0.09	0.12	0.12	0.24	0.13	0.00
GLW07X_L	0.02	0.01	0.10	0.17	0.12	0.23	0.13	0.02
GLW07X_R	0.16	0.02	0.03	0.08	0.06	0.11	0.06	0.89

Table AII.4 – Maximum simultaneous values on all wall uplifts for seismic test TEST_04

TEST007_04	GLW01Y_R	GLW02Y_L	GLW04X_L	GLW04X_R	GLW06Y_L	GLW06Y_R	GLW07X_L	GLW07X_R
GLW01Y_R	0.31	0.03	0.03	0.09	0.04	0.07	0.03	1.02
GLW02Y_L	0.02	0.27	0.05	0.08	0.08	0.18	0.10	0.13
GLW04X_L	0.06	0.01	0.11	0.07	0.09	0.16	0.07	0.02
GLW04X_R	0.12	0.04	0.06	0.22	0.12	0.23	0.13	0.14
GLW06Y_L	0.12	0.08	0.10	0.13	0.12	0.23	0.12	0.06
GLW06Y_R	0.12	0.04	0.06	0.22	0.12	0.23	0.13	0.14
GLW07X_L	0.04	0.12	0.06	0.10	0.11	0.20	0.13	0.06
GLW07X_R	0.31	0.03	0.03	0.09	0.04	0.07	0.03	1.02

Table AII.5 – Maximum simultaneous values on all wall uplifts for seismic test TEST_05

TEST028_01	GLW01Y_R	GLW02Y_L	GLW04X_L	GLW04X_R	GLW06Y_L	GLW06Y_R	GLW07X_L	GLW07X_R
GLW01Y_R	2.02	0.13	1.00	0.45	0.06	0.19	0.28	1.13
GLW02Y_L	0.70	0.26	0.64	0.02	0.01	0.23	0.24	0.97
GLW04X_L	1.32	0.02	2.16	0.17	0.07	0.32	0.11	0.57
GLW04X_R	1.50	0.02	1.05	0.59	0.08	0.07	0.30	0.07
GLW06Y_L	1.13	0.02	0.48	0.32	0.20	0.10	0.18	0.85
GLW06Y_R	0.70	0.17	0.31	0.28	0.09	0.64	0.36	1.67
GLW07X_L	0.22	0.04	0.14	0.36	0.01	0.38	0.45	2.49
GLW07X_R	0.16	0.04	0.04	0.02	0.04	0.23	0.30	3.20

Table AII.6 – Maximum simultaneous values on all wall uplifts for seismic test TEST_06

TEST028_02	GLW01Y_R	GLW02Y_L	GLW04X_L	GLW04X_R	GLW06Y_L	GLW06Y_R	GLW07X_L	GLW07X_R
GLW01Y_R	2.24	0.02	0.65	0.69	0.07	0.13	0.49	1.37
GLW02Y_L	1.42	0.27	2.97	0.13	0.03	0.22	0.22	1.59
GLW04X_L	1.66	0.01	3.55	0.14	0.04	0.14	0.12	2.20
GLW04X_R	1.31	0.12	0.10	0.76	0.07	0.27	0.57	1.44
GLW06Y_L	1.87	0.10	0.63	0.62	0.25	0.08	0.40	1.51
GLW06Y_R	0.88	0.05	1.28	0.31	0.03	0.92	0.54	3.00
GLW07X_L	0.16	0.06	0.66	0.25	0.04	0.76	0.70	3.90
GLW07X_R	0.07	0.05	0.66	0.10	0.11	0.49	0.59	4.07

Table AII.7 – Maximum simultaneous values on all wall uplifts for seismic test TEST_07

TEST028_03	GLW01Y_R	GLW02Y_L	GLW04X_L	GLW04X_R	GLW06Y_L	GLW06Y_R	GLW07X_L	GLW07X_R
GLW01Y_R	2.88	0.04	1.35	0.62	0.11	0.12	0.46	1.61
GLW02Y_L	1.46	0.31	1.01	0.15	0.09	0.56	0.27	0.67
GLW04X_L	1.48	0.06	4.37	0.15	0.05	0.20	0.29	2.74
GLW04X_R	0.81	0.13	1.66	0.95	0.09	0.61	0.10	0.48
GLW06Y_L	2.77	0.05	1.50	0.52	0.23	0.34	0.34	1.43
GLW06Y_R	1.28	0.01	0.96	0.55	0.07	1.11	0.55	3.48
GLW07X_L	0.19	0.14	0.10	0.61	0.05	0.73	0.76	2.85
GLW07X_R	0.09	0.04	0.04	0.28	0.14	0.70	0.68	4.62

Table AII.8 – Maximum simultaneous values on all wall uplifts for seismic test TEST_08

TEST028_04	GLW01Y_R	GLW02Y_L	GLW04X_L	GLW04X_R	GLW06Y_L	GLW06Y_R	GLW07X_L	GLW07X_R
GLW01Y_R	2.31	0.19	1.98	0.33	0.00	0.13	0.11	0.85
GLW02Y_L	1.40	0.35	0.82	0.15	0.05	0.49	0.26	0.82
GLW04X_L	2.19	0.14	2.02	0.31	0.03	0.11	0.13	0.76
GLW04X_R	0.72	0.06	0.85	0.62	0.08	0.25	0.12	0.80
GLW06Y_L	1.93	0.00	1.03	0.09	0.23	0.05	0.03	0.24
GLW06Y_R	0.76	0.08	0.35	0.21	0.15	0.74	0.33	2.09
GLW07X_L	1.43	0.20	0.71	0.30	0.13	0.65	0.45	1.66
GLW07X_R	1.04	0.10	0.51	0.11	0.09	0.26	0.17	2.77

Table AII.9 – Maximum simultaneous values on all wall uplifts for seismic test TEST_09

TEST028_05	GLW01Y_R	GLW02Y_L	GLW04X_L	GLW04X_R	GLW06Y_L	GLW06Y_R	GLW07X_L	GLW07X_R
GLW01Y_R	2.65	0.14	1.55	0.55	0.12	0.10	0.33	1.36
GLW02Y_L	1.44	0.32	0.71	0.06	0.04	0.50	0.20	0.38
GLW04X_L	2.27	0.12	3.45	0.26	0.10	0.22	0.19	2.22
GLW04X_R	0.03	0.01	0.66	0.85	0.01	0.49	0.18	2.03
GLW06Y_L	2.08	0.00	0.71	0.45	0.28	0.04	0.28	1.31
GLW06Y_R	0.07	0.09	0.82	0.39	0.01	0.88	0.48	2.26
GLW07X_L	0.51	0.05	0.22	0.31	0.01	0.86	0.64	3.19
GLW07X_R	0.23	0.05	0.10	0.07	0.18	0.51	0.46	3.62

Table AII.10 – Maximum simultaneous values on all wall uplifts for seismic test TEST_10

TEST028_06	GLW01Y_R	GLW02Y_L	GLW04X_L	GLW04X_R	GLW06Y_L	GLW06Y_R	GLW07X_L	GLW07X_R
GLW01Y_R	2.98	0.17	1.36	0.57	0.16	0.07	0.38	0.79
GLW02Y_L	1.90	0.34	0.74	0.05	0.01	0.45	0.19	0.20
GLW04X_L	2.49	0.02	4.40	0.21	0.07	0.28	0.33	2.98
GLW04X_R	0.37	0.08	1.44	0.92	0.10	0.64	0.18	0.67
GLW06Y_L	2.43	0.04	0.71	0.47	0.25	0.13	0.41	0.97
GLW06Y_R	0.67	0.03	0.98	0.57	0.03	1.00	0.47	3.30
GLW07X_L	0.29	0.04	0.70	0.41	0.09	0.87	0.70	3.79
GLW07X_R	0.18	0.04	0.62	0.21	0.21	0.61	0.56	3.95

Table AII.11 – Maximum simultaneous values on all wall uplifts for seismic test TEST_11

TEST050_01	GLW01Y_R	GLW02Y_L	GLW04X_L	GLW04X_R	GLW06Y_L	GLW06Y_R	GLW07X_L	GLW07X_R
GLW01Y_R	5.11	0.99	1.82	1.81	0.13	1.24	0.05	0.11
GLW02Y_L	4.92	1.21	1.88	1.87	0.18	1.15	0.14	0.57
GLW04X_L	1.06	0.46	9.90	0.31	0.03	1.63	1.53	6.16
GLW04X_R	4.92	1.21	1.88	1.87	0.18	1.15	0.14	0.57
GLW06Y_L	1.78	0.01	1.89	0.71	0.49	0.88	1.22	9.12
GLW06Y_R	3.55	0.18	1.97	0.77	0.03	1.82	0.87	5.74
GLW07X_L	1.25	0.47	9.86	0.29	0.03	1.65	1.54	6.16
GLW07X_R	1.93	0.01	2.15	0.76	0.44	0.99	1.26	9.15

Table AII.12 – Maximum simultaneous values on all wall uplifts for seismic test TEST_12

TEST050_02	GLW01Y_R	GLW02Y_L	GLW04X_L	GLW04X_R	GLW06Y_L	GLW06Y_R	GLW07X_L	GLW07X_R
GLW01Y_R	7.05	1.95	2.66	2.00	0.13	1.20	0.28	0.83
GLW02Y_L	6.96	2.10	2.93	2.03	0.23	1.18	0.30	0.02
GLW04X_L	0.11	0.87	11.62	0.53	0.06	2.33	2.00	8.34
GLW04X_R	5.54	1.97	2.99	2.09	0.22	0.95	0.41	0.09
GLW06Y_L	3.11	0.17	2.69	0.97	0.66	0.97	1.36	12.61
GLW06Y_R	0.74	0.72	11.50	0.50	0.04	2.64	2.03	8.07
GLW07X_L	0.74	0.72	11.50	0.50	0.04	2.64	2.03	8.07
GLW07X_R	3.34	0.09	2.89	1.08	0.57	1.16	1.47	12.64

Table AII.13 – Maximum simultaneous values on all wall slippage for seismic test TEST_01

TEST007_01	GLW02Y	GLW04X	GLW06Y	GLW07X
GLW02Y	0.05	0.01	0.02	0.01
GLW04X	0.05	0.02	0.02	0.01
GLW06Y	0.05	0.02	0.02	0.01
GLW07X	0.00	0.01	0.00	0.04

Table AII.14 – Maximum simultaneous values on all wall slippage for seismic test TEST_02

TEST007_02	GLW02Y	GLW04X	GLW06Y	GLW07X
GLW02Y	0.06	0.01	0.01	0.01
GLW04X	0.01	0.01	0.01	0.01
GLW06Y	0.02	0.01	0.02	0.01
GLW07X	0.01	0.00	0.00	0.03

Table AII.15 – Maximum simultaneous values on all wall slippage for seismic test TEST_03

TEST007_03	GLW02Y	GLW04X	GLW06Y	GLW07X
GLW02Y	0.05	0.01	0.01	0.01
GLW04X	0.01	0.02	0.01	0.01
GLW06Y	0.01	0.00	0.02	0.00
GLW07X	0.01	0.00	0.00	0.03

Table AII.16 – Maximum simultaneous values on all wall uplifts for seismic test TEST_04

TEST007_04	GLW02Y	GLW04X	GLW06Y	GLW07X
GLW02Y	0.05	0.01	0.01	0.00
GLW04X	0.02	0.02	0.01	0.00
GLW06Y	0.02	0.00	0.02	0.00
GLW07X	0.02	0.00	0.00	0.03

Table AII.17 – Maximum simultaneous values on all wall slippage for seismic test TEST_05

TEST028_01	GLW02Y	GLW04X	GLW06Y	GLW07X
GLW02Y	1.17	2.07	0.22	0.02
GLW04X	1.14	2.10	0.22	0.05
GLW06Y	1.13	2.02	0.30	0.19
GLW07X	0.86	2.05	0.20	0.56

Table AII.18 – Maximum simultaneous values on all wall slippage for seismic test TEST_06

TEST028_02	GLW02Y	GLW04X	GLW06Y	GLW07X
GLW02Y	1.91	3.32	0.83	0.15
GLW04X	1.26	3.49	0.79	0.77
GLW06Y	1.54	3.36	0.90	0.70
GLW07X	1.45	3.39	0.86	0.80

Table AII.19 – Maximum simultaneous values on all wall slippage for seismic test TEST_07

TEST028_03	GLW02Y	GLW04X	GLW06Y	GLW07X
GLW02Y	2.41	3.93	0.88	0.14
GLW04X	1.59	4.19	1.00	1.02
GLW06Y	1.90	4.07	1.18	0.96
GLW07X	1.74	4.12	1.02	1.05

Table AII.20 – Maximum simultaneous values on all wall slippage for seismic test TEST_08

TEST028_04	GLW02Y	GLW04X	GLW06Y	GLW07X
GLW02Y	1.07	3.99	0.53	0.06
GLW04X	0.86	4.09	0.45	0.46
GLW06Y	1.03	4.00	0.55	0.04
GLW07X	0.91	4.08	0.50	0.50

Table AII.21 – Maximum simultaneous values on all wall slippage for seismic test TEST_09

TEST028_05	GLW02Y	GLW04X	GLW06Y	GLW07X
GLW02Y	2.06	4.07	1.03	0.42
GLW04X	1.66	4.31	0.92	0.76
GLW06Y	1.92	4.14	1.08	0.03
GLW07X	1.70	4.29	0.91	0.76

Table AII.22 – Maximum simultaneous values on all wall slippage for seismic test TEST_10

TEST028_06	GLW02Y	GLW04X	GLW06Y	GLW07X
GLW02Y	2.52	4.25	0.96	0.48
GLW04X	1.85	4.54	1.16	0.84
GLW06Y	1.99	4.51	1.18	0.83
GLW07X	2.11	4.45	1.17	0.87

Table AII.23 – Maximum simultaneous values on all wall slippage for seismic test TEST_11

TEST050_01	GLW02Y	GLW04X	GLW06Y	GLW07X
GLW02Y	5.83	5.72	1.39	0.84
GLW04X	2.87	6.64	2.15	3.08
GLW06Y	0.19	4.38	2.58	0.90
GLW07X	2.63	6.62	2.16	3.12

Table AII.24 – Maximum simultaneous values on all wall slippage for seismic test TEST_12

TEST050_02	GLW02Y	GLW04X	GLW06Y	GLW07X
GLW02Y	7.21	5.99	2.63	0.78
GLW04X	4.24	6.97	2.16	4.16
GLW06Y	0.01	5.68	3.20	1.35
GLW07X	3.90	6.92	2.18	4.20

Table AII.25 – Maximum simultaneous values for all shear displacement for seismic test TEST_01

TEST007_01	GLW01Y_R	GLW02Y_L	GLW04X_L	GLW04X_R	GLW06Y_L	GLW06Y_R	GLW07X_L	GLW07X_R
GLW01Y_R	0.26	0.15	0.06	0.14	0.21	0.25	0.10	0.44
GLW02Y_L	0.13	0.17	0.06	0.14	0.18	0.22	0.09	0.21
GLW04X_L	0.06	0.09	0.21	0.11	0.11	0.06	0.13	0.25
GLW04X_R	0.18	0.06	0.08	0.20	0.20	0.26	0.16	0.27
GLW06Y_L	0.22	0.10	0.08	0.19	0.28	0.32	0.14	0.16
GLW06Y_R	0.22	0.10	0.08	0.19	0.28	0.32	0.14	0.16
GLW07X_L	0.21	0.07	0.16	0.18	0.23	0.17	0.21	0.07
GLW07X_R	0.12	0.08	0.08	0.04	0.06	0.06	0.03	0.67

Table AII.26 – Maximum simultaneous values for all shear displacement for seismic test TEST_02

TEST007_02	GLW01Y_R	GLW02Y_L	GLW04X_L	GLW04X_R	GLW06Y_L	GLW06Y_R	GLW07X_L	GLW07X_R
GLW01Y_R	0.25	0.13	0.09	0.11	0.26	0.27	0.17	0.05
GLW02Y_L	0.20	0.19	0.05	0.16	0.23	0.24	0.14	0.48
GLW04X_L	0.13	0.08	0.33	0.18	0.21	0.18	0.12	0.48
GLW04X_R	0.17	0.09	0.27	0.18	0.18	0.14	0.07	0.20
GLW06Y_L	0.25	0.13	0.09	0.11	0.26	0.27	0.17	0.05
GLW06Y_R	0.18	0.06	0.01	0.05	0.25	0.28	0.10	0.13
GLW07X_L	0.09	0.00	0.15	0.09	0.18	0.13	0.21	0.22
GLW07X_R	0.11	0.02	0.18	0.04	0.13	0.10	0.03	0.63

Table AII.27 – Maximum simultaneous values for all shear displacement for seismic test TEST_03

TEST007_03	GLW01Y_R	GLW02Y_L	GLW04X_L	GLW04X_R	GLW06Y_L	GLW06Y_R	GLW07X_L	GLW07X_R
GLW01Y_R	0.22	0.00	0.17	0.12	0.24	0.28	0.13	0.13
GLW02Y_L	0.10	0.16	0.25	0.09	0.14	0.18	0.12	0.31
GLW04X_L	0.13	0.04	0.44	0.16	0.14	0.10	0.09	0.30
GLW04X_R	0.16	0.07	0.42	0.17	0.18	0.14	0.09	0.27
GLW06Y_L	0.22	0.00	0.17	0.12	0.24	0.28	0.13	0.13
GLW06Y_R	0.22	0.00	0.17	0.12	0.24	0.28	0.13	0.13
GLW07X_L	0.09	0.04	0.23	0.12	0.17	0.19	0.19	0.07
GLW07X_R	0.10	0.06	0.34	0.09	0.04	0.01	0.04	0.66

Table AII.28 – Maximum simultaneous values for all shear displacement for seismic test TEST_04

TEST007_04	GLW01Y_R	GLW02Y_L	GLW04X_L	GLW04X_R	GLW06Y_L	GLW06Y_R	GLW07X_L	GLW07X_R
GLW01Y_R	0.24	0.41	0.45	0.15	0.21	0.21	0.11	0.33
GLW02Y_L	0.08	0.42	0.48	0.13	0.18	0.18	0.16	0.00
GLW04X_L	0.07	0.34	0.72	0.14	0.14	0.13	0.05	0.40
GLW04X_R	0.18	0.16	0.67	0.19	0.24	0.19	0.10	0.20
GLW06Y_L	0.09	0.25	0.46	0.10	0.25	0.24	0.15	0.16
GLW06Y_R	0.13	0.26	0.47	0.03	0.16	0.27	0.11	0.06
GLW07X_L	0.12	0.18	0.58	0.08	0.08	0.10	0.18	0.17
GLW07X_R	0.05	0.18	0.54	0.00	0.01	0.00	0.07	0.61

Table AII.29 – Maximum simultaneous values for all shear displacement for seismic test TEST_05

TEST028_01	GLW01Y_R	GLW02Y_L	GLW04X_L	GLW04X_R	GLW06Y_L	GLW06Y_R	GLW07X_L	GLW07X_R
GLW01Y_R	42.61	1.94	2.67	0.36	4.68	4.58	0.76	0.39
GLW02Y_L	42.27	1.94	2.68	0.53	4.79	4.48	1.00	0.64
GLW04X_L	11.80	0.57	2.85	0.47	1.51	1.03	0.56	0.09
GLW04X_R	9.60	0.05	2.63	1.42	0.20	0.64	1.87	3.37
GLW06Y_L	33.49	1.62	2.59	0.04	4.87	4.39	0.13	1.74
GLW06Y_R	42.15	1.94	2.76	0.21	4.67	4.59	0.63	0.21
GLW07X_L	9.70	0.06	2.64	1.38	0.21	0.62	1.88	3.38
GLW07X_R	0.31	0.34	2.70	0.31	1.47	0.88	1.17	4.26

Table AII.30 – Maximum simultaneous values for all shear displacement for seismic test TEST_06

TEST028_02	GLW01Y_R	GLW02Y_L	GLW04X_L	GLW04X_R	GLW06Y_L	GLW06Y_R	GLW07X_L	GLW07X_R
GLW01Y_R	77.57	3.44	2.89	0.09	7.17	6.91	0.25	1.52
GLW02Y_L	77.57	3.44	2.89	0.09	7.17	6.91	0.25	1.52
GLW04X_L	15.46	0.92	3.13	0.71	2.48	1.52	0.11	0.60
GLW04X_R	22.89	0.34	2.81	1.67	0.66	1.65	1.55	2.93
GLW06Y_L	75.18	3.35	2.87	0.55	7.29	6.43	0.92	0.86
GLW06Y_R	74.82	3.33	2.94	0.06	7.13	7.01	0.01	1.90
GLW07X_L	47.48	2.35	2.87	0.54	6.13	5.57	2.09	6.41
GLW07X_R	28.46	1.51	2.91	0.67	4.84	4.39	1.99	6.77

Table AII.31 – Maximum simultaneous values for all shear displacement for seismic test TEST_07

TEST028_03	GLW01Y_R	GLW02Y_L	GLW04X_L	GLW04X_R	GLW06Y_L	GLW06Y_R	GLW07X_L	GLW07X_R
GLW01Y_R	93.77	4.38	2.54	0.25	7.70	6.90	0.71	0.58
GLW02Y_L	93.77	4.38	2.54	0.25	7.70	6.90	0.71	0.58
GLW04X_L	17.48	1.35	2.73	0.86	2.52	1.67	0.13	0.49
GLW04X_R	17.18	0.20	2.51	2.60	0.96	1.79	2.68	4.74
GLW06Y_L	93.77	4.38	2.54	0.25	7.70	6.90	0.71	0.58
GLW06Y_R	90.78	4.28	2.58	0.50	7.60	7.68	0.36	2.77
GLW07X_L	45.32	2.52	2.55	1.18	5.42	4.88	3.13	8.49
GLW07X_R	34.19	2.10	2.55	1.20	4.39	3.59	3.11	8.55

Table AII.32 – Maximum simultaneous values for all shear displacement for seismic test TEST_08

TEST028_04	GLW01Y_R	GLW02Y_L	GLW04X_L	GLW04X_R	GLW06Y_L	GLW06Y_R	GLW07X_L	GLW07X_R
GLW01Y_R	33.51	2.09	2.00	0.64	4.08	3.55	0.75	2.75
GLW02Y_L	31.54	2.19	2.09	1.60	3.99	2.99	1.06	2.10
GLW04X_L	13.60	1.46	2.28	0.88	1.95	1.41	0.39	0.28
GLW04X_R	0.97	1.04	1.97	1.70	1.41	0.12	0.81	1.56
GLW06Y_L	33.29	2.06	2.02	0.75	4.44	3.74	0.67	2.37
GLW06Y_R	33.13	2.05	2.07	0.50	4.17	4.01	0.64	2.93
GLW07X_L	15.44	1.55	2.04	0.46	3.51	2.47	1.38	4.10
GLW07X_R	21.63	1.77	2.02	0.43	3.66	2.74	1.22	4.27

Table AII.33 – Maximum simultaneous values for all shear displacement for seismic test TEST_09

TEST028_05	GLW01Y_R	GLW02Y_L	GLW04X_L	GLW04X_R	GLW06Y_L	GLW06Y_R	GLW07X_L	GLW07X_R
GLW01Y_R	72.82	3.91	2.38	0.65	6.96	6.52	0.68	0.49
GLW02Y_L	72.79	3.92	2.31	1.47	7.03	6.28	1.53	2.78
GLW04X_L	19.74	1.59	2.58	1.00	2.58	2.01	0.33	0.35
GLW04X_R	8.99	0.89	2.23	2.26	0.29	0.83	1.77	3.73
GLW06Y_L	69.63	3.82	2.29	0.36	7.08	6.40	0.05	1.07
GLW06Y_R	67.51	3.67	2.40	0.23	6.56	6.65	0.55	3.14
GLW07X_L	41.22	2.70	2.31	0.29	5.49	4.77	2.20	6.09
GLW07X_R	37.09	2.51	2.37	0.40	4.77	4.63	2.09	6.26

Table AII.34 – Maximum simultaneous values for all shear displacement for seismic test TEST_10

TEST028_06	GLW01Y_R	GLW02Y_L	GLW04X_L	GLW04X_R	GLW06Y_L	GLW06Y_R	GLW07X_L	GLW07X_R
GLW01Y_R	91.34	4.41	2.79	1.80	8.21	7.21	1.91	3.67
GLW02Y_L	91.24	4.42	2.90	0.28	8.08	8.01	0.83	3.39
GLW04X_L	18.32	1.60	3.09	1.33	3.13	2.20	0.30	0.47
GLW04X_R	12.47	0.60	2.81	2.78	0.27	0.90	2.51	5.30
GLW06Y_L	91.22	4.41	2.85	0.63	8.47	7.84	0.62	0.23
GLW06Y_R	91.08	4.38	2.95	0.05	8.21	8.13	0.09	1.49
GLW07X_L	12.72	0.56	2.96	2.64	0.11	0.72	2.81	4.94
GLW07X_R	69.59	3.56	2.90	0.46	7.44	7.05	2.33	6.99

Table AII.35 – Maximum simultaneous values for all shear displacement for seismic test TEST_11

TEST050_01	GLW01Y_R	GLW02Y_L	GLW04X_L	GLW04X_R	GLW06Y_L	GLW06Y_R	GLW07X_L	GLW07X_R
GLW01Y_R	142.71	4.48	2.24	1.42	11.86	12.17	2.33	5.54
GLW02Y_L	133.22	7.94	1.60	1.02	15.94	17.36	1.19	5.14
GLW04X_L	18.49	1.82	2.78	1.40	3.68	2.82	0.05	1.24
GLW04X_R	70.32	3.92	2.41	5.96	7.49	6.37	5.93	11.51
GLW06Y_L	133.22	7.89	1.63	2.32	16.23	16.13	3.37	5.82
GLW06Y_R	133.22	7.75	1.72	1.59	15.88	17.45	2.61	8.73
GLW07X_L	91.79	4.61	2.38	4.44	9.54	8.72	7.43	18.26
GLW07X_R	94.12	4.67	2.44	4.61	10.30	10.11	7.40	19.60

Table AII.36 – Maximum simultaneous values for all shear displacement for seismic test TEST_12

TEST050_02	GLW01Y_R	GLW02Y_L	GLW04X_L	GLW04X_R	GLW06Y_L	GLW06Y_R	GLW07X_L	GLW07X_R
GLW01Y_R	143.09	3.61	2.23	2.01	13.89	14.78	2.36	6.32
GLW02Y_L	133.24	8.31	2.34	2.86	17.49	18.90	4.49	13.43
GLW04X_L	33.50	1.74	2.51	1.01	2.06	2.69	0.10	1.31
GLW04X_R	92.60	5.57	2.30	8.03	8.69	7.77	8.72	16.88
GLW06Y_L	133.22	8.21	2.33	2.38	19.01	21.84	2.48	9.25
GLW06Y_R	133.22	8.19	2.30	0.15	18.56	22.31	1.14	1.56
GLW07X_L	133.21	7.10	2.31	6.86	12.17	12.85	9.49	25.71
GLW07X_R	133.22	7.18	2.29	6.69	12.16	13.11	9.40	25.87

Table AII.37 – Maximum simultaneous values for all inter-storey drift for seismic test TEST_01

TEST007_01	GL_X	GL_Y	L1_X
GL_X	0.08	0.09	0.06
GL_Y	0.01	0.61	0.02
L1_X	0.06	0.08	0.07

Table AII.38 – Maximum simultaneous values for all inter-storey drift for seismic test TEST_02

TEST007_02	GL_X	GL_Y	L1_X
GL_X	0.07	0.10	0.06
GL_Y	0.01	0.65	0.01
L1_X	0.05	0.05	0.06

Table AII.39 – Maximum simultaneous values for all inter-storey drift for seismic test TEST_03

TEST007_03	GL_X	GL_Y	L1_X
GL_X	0.06	0.04	0.05
GL_Y	0.02	0.54	0.03
L1_X	0.05	0.06	0.06

Table AII.40 – Maximum simultaneous values for all inter-storey drift for seismic test TEST_04

TEST007_04	GL_X	GL_Y	L1_X
GL_X	0.06	0.08	0.05
GL_Y	0.03	0.55	0.03
L1_X	0.06	0.07	0.06

Table AII.41 – Maximum simultaneous values for all inter-storey drift for seismic test TEST_05

TEST028_01	GL_X	GL_Y	L1_X
GL_X	0.07	1.40	0.06
GL_Y	0.00	8.91	0.01
L1_X	0.05	1.00	0.06

Table AII.42 – Maximum simultaneous values for all inter-storey drift for seismic test TEST_06

TEST028_02	GL_X	GL_Y	L1_X
GL_X	0.07	1.59	0.06
GL_Y	0.02	14.46	0.03
L1_X	0.06	2.29	0.07

Table AII.43 – Maximum simultaneous values for all inter-storey drift for seismic test TEST_07

TEST028_03	GL_X	GL_Y	L1_X
GL_X	0.07	2.29	0.05
GL_Y	0.03	17.02	0.01
L1_X	0.06	3.84	0.06

Table AII.44 – Maximum simultaneous values for all inter-storey drift for seismic test TEST_08

TEST028_04	GL_X	GL_Y	L1_X
GL_X	0.09	1.93	0.09
GL_Y	0.05	6.85	0.05
L1_X	0.09	2.41	0.10

Table AII.45 – Maximum simultaneous values for all inter-storey drift for seismic test TEST_09

TEST028_05	GL_X	GL_Y	L1_X
GL_X	0.09	2.86	0.07
GL_Y	0.04	13.94	0.04
L1_X	0.06	2.93	0.08

Table AII.46 – Maximum simultaneous values for all inter-storey drift for seismic test TEST_10

TEST028_06	GL_X	GL_Y	L1_X
GL_X	0.08	2.90	0.07
GL_Y	0.05	17.84	0.04
L1_X	0.08	2.90	0.07

Table AII.47 – Maximum simultaneous values for all inter-storey drift for seismic test TEST_11

TEST050_01	GL_X	GL_Y	L1_X
GL_X	0.07	29.37	0.04
GL_Y	0.01	29.97	0.00
L1_X	0.03	29.48	0.08

Table AII.48 – Maximum simultaneous values for all inter-storey drift for seismic test TEST_12

TEST050_02	GL_X	GL_Y	L1_X
GL_X	0.09	25.63	0.07
GL_Y	0.03	30.49	0.02
L1_X	0.06	29.48	0.07

FRF estimates

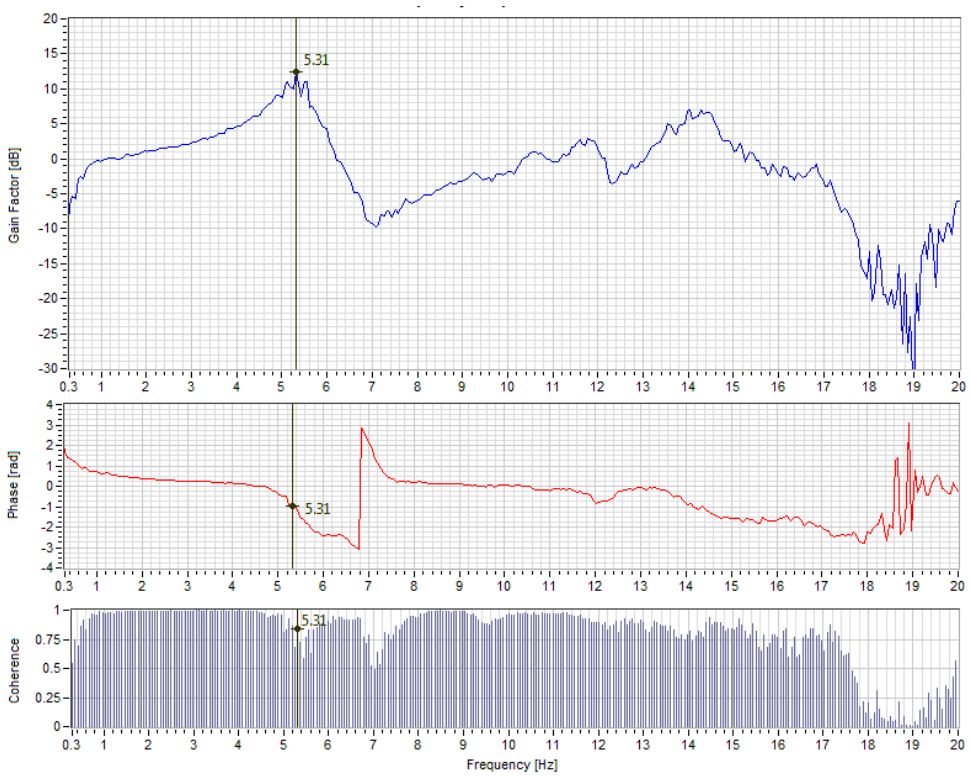

Figure AII.1: Frequency response function, phase and coherence (Cat 1): ACC MESA TRANS; ACC_L1_C3_X_NE_T

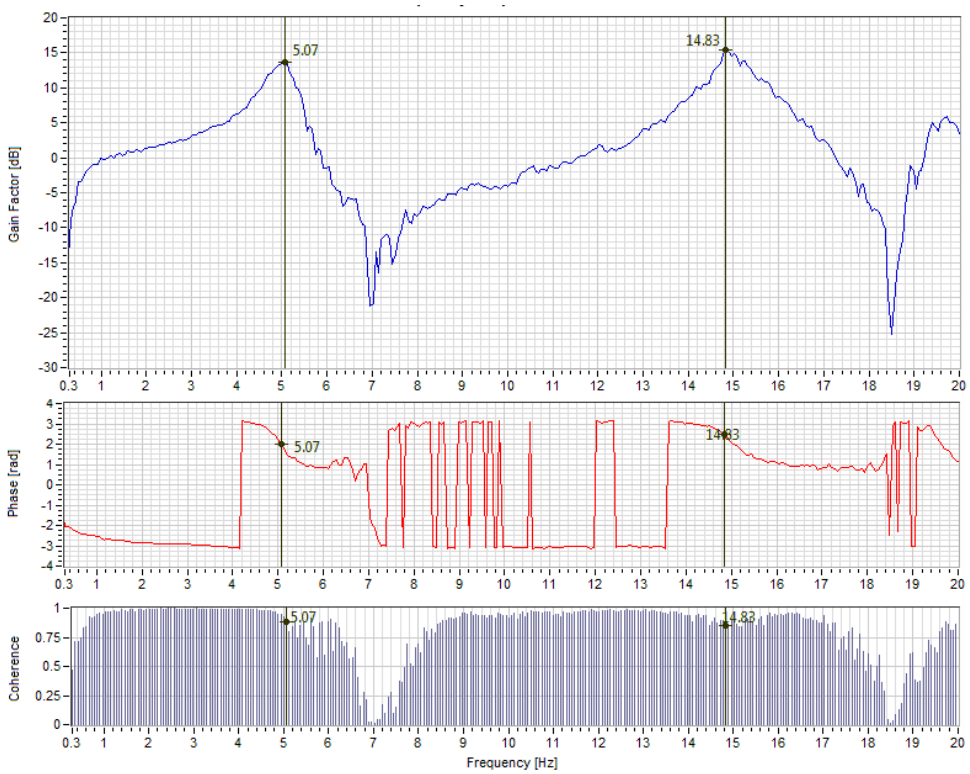

Figure AII. 2: Frequency response function, phase and coherence (Cat 1): ACC MESA TRANS; ACC_L1_C3_Y_NE_L

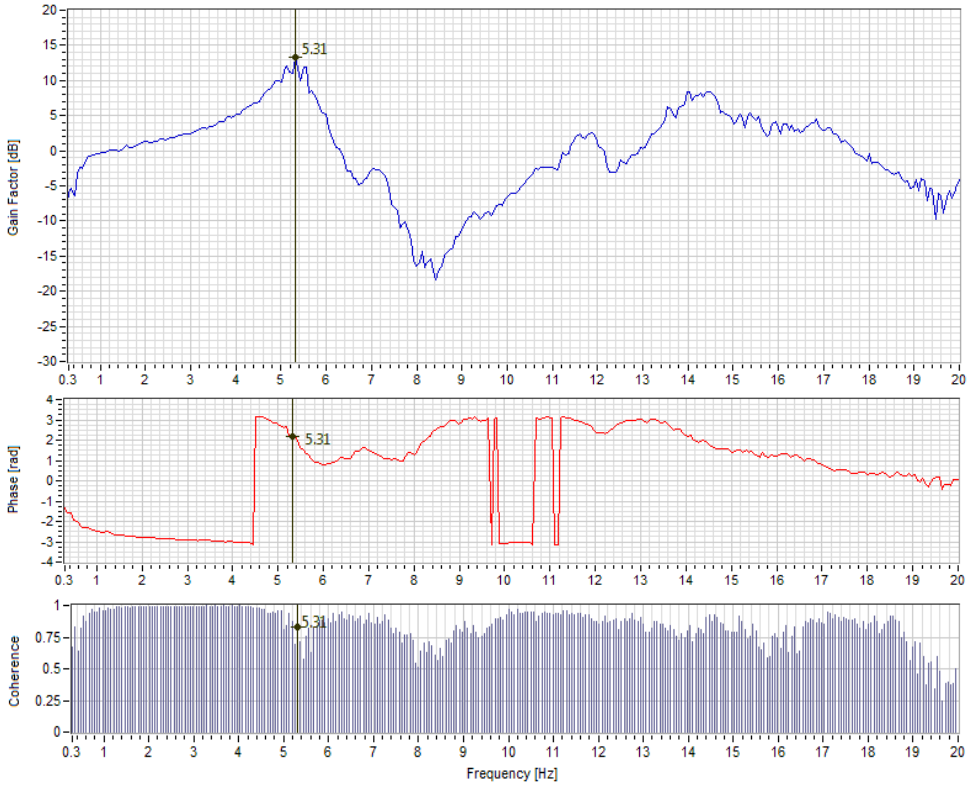

Figure AII. 3: Frequency response function, phase and coherence (Cat 1): ACC MESA TRANS; ACC_L1_A1_X_SW_T

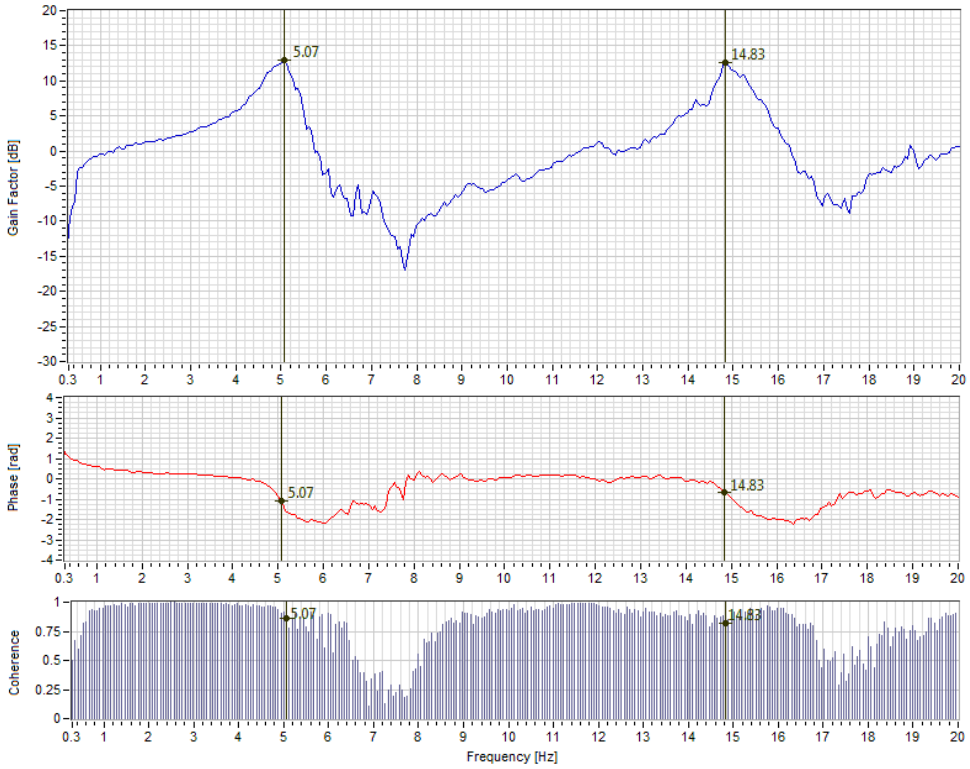

Figure AII. 4: Frequency response function, phase and coherence (Cat 1): ACC MESA LONG; ACC_L1_A1_Y_SW_L

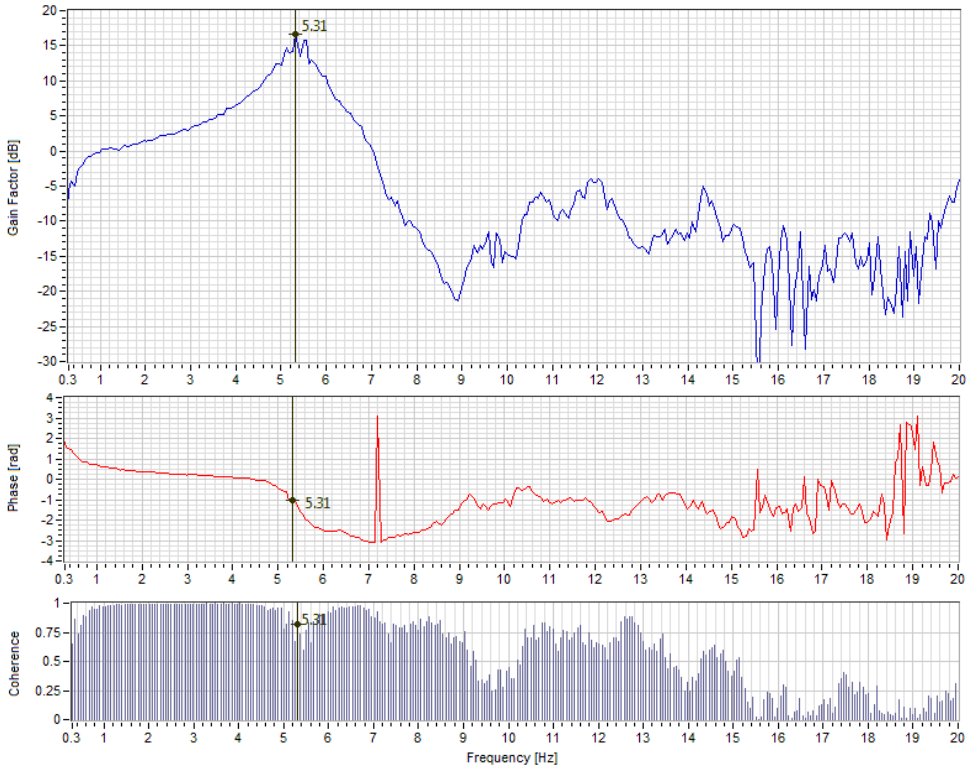

Figure AII. 5: Frequency response function, phase and coherence (Cat 1): ACC MESA TRANS; ACC_RL_C3_X_NE_T

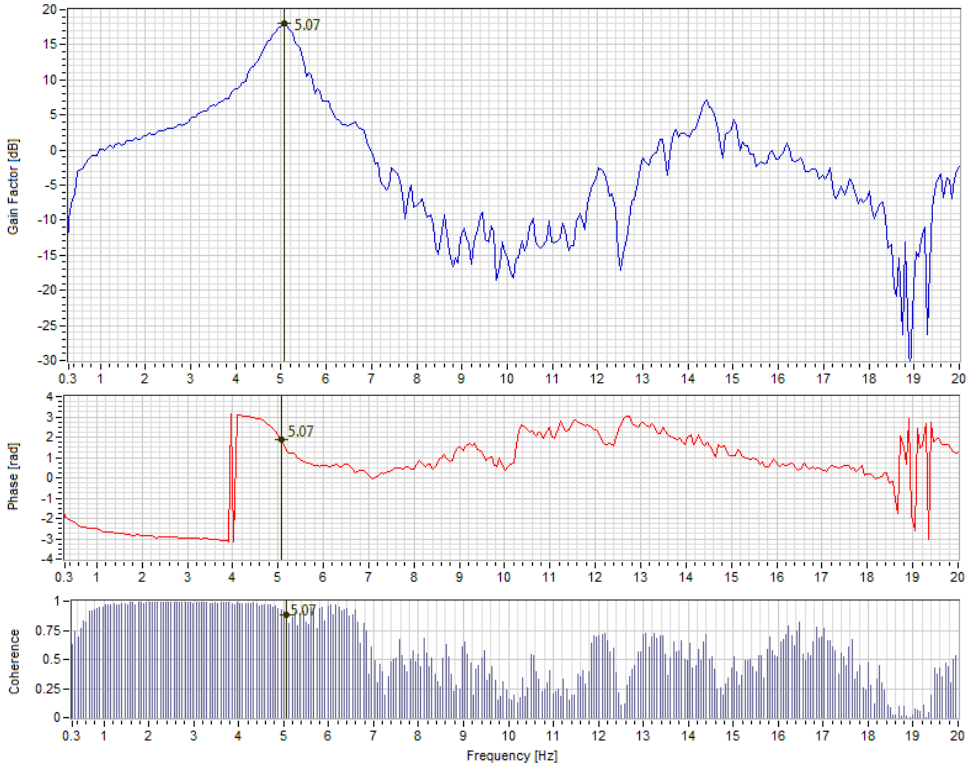

Figure AII. 6: Frequency response function, phase and coherence (Cat 1): ACC MESA LONG; ACC_RL_C3_Y_NE_L

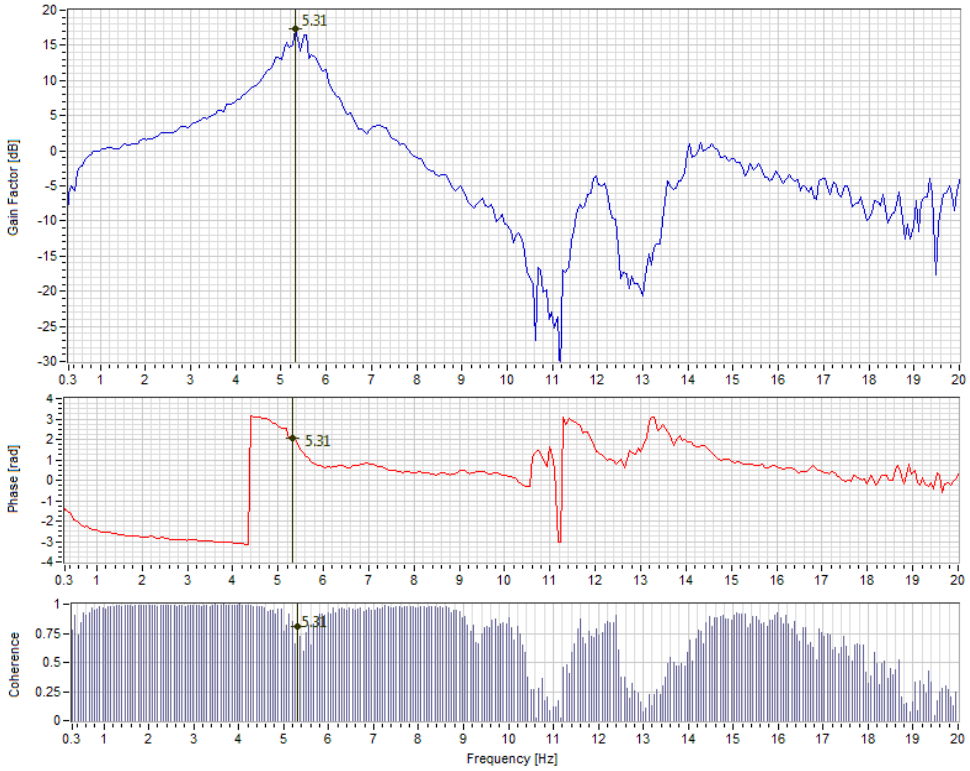

Figure AII. 7: Frequency response function, phase and coherence (Cat 1): ACC MESA TRANS; ACC_RL_A1_X_SW_T

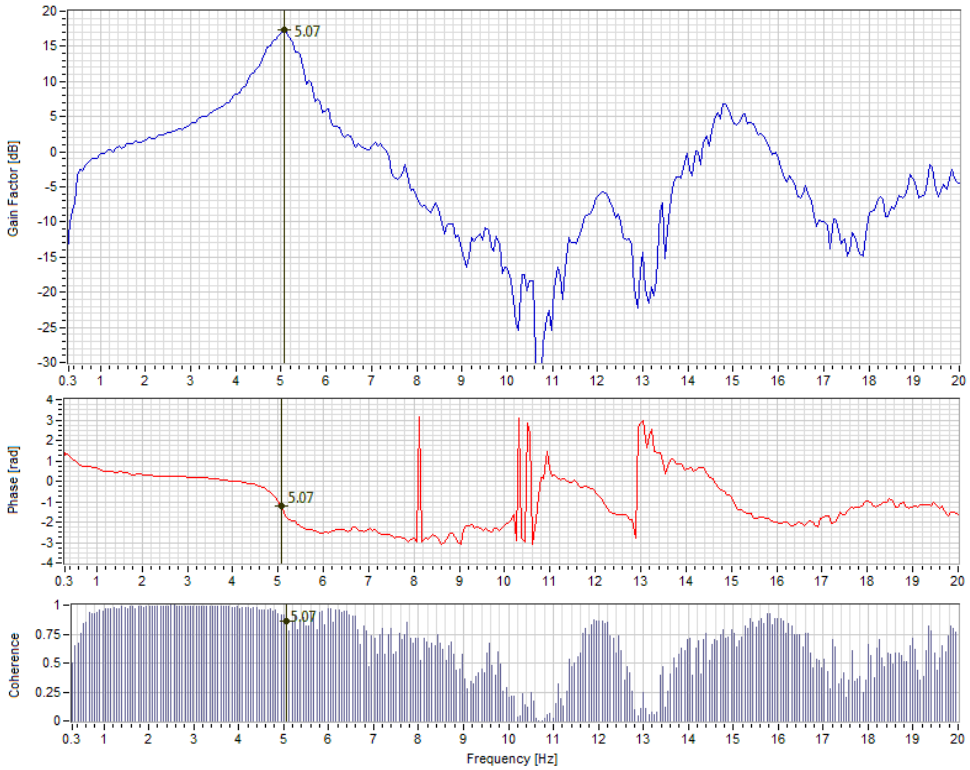

Figure AII. 8: Frequency response function, phase and coherence (Cat 1): ACC MESA LONG; ACC_RL_A1_Y_SW_L

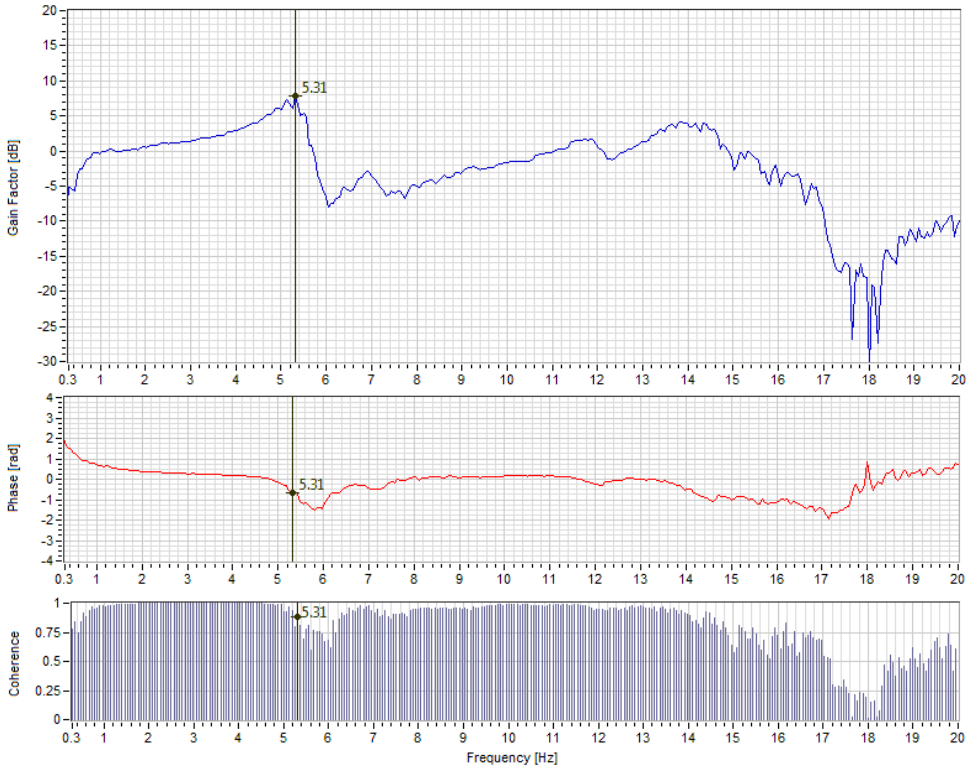

Figure AII. 9: Frequency response function, phase and coherence (Cat 1): ACC MESA TRANS; ACC_GL_A3_X_SE_T

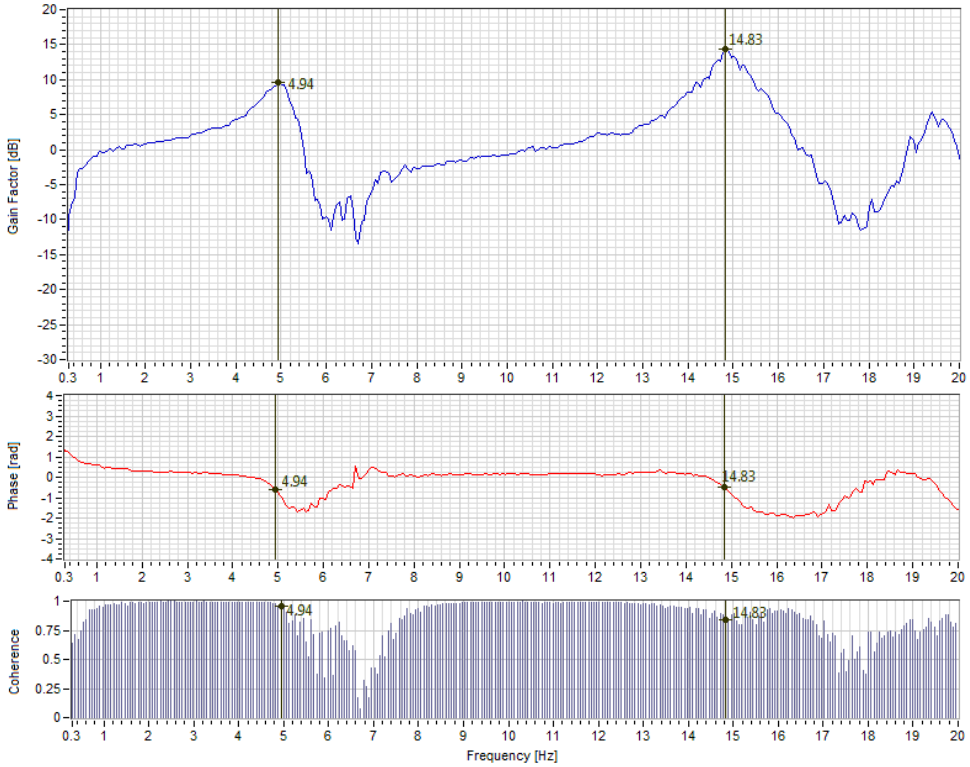

Figure AII. 10: Frequency response function, phase and coherence (Cat 1): ACC MESA LONG; ACC_GL_A3_Y_SE_L

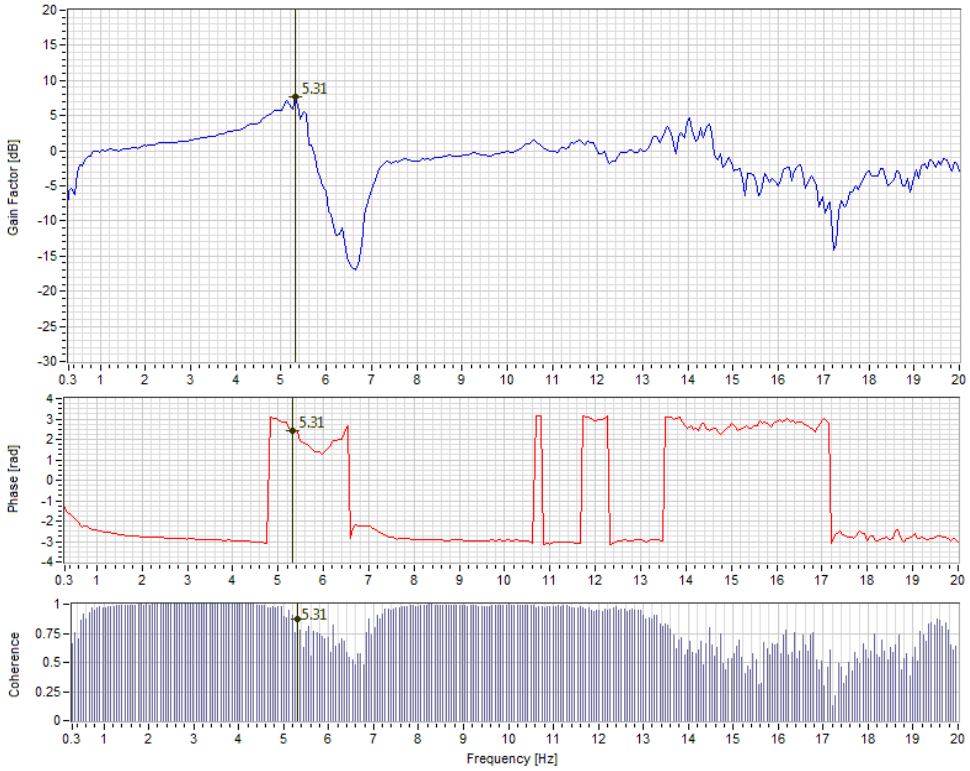

Figure AII. 11: Frequency response function, phase and coherence (Cat 1): ACC MESA TRANS; ACC_GL_C1_X_NW_T

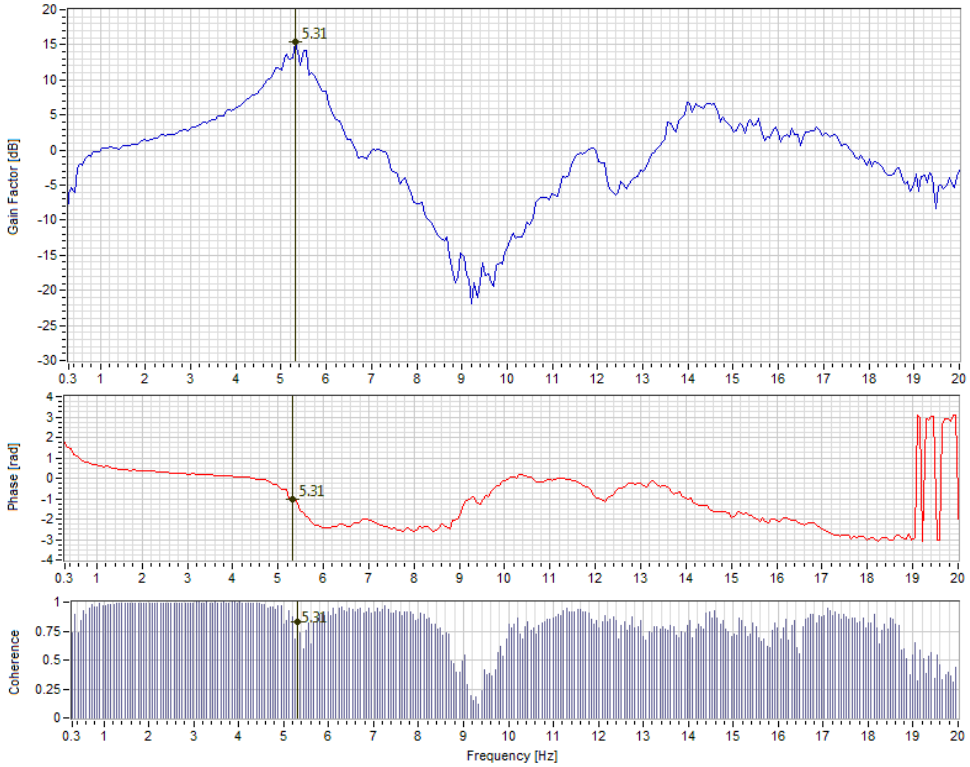

Figure AII. 12: Frequency response function, phase and coherence (Cat 1): ACC MESA TRANS; ACC_L1_A3_X_SE_T

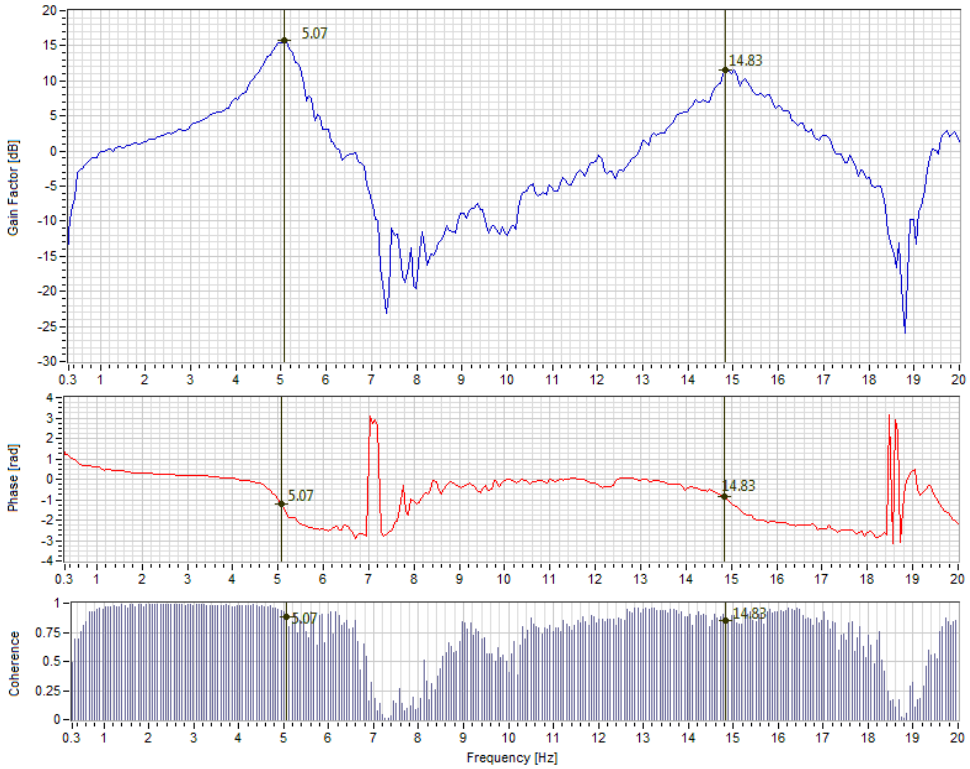

Figure AII. 13: Frequency response function, phase and coherence (Cat 1): ACC MESA LONG; ACC_L1_A3_Y_SE_L

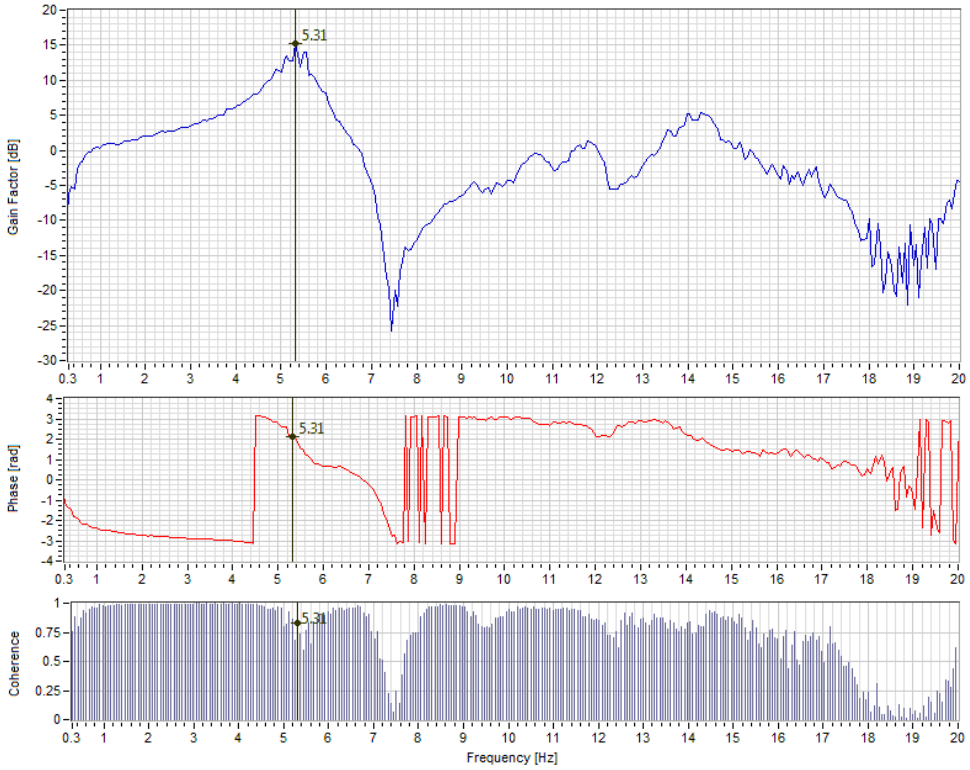

Figure AII. 14: Frequency response function, phase and coherence (Cat 1): ACC MESA TRANS; ACC_L1_C1_X_NW_T

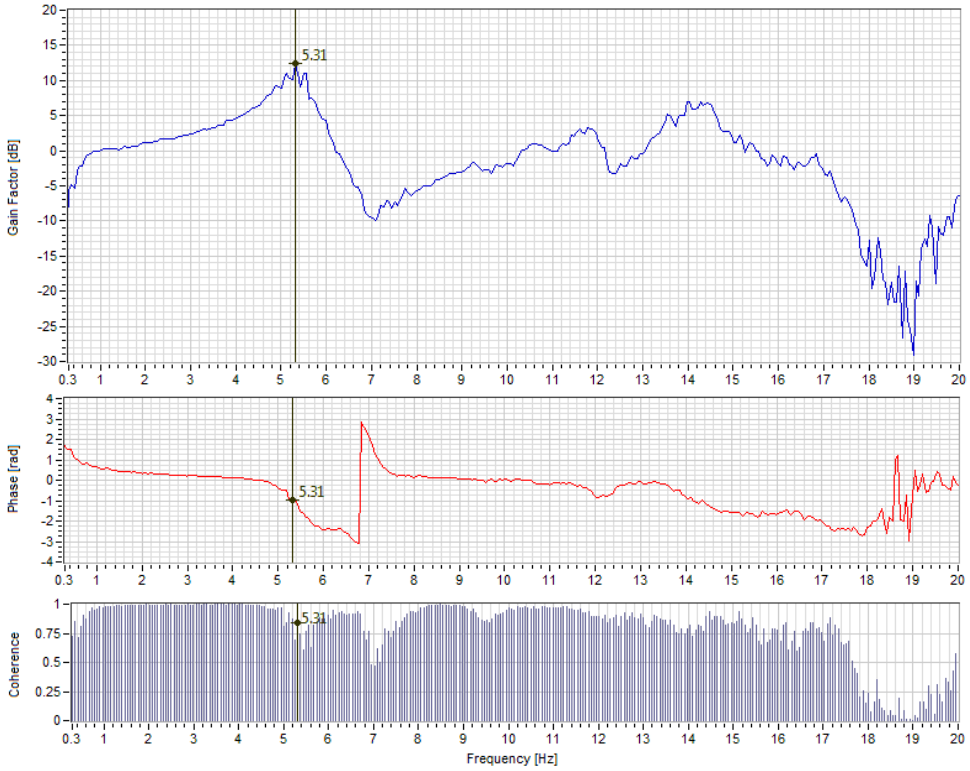

Figure AII. 15: Frequency response function, phase and coherence (Cat 1): ACC MESA TRANS; ACC_L1_C2_X_N_T

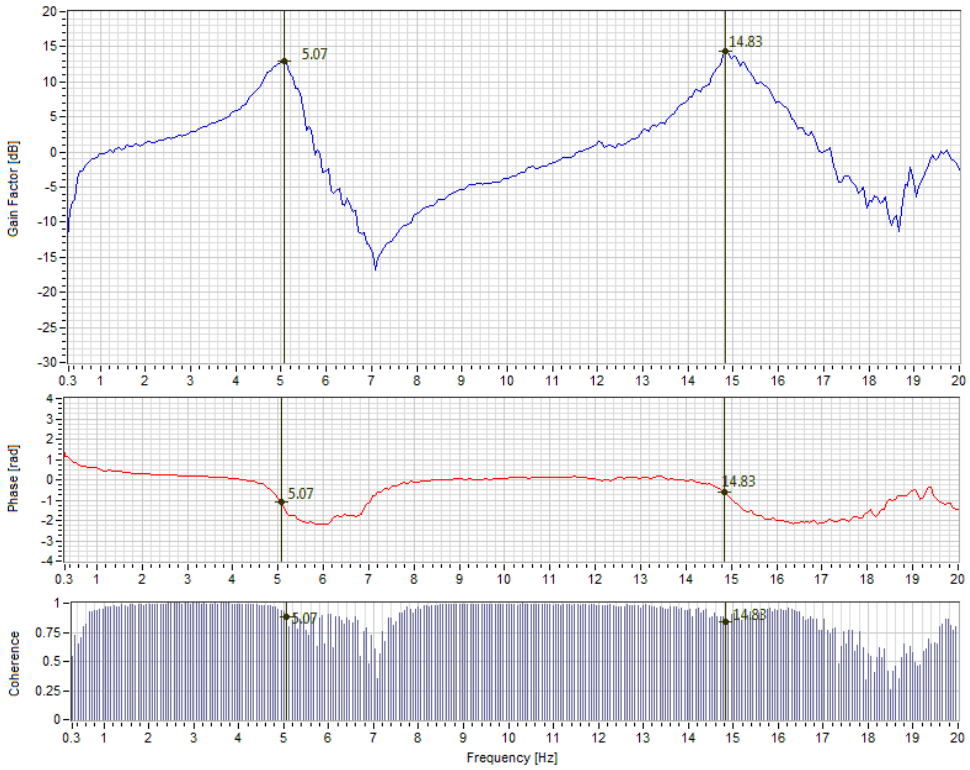

Figure AII. 16: Frequency response function, phase and coherence (Cat 1): ACC MESA LONG; ACC_L1_C2_Y_N_L

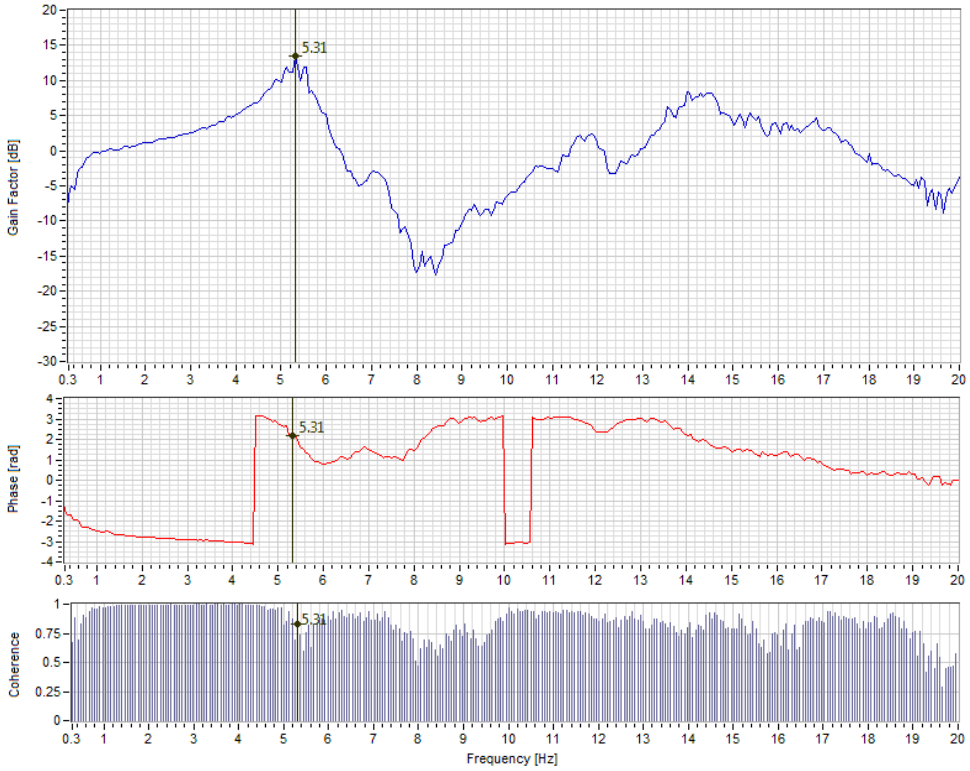

Figure AII. 17: Frequency response function, phase and coherence (Cat 1): ACC MESA TRANS; ACC_L1_A2_X_S_T

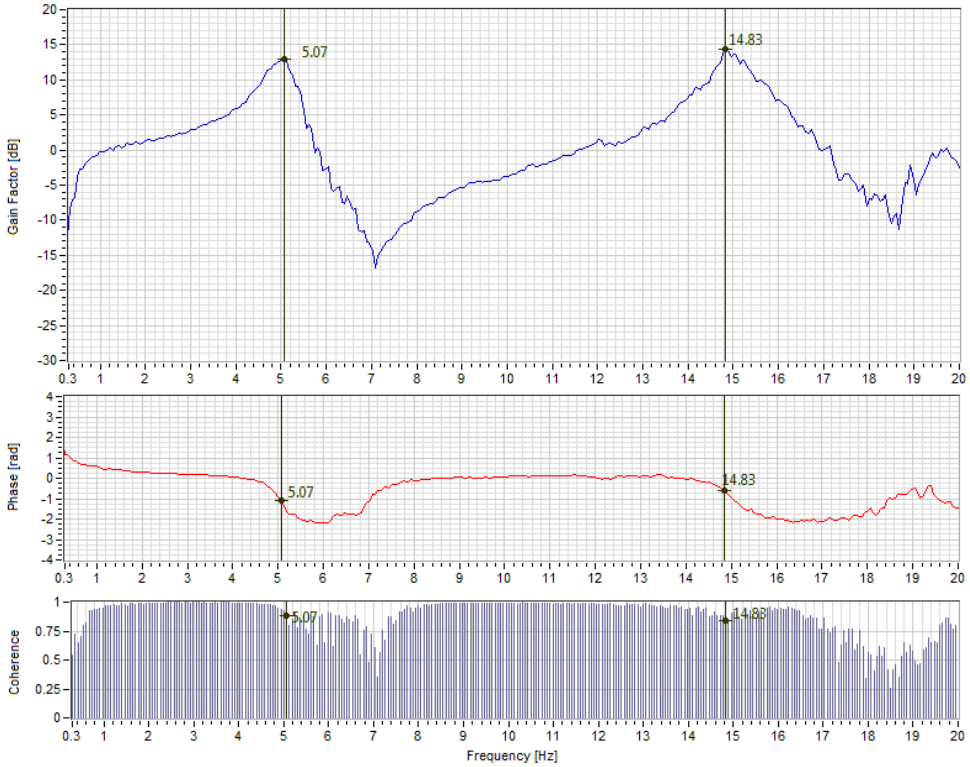

Figure AII. 18: Frequency response function, phase and coherence (Cat 1): ACC MESA LONG; ACC_L1_A2_Y_S_L

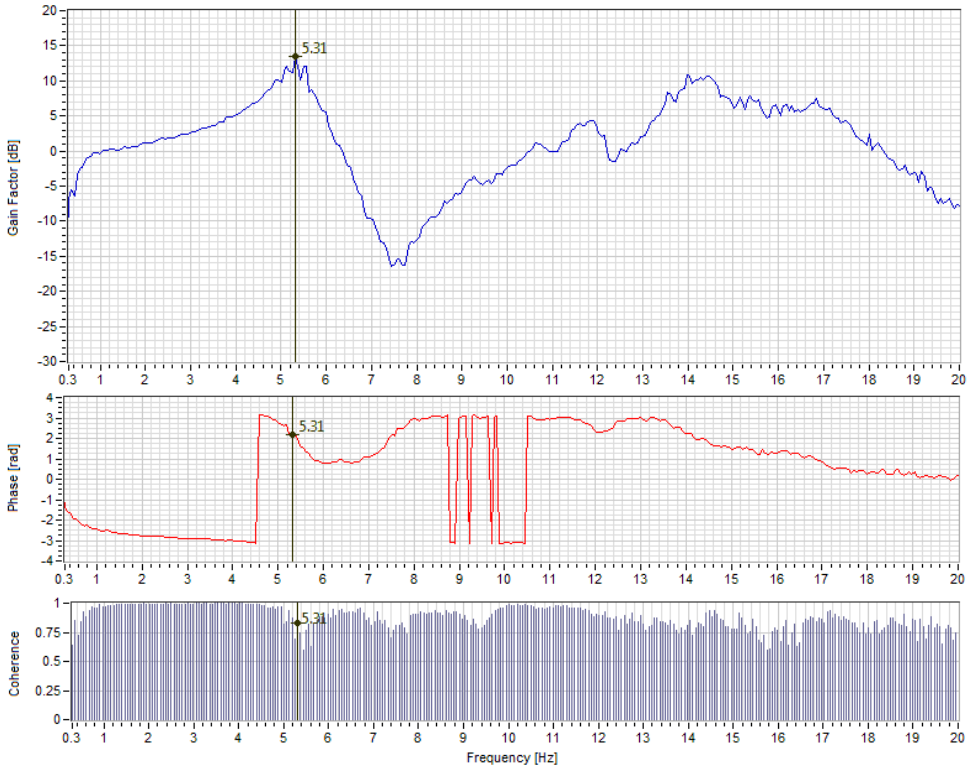

Figure AII. 19: Frequency response function, phase and coherence (Cat 1): ACC MESA TRANS; ACC_L1_B1_X_W_T

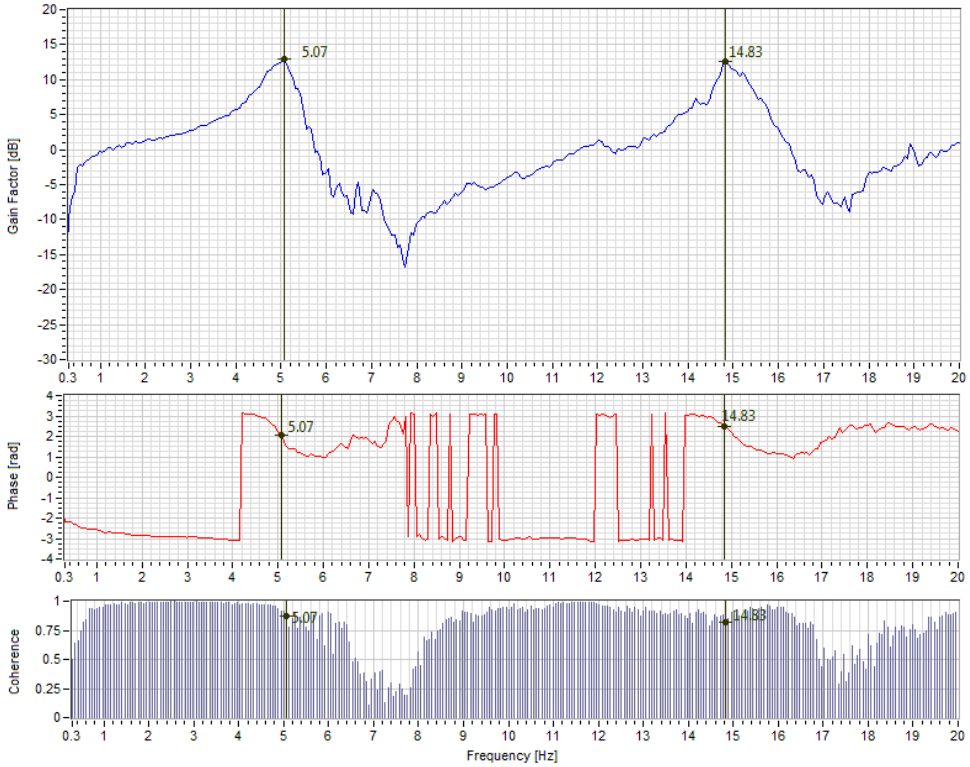

Figure AII. 20: Frequency response function, phase and coherence (Cat 1): ACC MESA TRANS; ACC_L1_B1_Y_W_L

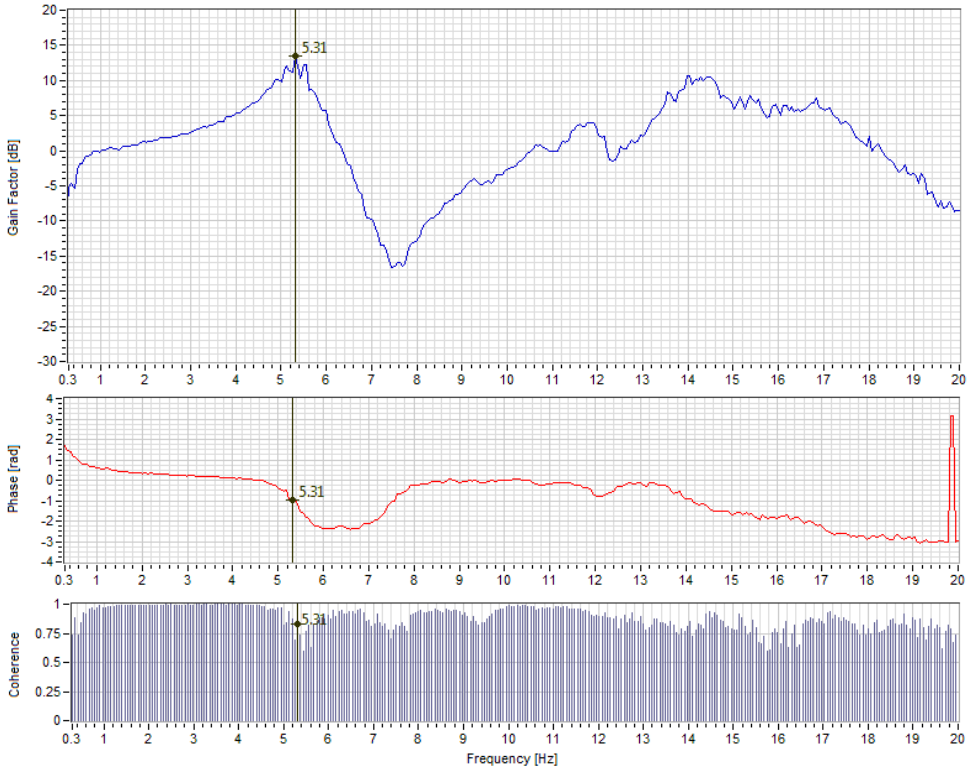

Figure AII. 21: Frequency response function, phase and coherence (Cat 1): ACC MESA TRANS; ACC_L1_B2_X_I_T

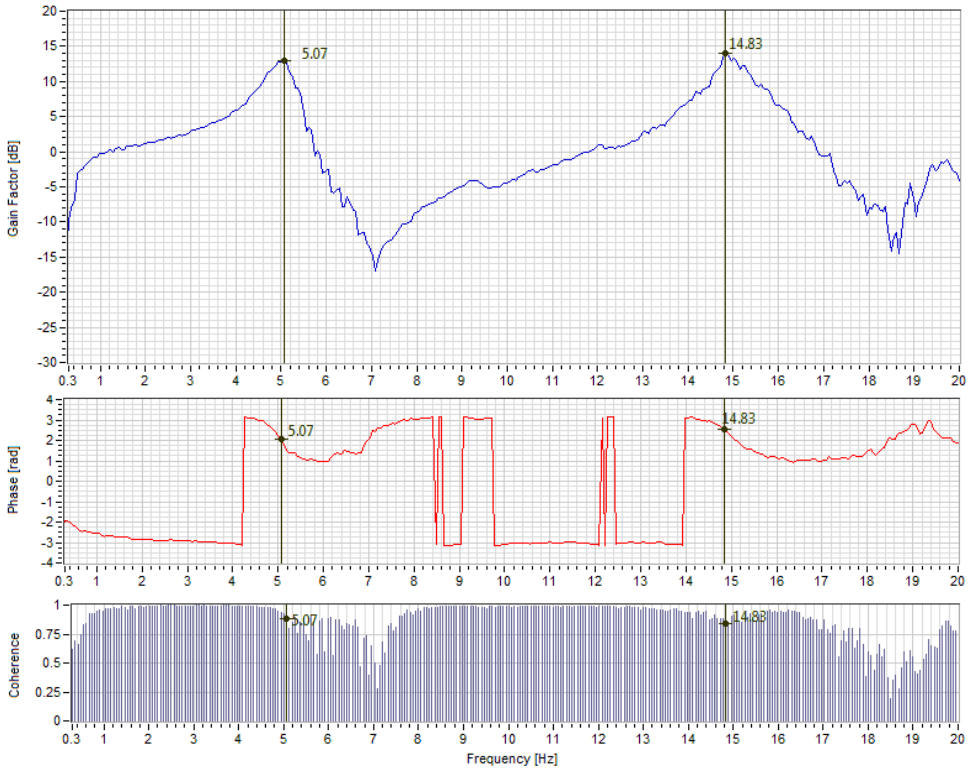

Figure AII. 22: Frequency response function, phase and coherence (Cat 1): ACC MESA LONG; ACC_L1_B2_Y_I_L

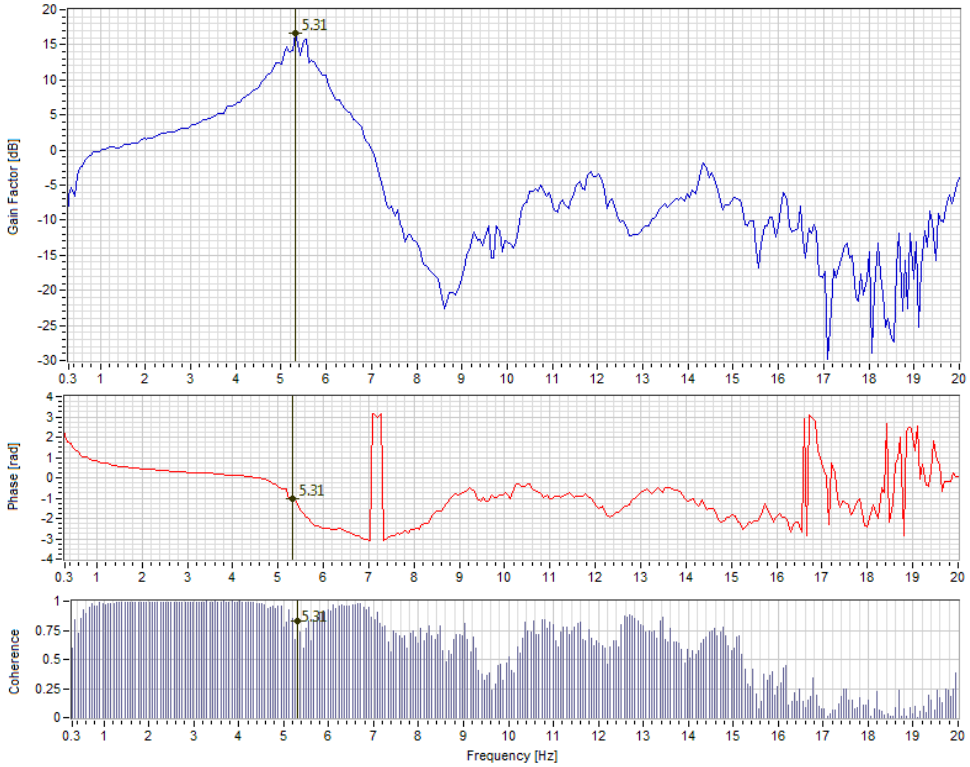

Figure AII. 23: Frequency response function, phase and coherence (Cat 1): ACC MESA TRANS; ACC_RL_C2_X_N_T

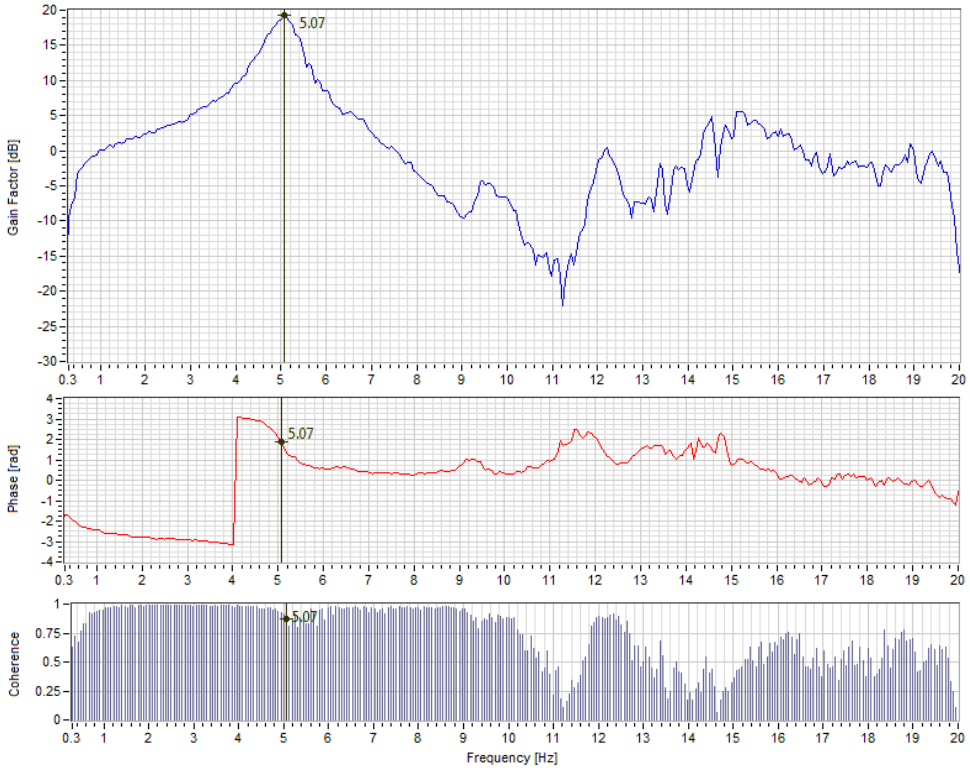

Figure AII. 24: Frequency response function, phase and coherence (Cat 1): ACC MESA LONG; ACC_RL_C2_Y_N_L

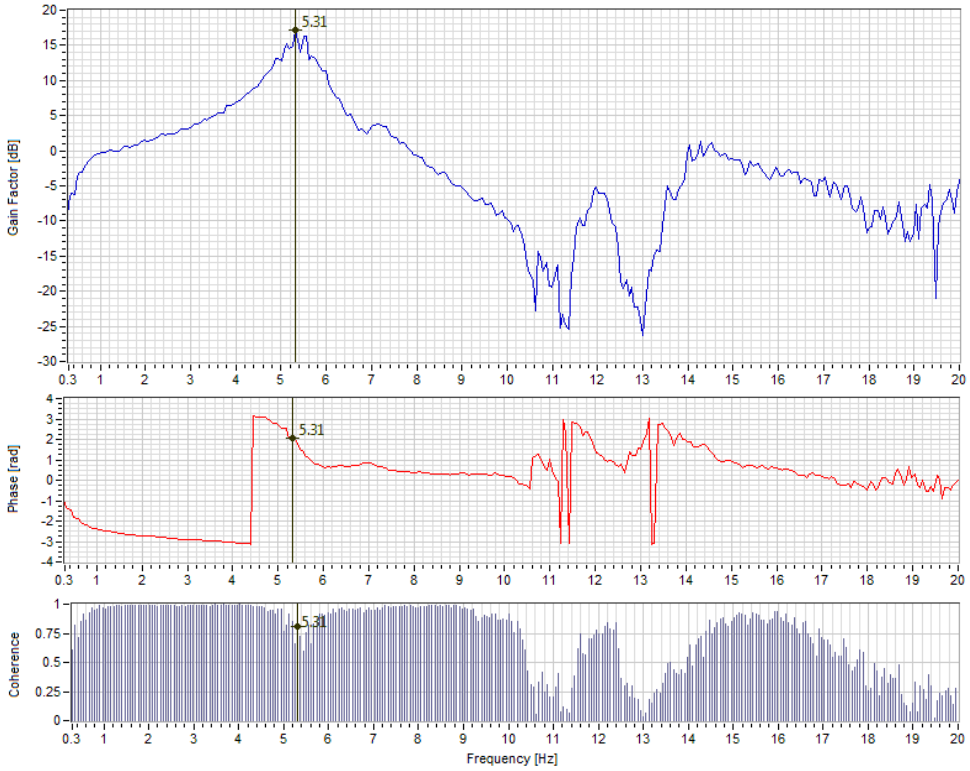

Figure AII. 25: Frequency response function, phase and coherence (Cat 1): ACC MESA TRANS; ACC_RL_A2_X_S_T

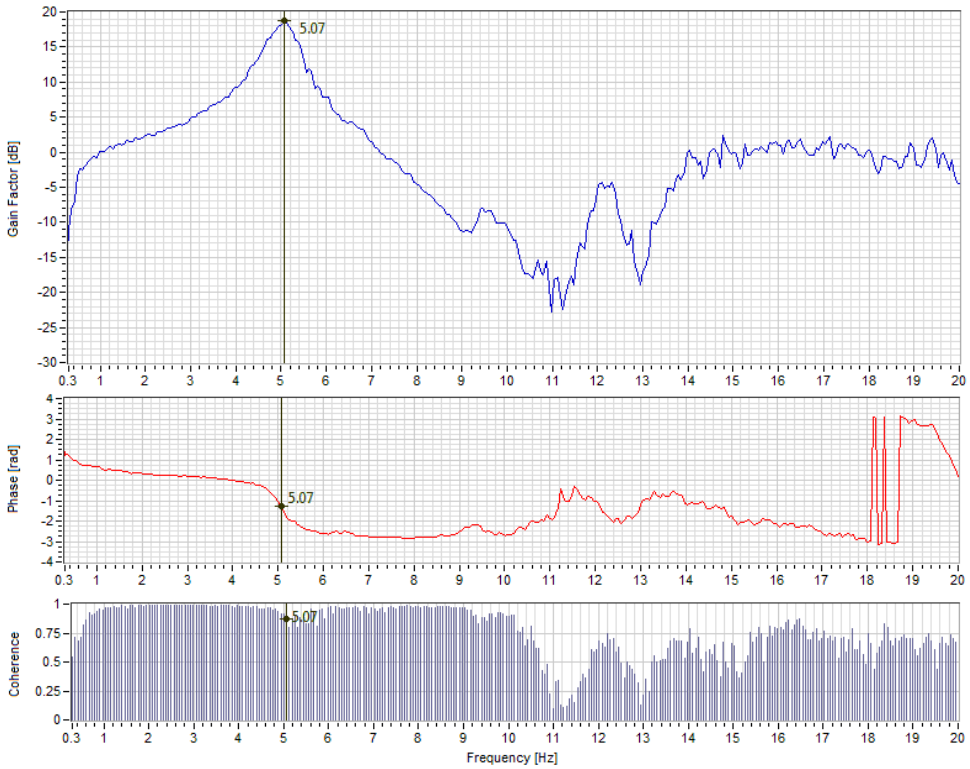

Figure AII. 26: Frequency response function, phase and coherence (Cat 1): ACC MESA LONG; ACC_RL_A2_Y_S_L

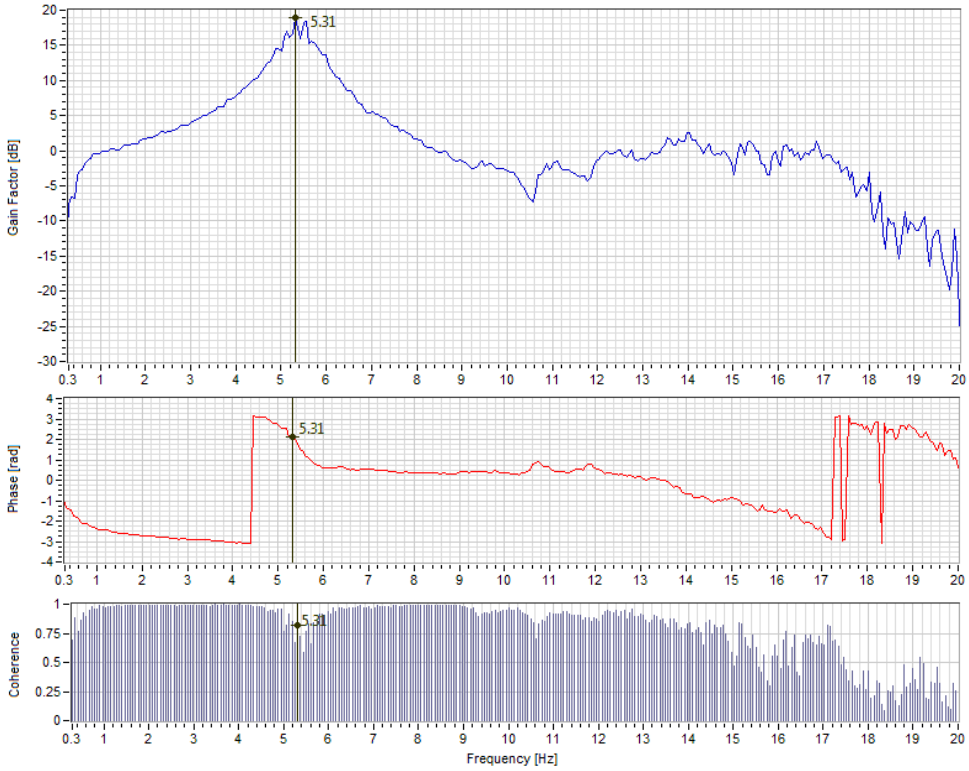

Figure AII. 27: Frequency response function, phase and coherence (Cat 1): ACC MESA TRANS; ACC_RL_B1_X_W_T

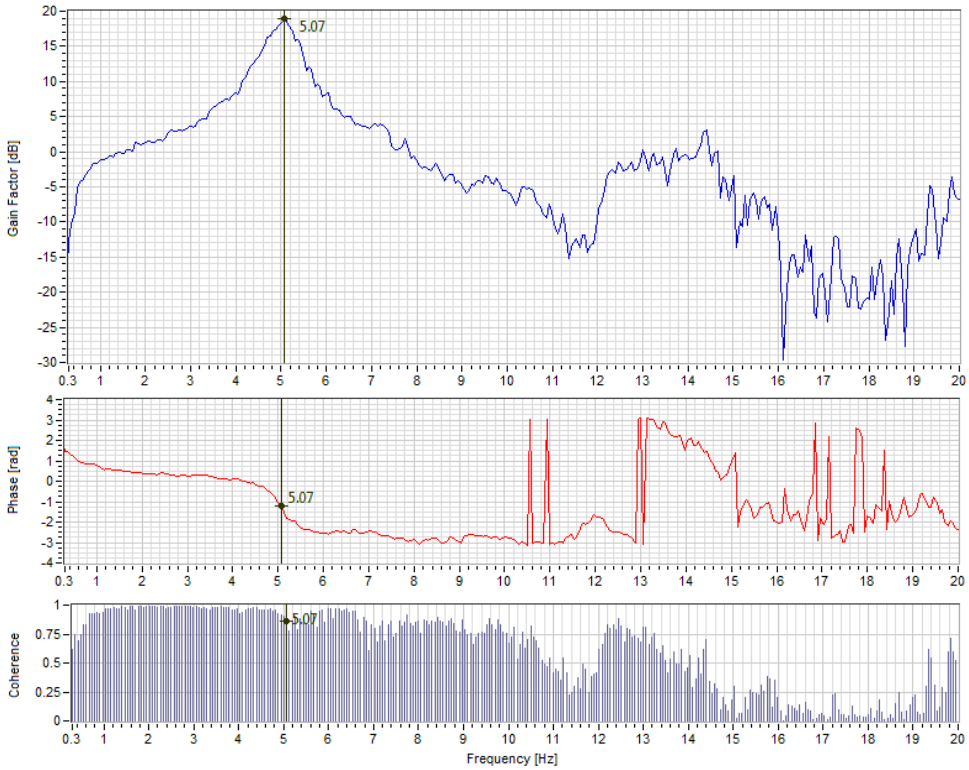

Figure AII. 28: Frequency response function, phase and coherence (Cat 1): ACC MESA LONG; ACC_RL_B1_Y_W_L

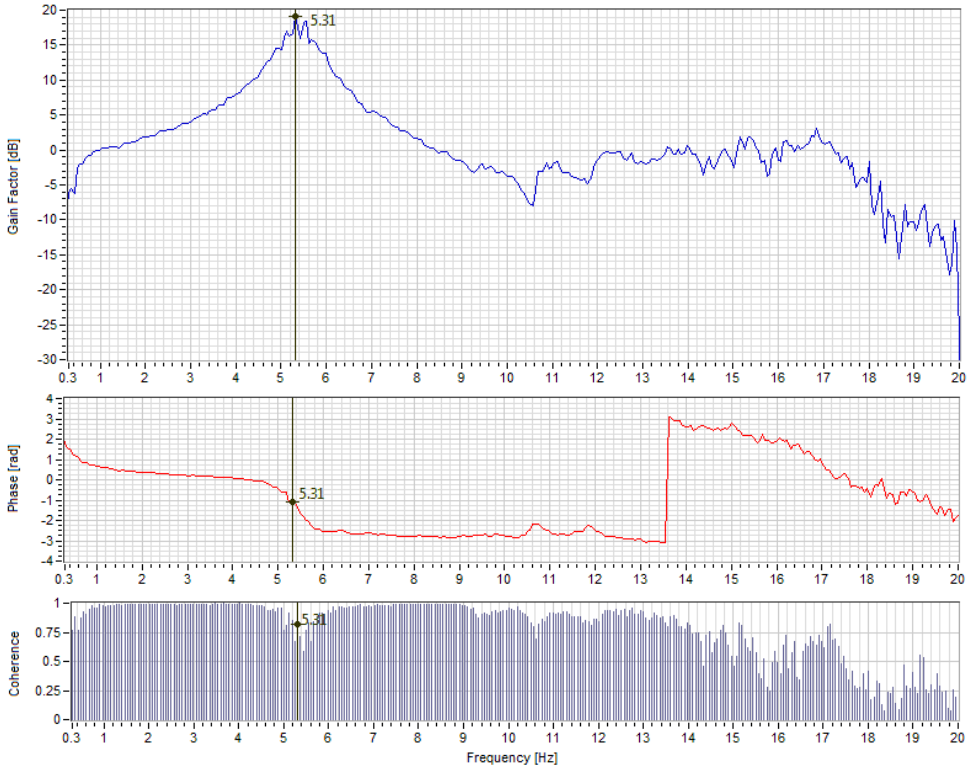

Figure AII. 29: Frequency response function, phase and coherence (Cat 1): ACC MESA TRANS; ACC_RL_B2_X_I_T

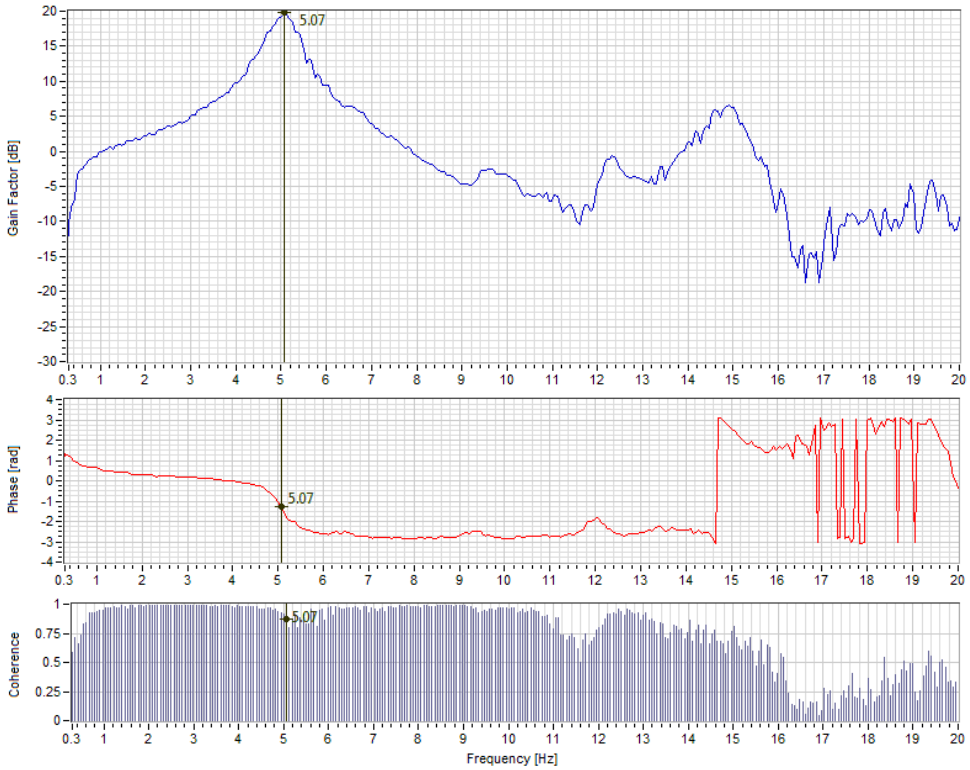

Figure AII. 30: Frequency response function, phase and coherence (Cat 1): ACC MESA LONG; ACC_RL_B2_Y_I_L

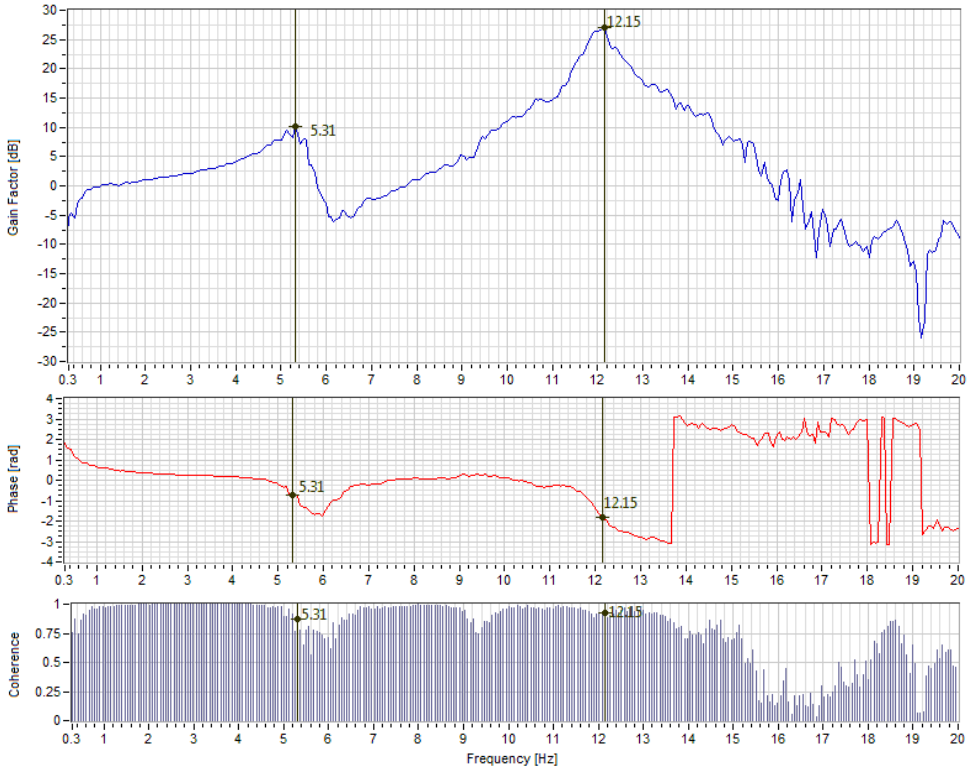

Figure AII. 31: Frequency response function, phase and coherence (Cat 1): ACC MESA TRANS; ACC_GLW03Y_I_T

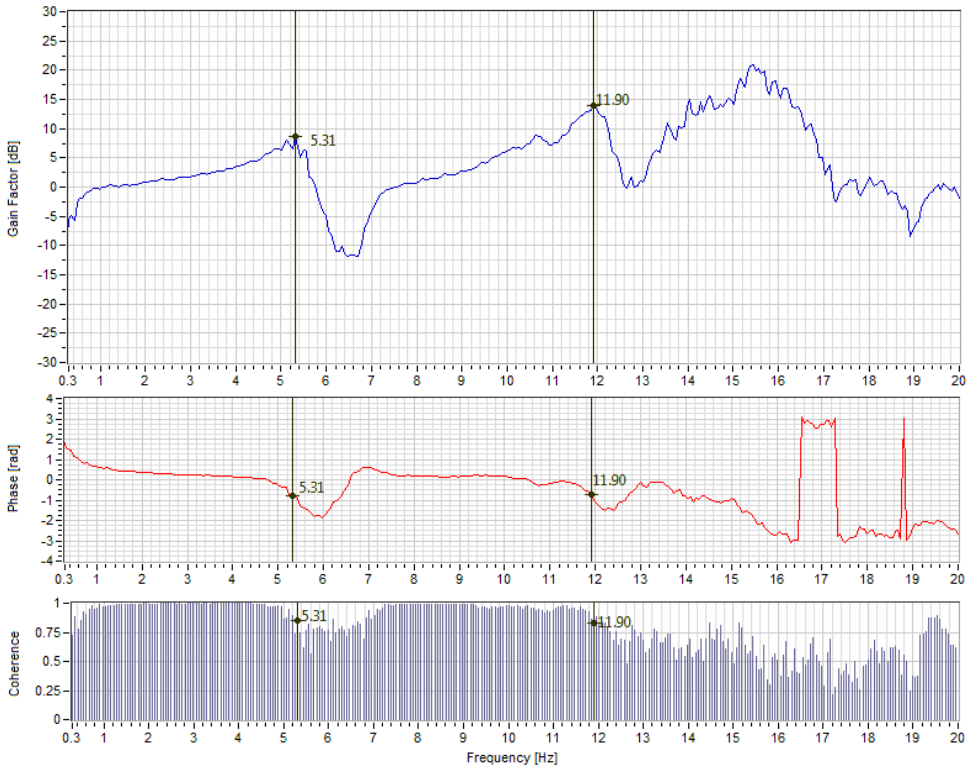

Figure AII. 32: Frequency response function, phase and coherence (Cat 1): ACC MESA TRANS; ACC_GLW04Y_I_T

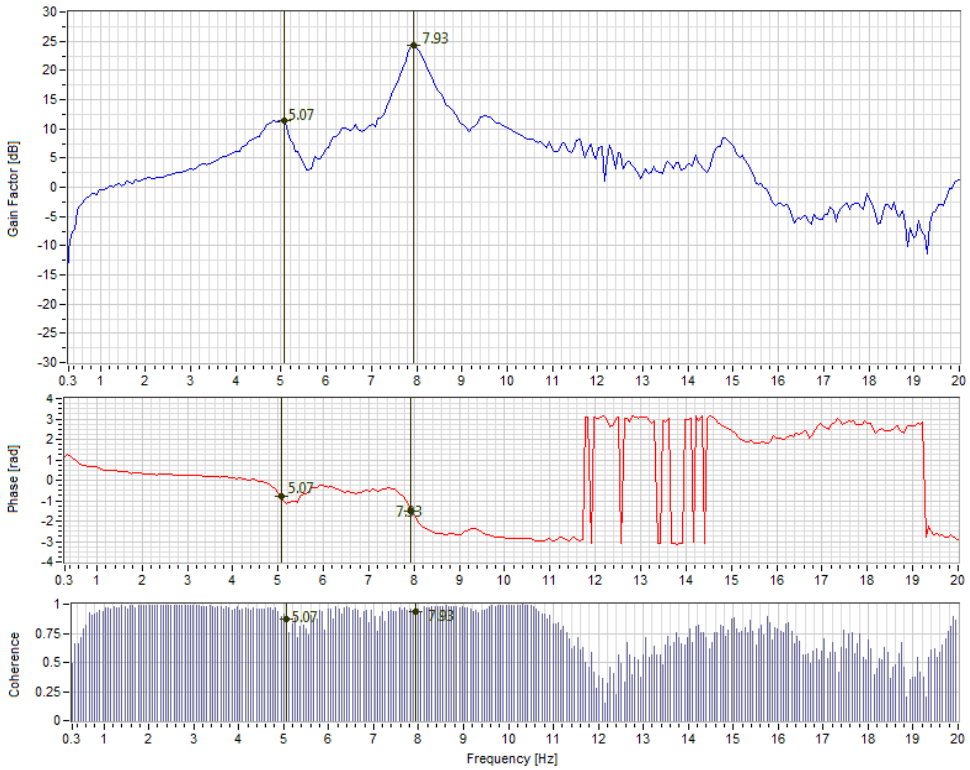

Figure AII. 33: Frequency response function, phase and coherence (Cat 1): ACC MESA LONG; ACC_GLW04X_I_L

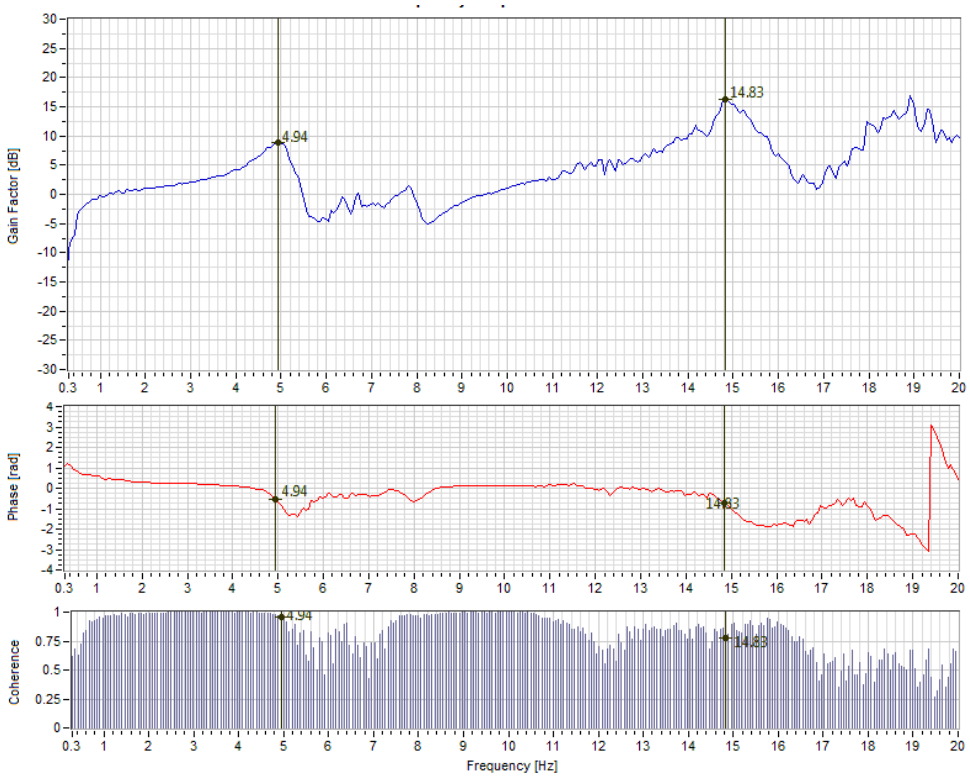

Figure AII. 34: Frequency response function, phase and coherence (Cat 1): ACC MESA LONG; ACC_GLW05X_I_L

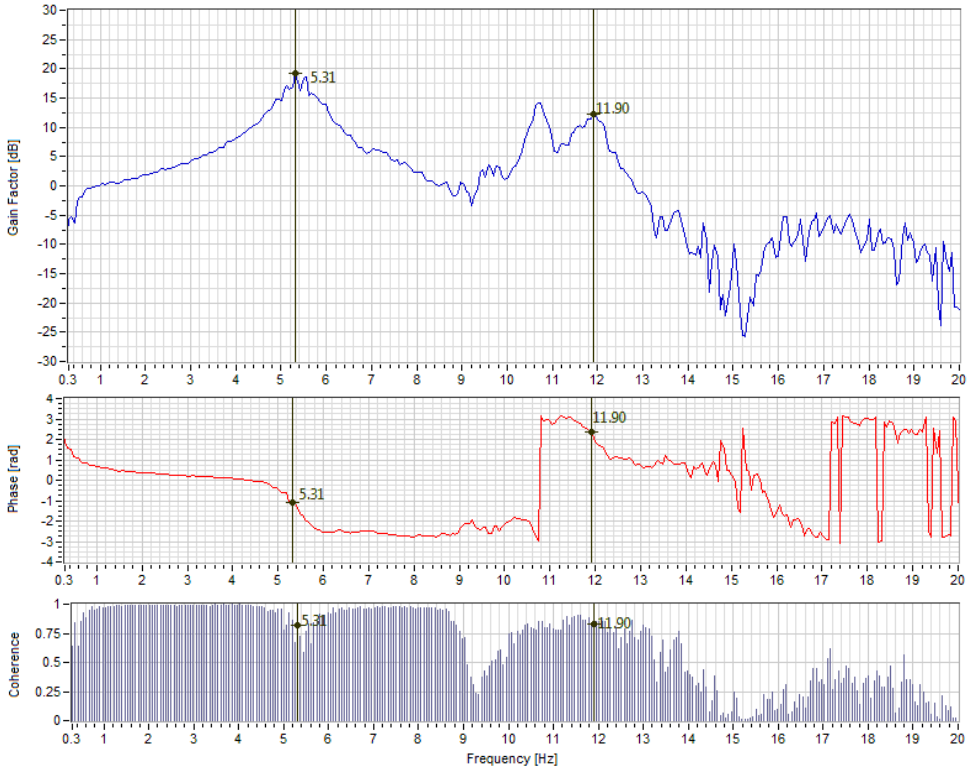

Figure AII. 35: Frequency response function, phase and coherence (Cat 1): ACC MESA TRANS; ACC_L1W03Y_I_T

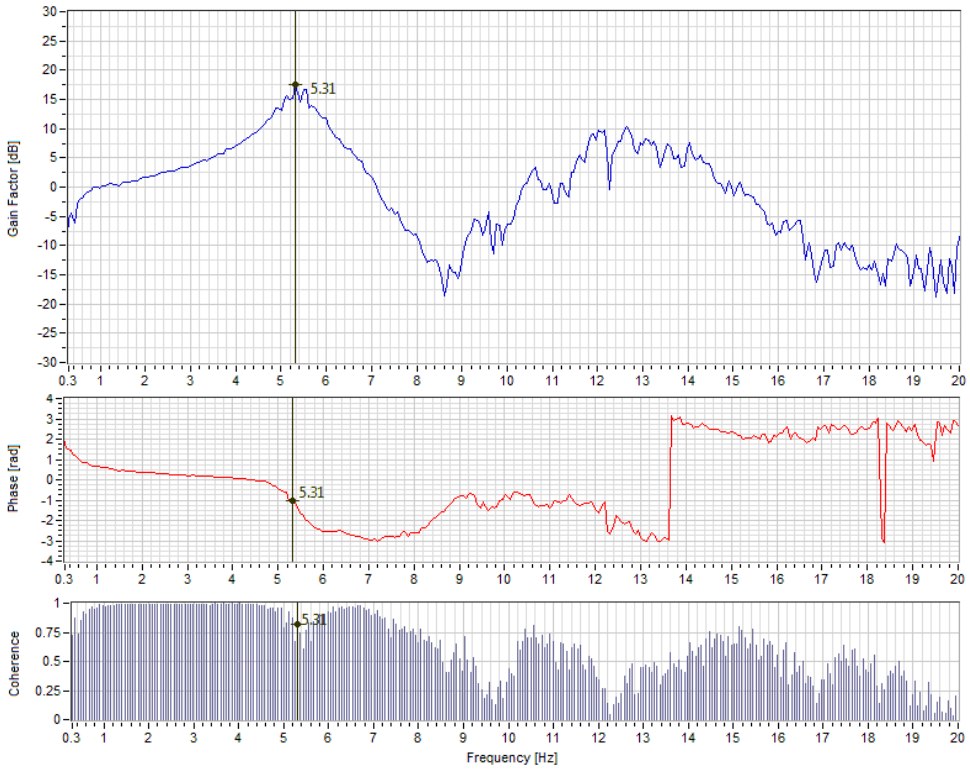

Figure AII. 36: Frequency response function, phase and coherence (Cat 1): ACC MESA TRANS; ACC_L1W04Y_I_T

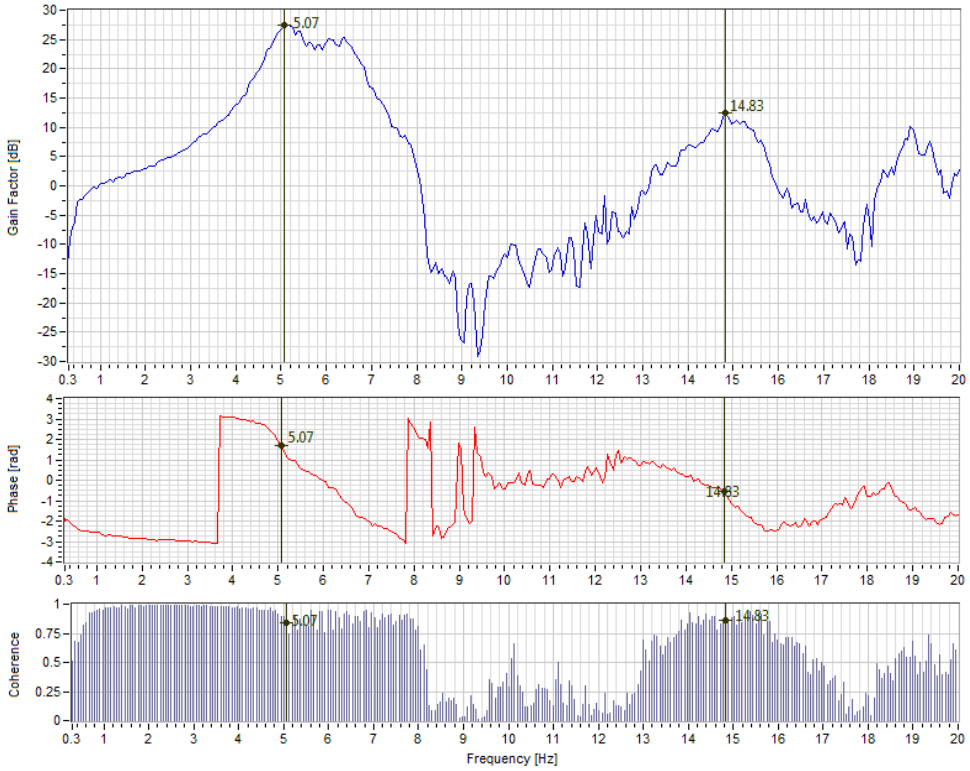

Figure AII. 37: Frequency response function, phase and coherence (Cat 1): ACC MESA LONG; ACC_L1W04X_I_L

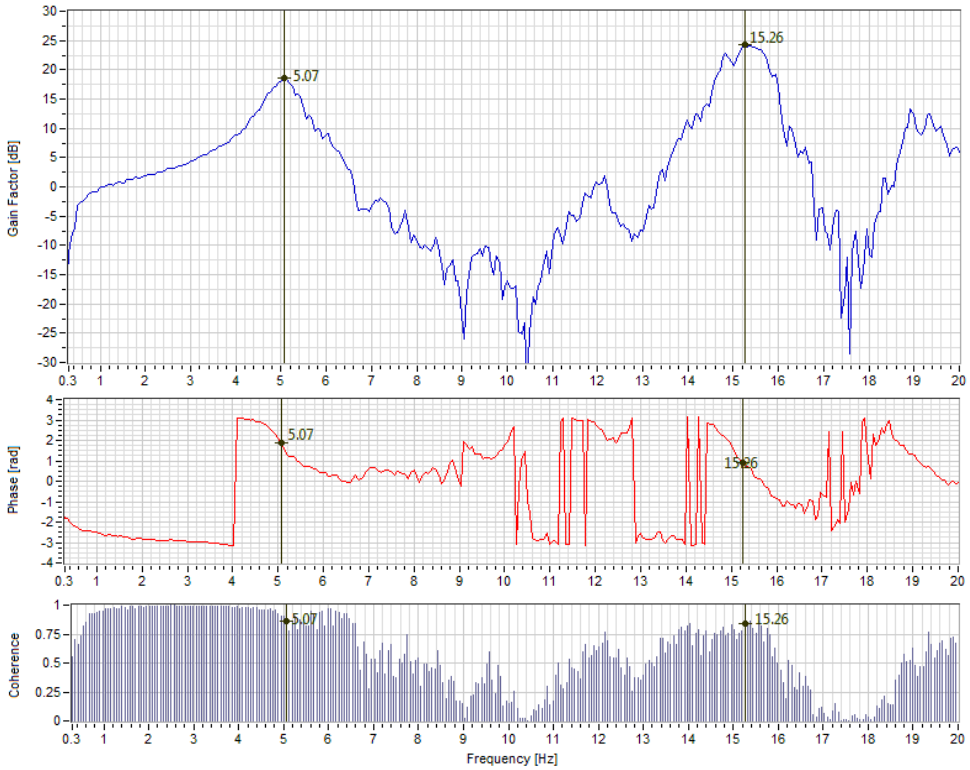

Figure AII. 38: Frequency response function, phase and coherence (Cat 1): ACC MESA LONG; ACC_L1W05X_I_L

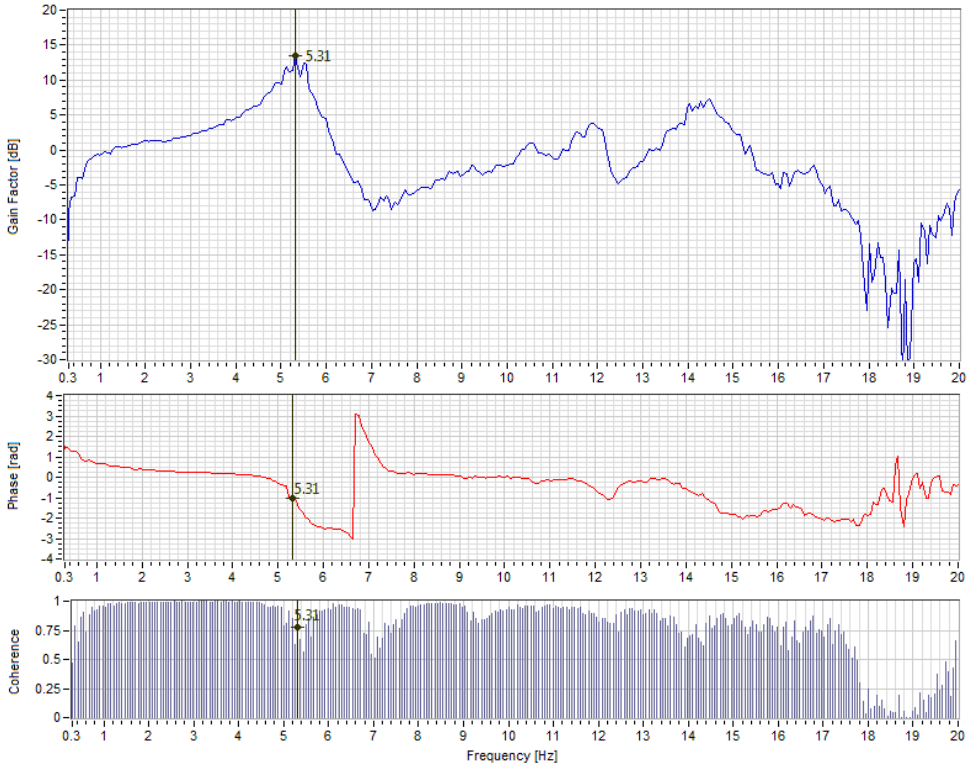

Figure AII.39: Frequency response function, phase and coherence (Cat 7): ACC MESA TRANS; ACC_L1_C3_X_NE_T

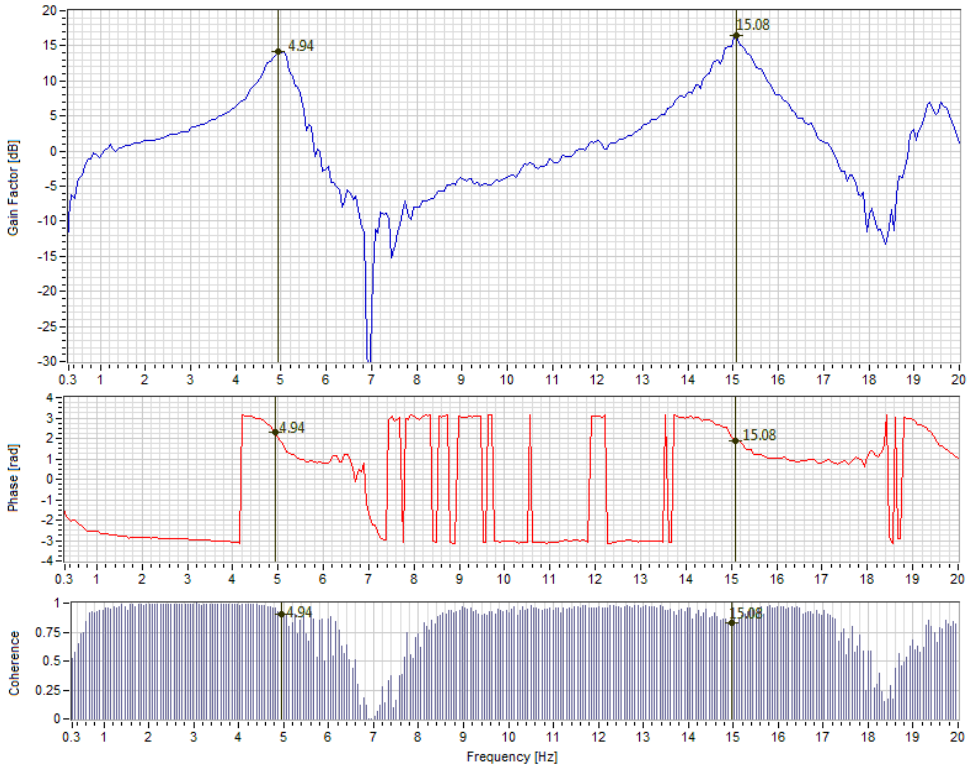

Figure AII. 40: Frequency response function, phase and coherence (Cat 7): ACC MESA TRANS; ACC_L1_C3_Y_NE_L

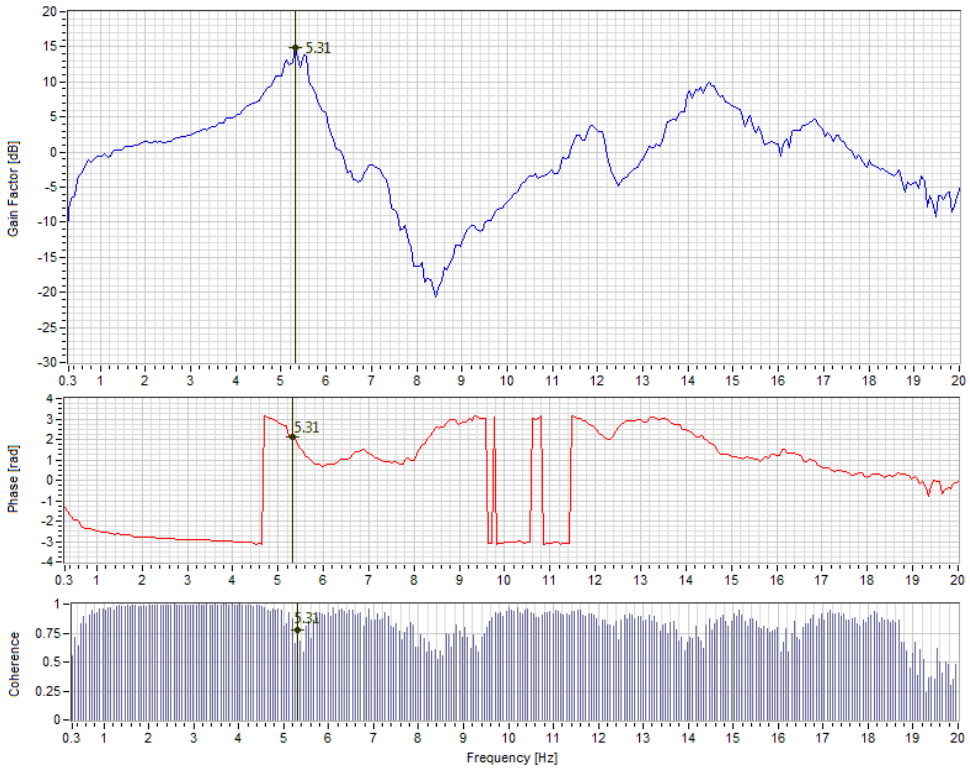

Figure AII. 41: Frequency response function, phase and coherence (Cat 7): ACC MESA TRANS; ACC_L1_A1_X_SW_T

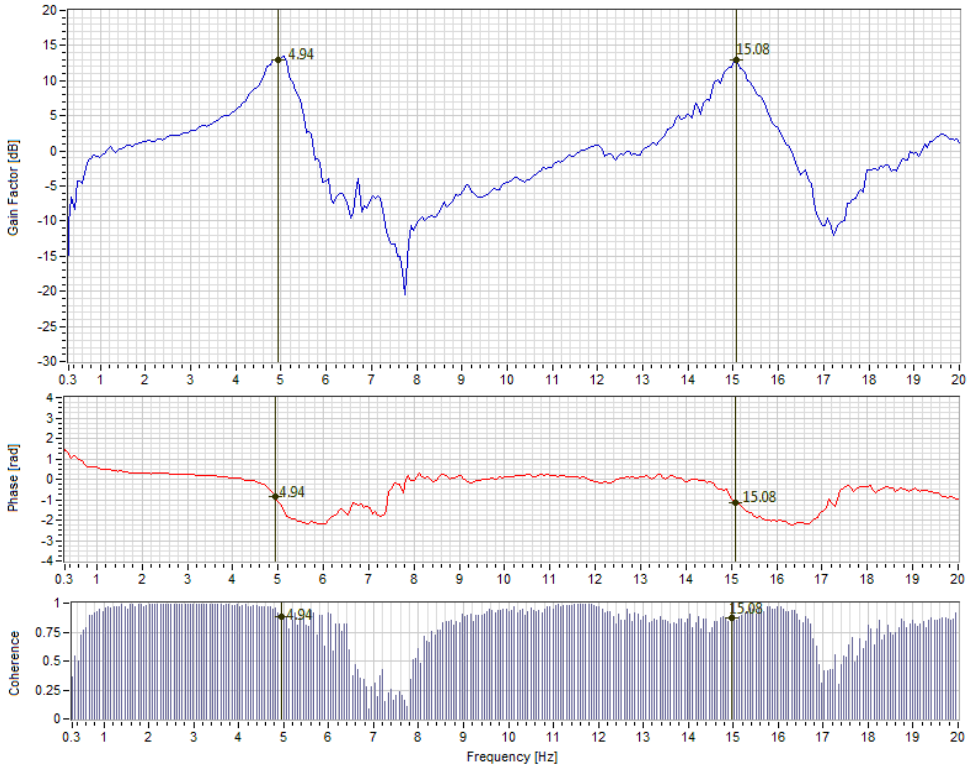

Figure AII. 42: Frequency response function, phase and coherence (Cat 7): ACC MESA LONG; ACC_L1_A1_Y_SW_L

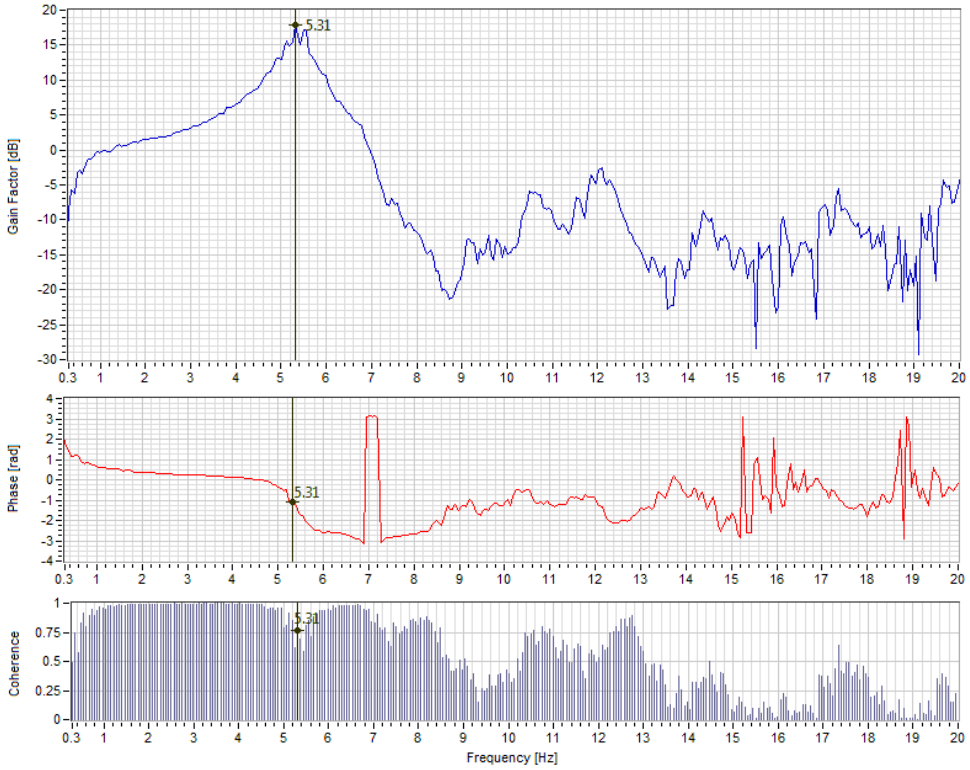

Figure AII. 43: Frequency response function, phase and coherence (Cat 7): ACC MESA TRANS; ACC_RL_C3_X_NE_T

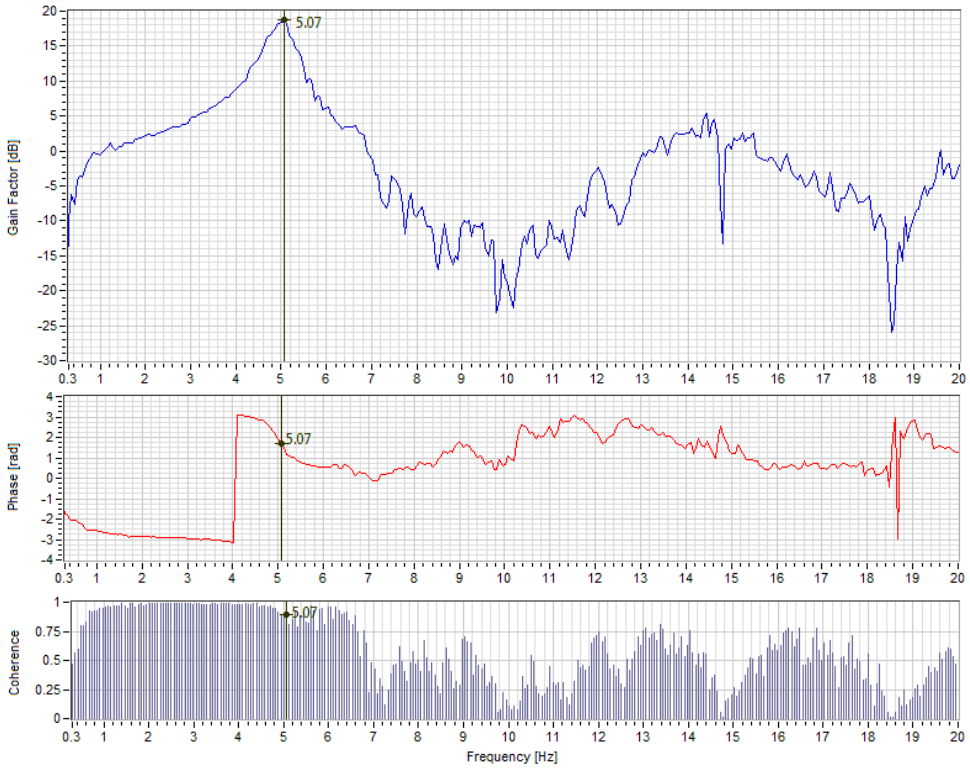

Figure AII. 44: Frequency response function, phase and coherence (Cat 7): ACC MESA LONG; ACC_RL_C3_Y_NE_L

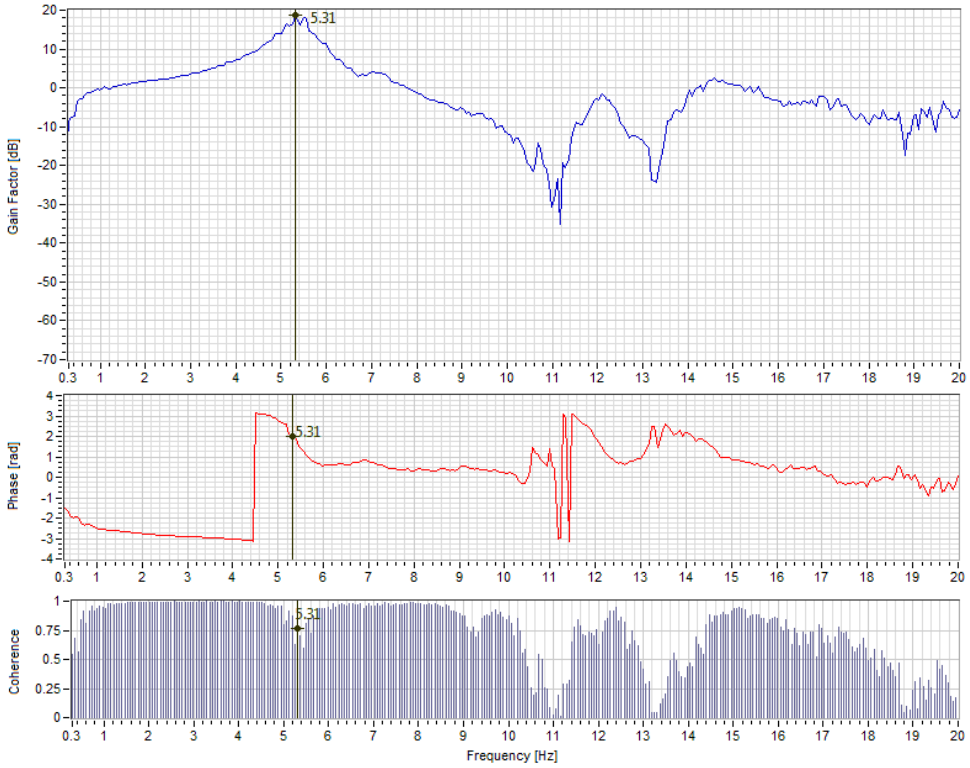

Figure AII. 45: Frequency response function, phase and coherence (Cat 7): ACC MESA TRANS; ACC_RL_A1_X_SW_T

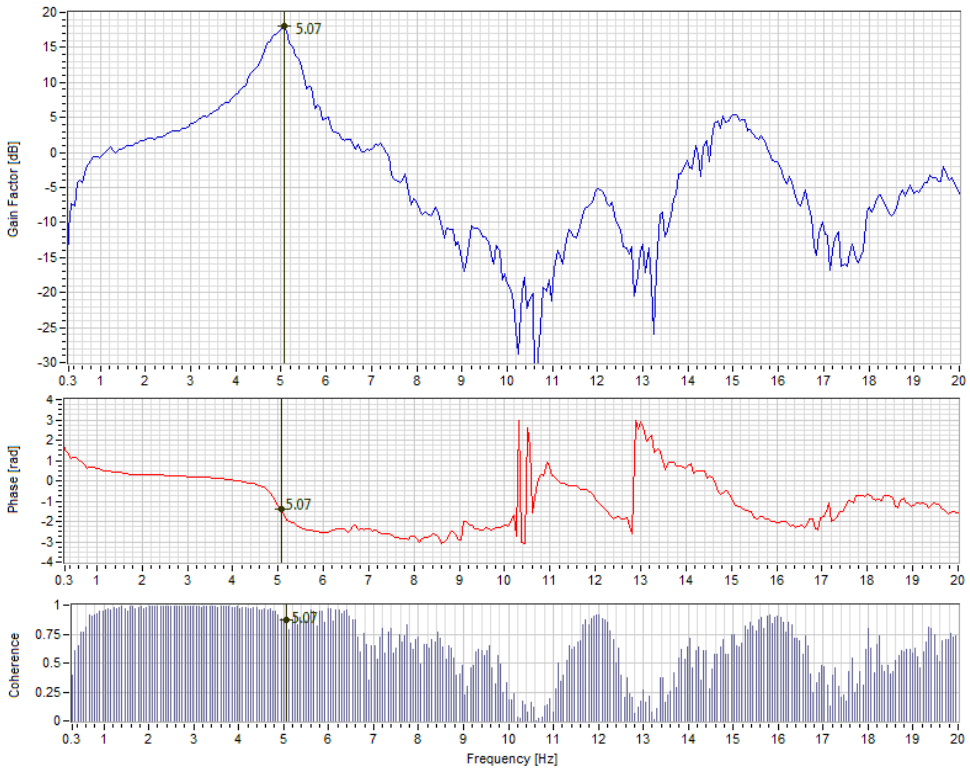

Figure AII. 46: Frequency response function, phase and coherence (Cat 7): ACC MESA LONG; ACC_RL_A1_Y_SW_L

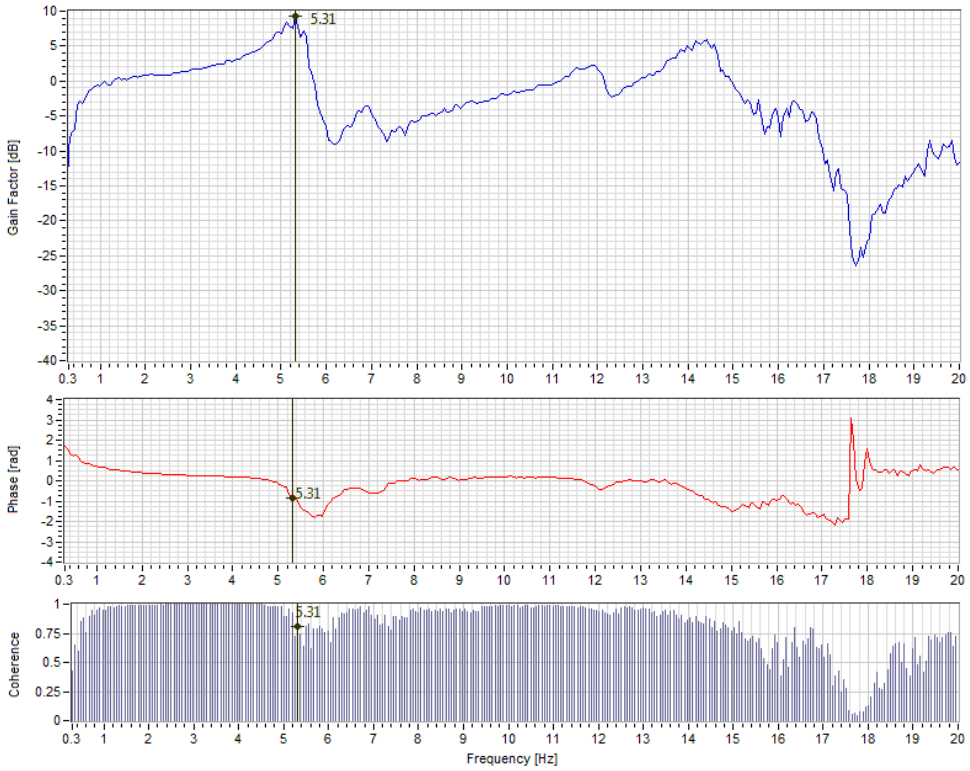

Figure AII. 47: Frequency response function, phase and coherence (Cat 7): ACC MESA TRANS; ACC_GL_A3_X_SE_T

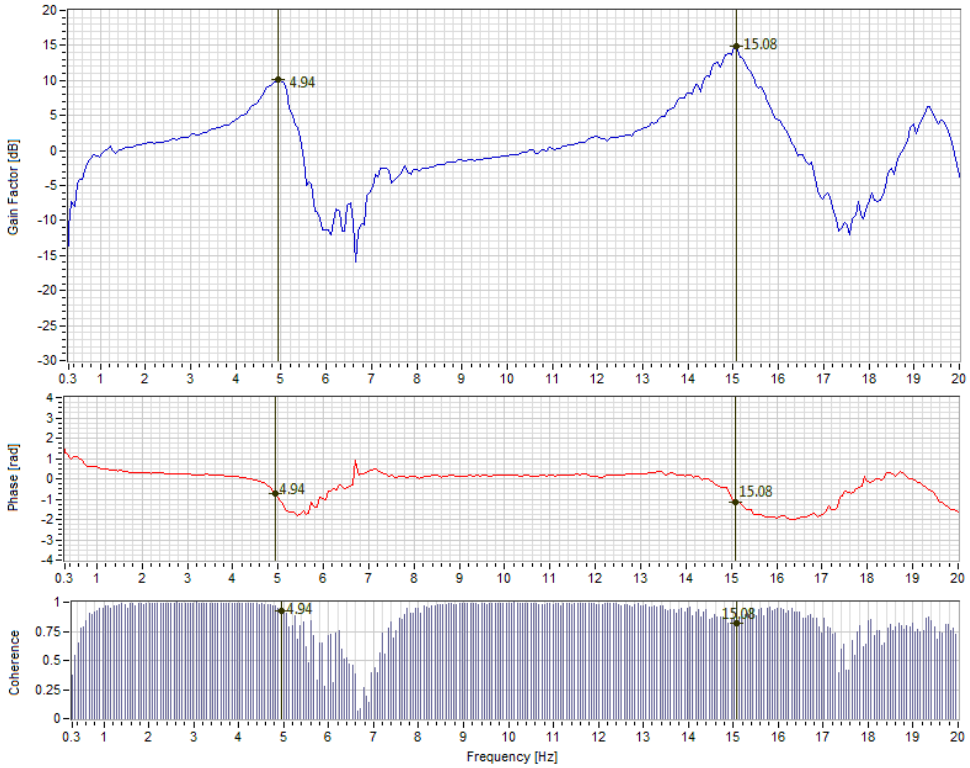

Figure AII. 48: Frequency response function, phase and coherence (Cat 7): ACC MESA LONG; ACC_GL_A3_Y_SE_L

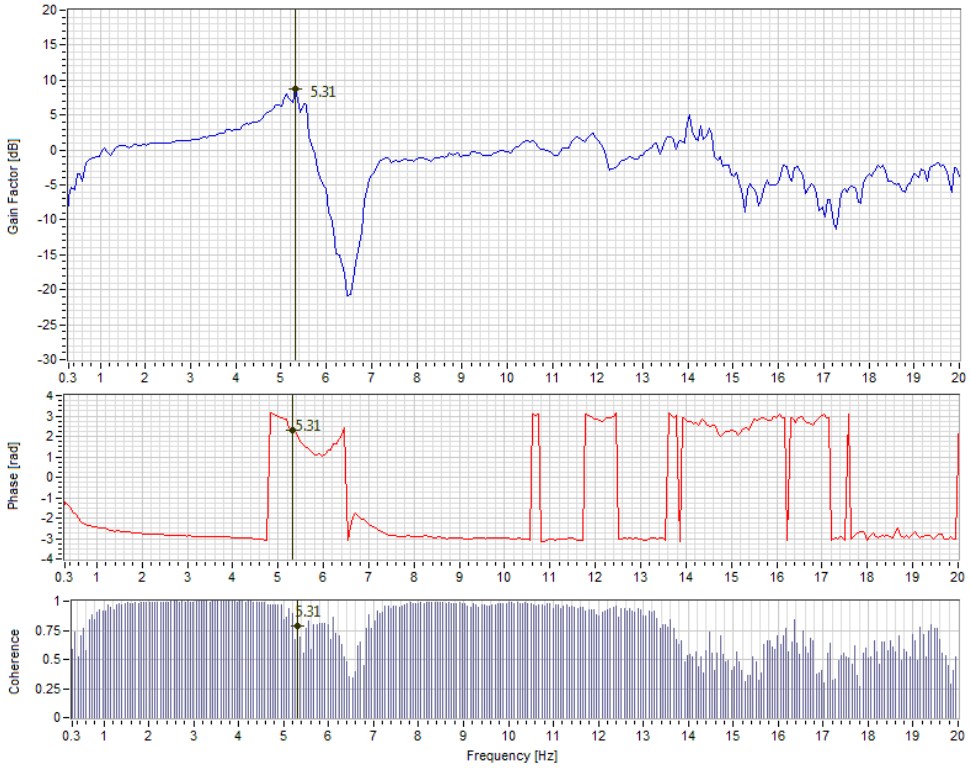

Figure AII. 49: Frequency response function, phase and coherence (Cat 7): ACC MESA TRANS; ACC_GL_C1_X_NW_T

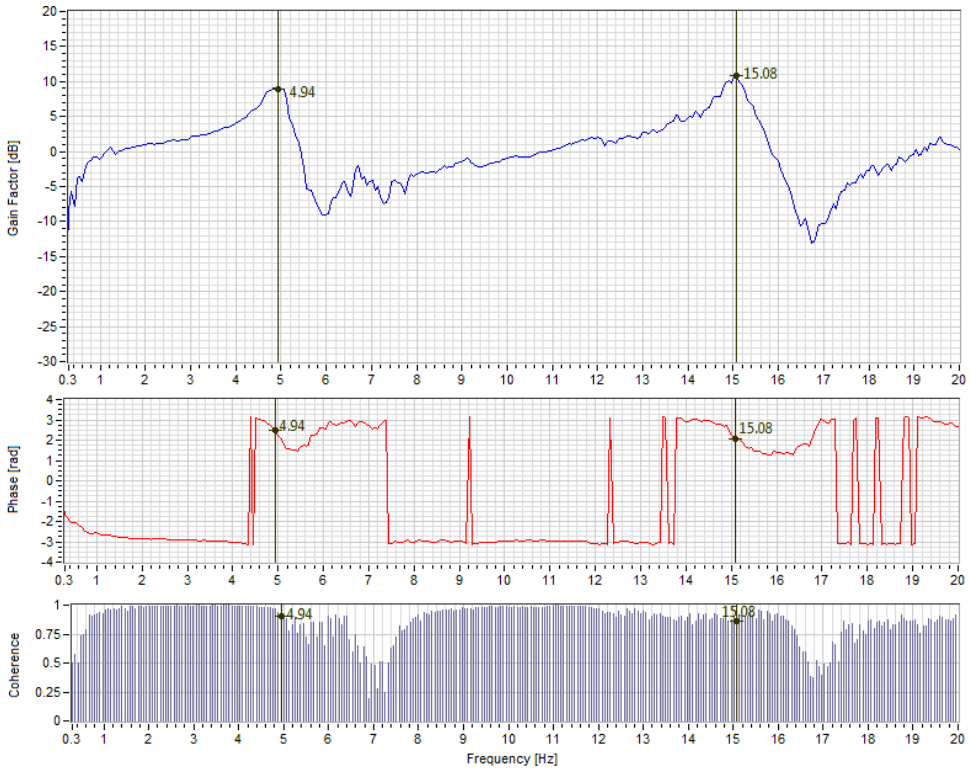

Figure AII. 50: Frequency response function, phase and coherence (Cat 7): ACC MESA LONG; ACC_GL_C1_Y_NW_L

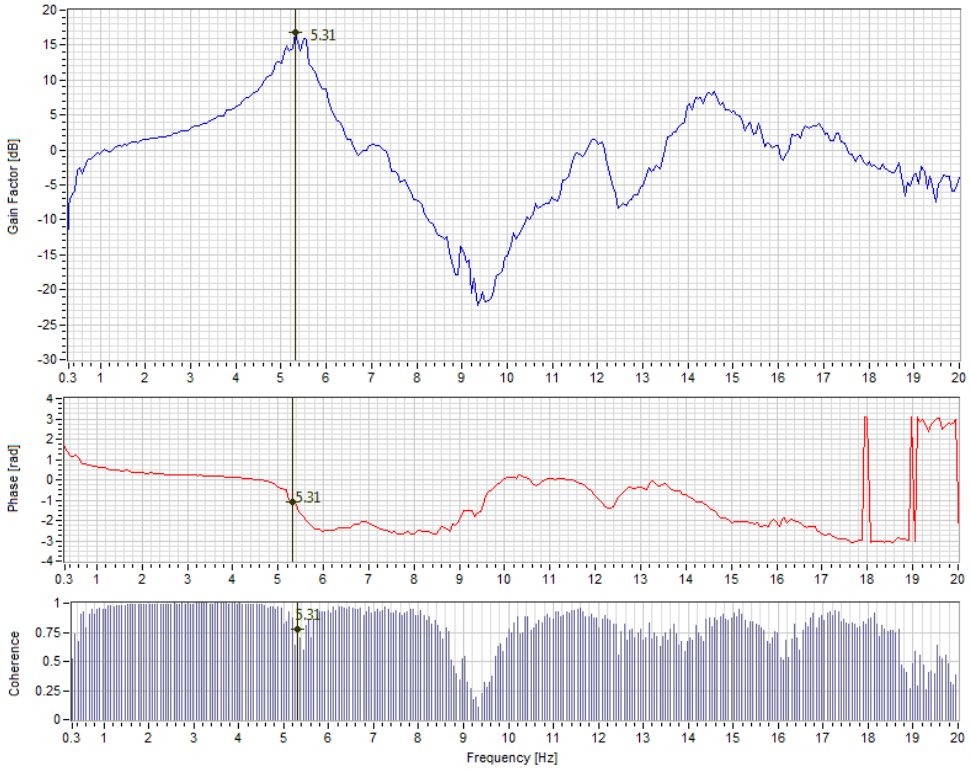

Figure AII. 51: Frequency response function, phase and coherence (Cat 7): ACC MESA TRANS; ACC_L1_A3_X_SE_T

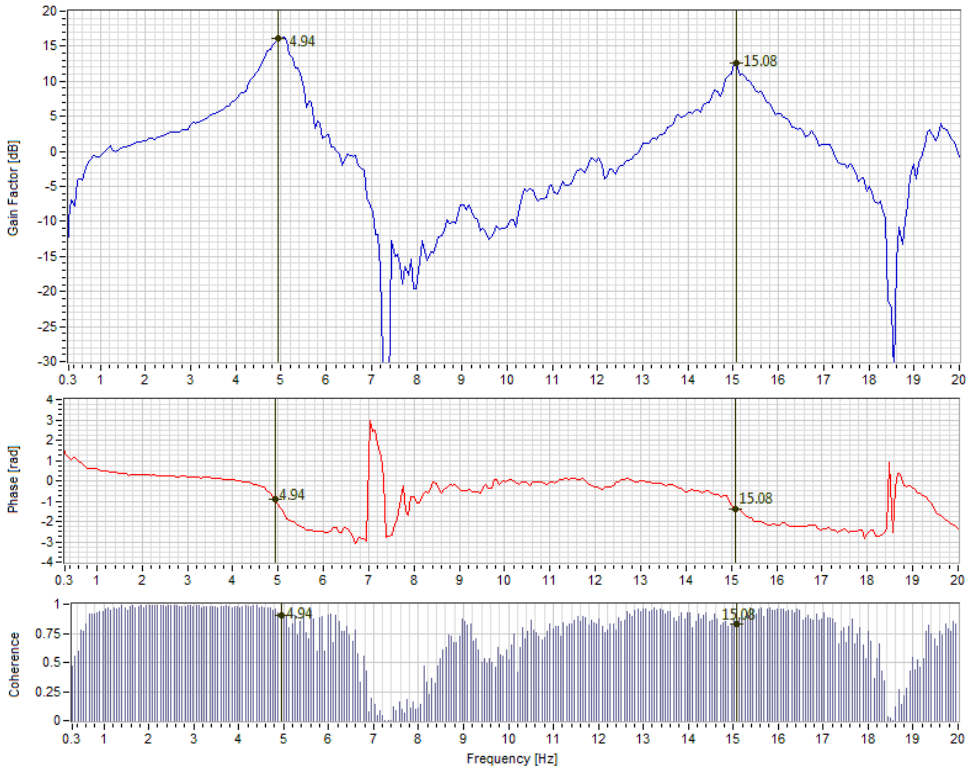

Figure AII. 52: Frequency response function, phase and coherence (Cat 7): ACC MESA LONG; ACC_L1_A3_Y_SE_L

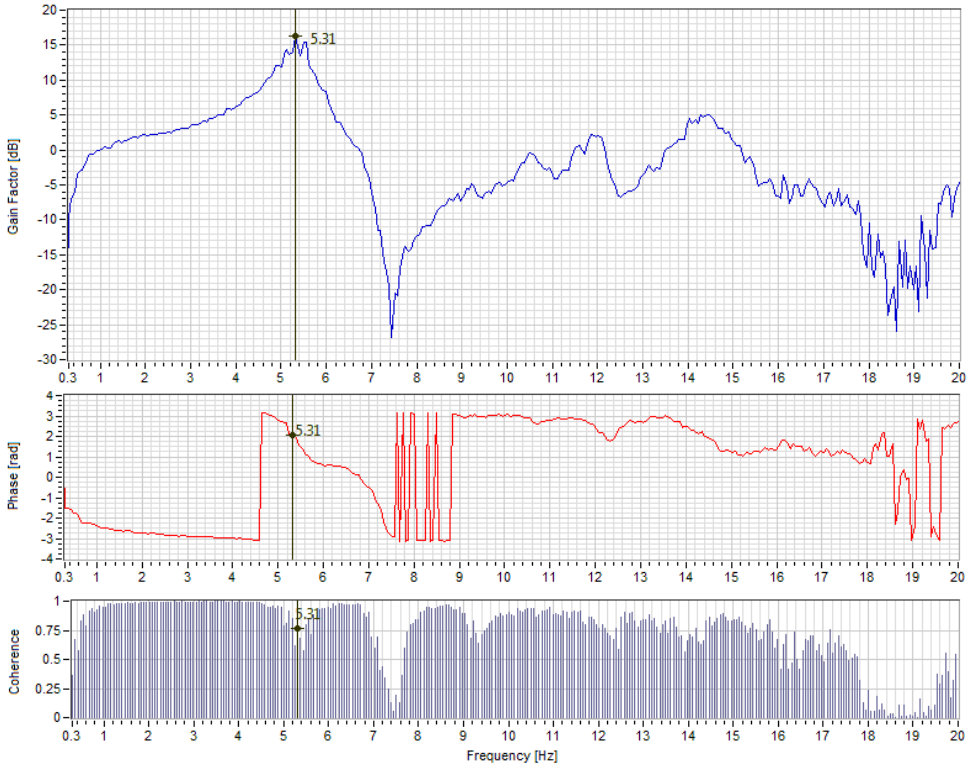

Figure AII. 53: Frequency response function, phase and coherence (Cat 7): ACC MESA TRANS; ACC_L1_C1_X_NW_T

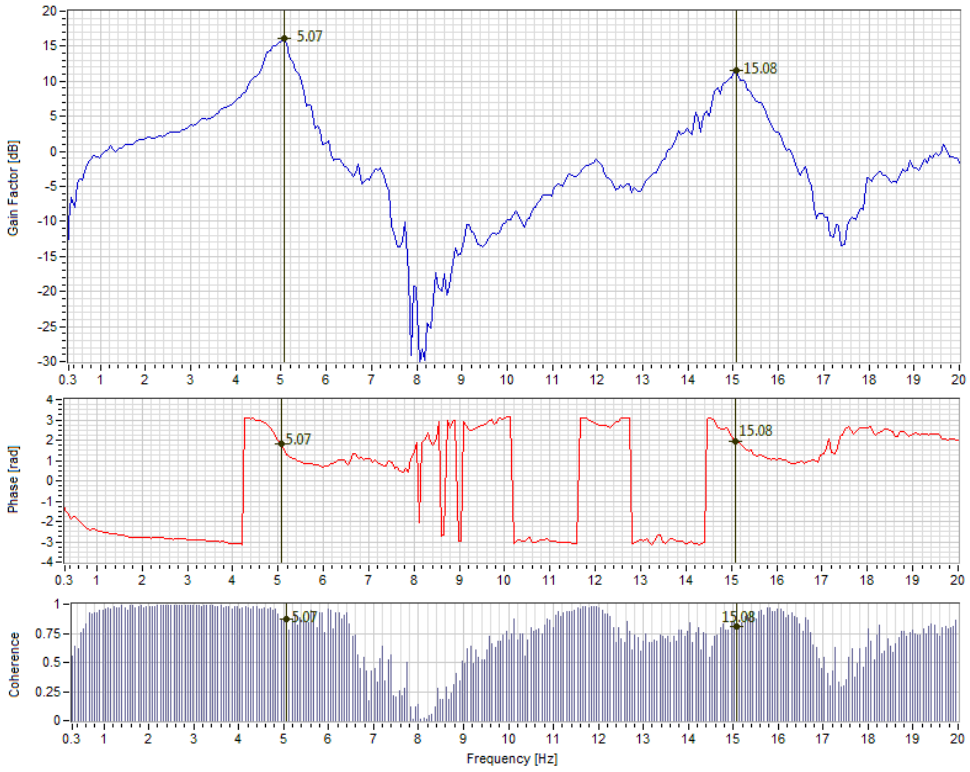

Figure AII. 54: Frequency response function, phase and coherence (Cat 7): ACC MESA LONG; ACC_L1_C1_Y_NW_L

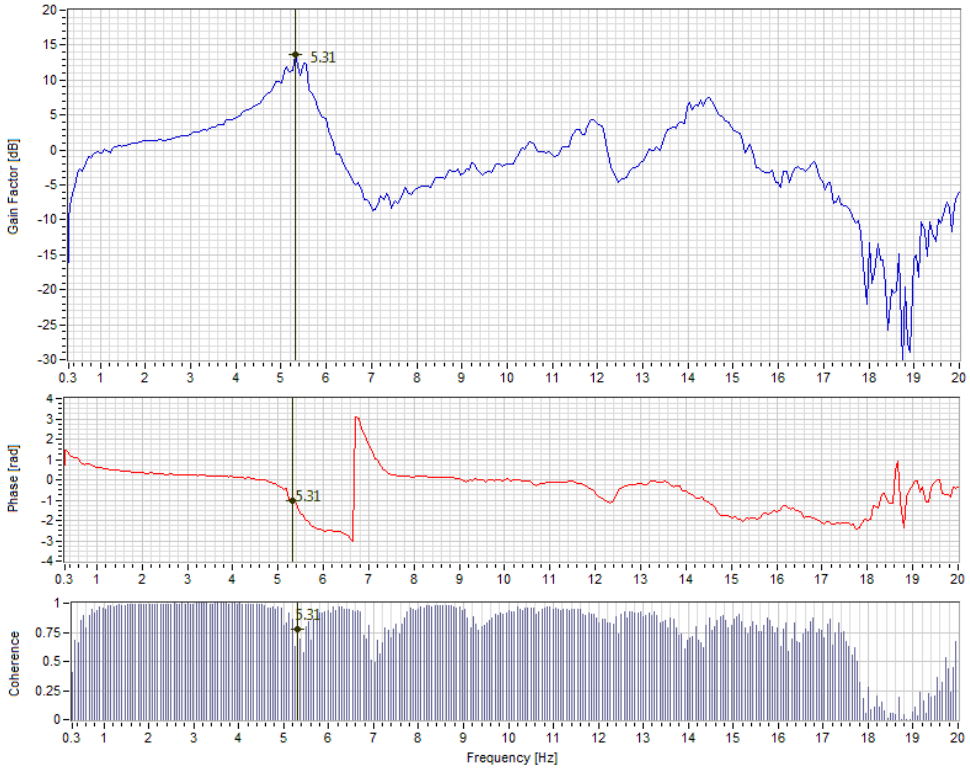

Figure AII. 55: Frequency response function, phase and coherence (Cat 7): ACC MESA TRANS; ACC_L1_C2_X_N_T

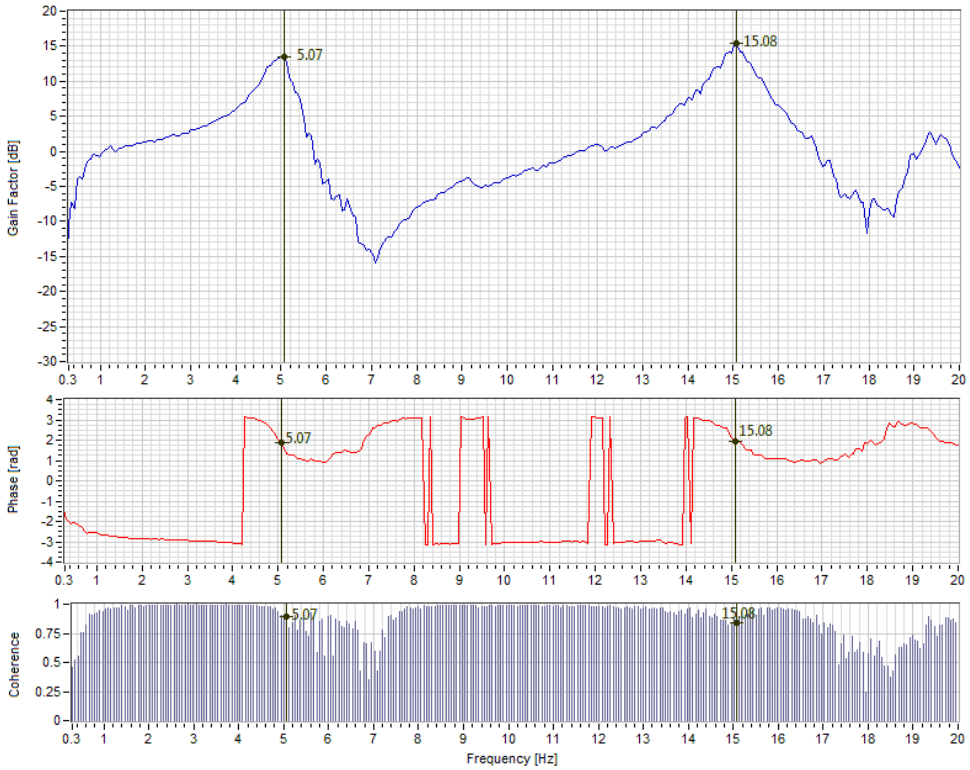

Figure AII. 56: Frequency response function, phase and coherence (Cat 7): ACC MESA LONG; ACC_L1_C2_Y_N_L

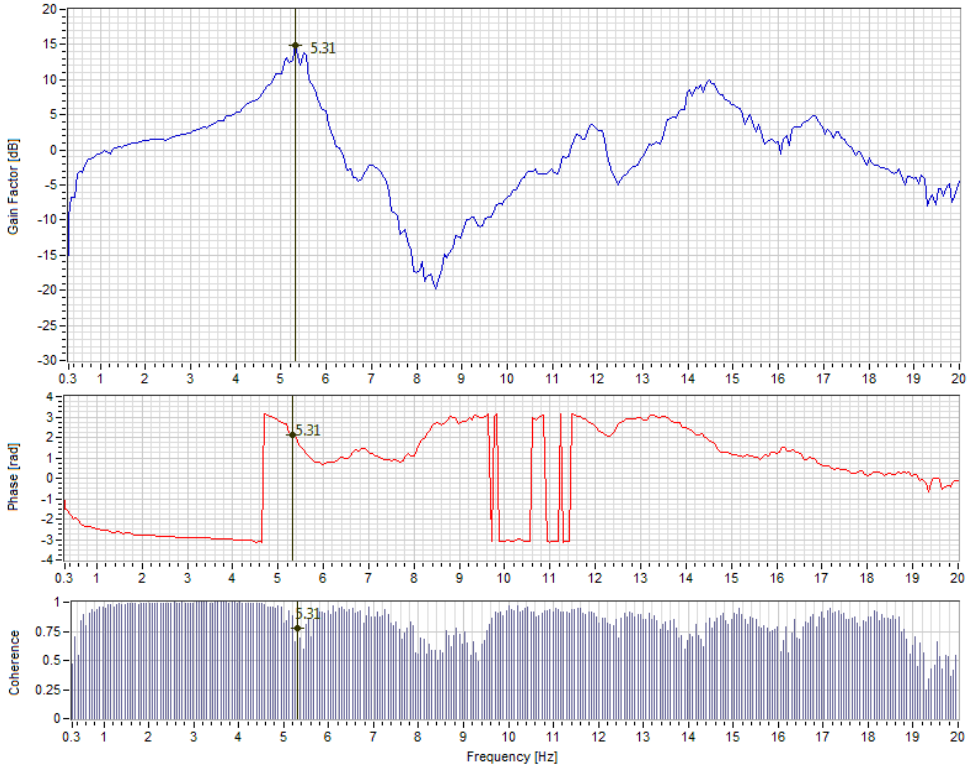

Figure AII. 57: Frequency response function, phase and coherence (Cat 7): ACC MESA TRANS; ACC_L1_A2_X_S_T

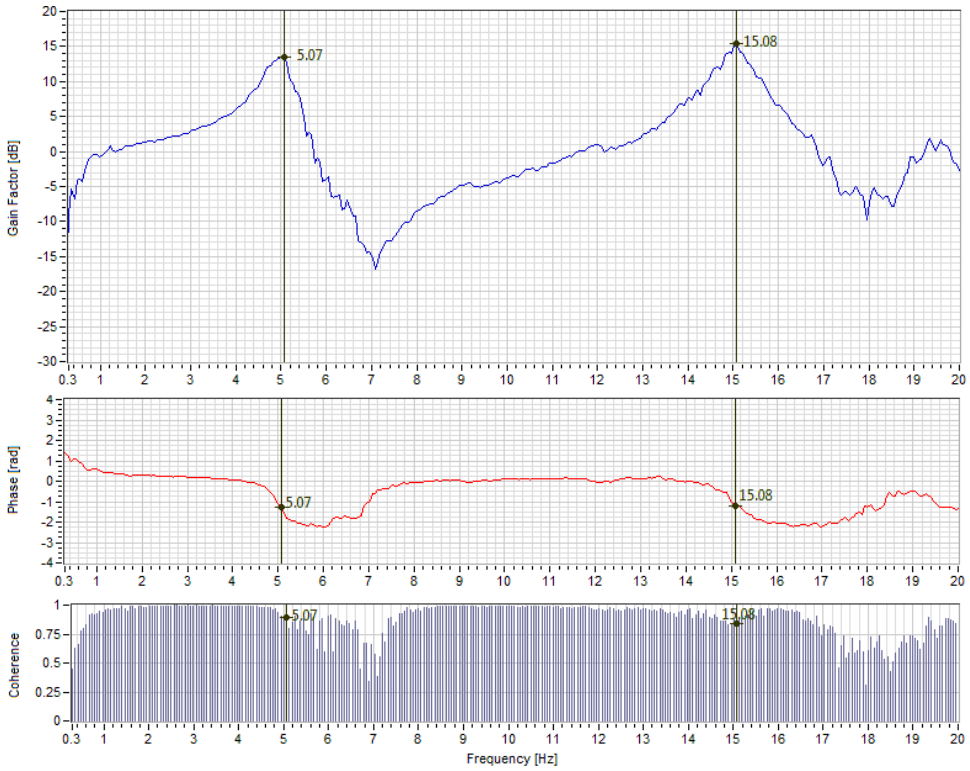

Figure AII. 58: Frequency response function, phase and coherence (Cat 7): ACC MESA LONG; ACC_L1_A2_Y_S_L

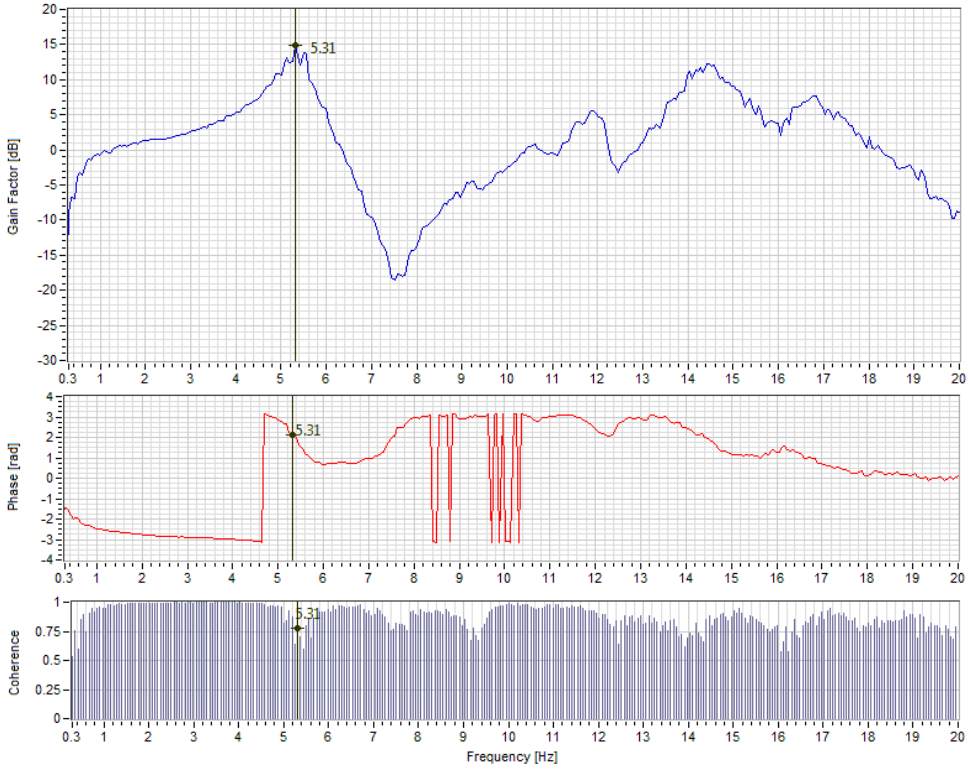

Figure AII. 59: Frequency response function, phase and coherence (Cat 7): ACC MESA TRANS; ACC_L1_B1_X_W_T

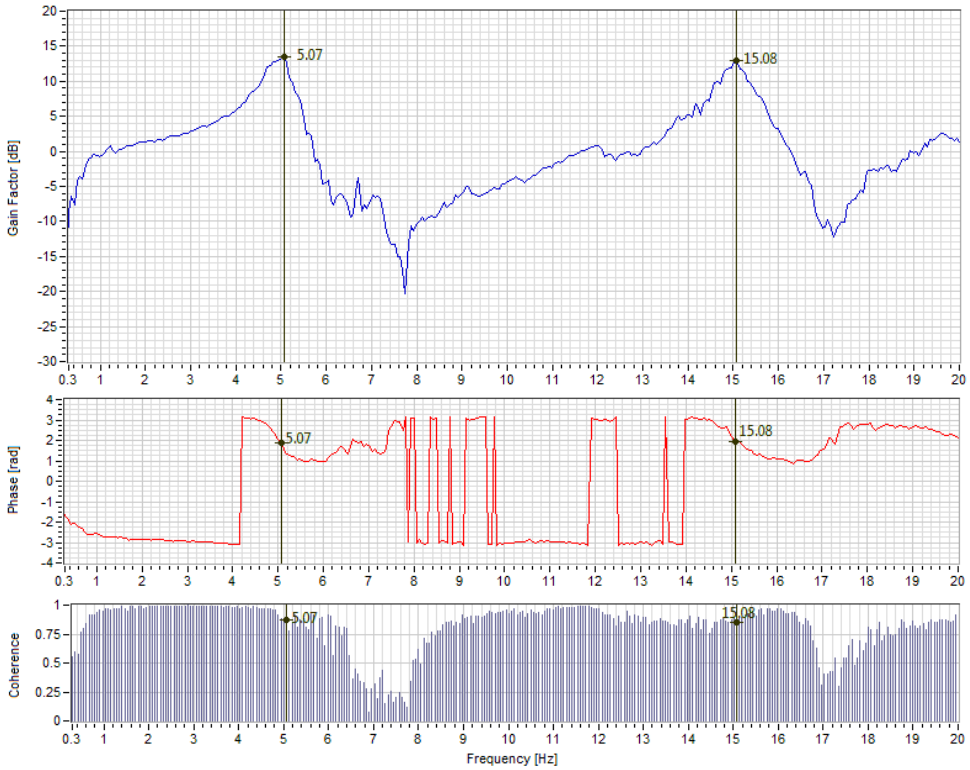

Figure AII. 60: Frequency response function, phase and coherence (Cat 7): ACC MESA TRANS; ACC_L1_B1_Y_W_L

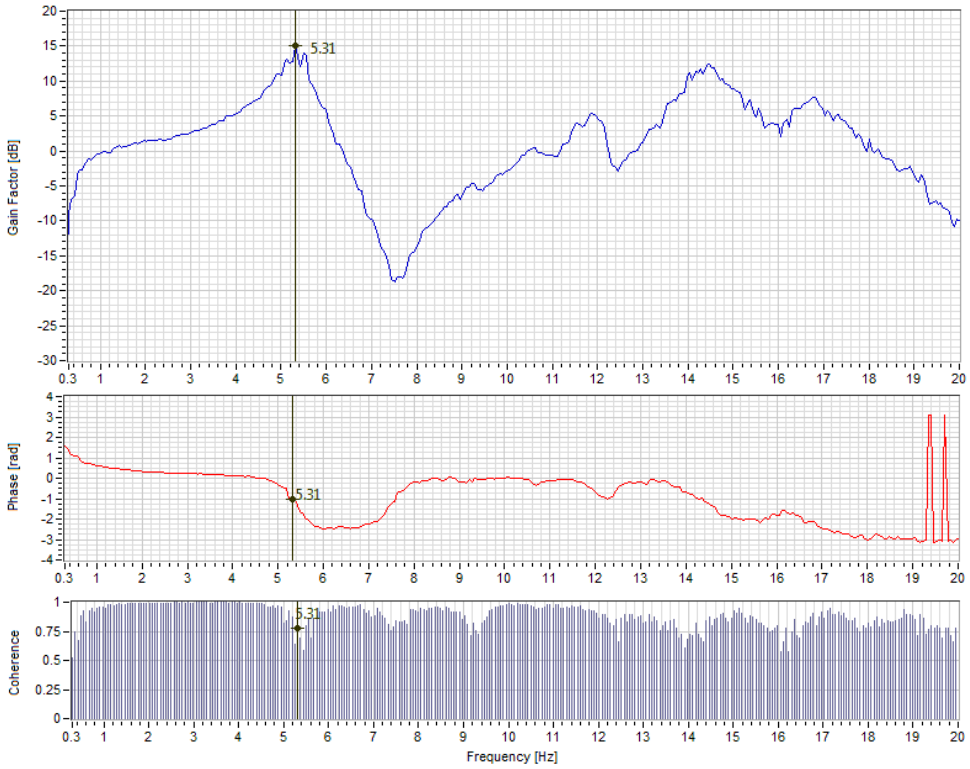

Figure AII. 61: Frequency response function, phase and coherence (Cat 7): ACC MESA TRANS; ACC_L1_B2_X_I_T

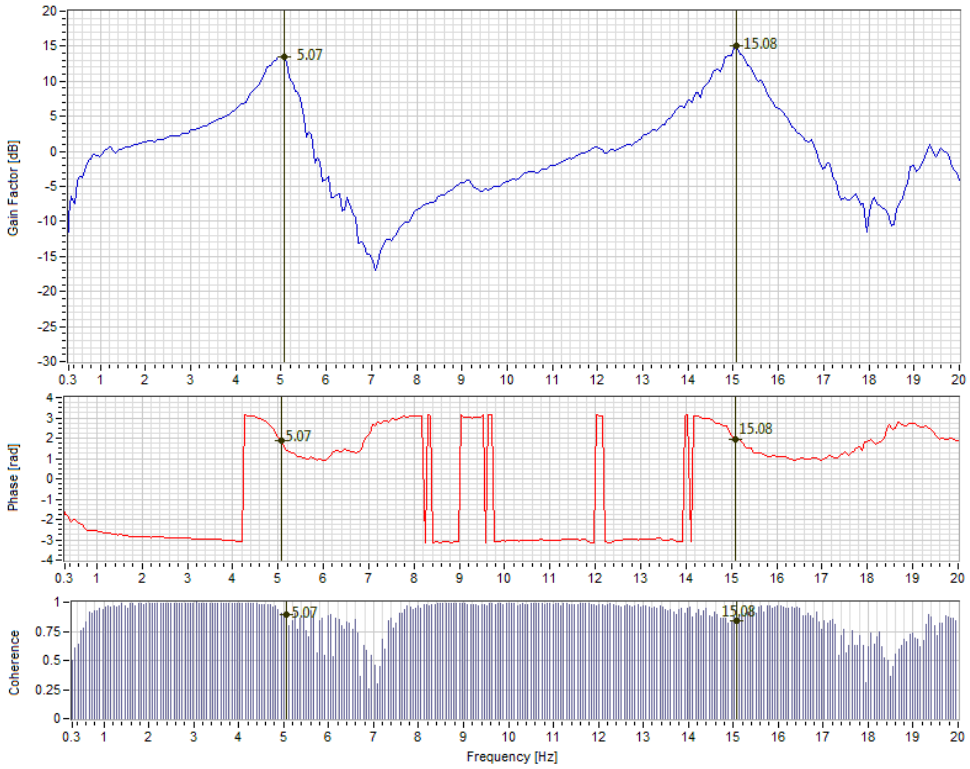

Figure AII. 62: Frequency response function, phase and coherence (Cat 7): ACC MESA LONG; ACC_L1_B2_Y_I_L

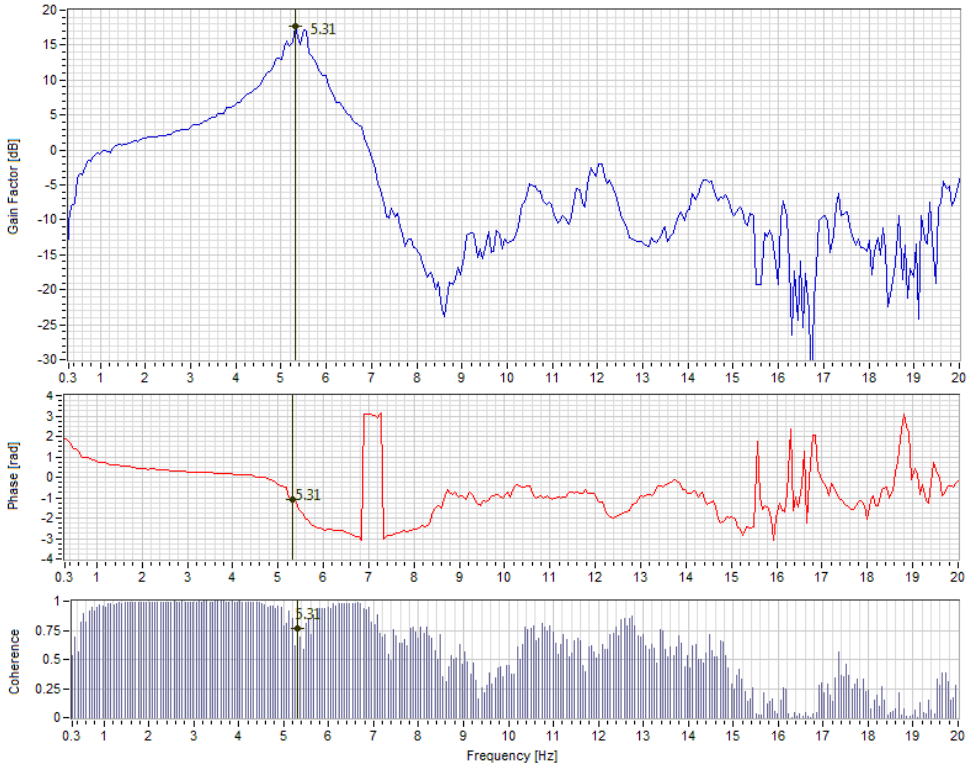

Figure AII. 63: Frequency response function, phase and coherence (Cat 7): ACC MESA TRANS; ACC_RL_C2_X_N_T

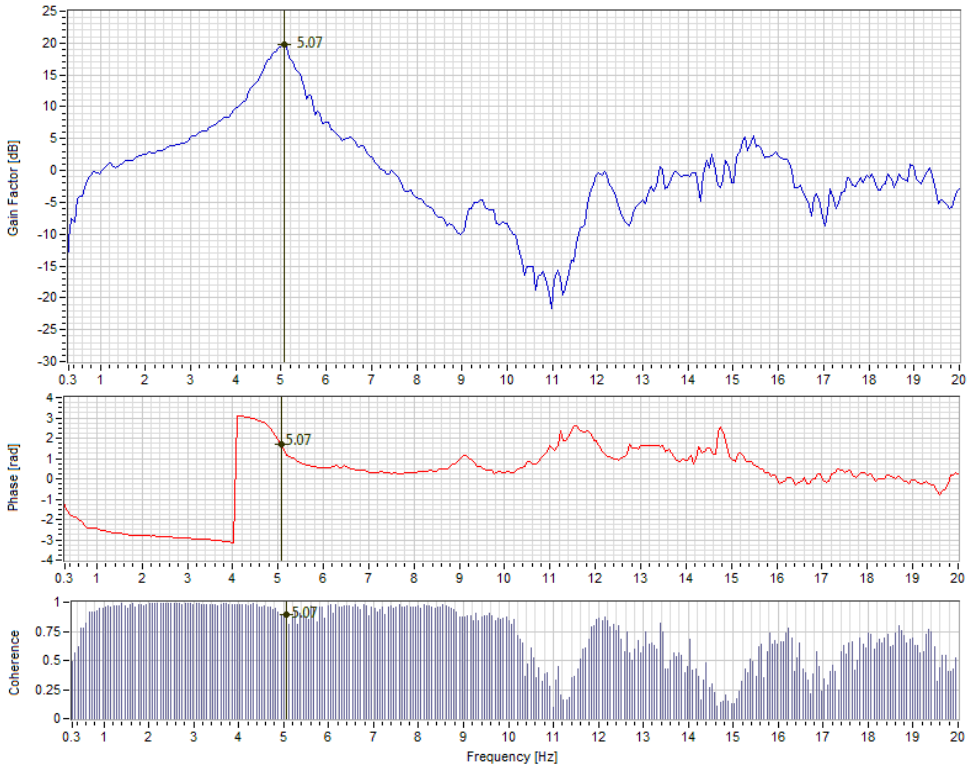

Figure AII. 64: Frequency response function, phase and coherence (Cat 7): ACC MESA LONG; ACC_RL_C2_Y_N_L

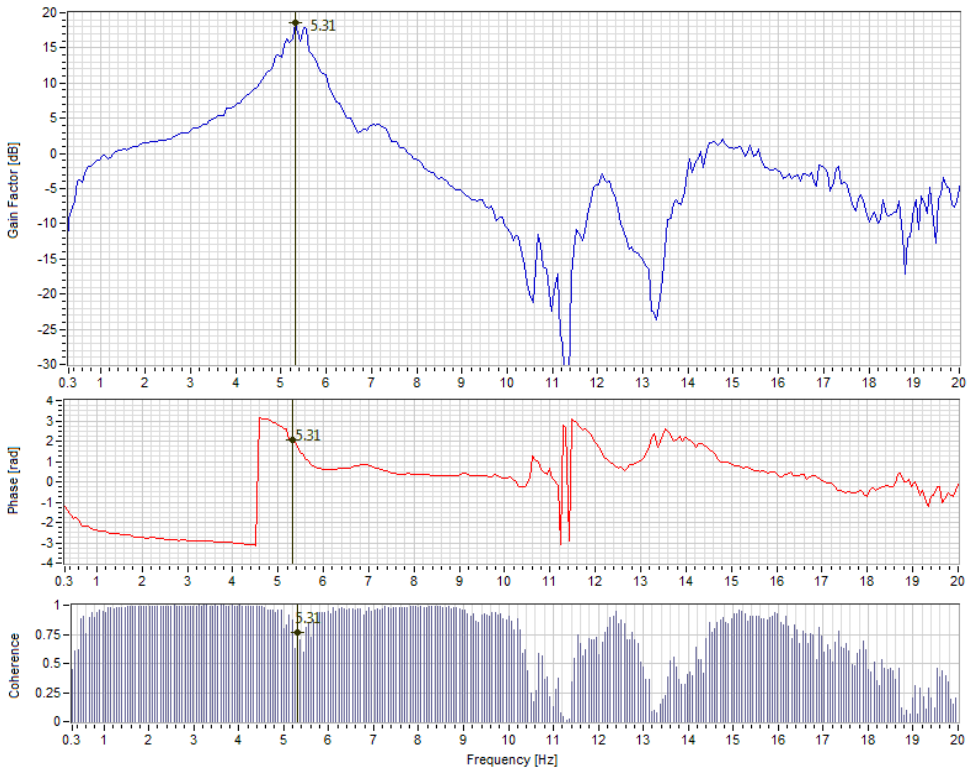

Figure AII. 65: Frequency response function, phase and coherence (Cat 7): ACC MESA TRANS; ACC_RL_A2_X_S_T

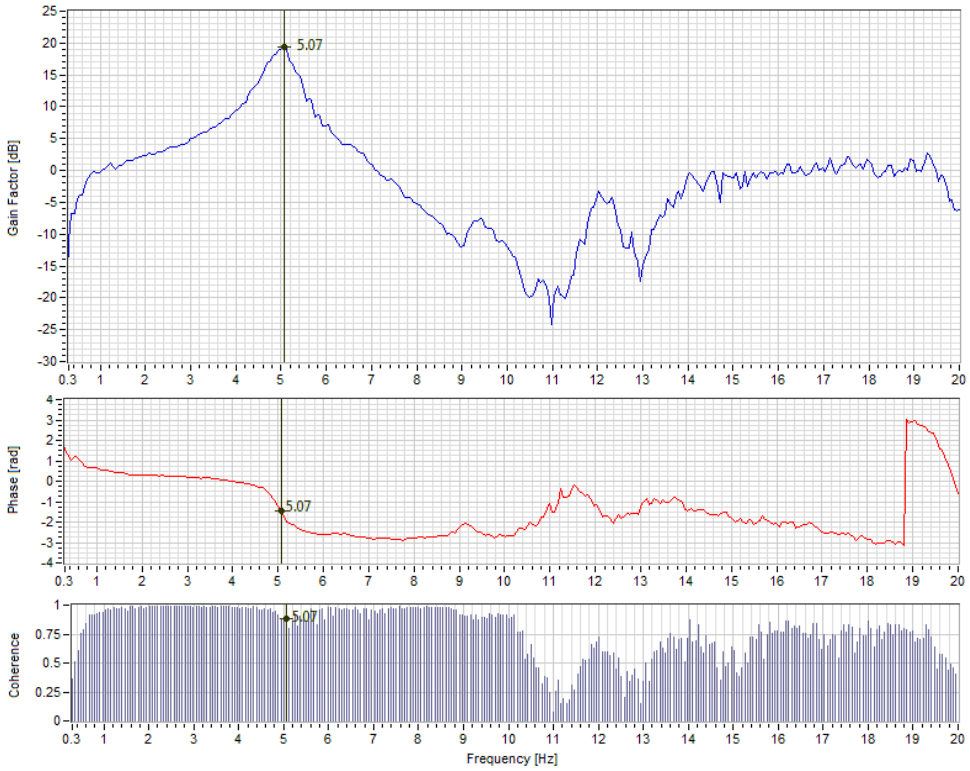

Figure AII. 66: Frequency response function, phase and coherence (Cat 7): ACC MESA LONG; ACC_RL_A2_Y_S_L

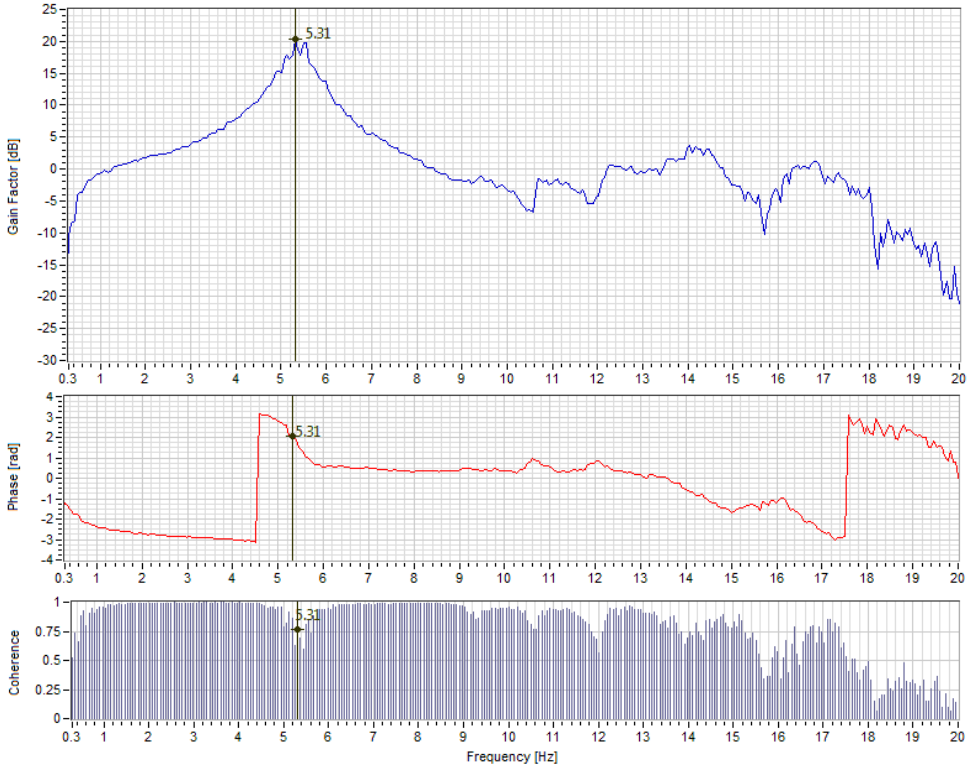

Figure AII. 67: Frequency response function, phase and coherence (Cat 7): ACC MESA TRANS; ACC_RL_B1_X_W_T

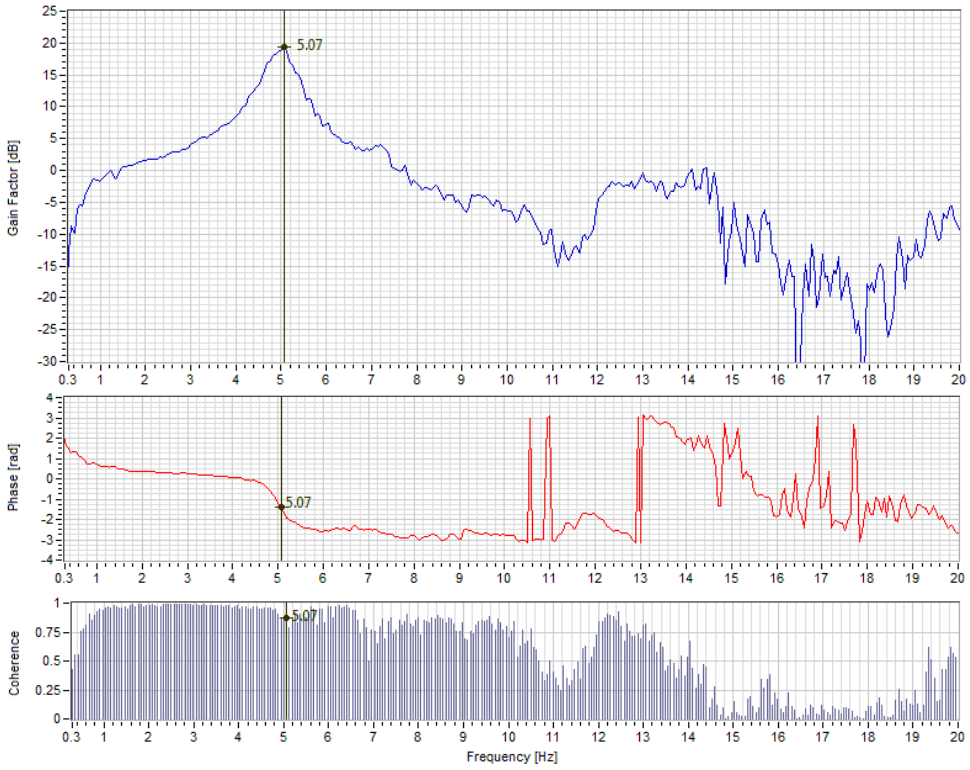

Figure AII. 68: Frequency response function, phase and coherence (Cat 7): ACC MESA LONG; ACC_RL_B1_Y_W_L

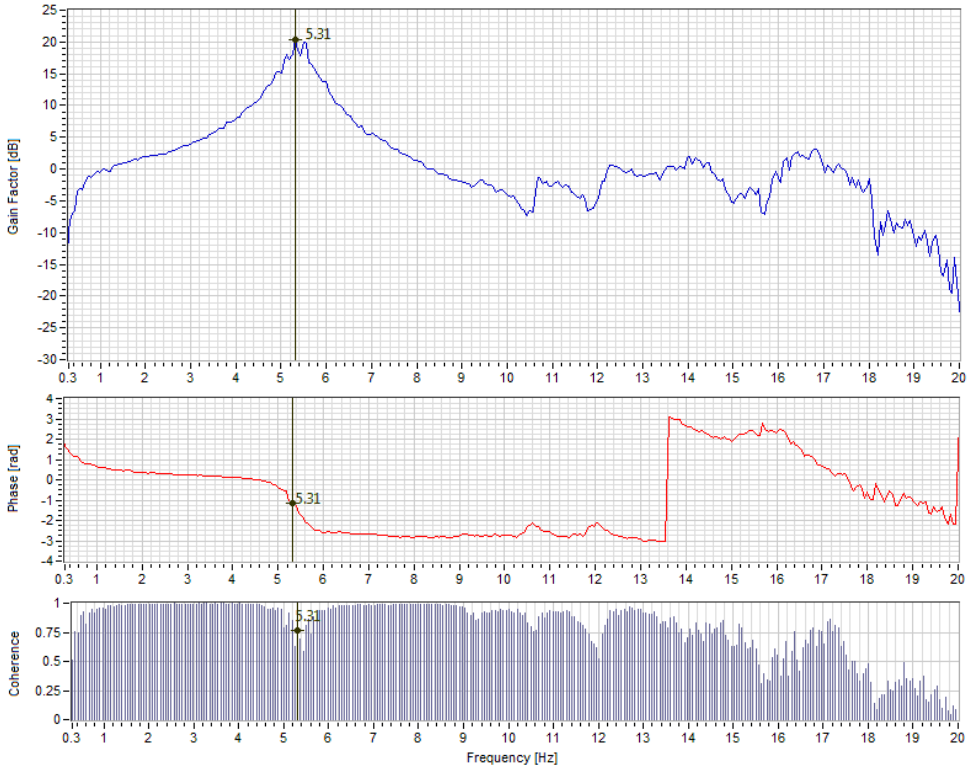

Figure AII. 69: Frequency response function, phase and coherence (Cat 7): ACC MESA TRANS; ACC_RL_B2_X_I_T

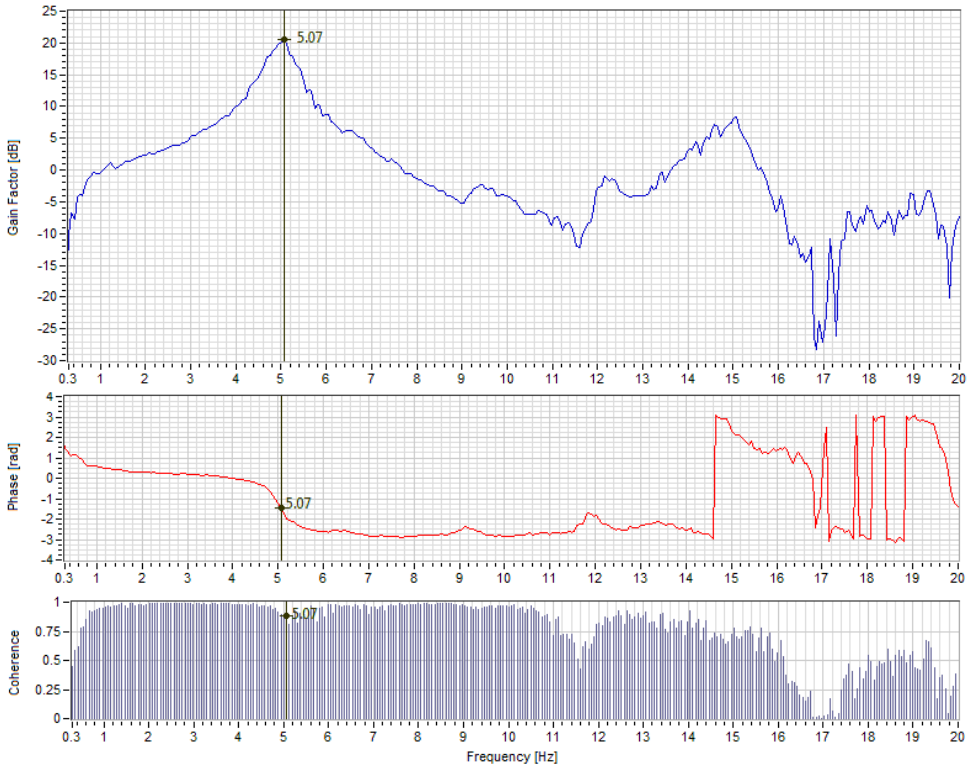

Figure AII. 70: Frequency response function, phase and coherence (Cat 7): ACC MESA LONG; ACC_RL_B2_Y_I_L

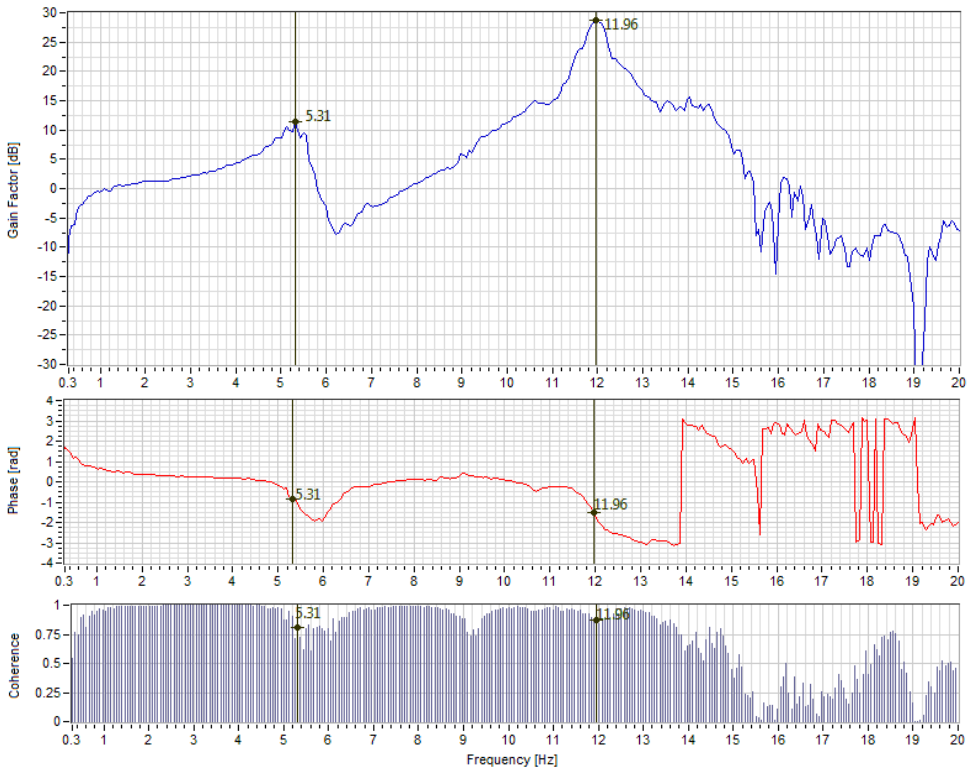

Figure AII. 71: Frequency response function, phase and coherence (Cat 7): ACC MESA TRANS; ACC_GLW03Y_I_T

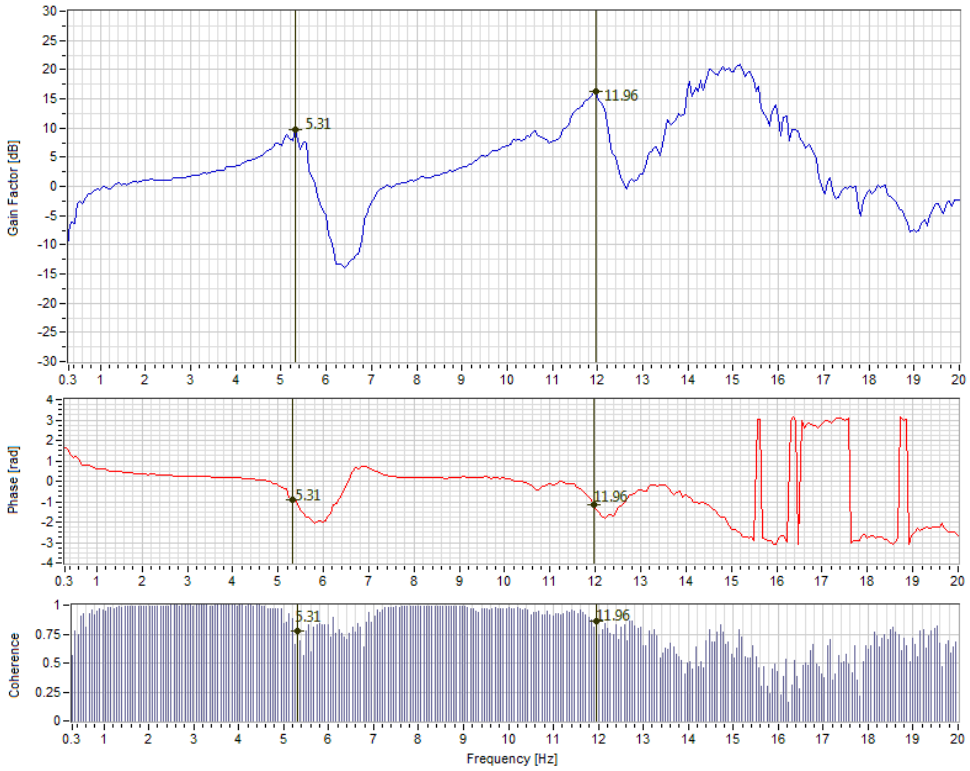

Figure AII. 72: Frequency response function, phase and coherence (Cat 7): ACC MESA TRANS; ACC_GLW04Y_I_T

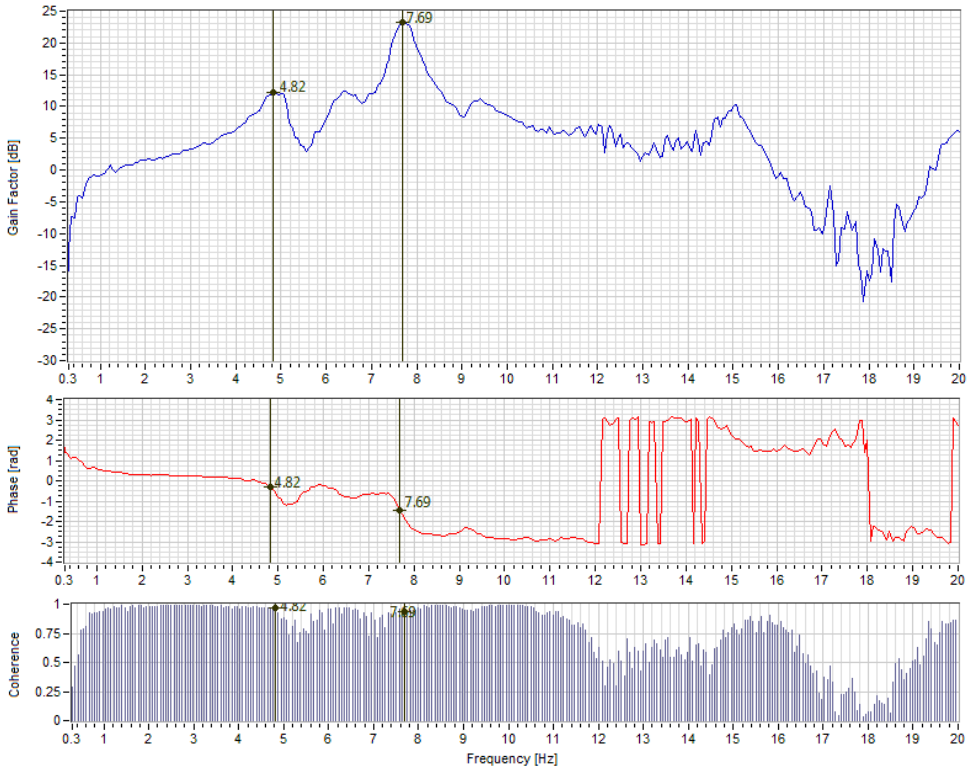

Figure AII. 73: Frequency response function, phase and coherence (Cat 7): ACC MESA LONG; ACC_GLW04X_I_L

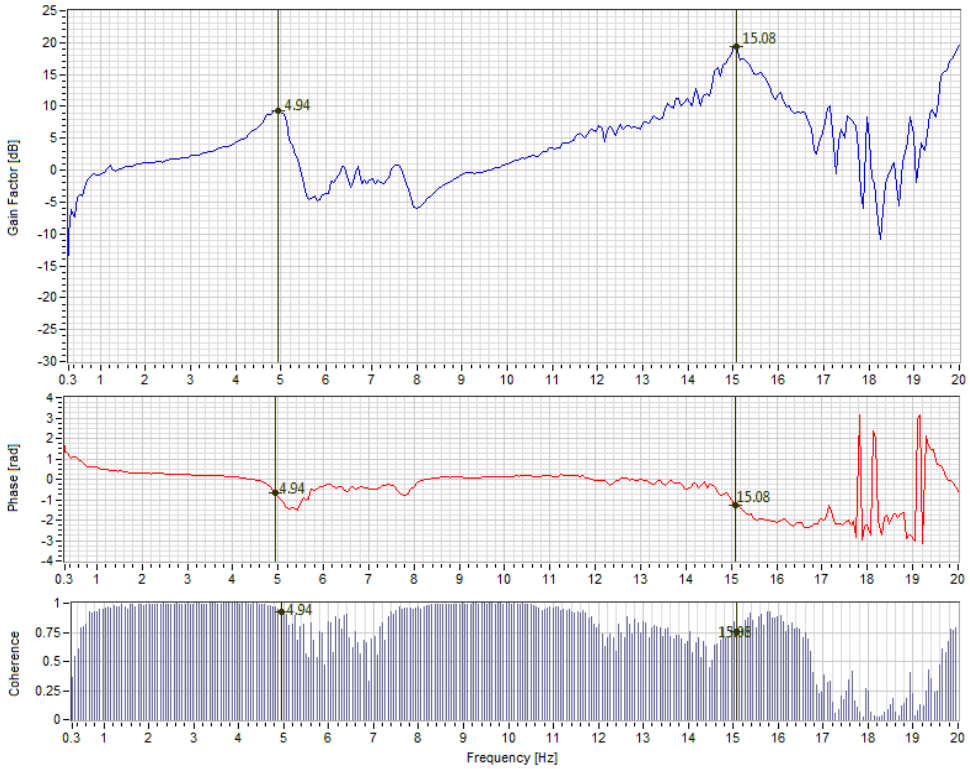

Figure AII. 74: Frequency response function, phase and coherence (Cat 7): ACC MESA LONG; ACC_GLW05X_I_L

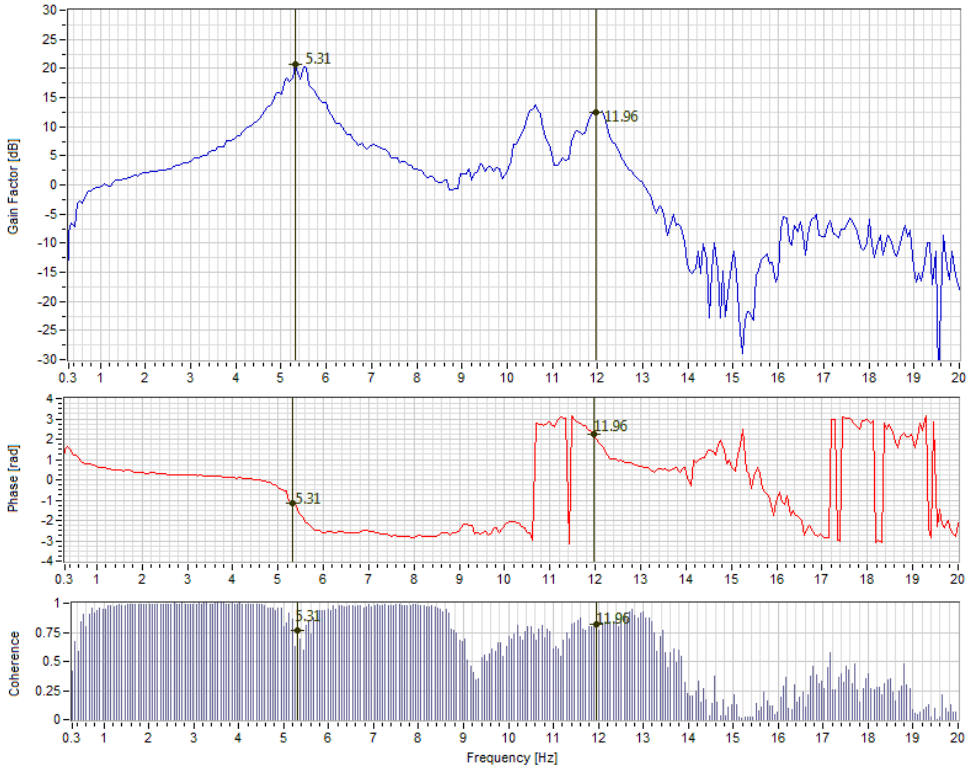

Figure AII. 75: Frequency response function, phase and coherence (Cat 7): ACC MESA TRANS; ACC_L1W03Y_I_T

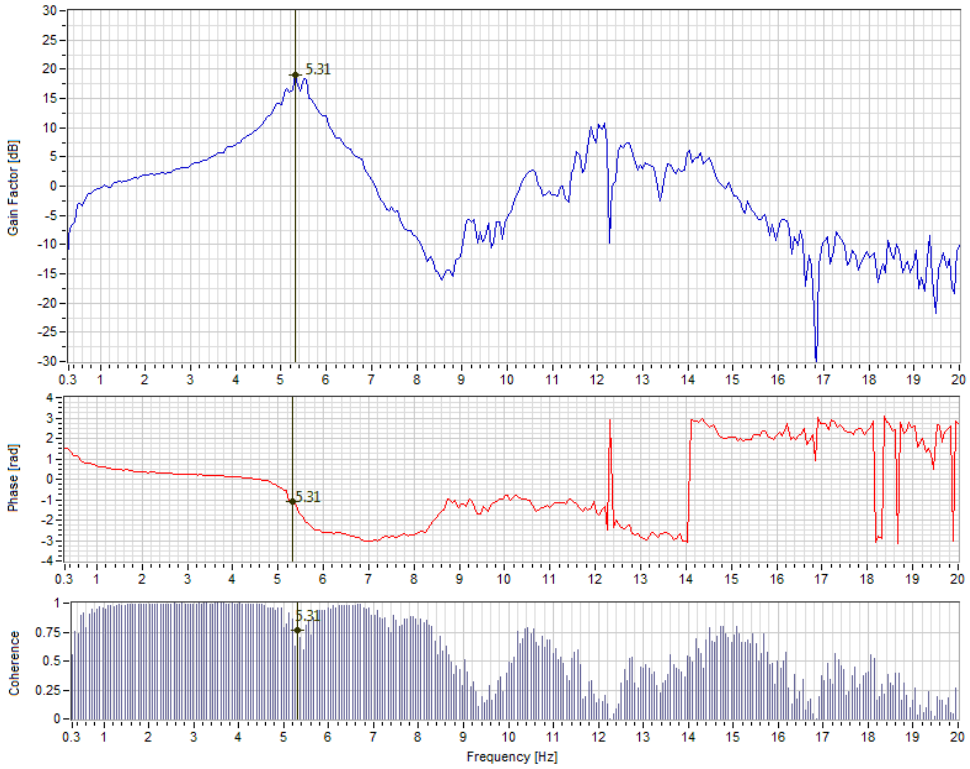

Figure AII. 76: Frequency response function, phase and coherence (Cat 7): ACC MESA TRANS; ACC_L1W04Y_I_T

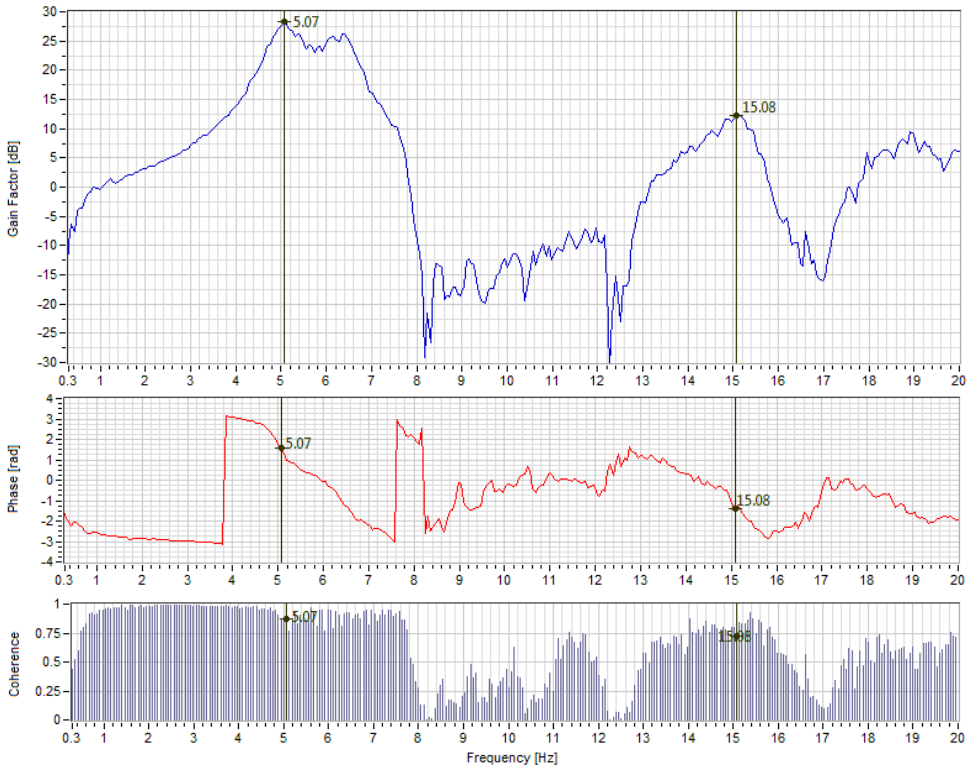

Figure AII. 77: Frequency response function, phase and coherence (Cat 7): ACC MESA LONG; ACC_L1W04X_I_L

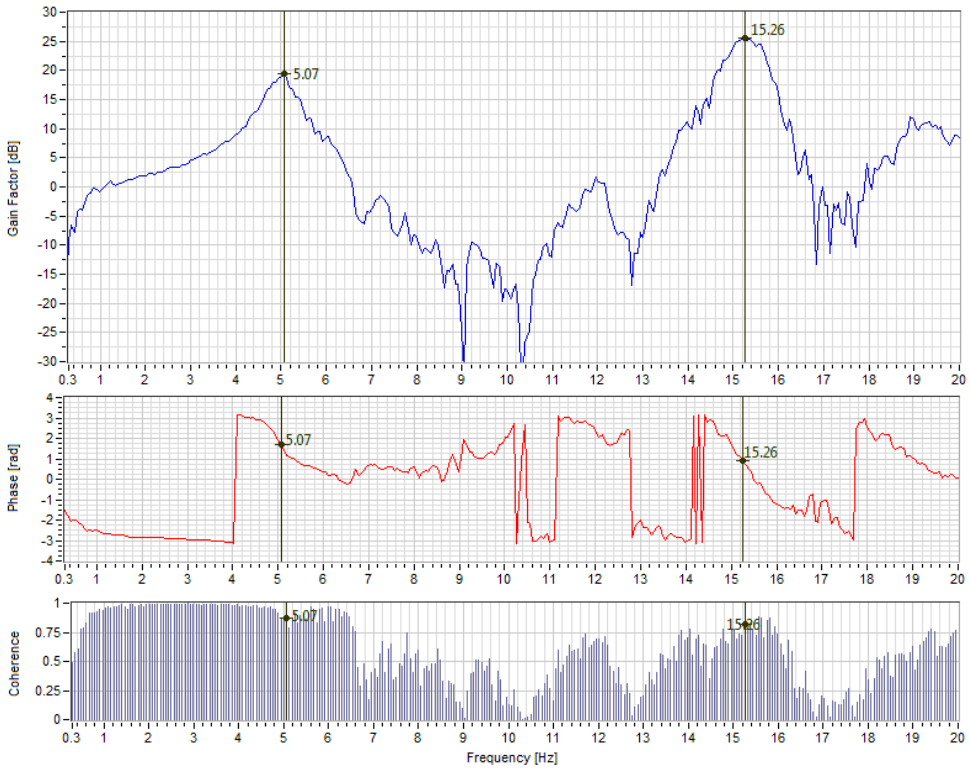

Figure AII. 78: Frequency response function, phase and coherence (Cat 7): ACC MESA LONG; ACC_L1W05X_I_L